CYCLOPEAN

cyclopean concrete noun
: concrete with large embedded stones

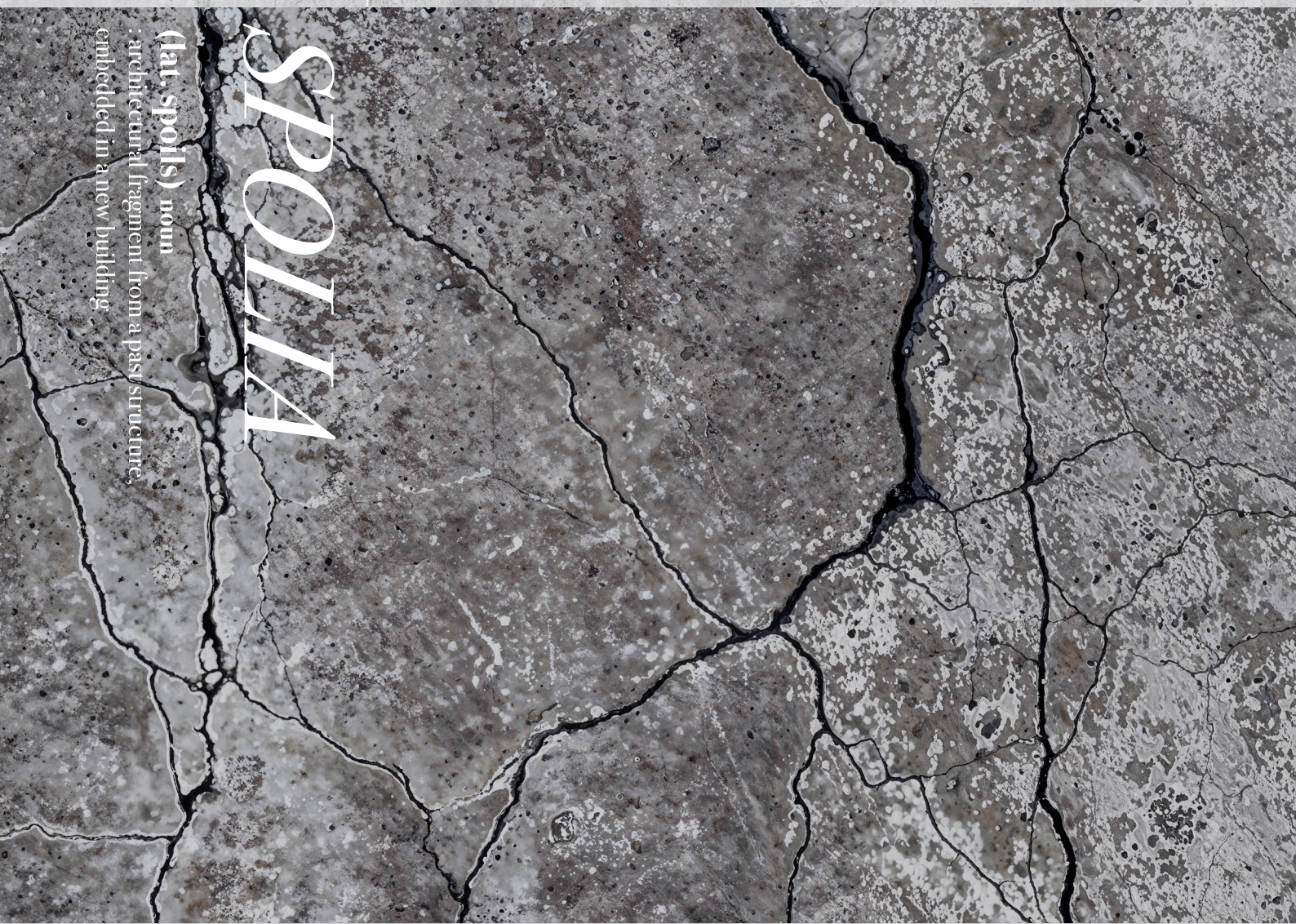

SPOLIA

(lat. spolia) noun
: architectural fragment from a past structure embedded in a new building

Cyclopean Spolia

From Concrete Waste To Load-Bearing Precast Walls

Mauritz von Kardorff - 5145163

19.06.2025

First Mentor

Dr. Olga Ioannou

Second Mentor

Dr.ir. Branko Šavija

Acknowledgements

I would like to thank my mentors Dr. Olga Ioannou and Dr.ir. Branko Šavija for their continuous guidance during the development of this thesis. Their invaluable support has helped me to investigate concrete walls from multiple perspectives and enabled a bigger picture view.

For the advice and support during the experiments, I would like to thank Dr.ir. Fred Veer.

Furthermore, I would like to thank Floor Hoogenboezem and Tim Jonathan for providing me with a space to explore concrete rubble at the Green Village. I would also like to express my sincere gratitude to Jean-Paul de Garde and his team, who had my back during the production of the samples and provided me with every tool necessary.

I would also like to send my gratitude and best wishes to Maxence Grangeot in Lausanne. He enabled a visit of the laboratories at EPFL and it was great to be in conversation with fellow rubble enthusiasts.

I would also like to thank Sander Bentvelsen, who assisted the sample preparation for the Algorithm Experiments.

Furthermore, the preparation and production of all 31 Arrangement Experiment walls simultaneously, would not have been possible without Artemis Rovoli who took time out of their own Master Thesis to mix and pour concrete with me.

Executive Summary

While the construction industry searches for alternatives to concrete due to its high carbon footprint, its demolition waste is currently either downcycled or landfilled. This thesis presents a scalable method for reclaiming large concrete rubble fragments as structural, load-bearing precast walls. A horizontal prefabrication workflow was designed that not only produces airtight, load-bearing walls from reclaimed concrete waste but also enables new possibilities for architectural expression. Using a computational design workflow, the structural performance of multiple rubble arrangements was investigated at a 1:10 scale. Furthermore, a wall system was designed to explore future applications of load-bearing rubble elements and integrate them into established production methods. Through an environmental analysis focusing on waste reduction, circularity, and a cradle-to-gate study, a 50% reduction in embodied carbon compared to conventional precast walls was demonstrated. Overall, the work showed that a prefabrication process has the potential to scale the use of concrete waste as a load-bearing element and produce prefabricated walls with integrated concrete waste.

Glossary

Acronym	Full Term
AI	Artificial Intelligence
CDW	Construction & Demolition Waste
CCDW	Concrete Construction & Demolition Waste
CE	Circular Economy
CS	Cyclopean Spolia
DIC	Digital Image Correlation
DIN	Deutsches Institut für Normung
DIC	Digital Image Correlation
EPD	Environmental Product Declaration
FIFO	First In, First Out
FDP	Void Ratio
FAH	Uniform Course Height
FAV	Vertical Interlocking
FFP	Rectangularity of Units
GWP	Global Warming Potential
ITZ	Interfacial Transition Zone
KPI	Key Performance Indicator
LCA	Life Cycle Assessment
LIFO	Last In, First Out
NFP	No-Fit Polygon
PENRT	Primary Energy Non-Renewable Total
PRECS	Piecewise Reuse of Extracted Concrete in new Structures
RCA	Recycled Concrete Aggregate
RVE	Representative Volume Element
SF	Shape Factor
SSD	Saturated Surface Dry
UTM	Universal Testing Machine

Table of Contents

Introduction

Summary

The Introduction gives an overview of the current challenges associated with concrete production and its disposal. The first sections explain the notion of spolia and highlight the opportunities for the integration of concrete demolition waste for structural applications. The background of the study is explained and the process vision, which acts as the base for this work, is laid out. The following sections describe this paper's impact, the outcomes and outputs of the process and the research questions.

1.1. Cyclopean Spolia

Spolia (lat. *spolium* = spoils/prey) are building materials from existing structures, which are repurposed for new architectural elements. It traditionally refers to the reuse of valuable building materials like stone or marble in a new building and was widespread during the Roman Period (Kinney, 2001). The practice not only served as an economic and practical alternative to new sources of material, but it preserved stories from the past in present architecture.

Figure 1 Spolia Wall of Parikia Castle, Parikia,13th Century (https://www.deutschefotothek.de/documents/obj/71483733)

Figure 2 Mezquita Catedral, Cordoba, 8th Century (https://smarthistory.org/the-great-mosque-of-cordoba/)

Examples of spolia can be found on multiple scales and purposes. The reclaimed building materials could be entire building components, like the columns in the Mezquita Catedral in Cordoba for example (Figure 2), or just fragments of old buildings, like the Parikia Castle on Paros, built in the 13th century. Both buildings adapted their design to the local material they found. In Cordoba, the structure was customized to account for the different lengths of the columns found. In Parikia, the fragments were treated like natural stones and use local masonry techniques to reach a stable arrangement.

Today, the concept of spolia could provide us with a new perspective on how to treat our material resources. Based on the numbers, concrete can be considered the largest source for modern spolia. By weight, 30% of our waste consists of it (Böhmer et al., 2008). In 2025, 201 years after the invention of Portland Cement (Scrivener & Snellings, 2022), we perceive it as low-value material with high costs affiliated with its disposal (Grangeot, Wang, Beyer, et al., 2024b).

What if we challenged this view?

What if we changed our perception of waste?

Could our buildings become quarries?

What if a new method could increase the material value of concrete waste?

Could concrete rubble ever be treated like a precious natural stone?

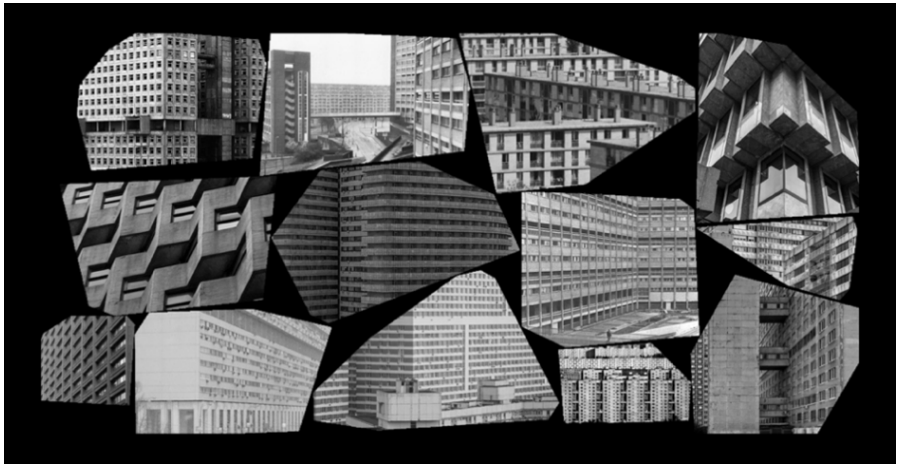

Figure 3 Concept Collage

This research proposes *'Cyclopean Spolia'* (CS). A method which gives a second life to the remains of concrete buildings and integrates them into new load-bearing structures. It develops an approach that combines existing knowledge from working with concrete rubble, prefabrication methods and computational tools. The process uses digital scanning and packing algorithms to handle the irregularity of concrete rubble and analyses how the arrangement of the stones influences the structural performance of new load-bearing elements.

Problem Statement

As the backbone of the built environment, concrete is the key material which shapes our modern world. In the 20th century, it became the most popular structural material, but the urbanisation of the past 30 years drove the consumption to unprecedented levels. China alone poured more concrete between 2010 and 2013 than the US did in the entire 20th century (USGS, n.d.) and concrete is projected to outweigh all biomass on the planet in the 21st century (Elhacham et al., 2020). The reasons for its success are the material's unique advantages like the adaptability to various shapes linked with a high compressive strength and low maintenance costs. Furthermore, it presents excellent thermal storage capacities and is flexible to build with. However, concrete production contributed to 5% of global C02 emissions in 2021 (Statista, 2024b, 2024a) and sand, one of its main resources, starts to become scarce (UNEA, 2022).

- Between 2010 and 2013, China alone poured more concrete than the US did in the entire 20th century -

Furthermore, concrete presents us with another challenge. Its waste accounts for about 30% of the total mass of waste in Europe (Böhmer et al., 2008). Current demolition methods turn the material into irregular-sized rubble, which get crushed down and either used as infill material for road fills, as aggregates for new concrete, or, like 80% of construction waste (Uotila et al., 2024), the concrete gets landfilled.

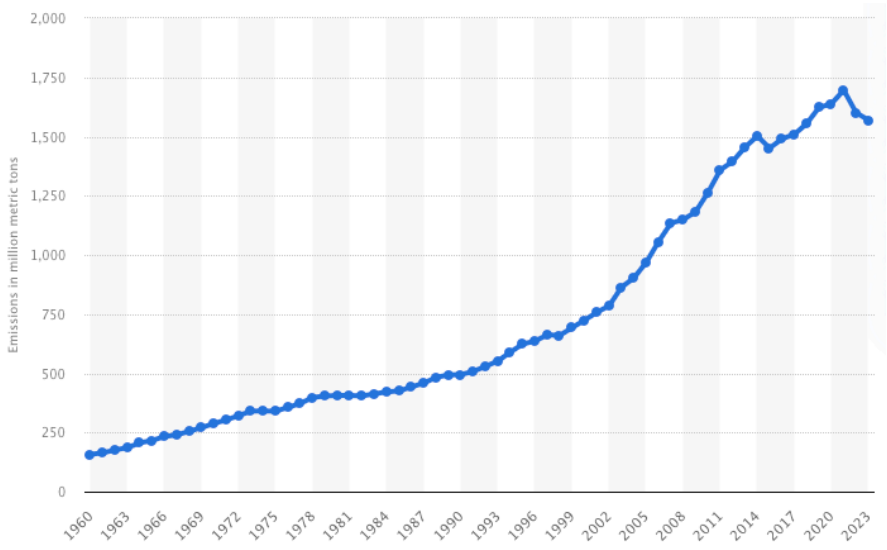

Figure 4 Carbon dioxide emissions from the manufacture of cement worldwide from 1960 to 2023 (Statista, 2024)

However, many concrete buildings are demolished due to functional obsolescence, not because the material has reached the end of its structural capacity. This presents an opportunity to reuse these components in new structural applications.

Today, this is a rarely practised method, though. Industrial processes for the reuse of building products do not exist yet, which leads to increased manual labour during construction and an increased complexity in planning the building. Entire concrete elements are difficult to extract without breaking them, their weight leads to high transport costs and the non-standard elements have to be integrated into the design of the new building (Küpfer & Fivet, 2023).

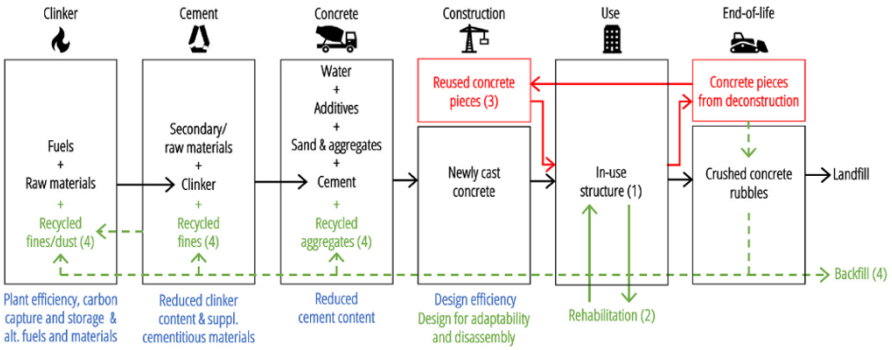

Figure 5 "Concrete value chain. In black, conventional concrete production and service cycle. In colors, strategies to lower the DEI of concrete: direct strategies in blue, circular strategies in green, circular reuse strategies in red. Numbers indicate the circular strategy priority to lower DEI" (Adapted by Küpfer et al., 2023, based on Habert et al., 2020)

There are clear opportunities to overcome these challenges, though. Firstly, the industry has an incentive to search for alternatives, due to the scarcity of sand (UNEA, 2022) and the high carbon footprint of cement. This is also a major goal of political policies and government funding (European Commission, 2020). In recent years, researchers developed frameworks for circular concepts for concrete (e.g. Figure 5) and technological advances offer computational tools, which enable precise and efficient planning with non-standardized elements. The simultaneous digitization of prefabrication processes for the construction industry facilitates mass customization of building products (Khan et al., 2021). All of these developments lead to new opportunities for reuse and reclamation. This thesis develops a method which harnesses these factors and designs a scalable production method to reclaim concrete rubble.

1.2. Personal Background

This master thesis was inspired by the project 'Mosaic Walls' from the CORE studio at TU Delft. It was developed by the author, together with Laila Hany, Tamara Lalyko, and Annebel van der Meulen between September and November 2024. The topic of the studio was 'Robotics in the Construction Industry'. To enable a construction process with concrete rubble, the team developed a stacking algorithm to build a 1:5 prototype with a UR 5 Robot.

The project showed the potential of building with concrete rubble as a structural component and proved a new approach for packing algorithms, which uses tessellations as a base for stacking. Even though the robotic stacking performed well for the 1:5 prototype, the project showed that the vertical free assembly requires a level of precision which is difficult to maintain on-site. As a result, this master thesis investigates a horizontal precast approach, which promises a higher scalability for structural rubble walls.

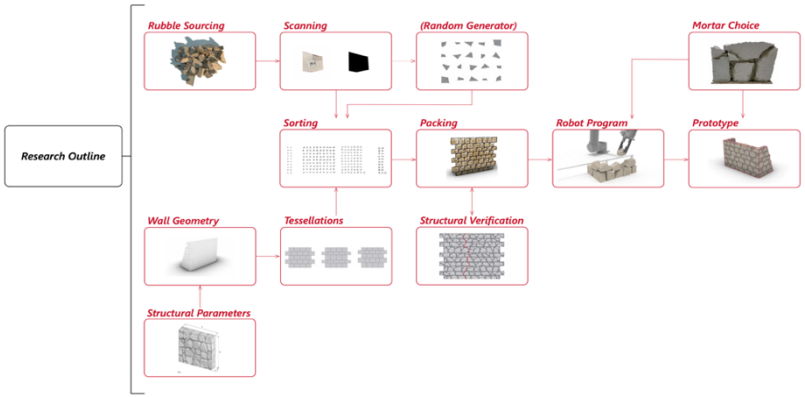

Figure 6 Mosaic Walls Workflow (Hany et al., 2024)

1.3. Vision

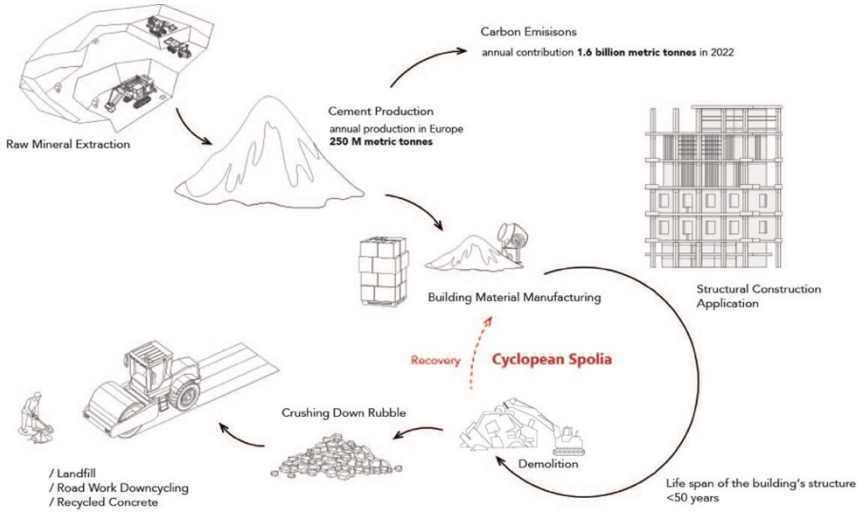

Figure 7 Cyclopean Spolia Diagram (adapted from Mosaic Walls (2024))

The above diagram shows how Cyclopean Spolia integrates into the current product cycle of concrete. Several research papers suggest a change in demolition methods and design, to enable the direct reuse of building parts (Küpfer et al., 2023, 2024; Uotila et al., 2024). Because this development will take a long time to be implemented, this research focuses on the concrete construction demolition waste (CCDW) created by traditional demolition methods. Due to different shapes, properties and sizes, direct reuse of these elements is a challenge (Grangeot, Wang, Beyer, et al., 2024b). Therefore, a method is developed which creates a new homogenous structural element out of several diverse elements. According to Marshall & Grangeot (2024), the process for a load-bearing concrete element should be inside a factory for economies of scale and to create a competitive building product. The vertical stacking construction method is therefore adapted to suit a horizontal prefabrication of the walls. The following potential advantages have been identified:

I. ability to fill all gaps and generate air tightness
II. eliminate the need for structural integrity during the construction process
III. enable the use of a nesting algorithm
IV. create a higher degree of freedom for rubble placement
V. enable vibration for setting the concrete
VI. compensation for the variety of rubble thicknesses

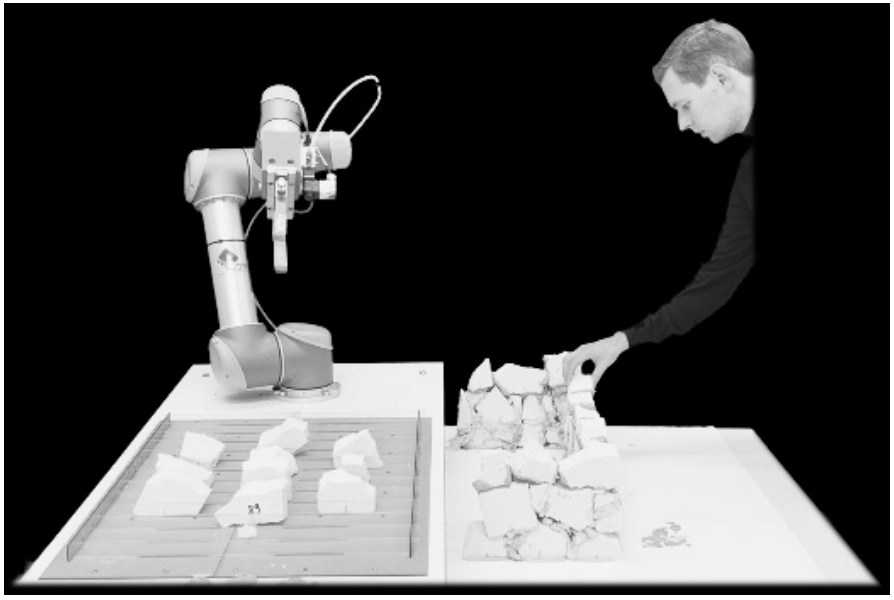

Figure 8 For Vertical Assemblies, Structural Integrity has to be provided for the assembly process, therefore a stacking algorithm is needed

To realize a horizontal fabrication with concrete rubble, the following workflow is envisioned and taken as a base for the research (a more detailed description of the process can be found in 4.5.4 - Prefabrication Process on page 131)

I. A concrete building gets demolished
II. The concrete rubble is transported to a waste treatment plant with adjacent CS Walls factory unit
III. Rubble gets sieved and separated
IV. Diameters under 250mm and thicknesses over 300mm are transferred to regular waste treatment
V. Diameters of 250mm - 750mm and 750mm-1500mm are 2D scanned, tagged and stored in silos for CS Walls
VI. Walls are ordered in specific dimensions and rubble diameters
VII. An algorithm decides on the rubble placement first in first out
VIII. The formwork size is adjusted on a stationary tilting table
IX. Placeholder and lintels for windows and doors are placed
X. A rebar frame is placed around the wall
XI. Rubble is transferred to horizontal formwork by crane
XII. The voids are filled with concrete
XIII. Formwork is removed after at least 18 hours
XIV. The CS Wall is tilted vertically
XV. The CS Wall gets transported on-site

Even though the use-case of the Cyclopean Spolia Walls will be similar to the original use of the concrete, the flexibility and structural performance of the product will be decreased. Therefore, a clear categorization according to the R-Ladder of Circularity (Cramer, 2022) is difficult. This paper uses the words 'reclaiming' and 'integration' when it describes the new use of the rubble.

1.4. Research Question

1.4.1. Main Research Question

How can parallel-sided concrete rubble waste be reclaimed and integrated into load-bearing prefabricated concrete walls to improve structural performance, design freedom and scalability?

1.4.2. Sub Questions

Literature Review

What are the current methods to reclaim concrete rubble without crushing it?

What are the key technical, material and design challenges that require further exploration in load-bearing concrete rubble research?

What are the key factors necessary to design Cyclopean Spolia Walls?

Structural Tests

How can digital tools facilitate the scalability of load-bearing rubble walls?

How does the arrangement and the diameter of concrete rubble affect the structural performance of load-bearing walls under compression?

System Design

How can a prefabrication process enhance the design freedom of load-bearing concrete rubble walls?

How can Cyclopean Spolia Walls be designed to integrate into existing prefabrication and construction processes?

Environmental Impact

How does the integration of concrete rubble affect the environmental performance of load-bearing concrete walls?

1.5. Impact

This research aims to reduce the carbon footprint of concrete walls and proposes a new option for construction waste treatment. The prefabrication process developed uses accessible computational methods to treat the irregularity of the material and contributes to the scalability of the reclamation of concrete rubble. The structural tests compare stone arrangements and investigate the design freedom of walls made from concrete waste. With a physical model, a construction system is demonstrated and the aesthetical appeal of CS walls are shown. Both are essential to the adoption of these walls, which have the potential to offer similar advantages to concrete in terms of maintenance, heat storage, acoustics and fire resistance. An environmental study demonstrates the main advantage of the product, which is the reduction of waste and a lower carbon footprint.

1.6. Research Outcomes

The research designs a process for the prefabrication of structural concrete walls with embedded parallel-sided large concrete construction waste elements. Furthermore, structural experiments help determine the performance of multiple stone arrangements with regards to design freedom enabled by horizontal precast methods. To enable the arrangement of stones within a boundary surface regardless of the database size, a nesting algorithm is introduced and its performance compared to a structural stacking algorithm. Finally, a 1:10 demonstrator is designed and built, which showcases the workflow and the aesthetics of the resulting wall.

These measures add to our understanding of the feasibility of working with load-bearing concrete rubble on a larger scale.

1.7. Research Outputs

The thesis comprises this research report, which includes a literature review, a documentation and analysis of the experiments, the wall system design and an environmental analysis. Furthermore, a computational design workflow for the production of prefabricated concrete rubble walls is developed and tested during the experiments. Throughout the thesis, 31 wall prototypes and 24 concrete samples are built and tested. Additionally, six 1:10 demonstrator walls are presented in a display shelf.

1.8. Methodology

As demonstrated in the research diagram, this thesis examines Cyclopean Spolia Walls around three main pillars. Structural Tests, a System Design and their Environmental Impact. The pillars offer an overview of what Cyclopean Spolia Walls could look like. They build upon each other and create a bigger picture, necessary to discuss the feasibility of upscaling the method.

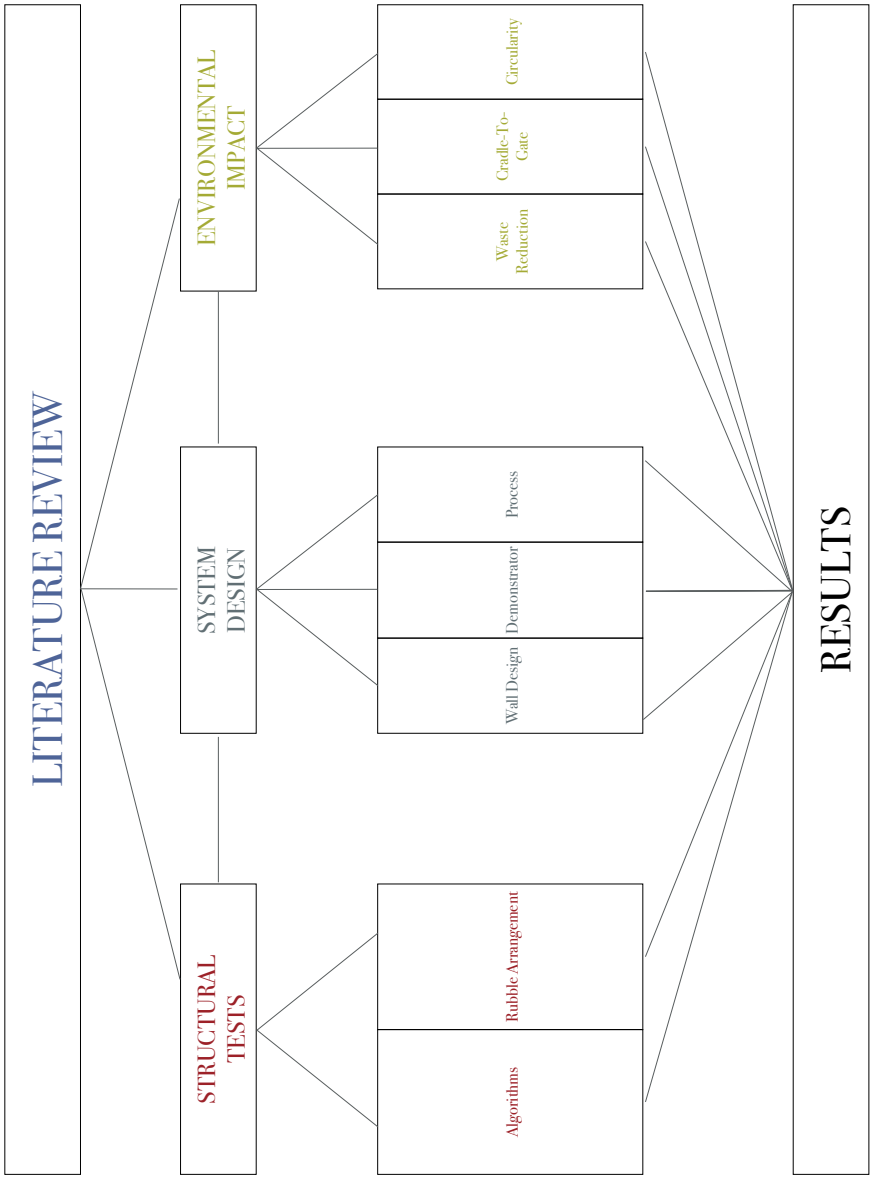

Figure 9 Research Diagram With Three Research Pillars

Literature Review

The pillars are influenced by findings of the literature review, which examine concrete rubble and the steps necessary to design a prefabricated concrete. It is therefore structured around the following themes, which follow the construction process of CS Walls.

1_Rubble Supply - Concrete Demolition Methods
2_Examples - Load-Bearing CCDW Atlas
3_Handling - Lifting and Scanning
4_Computation - CCDW Algorithms
5_Construction - Precast Concrete Walls
6_Filler Material - Cement and Aggregate Behaviour

The academic research papers for this literature review were accessed through two online portals (Scopus and Google Scholar) and through reference lists from papers read throughout the process. Additionally, general information about concrete, precast methods and norms were found in the TU Delft library and its database. To include non-academic CCDW reuse methods and reference projects, sources like blogs, magazines, architecture websites and online video platforms were consulted.

Structural Tests

Structural tests offered a base to understand the mechanical behaviour of parallel rubble embedded in virgin concrete. Due to the heavy weight of concrete rubble from buildings, the tests have been carried out in a 1:10 scale with self-produced rubble. In a first phase, they compare the structural performance of two algorithms used to arrange stones within a wall. A second phase compares two different rubble diameters, two infill ratios, an unreinforced wall and a wall which combines large rubble and small rubble. All computational calculation times stated in the structural tests refer to a personal computer equipped with an Apple M2 Max chip wih a 12-core CPU and 64 GB of RAM. The Python scripts were executed using Python 3.9.6. and can be found in chapter the appendix.

System Design

A major part of this thesis is the design of a reproducible prefabricated wall system. This was developed from the findings of the first pillar and based on the use case of a three story high building. Additionally, a transport and assembly system has been designed to overcome the constrains of rubble walls and to show the connection details of the walls. The final part of this pillar is centred around the aesthetics of Cyclopean Spolia Walls. It focuses on the concrete surface, with regard to rubble thickness, rubble size and the forms which can be included in a wall. To demonstrate it in an appealing way, a 1:10 model of six walls was built. This pillar therefore shows the appeal and feasibility of Cyclopean Spolia.

Environmental Impact

In addition to the aesthetics and memory that CS walls offer, their reduced environmental impact is one of their major advantages. To back this up, the final pillar examines the system designed beforehand and performs a comparative cradle-to-gate life cycle analysis for its manufacturing phase. CS Walls are compared to similar wall structures, based on a case study. Furthermore, the waste reduction that load bearing rubble elements offer is discussed and its circularity assessed.

Literature Review

Summary

The Literature Review section starts with the Load-Bearing CCDW Atlas. It provides an overview of the current state of concrete rubble reclamation methods and uncovers opportunities for the scalability of the Cyclopean Spolia. After this, the literature review investigates current demolition methods to portray the supply of material and gathers knowledge about the physical handling and digital scanning of large rubble elements. To inform the arrangements and design variabilities of the rubble, the research compares nesting and stacking algorithms, which are used to produce the specimens for the experiments. Due to the scarcity of papers on structural concrete rubble reclamation, the section provides an overview of the behaviour of cement paste and aggregates, which informed the structural tests.

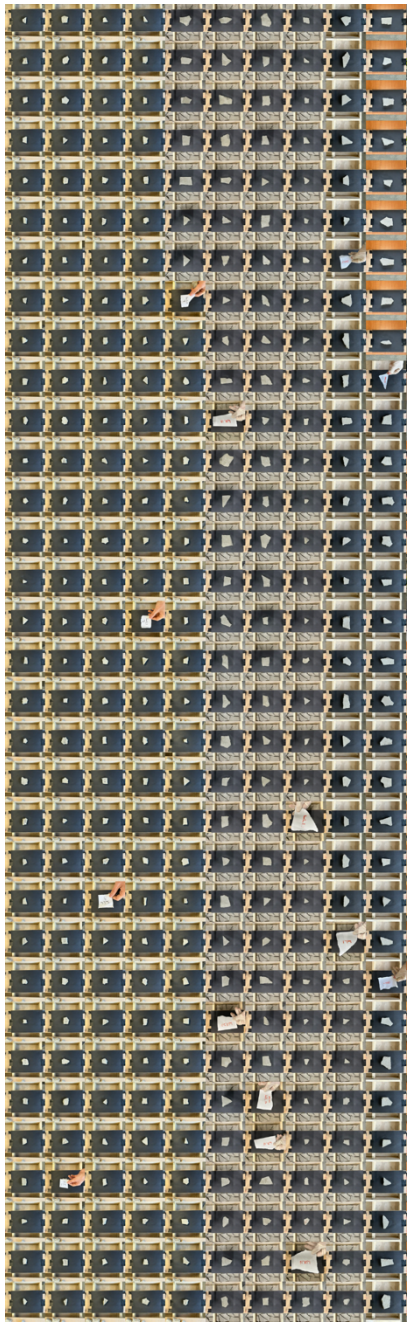

2.1. Concrete Rubble

2.1.1. Concrete Demolition

The common abbreviation CDW stands for Construction & Demolition waste, which actually describes two types of waste. Construction waste is everything which arises during the erection of a building, like excavation soil, offcuts, or packaging. Demolition waste is the material produced at a building's end of life. This commonly includes Stony Waste (concrete, mortar, etc.), Non-Stony Waste (metals, wood, glass, etc.), Hazardous Waste (asbestos, paints, oils, etc.) and Other Waste like organic material for example (Llatas, 2013). The demolition methods most commonly used in Central Europe be found in Table 1 below.

Mechanical Processes	Mechanical equipment is used to crush or bring down constructions.
Thermal Processes	Materials are fused and separated from the structure.
Abrasive Processes	Constructed elements are cut into smaller pieces using abrasive saws.
Explosive Processes	Structures are collapsed using explosive charges at strategic points of the structure.
Electrical Processes	Electrical discharges are conducted through the elements causing breakage.
Chemical Processes	Use of highly expansive chemicals, which cause fragmentation of constructed elements.

Table 1 Common Demolition Methods (based on Coelho & De Brito, 2013)

All methods are used for concrete structures. Mechanical, abrasive and explosive processes are the most common, whereas thermal, electrical and chemical processes are used for specialized applications (Coelho & De Brito, 2013).

2.1.2. Concrete Deconstruction

The term 'demolition' has to be set apart from the term 'deconstruction'. The former stands for a destructive process, whereas the latter describes a process which preserves and separates construction materials at their end of life (Coelho & De Brito, 2013). This method is increasingly applied for environmental, but also for economic reasons, as the disposal of cleanly separated CDW is significantly cheaper than for mixed CDW (Coelho & De Brito, 2013). This represents and incentive for companies to separate waste, and offers opportunities to develop methods which remove materials from the waste stream. With 5 t of CDW per capita per year in the EU alone, the potential to recover this waste is vast (Eurostat, 2022). After soil, concrete is the largest component in demolition waste (*Database - Waste - Eurostat*, n.d.), and represents up to 40% of the waste generated (Gálvez-Martos et al., 2018). Currently, concrete is mostly crushed to smaller pieces and landfilled, downcycled as backfilling (Baldania & Bhogayata, 2023; Vermeulen, 2016) or turned into recycled aggregate concrete (RAC) (Tam et al., 2018). Contrary to public perception, RAC do not show a significant reduction in carbon emissions compared to

period	1967–1998			1999–2010		2011–2022	
	pioneering period			development period		diversification period	
practice trend	A early reuse of precast concrete components in Germany	B first large-scale experiments reusing precast concrete panels	C pioneering reuse of cast-in-place concrete for like-for-like applications	D research and application reusing German mass-housing precast concrete panels in low-rise projects	E aborted large-scale projects reusing precast-concrete components	F diversification of precast concrete reuse	G new applications reusing cast-in-place concrete pieces
							
total number of case studies (including built ones)	17 (14)	3 (3)	1 (1)	30 (25)	4 (2)	10 (4)	12 (5)
location	D	S, NL	S	D (NL, F)	NL, S, USA	Europe	Europe, USA

Table 2 Application Of PRECS (Küpfer et al., 2023)

concrete with natural aggregates (Marinković et al., 2010; Marinković & Carević, 2019). In addition to crushing down the material, multiple methods to reclaim larger concrete parts have been applied in the past (Huuhka et al., 2015) and the attention to them has grown recently. As the literature is still scarce, Küpfer et al. (2023) collected the available knowledge on Piecewise Reuse of Extracted Concrete in new Structures (PRECS) in a comprehensive overview, which is represented in Table 2 above. They categorize PRECS in three periods, whereas the current development contributes to the diversification of the method, with a focus on cast-in-place concrete. In addition, the FCRBE (2021) laid out how concrete building parts can be reclaimed for different purposes (see Figure 10).

2.1.3. Concrete Rubble Sources

However, in relation to the local market, deconstruction is not always economically feasible (Coelho & De Brito, 2013). In these cases, the concrete can still be saved from common downcycling streams. To achieve this, larger concrete rubble fragments (red square in Figure 10) are reclaimed and turned into new construction elements. The example approaches were already discussed in the previous chapters, but their

material sources are rarely laid out in detail. According to FCRBE (2021), the best concrete waste candidates to reclaim are fragments with little rebar, as this prevents injuries during handling. Like Grangeot et al. (2023), they also state that floor slabs and walls mostly produce rubble with two parallel faces, whereas beams and columns usually break into irregular blocks of the size between the reinforcement bars (FCRBE, 2021). This offers an opportunity for their reintegration into construction processes. Therefore, parallel rubble becomes the main material for Cyclopean Spolia Walls, as it offers the potential of 2D scanning. Existing methods are laid out and discussed in detail in the following chapter.

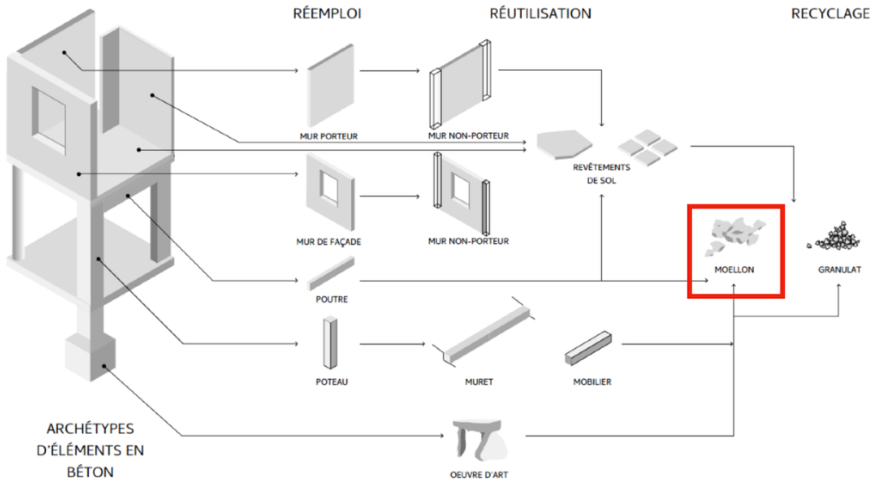

Figure 10 Solutions For Reclaiming Concrete Parts Of Buildings, Reuse / Remanufacture / Recycling (FCRBE, 2021)

Load-Bearing CCDW Atlas

Concrete reuse is widely discussed and often based on novel ways of planning or demolition (Küpfer et al., 2023, 2024; Uotila et al., 2024). To reclaim rubble from traditional demolition methods, the majority of human waste, is still new though. Only a handful of academic papers are available. However, rubble found its way into architecture, art and even local landscaping. The Load-Bearing CCDW Atlas maps known projects and existing research, which directly work with structural concrete rubble methods, based on parallel-sided rubble. To summarize them, a table is created which compares the existing approaches. Each project description starts with a process timeline, which is followed by a brief description of the approach. The overview starts with current academic research, sorted by year of publication and moves on to non-academic approaches. The aim is not only to show the potential and variety of reclaimed rubble methods, but also to demonstrate how recent the development is and how little we know about it. The atlas concludes with an overview of the existing knowledge from these applications and their influence on Cyclopean Spolia. The text does not use in-text citations when the projects themselves are described, as the source is always the main paper cited in the title.

	Year	Place	Author	Method	Stone Preparation	Scale	Estim. Max. Rubble Weight	Rubble Source	Stone Arrangement	Estim. Database Size	Potential for scaled prefabrication	Why
Masonry Walls from Reclaimed Concrete Demolition Waste	2024	Lausanne CH	Oreb et al.	Structural tests of horizontally stacked rubble masonry walls and weaker mortar	none	1:1	< 50 kg	Local Waste Treatment Plant	manual	ca x3	1/5	On Site Manual Labour Required
From Concrete Waste to Walls	2024	Lausanne CH	Grangeot et al.	Robotic stacking of vertical raw concrete rubble elements with mortar	none	1:1	> 100 kg	Local Waste Treatment Plant	2D – Image Convolution Based (Wang et al., 2024)	ca x3	3/5	A controlled environment is beneficial for the robotic stacking process
An Investigation into Machine Learning Matchmaking for Reused Rubble Concrete Masonry Units (RR-CMU)	2024	Lausanne CH	Marshall & Grangeot	Rubble match-making via machine learning algorithm to cast modular panels	none	n/a	> 50 kg	Local Waste Treatment Plant	2D – Image Convolution Based (Wang et al., 2024)	ca x3	5/5	Modular panelisation, high potential for prefabrication
Cyclopean Cannibalism	2017	Boston USA	Clifford & McGee	Revival of ancient masonry methods with CDW and computational methods	precise carving of the stones	1:1	> 300 kg	Local Waste Treatment Plant	n/d	n/d	4/5	Controlled environment beneficial for precise stone preparation. Assembly could happen locally
Mosaic Walls	2024	Delft NL	Hany et al.	Robotic stacking of large stones with manual placement of infill stones and mortar	none	1:5	> 2 kg	Broken aerated concrete blocks	2D – Tessellation Based, Stacking and Nesting (Hany et al., 2024)	x2	2/5	A controlled environment is beneficial for the robotic stacking process. Buttresses make transport
Missing Pieces	2023	Cape Cod USA	Ensamble Studio	Creation of an art piece made of large vertically stacked concrete rubble elements connected with steel	none	1:1	> 100 kg	Self-made	n/a	x1	3/5	Was prefabricated and then shipped, but not in controlled indoor environment
Urbanite	NA	USA	Various	Remanufacturing of concrete rubble elements for landscaping into pathways and retaining walls	sometimes	1:1	< 100 kg	Local Waste Treatment Plant	n/a	x1	1/5	Manual on-site placement required
Cyclopean Spolia	2025	Delft NL	von Kardorff	Horizontal prefabrication of load-bearing rubble walls	none	1:10	> 2 kg	Self-made	Nesting (Deepnest, 2025) & Stacking (Wang et al., 2024)	x1.1 - x5	5/5	Horizontal prefabrication process

Table 3 Reclaimed Load Bearing Parallel Sided Concrete Rubble Methods Analysed In The Load-Bearing CCDW Atlas

Masonry Walls from Reclaiming Construction Demolition Waste (Oreb et al., 2024)

Process overview:

I. source concrete demolition waste
II. photogrammetric 3D scanning of the stones
III. digital reconstruction of the stones and sorting into an inventory
IV. development of the walls with a stacking algorithm for placement optimization
V. formwork construction
VI. layer-by-layer assembly with horizontally placed rubble and mortar
VII. intermediate layer image capture to create a full digital twin of the walls as constructed
VIII. structural tests

Figure 11 Wallets After The Diagonal Compression Tests (Orev et al., 2024)

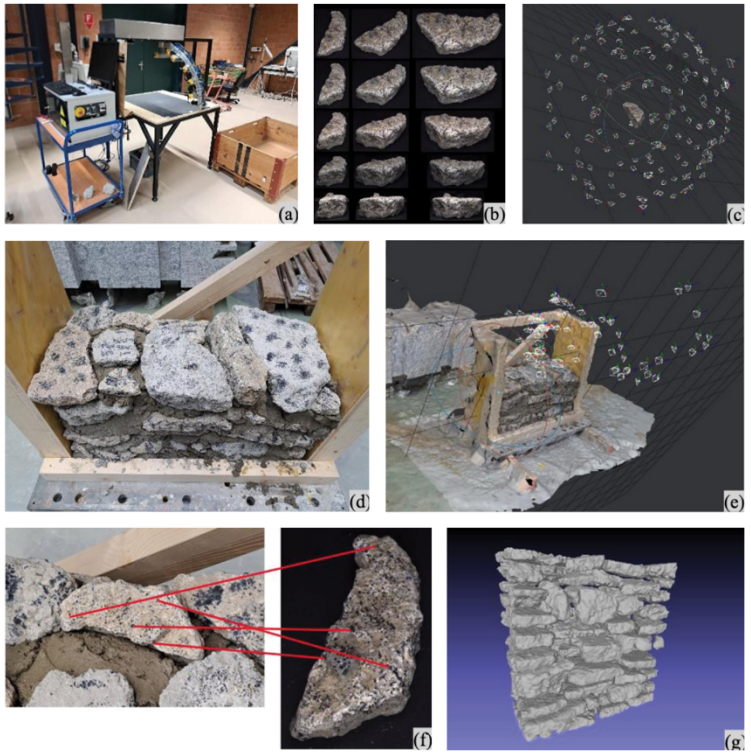

Figure 12 3D Scanning Process (Oreb et al., 2024)

Oreb et al. (2024) developed a workflow which treats concrete rubble like masonry elements. In their research, they horizontally stacked concrete with a diameter between 10cm to 40cm with the use of mortar. Together with the compression tests by Grangeot, Bastien-Masse, et al. (2024) it is the only project found, which provides a structural assessment of concrete rubble wall elements and is therefore a key reference for Cyclopean Spolia Walls.

Their concept relies on the mortar being the weakest part of the structure. After a test on three concrete samples from the rubble, they

Wall name	f_c (MPa) EN 1052-1 [29]	E (GPa) EN 1052-1 [29]	E/f_c
W1	5.10	7.096*	1390
W2	8.32	5.430	653
W3	6.38	5.877	921
W4a	-	3.820	-
W4b	9.56	4.001	418
Mean ± Standard deviation (*CoV: Coefficient of Variation*)	7.34 ± 1.72 (23%)	5.245 ± 1.220 (23%)	846 ± 417 (49%)

Table 5 Results of Simple Compression Tests on Wallettes (Oreb et al., 2024)

Wall name	f_t (MPa)			G (GPa)
	ASTM [34] (α=0.707)	RILEM [33] (α=0.5)	Brignola et al. [35] (α=0.35)	ASTM [32] (α=0.707)
DCW_A	0.483	0.342	0.239	1.273
DCW_B	0.556	0.393	0.275	1.374
DCW_C	0.726	0.514	0.360	1.799
Mean ± Standard deviation (*CoV: Coefficient of Variation*)	0.592 ± 0.130 (22%)	0.419 ± 0.092 (22%)	0.293 ± 0.065 (22%)	1.482 ± 0.279 (19%)

Table 5 Results of Diagonal Compression Tests (Orev et al., 2024)

still showed a strength between 25 and 40MPa. With M10 mortar, they chose a weaker binder for the concrete. This enabled quality control of the structure, even though the strength of each concrete element was unknown, as weaker binder leads to failures in the mortar or at the interface transition zone (ITZ).

To test the structural integrity, they produced seven wallets of 90cm x 90cm x 40cm, of which four were tested under simple compression and three were tested under diagonal compression. Linear variable differential transformers (LVDT) and digital image correlation (DIC) results showed that the cracks propagated along the interfaces between stones and mortar, which reflects typical masonry failure behaviour and proves the quality-control concept of a weaker mortar. The walls have compressive strength between 5.1 MPa and 9.6 MPa and a Modulus of Elasticity between 3.8 GPa and 7 GPa. For the diagonal tests, the wallets were rotated by 45 degrees to determine their tensile strength. A key finding for Cyclopean Spolia Walls is in the results of the final wallet. Because the large stones were used first, this wallet contained smaller rubble elements and more mortar. Even though the mortar was the weaker element, the structure showed higher tensile strength than the other specimens. According to Oreb et al. (2024), this suggests a more homogenous construction. This could indicate that a horizontal production with a gap-filling binder like the CS process plans could lead to stronger, hence more homogenous elements.

Compared to traditional stone masonry (Type A) and concrete walls from residential constructions, the wallets tested by Oreb et al. (2024) show better mechanical properties (compressive strength and modulus of elasticity) than the former, but lower properties than the latter. The density of the wallets is however 53% higher than hollow brick masonry walls, which could increase transport emissions, but have a positive effect on their volumetric heat capacity.

To conclude, the method proposed by Oreb et al. (2024) is a promising alternative to regular masonry in regards to mechanical properties and its efficient use of resources. The process is not automated however and still heavily relies on manual labour. Furthermore, the formwork adds a layer of complexity, not present in brick masonry.

Material	f_c (MPa)	f_t (MPa)	E (MPa)	G (MPa)	ρ (kN/m^3)
Stone masonry with lime mortar (type A) [36]	1.4 (30%)	0.039 (24%)	870 (21%)	290 (21%)	19
Concrete demolition waste masonry	7.34 ± 1.72 (23%)	0.592 ± 0.130 (22%)	5245 ± 1220 (23%)	1482 ± 279 (19%)	23
Brick masonry [37] *	5.0 – 8.0	-	3500-5600	875-1400	15
Concrete (C25/30) [38]	25	2,6	31000	12916	24

*** Note:** Hollow bricks (voids < 40%) with cement mortar

Figure 13 Comparing Concrete Demolition Waste Masonry With Traditional Building Methods

Structural Concrete Rubble Arrangements (Grangeot, Wang, Beyer, et al., 2024b)

Process overview:

I. source large flat rubble pieces from the recycling centre
II. 2D scan with a regular camera on a dark surface
III. digitalise outline
IV. cluster rubble by size and shape
V. find structurally safe arrangement with a stacking algorithm
VI. choose the final assembly based on: uniform course height (FAH), vertical interlocking (FAV), void ratio (FDP), and rectangularity of rubble units (FFP).
VII. build a formwork
VIII. place lifting anchor with a drill
IX. lift and place a stone into the formwork
X. fill voids manually with mortar
XI. repeat steps VIII - X until the wall is finished

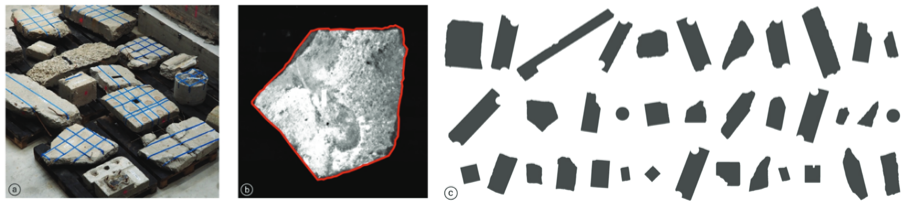

Table 14 Scanning process by Grangeot et al. (2024) (a) Scanning configuration of concrete debris, (b) canny edge detection output on top-view image, (c)

To reclaim concrete construction demolition waste into a structural element, Grangeot et al. (2024) use rubble fragments as the major structural element of thin single-leaf masonry walls. To achieve this, flat concrete waste elements are stacked vertically on top of each other, without any alteration or preparation of the rubble. The concrete pieces are sourced from a local construction waste recycling facility. To fill the gaps, mortar and smaller rubble are placed in between the larger elements. To render the process more feasible, only regular equipment typically used on construction sites and in factories is used. This lowered the skills needed to assemble the wall and made the process more economical. Therefore, only drills and hoisting equipment are needed. As in most concrete rubble studies, the rebar included in some rubble fragments is not discussed in detail.

As the rubble used comes from walls or floor slabs, it is parallel on both sides. It is thus possible to create a 2-D digital scan of the concrete waste elements, which is processed with the OpenCV Python library (Culjak et al., 2012). This simplification from a three-dimensional shape into a two-dimensional outline reduces the effort for scanning and the following computing power for the algorithm. The rubble thickness is measured by hand, but could also be measured with a sensor from a

Components in formulation	Model-based					Model-free	
	LS + HF	LS		HF		RL	
	Ours	Johns et al. (2020)	Lambert and Kennedy (2012)	Liu et al. (2021)	Thangavelu et al. (2018)	Menezes et al. (2021)	Liu et al. (2018)
Masons' rules-of-art							
Tight packing	×	×	×		×	×	×
Straight course	×			×	×		
Interlocking	×	×		×	×		
Wedging	×						
Placement stability							
Stable footing	×			×	×		
Inward sloping	×	×		×	×		
Gravity	×	×		×	×	×	×
Lateral load	×				×		×
Others							
Physical experiment		×		×	×		×
2D/3D	2D	3D	2D	3D	2D	3D	2D

Table 6 Wang et al. (2024)

crane if the distance remains constant. To account for inaccuracies, the outline is offset by 1.5cm as a margin of error.

To plan the placement of the stones into predefined wall dimensions, they based their algorithm on the image convolution-based process developed by Wang et al. (2024). It is aimed at stacking non-uniform natural stones based on 2D scans and uses the traditional masonry method of stone wedging to improve the structural performance of the wall. The stability verification is based on contact points to the right and left of the stone's centre of mass. Because the algorithm works with image processing, based on binary images, and the next best-fit approach, it can place a stone within 8 seconds (50000 pixels raster with an Intel Core (TM) i7-10700 CPU 2.90 GHz). The approach is further analysed in 2.3.2 on page 43. The algorithm produces multiple wall options which are ranked based on their height and void ratio. These were then evaluated by the team, to choose the best one, based on masonry regularity (Borri et al., 2015). The assessment methods are 'uniform course height (FAH), vertical interlocking (FAV), void ratio (FDP), and rectangularity of rubble units (FFP)' (Grangeot, Wang, Beyer, et al., 2024b) based on Almeida et al. (2016).

Indices (%)	HI 01	HI 02	HI 03	HI 04	HI 05	HI 06	HI 07	BT 01	OP 01	OP 02	OP 03	OP 04	OP 05	OP 06	OP 07	OP 08
F_{DP}	13	14	16	16	21	23	23	19	22	25	25	25	25	26	27	27
F_{AH}	1	2	1	4	3	5	4	3	4	3	4	2	7	1	14	4
F_{AV}	40	58	40	42	37	27	47	73	28	28	5	24	5	29	6	30
F_{FP}	6	7	6	5	8	9	11	9	8	7	7	9	8	7	8	9

Table 7'Comparison of geometric indices of irregular masonry walls. Historic examples using unsquared stones are ranked from most regular (HI01) to most irregular pattern (HI07) [17]. The built solution is BT01. The eight best stacking options are OP01–08' (Grangeot et al., 2024)

To build the chosen layout, a wooden formwork is placed, which ensures the stability of the wall during assembly. Then, the centre of gravity is determined for each stone (see method explained in 3.1.1.). Based on this point and the rotation of the element in the final pattern, a robot drills into the flat side of the rubble and places a removable lifting anchor. Stones over 100kg receive two anchors, each placed at the centre of gravity of half the stone's centre of gravity. Stones above 15kg receive one anchor and lighter stones are placed manually. A hoisting machine then lifts the stone and places it inside the formwork at the position determined by the algorithm. To fill the voids between the stones, mortar is placed by hand.

The full-scale demonstrator is 2250mm high and includes concrete waste elements with a thickness of up to 320mm. A structural compressive load test confirmed a lower bound resistance of 2MPa. The wall construction took 40h (6.6h/m2), out of which 70% of the time accounted for the manual void filling.

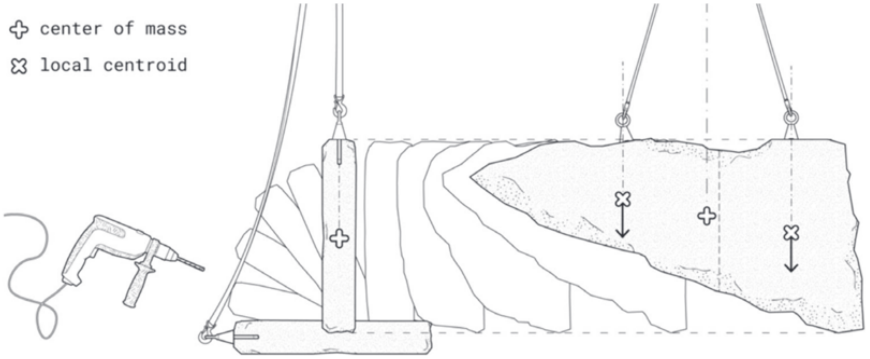

Figure 15 Orientation and Lifting of the Rubble (Grangeot et al, 2024)

Figure 16 (a) Final Demonstrator, (b) Rubble Lifting (Grangeot et al., 2024)

An Investigation into Machine Learning Matchmaking for Reused Rubble Concrete Masonry Units (RR-CMU) (Marshall & Grangeot, 2024)

Process overview:

I. source rubble from the recycling centre
II. lift rubble on wooden slats
III. 3d scan rubble
IV. transfer images to mesh
V. machine learning algorithm matches rubble edges
VI. physical comparison to the result of the algorithm

To produce 'Reused Rubble Concrete Masonry Units (RR-CMU)', Marshall & Grangeot (2024) developed a framework to match two concrete rubble elements to integrate them into modular load-bearing concrete panels. The gaps would be filled with new concrete around the concrete demolition waste. Their project focuses on the matching process and they have not yet produced a prototype of a RR-CMU. Concrete elements were 3d scanned from all sides except from the bottom and a digital mesh was created for each. Their machine learning algorithm analysed the short edges of each rubble piece to find a second element with the least amount of gaps. Physical tests carried out after the simulations showed that the tolerance was only between 10-20mm deviation. This was also due to damage during the handling of the element. Their focus was to maximise the volume of concrete waste per panel to minimise new cement use. Furthermore, Marshall & Grangeot carried out an LCA study, comparing a traditional concrete panel to RR-CMUs (See Table 8 and Table 10)

Table 1. Reused Rubble CMU – 30m² of wall

	A1 - Raw Materials for Façade Contractor					A2 - Transport of Raw Materials			A1 + A2
MATERIAL	Volume (m3)	Density (kg/m3)	Weight (kg)	Emissions factor ($kgCO_2eq/kg$)	A1-A3 GWP ($kgCO_2eq$)	Distance to Site (km)	Truck ($kgCO_{2eq}$ /ton km)	A2 -Transit ($kgCO_2eq$)	A1-A2 GWP ($kgCO_2eq$)
Concrete (Reclaimed)	1.7	2300	3910	0	0	100	0.07	27.4	27.4
New Concrete	0.15	2300	356	0.1	36.6	300	0.07	7.47	44.1
Grout Infill	0.24	2300	557	0.1	57.3	300	0.07	11.69	69.0
									140.4

Table 10 LCA of RR-CMU (Marshall & Grangeot, 2024)

Table 2. Concrete Wall – 30m² of wall

	A1 - Raw Materials for Façade Contractor					A2 - Transport of Raw Materials			A1 + A2
MATERIAL	Volume (m3)	Density (kg/m3)	Weight (kg)	Emissions factor ($kgCO_2eq/kg$)	A1-A3 GWP ($kgCO_2eq$)	Distance to Site (km)	Truck ($kgCO_{2eq}$ /ton km)	A2 -Transit ($kgCO_2eq$)	A1-A2 GWP ($kgCO_2eq$)
15cm thick Concrete	4.28	2300	9833	0.1	1,012	300	0.07	206.5	1,219
OSB Formwork	0.6	650	390	0.1	39	300	0.07	8.2	47.2
Steel Rebar	0.04	7750	299	2.3	688	300	0.07	6.3	694.6
									1,961

Table 9 LCA of a regular concrete wall

Based on the assumption that the reclaimed concrete has 0% emissions, the RR-CMUs produce only 15% kgC02eq of an equivalent concrete wall. The authors argue that the process should happen inside a factory for economies of scale and that it has the potential to create a competitive building product for compression-only walls or vaults. It was beyond the scope of the study to consider the 'stability of the unit and capacity to resist force' (Marshall & Grangeot, 2024). The tests carried out for Cyclopean Spolia in this paper aim to contribute to this.

This research disclosed several challenges for concrete rubble reclamation. Damage during handling occurs easily, due to the brittle nature of the concrete and the high weight. If the scanning occurs before transport, care needs to be taken to prevent falsification of the assumed shape. The authors therefore recommend to include a 20mm tolerance in the 3D model. They mention that the entire process took a lot of time, including the assembly of timber slats for scanning, the digital process of building the mesh, running the algorithm, assigning and tracking the rubble and the transport of the rubble. They recommend a specialised production line for rubble with handling equipment. They also argue that even though some of the rubble might have reinforcement, the analysis of its remaining performance against tensile forces is too complex. Therefore, they recommend their use for compression-only structures.

Their paper touches on a more industrialized approach to the reclamation of concrete rubble. If future structural tests show that minimising the distance between waste elements is recommended, their algorithm can largely decrease the amount of cement needed to create a new panel.

Cyclopean Cannibalism (Clifford & McGee, 2018)

Process overview:

I. design wall geometry
II. source a selection of demolition debris as raw material
III. turn each stone on a chosen backside
IV. 3d scan 5 sides of rubble (ignoring the back side)
V. create a point cloud geometry
VI. find the largest polygon possible per stone with a recursive algorithm
VII. stock database with those polygons
VIII. the algorithm sets a stone into the wall and orients the polygon around its depth axis to find the best fit
IX. the algorithm ensures that the stone can be set from above and that all stones overlap each other without any gap
X. iteratively run stability checks for the entire assembly
XI. carve units with a six-axis robotic arm, so that side faces become planar
XII. trace the global surface geometry curve on the stone for fitting
XIII. chip off excess material on the form to maintain global surface geometry
XIV. stack stones in assembly order

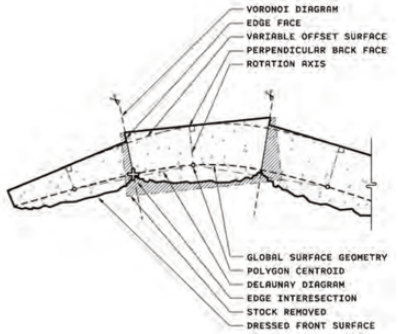

Figure 18 Geometric Operations of the Virtual Process (Clifford and McGee, 2018)

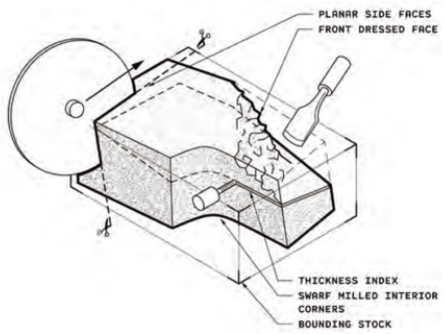

Figure 18 Carving Process (Clifford and McGee, 2018)

Clifford and McGee bridge the ancient art of stone fitting with contemporary computational design and fabrication tools. Their term 'Cyclopean Cannibalism' is based on the notion that architecture should consume itself after its end of life, thus cannibalise. They see the ancient craft of 'Cyclopean Masonry' as a key to the contemporary reconsumption of architectural material. In his Theogony, the ancient Greek poet Hesiod described stone structures, which are made up of stones so large, that only Cyclops from the race of giants could have moved them. Their 2017 'The Cannibal's Cookbook' lays out the numerous ways of large stone masonry, which has been discussed in the previous section.

Based on their findings, they developed a process to use contemporary tools and large-scale building rubble to build a 2017 version of a cyclopean masonry wall.

For their prototype, they chose the Ashlar wall type from the Inkas, which showed only rough coursing and creates polygonal shapes of the stones. In this ancient technique, large stones are carefully chosen and

Figure 19 The Finished Wall (Clifford & McGee, 2018)

carved to match one another. Depending on the amount of carving, the placement of the stones created unique gaps, which had to be filled by the next element. The masons therefore selected the stone which most closely fit the gaps and then carved off any excess material with a so-called hammerstone. This technique allowed a close fit of the large boulders and created a nearly surreal pattern in regard to its size. The correct choice of stone was crucial to minimize the carving needed and this is where Clifford and McGee saw the potential of computational tools. They translated this system into a contemporary workflow, which enables large construction demolition waste elements to be used as new material. Clifford and McGee did not limit themselves to concrete only but also included limestones or other solid materials from building demolitions. The main difference between the ancient and the contemporary method is the ability of Clifford and McGee to plan the entire wall in a top-down approach. This enabled them to design a prototype with an undulating shape, which would have been difficult to achieve with the ancient bottom-up approach.

- [The] act of reconsuming becomes a character trait in the resultant architectures' (Clifford and McGee, 2018) -

Clifford and McGee built their wall as follows:
First, they digitally design the wall geometry, setting its overall form, curvature and dimensions (6600mm x 2300mm with a thickness range between 100mm - 312mm). The raw material is then sourced from a local waste treatment facility. It contains a variety of demolition debris with fragments of concrete and natural stones. The chosen rubble units are then oriented so that one side becomes the backside and the other surfaces can be modified. All sides, except for the backside are 3D scanned and the geometry is transferred into a point cloud, which captures the contours and irregularities of each piece. An algorithm then finds the largest polygon possible within the contour of the stone. These polygons are then transferred into a database. To integrate the polygons within the designed wall geometry, the team uses a recursive algorithm which virtually assesses the stone. It positions each stone by aligning the element around its depth axis, finding its optimum orientation. At the same time, it ensures that each stone can be placed from above into the wall, while a constant overlap is maintained. As the stones will be carved to ensure a snug fit, no gaps are allowed. To

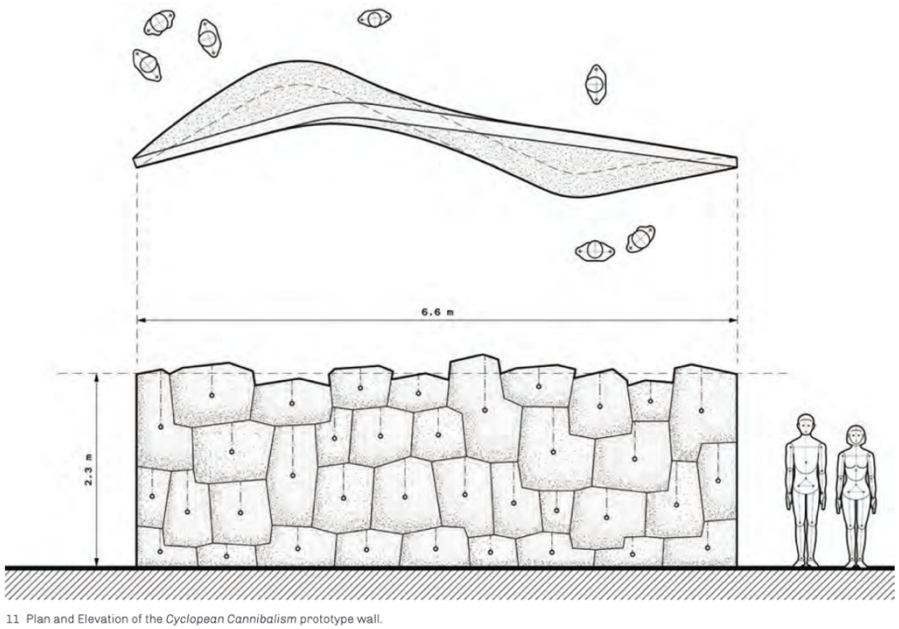

11 Plan and Elevation of the *Cyclopean Cannibalism* prototype wall.

Figure 20 Plan and Elevation of the Wall (Clifford & McGee, 2018)

ensure the structural integrity of the wall, stability checks are run iteratively for the entire assembly. After the virtual workflow, the stones get carved with a six-axis robotic arm. The side faces are cut straight to match the algorithm's defined form within the rubble. In parallel, a curve representing the wall's global surface curve is carved into the stone for fitting and to preserve the wall's intended undulating shape. Lastly, the stones are stacked precisely on top of each other, in the sequence defined by the algorithm. This top-down approach enables a new shape, an efficient use of the chosen stones and a prefabrication process.

'cyclopean masonry as a living system that ingests urban debris to generate new, flexible building systems' (Clifford and McGee, 2018)

Clifford and McGee's algorithm differs from regular packing algorithms. The usual aim is to reduce the gap between the elements, whereas here the gaps have to be completely filled by material. The elements are therefore allowed to overlap, as the excess stone will be carved away. This approach is interesting in regard to reclaiming waste elements. As the raw material is currently not conceived as 'precious' and is economically cheap, the loss of the excess stone becomes secondary. The final prototype used 73% of the initially scanned rubble. Clifford and McGee are the only academic research to date on construction rubble, which realized a full-scale prototype without the use of newly sourced material. Their wall consists of 100% of structural elements which would otherwise have been discarded.

Mosaic Walls (Hany et al., 2024)

Process overview:

I. rubble production from AAC blocks
II. numbering the rubble
III. scanning with OpenCV
IV. creation of a bespoke tessellation pattern
V. stacking algorithm for large stones
VI. nesting algorithm for small stones as infill
VII. robotic placement of the large stones
VIII. manual placement of the small stones and the mortar

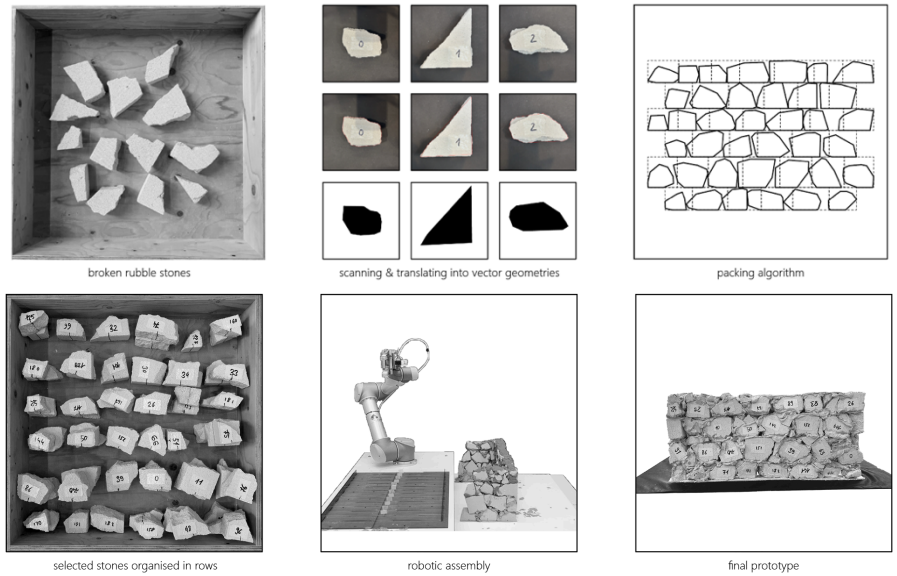

Figure 21 Mosaic Walls Process (Hany et al., 2024)

The Mosaic Walls project developed a workflow for the digital planning of concrete rubble elements on a 1:5 scale. It aimed at a freestanding assembly without formwork. To achieve this, the rubble stones were interlocked to connect buttresses to the main wall. After the production of rubble from 5cm thick AAC blocks, the stones were photographed, and the outline was detected with OpenCV (Culjak et al., 2012). The detected points were converted into Rhino line objects and added to a database. The algorithm is based on tessellation patterns with randomized widths and heights within a predetermined range, which the designer can define. It levels each row out and creates strict horizontal lines which structure the assembly. The stones first get sorted and the algorithm searches for the stone which resembles the cell area and aspect ratio the closest. After that, the next cell gets adapted based on the previously placed rubble element. Due to the size of the cells, the algorithm favours the top 50% of stone diameters. This leaves large gaps between the stones which get filled with the smaller half of the rubble. Here, the 2D nesting algorithm OpenNest (*OpenNest - Parametric House*, 2020) is used. The gaps which remain get filled with mortar during the assembly process. Due to the 2D approach, a pre-sorting of the database and the case-by-case search query, the algorithm is comparatively low in complexity and therefore resource efficient. Its main disadvantage is the reliance on large rubble databases though. Due to the predetermined size of the cell, the structural overlap of the stones only works if it can pick from a large variety of stone geometries. The Mosaic Walls project showed that roughly three times the amount of stones is needed in the database to find enough geometries for a structurally reliable wall.

The assembly was realized with a UR5 robot, which placed the large stones. The small stones and the mortar were placed manually. The comparison of preliminary handpicked arrangements with the final assembly showed that the algorithm successfully enabled a structural system.

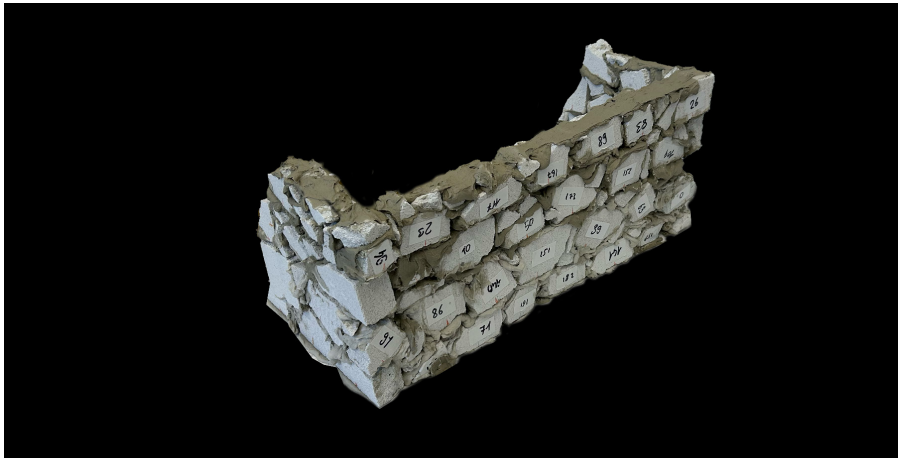

Figure 22 Robotically Assembled Prototype

Missing Pieces, Ensamble Studio, 2023

Process overview:

I. placement of a plastic sheet on the floor as formwork
II. placement of a rebar net and pouring of concrete over it
III. demolition of the concrete element
IV. horizontal test reassembly of the rubble
V. vertical assembly of the entire wall
VI. disassembly
VII. shipment to Cape Cod
VIII. reassembly

Figure 23 Missing Pieces assembled in Cape Cod (https://www.ensamble.info/missingpieces)

Figure 24 Process (https://www.ensamble.info/missingpieces)

In 2023, Ensamble Studio realized the art sculpture 'Missing Pieces' in Cape Cod, Massachusetts. The installation takes inspiration from the Japanese art of 'Kintsugi' (*kin* (gold), *tsugi* (joint)). This traditional craft uses golden glue to reassemble broken ceramic and give new value to an otherwise lost piece of art. The joint becomes the new defining element (Keulemans, 2016). To build this sculpture, the team at Ensamble Studio first studied a small-scale prototype (Fig 26). Then, they produced a horizontal formwork out of a large plastic sheet, to create a desired uneven surface of the concrete. They filled the formwork with concrete and a rebar net and let it dry. Then they proceeded to demolish the newly created wall to create randomly sized rubble elements. To reconnect these elements and build the sculpture, they were lifted vertically with a small crane and connected via steel rods, which were drilled into the borders of the rubble. The finished wall was then shipped in pieces from Spain to Cape Cod in the USA (Ensamble Studio, 2023). This project is different to approaches which reuse existing building demolition waste, due to the source of the debris. Ensamble Studio builds a wall with the sole benefit of using the broken elements. It is difficult to know from the sources if they reassemble the elements back to the same positions they were in before. This would be in line with the Kintsugi craft, which keeps the original placement of the broken elements. Their workflow does not seem to include digital tools and is highly manual, only including a demolition excavator, a small crane and regular tools.

'Missing Pieces' explores the aesthetic of broken concrete and celebrates the joints as something precious. Their assembly and aesthetic can therefore serve as a reference for creating a functional prefabricated wall, where the gaps they create are filled with mortar.

Figure 25 Small Scale Model (https://www.ensamble.info/missingpieces)

Urbanite

Urbanite is a method of using concrete demolition elements for landscaping projects. There is currently no academic research on this subject, but several online sources explain do-it-yourself methods on how to source, place and work with concrete rubble for landscaping. The results range from walkways, flower beds, patios, fire pits or even retaining walls (Tate, n.d.). The articles have in common that they use knowledge from natural stone construction and transfer it to working with concrete rubble. Advantages are the low cost of the raw materials and often an easy access through local waste sites. Most articles also mention the environmental benefit of the reclamation of the waste elements. The use cases found in landscape design are wide. Examples of pathways, patios, stepping stones, garden walls and even retaining walls can be found (Figure 26). The projects show the raw use of the concrete rubble elements, but examples of the preparation of stones into the desired form through cutting and material removal are also available (Figure 27).

Figure 26 Retaining Wall (https://www.youtube.com/watch?v=aM4FWhb75mE)

Figure 27 Garden Wall (https://www.taproot.us/building-stone-walls-with-urbanite/)

Figure 28 Pavement (https://anoregoncottage.com/broken-concrete-patio/)

Further Methods

To name some further methods, CCDW is also used for gabion retaining walls (Collaud et al., 2023; Paschoalin Filho et al., 2020), as an infill for concrete blocks to engrave the memory of buildings (v studio, 2017) or as a computational concept for the transformation of construction waste into new forms (Certain Measures, 2015). The methods presented in the previous section were chosen due to their potential for scalability, the raw use of rubble and a focus on structural use cases.

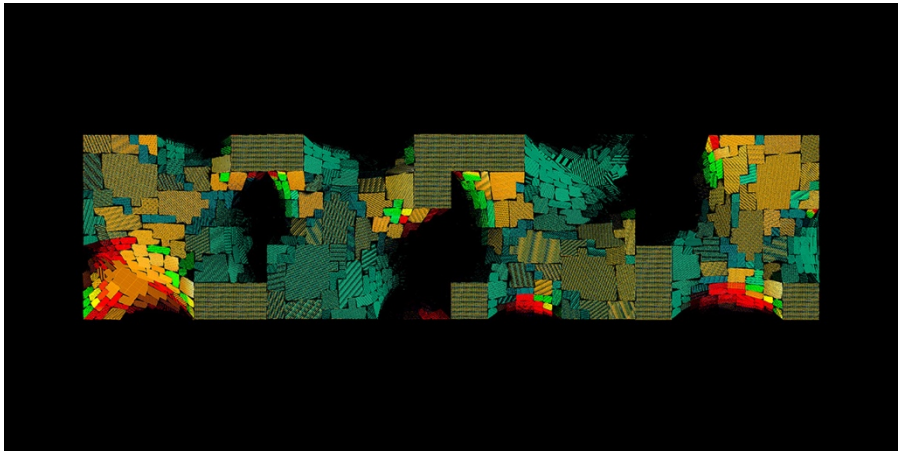

Table 29 Mine The Scrap (Certain Measures, 2015

2.1.4. Key Takeaways

The previously described projects show the diversity of approaches to the reclamation of concrete rubble into structural elements. This section explains key takeaways from these tested methods, which are implemented for Cyclopean Spolia.

Structural Performance

Due to the variety of concrete strengths in rubble elements, the structural performance of reclaimed building components is difficult to measure. The use of a weaker mortar, as shown by Oreb et al. (2024) ensures a controlled failure within the structure. The cracks appear inside the binder or the ITZ and not in the CCDW. This enables predictability, which is key to the introduction of rubble components into the market. Furthermore, they showed that walls with a higher filler/rubble ratio display higher tensile strength. They explain it with the increased homogeneity, which resulted from the reduced presence of large voids and an improved interlocking between rubble and binder. This presents an opportunity for prefabricated CS Walls to increase homogeneity through the filler/rubble strength ratio and the arrangement of the CCDW.

- The use of a weaker mortar, as shown by Oreb et al. (2024) ensures a controlled failure within the structure. -

Both studies which conducted structural tests (Grangeot, Bastien-Masse, Parascho, et al., 2024; Oreb et al., 2024) found that their respective method showed enough compressive strength to be used as load-bearing walls, according to Swiss building codes.

- According to Swiss building codes, the prototype wall could therefore be introduced for a three-story residential building. -

The wall built by Grangeot, Bastien-Masse, et al. (2024) was tested to the maximum capacity of the setup and showed a lower compressive strength boundary of 2MPa. The crack behaviour obtained by DIC and LVDT confirmed the behaviour of the slender wall as similar to stone masonry structures or cracked unreinforced concrete walls. Based on this, the resistance of the prototype is conservatively expected at 3 to 8 MPa. According to Swiss building codes, the prototype wall could therefore be introduced for a three-story residential building. The prototypes from Oreb et al. (2024) showed a structural performance of 5.1 MPa to 9.6 MPa, which surpassed the compressive strength of traditional stone masonry and showed a similar performance to brick masonry. These insights prove the potential which lies in structural reclamation processes for concrete rubble.

Digital and Computational Tools

Four different algorithms were identified in the Atlas. Clifford & McGee (2018) required a three-dimensional algorithm which overlayed the stones without the creation of gaps. It also defined the cutting pattern to prepare the stone for assembly. Another 3D algorithm is the one developed by Marshall & Grangeot (2024). Their machine-learning approach matches concrete rubble edges and minimises gaps between

them. However, these previously mentioned approaches do not target a workflow with gaps between the rubble elements.

Thus, the 2d open-source stacking algorithm developed by Wang et al. (2024) which is used by both projects at EPFL (Grangeot, Bastien-Masse, Parascho, et al., 2024; Oreb et al., 2024) is an accessible code, which is promising for CS Walls. Its pixel-based method is computationally efficient and compares multiple arrangements. Furthermore, it involves advanced structural analysis, which is discussed in 2.3.2 Stacking Algorithms. Similar to the algorithm by Wang et al. (2024), the Mosaic Walls (Hany et al., 2024) approach is also based on 2D scans and combines stacking and nesting approaches.

Nonetheless, another approach should be considered. A horizontal laying of concrete rubble, together with a filler material that generates homogeneity in the wall, could enable the use of a simple 2D nesting algorithm. No project has tested this approach to date, but it could facilitate the choice of rubble and extend the designer's freedom due to the lack of structural restrictions within the algorithm. This approach is discussed in 2.3.1 Nesting Algorithms.

Construction Methods

The reference projects showed a variety of methods employed to reclaim concrete rubble. The academic papers from EPFL both used formwork to realise the structure. Grangeot, Wang, et al. (2024) stacked the elements vertically with a hoisting machine and manually poured the mortar. They found that an automation process for the mortar would significantly lower the construction time, as the manual process consumed 70% of the time. Oreb et al. (2024) also used a formwork, but stacked smaller rubble horizontally on top of each other. This required manual labour. Only the Mosaic Walls project realised an assembly without formwork. This required the introduction of buttresses into the wall, though, and relied on the immediate adhesion of the mortar, which would be difficult to realise in a full-scale prototype. The vertical dry stacking without formwork from Ensamble Studio (2023) is disregarded here, as the assembly was not prepared to bear loads.

These examples show that vertical stacking is difficult to achieve without formwork and manual labour. This supports the horizontal process investigated for Cyclopean Spolia Walls, which enables an automated introduction of the filler with conventional methods and removes structural requirements during the assembly stage.

It has to be noted that all projects disregard long rebars which protrude out of the CCDW. There are no accessible large-scale rubble scans, which give insight into typical shapes from CCDW. Nevertheless, it can be assumed that the rebar from tensile building components (eg. floor slabs), could cause problems for vertical stacking if the rubble is not further processed.

Stories of Rubble

The projects show the variety of architectural expressions and stories which concrete rubble carries. The sculpture by Ensamble Studio (2023) shows the Zeitgeist for materials which represent an aesthetic of the memory embedded in reclaimed materials. Even though they produced the rubble themselves, the plastic sheet formwork gave the concrete a texture which imitated a natural surface with a history. The embedding of rubble, which conveys a former function, like the apparent column

sections or beams in Grangeot, Wang, et al.'s work (2024), similarly places a notion of the past into the structures. This culminates in the book Cyclopean Cannibalism (Brandon Clifford, 2021), where ancient methods are described and brought to the modern age with Cyclops as the storyteller of the past. The prior project by Clifford & McGee (2018) presented the bridge between digital tools and ancient crafts to create surreal connections between different types of stones and rubble.
Overall, the examples show that concrete rubble components have the potential for a successful implementation as a tool for architectural expression and storytelling, which is key for their longevity and the adoption of the technique.

Conclusion

The Atlas showed an overview of seven concrete rubble projects, which show the variety of existing approaches. Even though the field of research is still scarce, the existing papers show a promising development and a potential for the scalability of concrete rubble structures. LCA studies suggest that embedded rubble elements can decrease the carbon footprint by up to 90% compared to standard concrete elements (Marshall & Grangeot, 2024). Several studies see automation as the key to the scalability of rubble walls. The process in this Master Thesis caters to this and shows a possible path to the prefabrication of structural concrete rubble walls.

2.2. Rubble Handling

2.2.1. Methods of Lifting

Parallel concrete rubble used for Cyclopean Spolia has a diameter between 25cm to 150cm and a thickness between 20cm to 30cm. This results in weights of around 15kg to 400kg with a typical concrete density of 2400 kg/m3 (Ansys, n.d.). The Health Council of the Netherlands recommend weights above 23kg to be lifted with the help of machines (Gezondheitsraad, 2012). The machines used to lift the rubble have to be carefully chosen, as damage can occur to the edges, which compromises the scanning results (Marshall & Grangeot, 2024). To prevent this, proper handling is key to the accuracy of the process.

Figure 30 Concrete Gripper For Landscape Works
(https://bbfscaffoldingtowers.co.uk/products/probst-concrete-step-handles-tsz-uni-53100338)

For vertical processes, Grangeot et al. (2024) developed a method, where anchors are robotically drilled into the edges of parallel sided rubble fragments. The holes are placed with regard to the stone's centre of gravity to determine the placement angle. An overhead crane then lifts the stones and positions them within the formwork. Figure 31 demonstrates this process. A horizontal prefabrication process can rely on more common concrete lifting methods, like block grabbers used in landscaping for example (see Figure 30). Smaller fragments up to 250kg could even be lifted with vacuum grippers (Movomech, n.d.), to ensure that the edges stay intact and to enable tighter cavities.

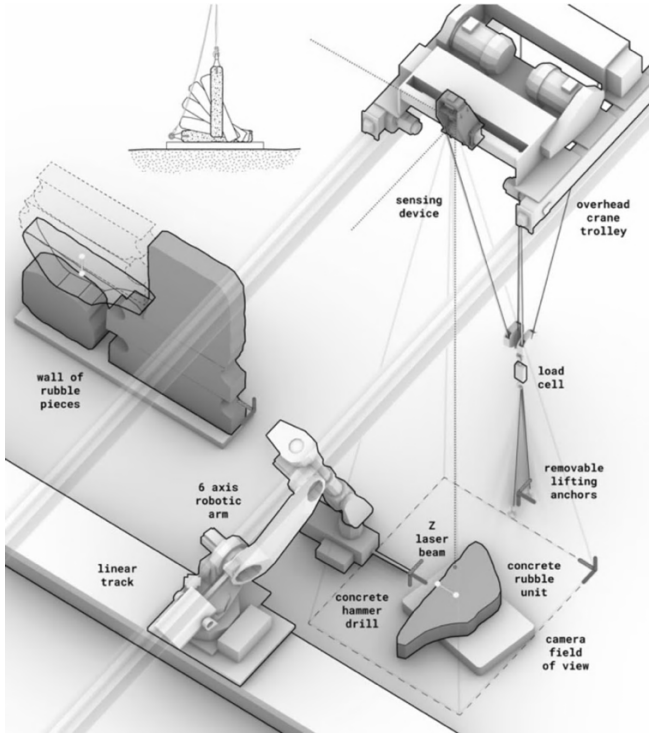

Figure 31 Lifting And Placement Process For Vertical Stacking (Grangeot et a., 2024)

2.2.2. Methods of Scanning

To enable digital processing for the arrangement and placement of concrete rubble, a digital twin has to be generated. Hence, the stones are scanned and transferred into a dataset.

- To facilitate scalability, the scanning process for CS walls should be as accessible as possible -

Current research on irregular stone scanning can be categorised into methods based on 3D scanning, like Johns et al. (2023), Clifford & McGee (2018) and Marshall & Grangeot (2024) and methods which rely solely on 2D scans, like Grangeot et al. (2024) or Hany et al. (2024). The aforementioned studies used 3D scanning either due to the irregularity of the geometries they worked with or because they wanted to accurately match the edges of rubble. Johns et al. (2023) chose for a LiDAR scanner together with photogrammetry, to create an accurate 3D representation of the stones and the surrounding site. This method enables every possible shape of the stone to be processed but requires a high computational power with several minutes of calculation time per element placed. If the focus is on parallel-sided rubble and an accurate representation of the edge geometry is secondary, outlines from a 2D scan can suffice (Grangeot, Wang, Beyer, et al., 2024b). To facilitate scalability, the scanning process for CS walls should be as accessible as possible. Thus, the 2D method is a promising alternative to complex 3D scans, because it also lowers the amount of data captured and simplifies the computational arrangement processes.
The most accessible option is to use a monochrome surface and a regular phone camera, as shown in the Mosaic Walls project (Hany et

al., 2024). Due to the thickness of the stone, its top surface does not align with the bottom surface, which leads to a distortion of the scan, where the stone appears larger than in reality. This distortion can be compensated when the distance of the camera and the height of the stone is captured (see Figure 33 below).

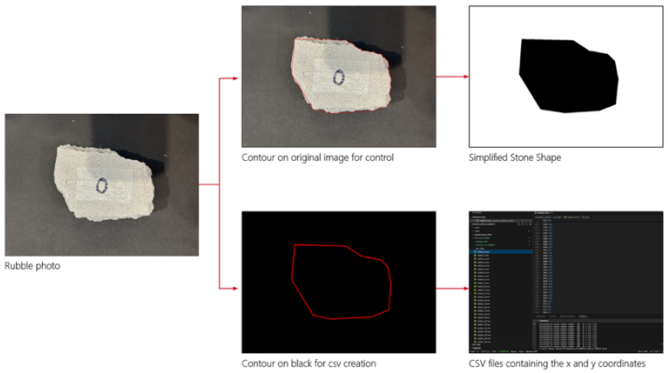

Figure 32 2D Scanning Process with Photos and OpenCV

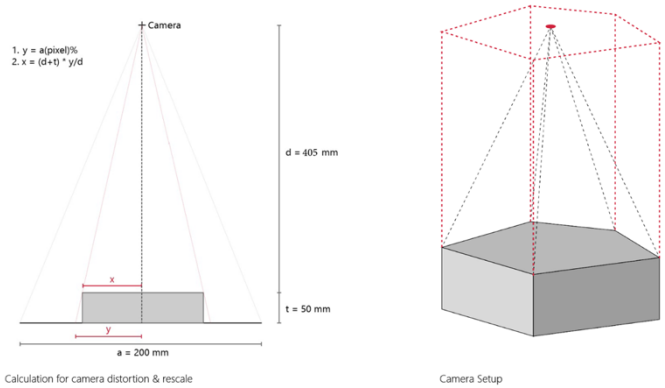

Figure 33 Camera Setup and Distortion Calculation (Hany et al., 2024)

The images can then be processed with the Python plugin OpenCV (Culjak et al., 2012), which returns the contour line of the stone. This data can be used for pixel-based algorithms, like the one developed by Wang et al. (2024) or transferred into vector-based programs to work with plugins like OpenNest (*OpenNest - Parametric House*, 2020), DeepNest (Deepnest, 2025), or the algorithm developed in Mosaic Walls (Hany et al., 2024).

However, this approach is highly dependent on a controlled environment. To prevent inaccuracies during the assembly process, Marshall & Grangeot (2024) thus recommend a 20mm tolerance for the scan of real-size rubble. This translates to a 2mm offset for the 1:10 scale used in the CS project. To improve accuracy, Grangeot et al. (2024) recommend image segmentation approaches like Segment Anything (Kirillov et al., 2023), which are less sensitive to lighting conditions. A preliminary test, done by the author can be seen in Figure 34.

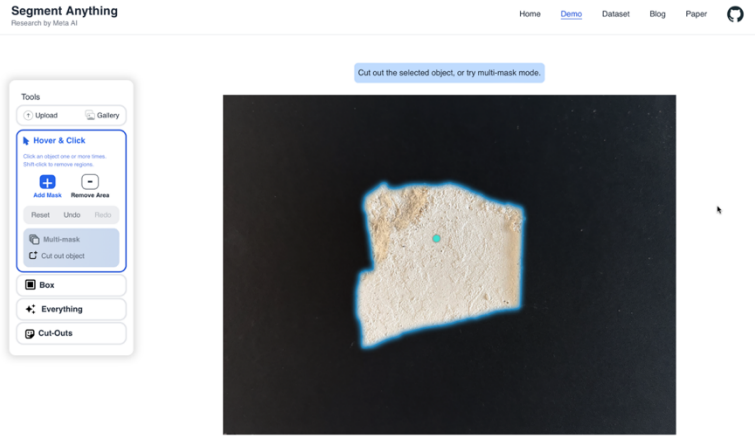

Figure 34 Segment Anything Test With Rubble

2.3. CCDW Algorithms

Packing algorithms are the main method found in literature to digitally arrange concrete fragments into rubble walls. These tools are widely adopted in industries where material utilisation is crucial. This can range from 2D packing algorithms for material cutouts in the automobile, clothing or aviation industry (Guo et al., 2022) to 3D bin packing algorithms in the logistics industry. The algorithms are divided into regular and irregular problems, which are determined by the variability of the shapes needed to fit into the given outline (see Figure 35 and Table 11).

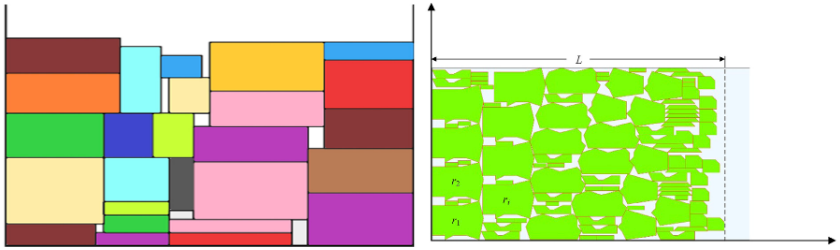

Figure 35 Regular- (Left) and Irregular 2D Packing Problems (Guo et al., 2022)

Classification			Applications	Example	Quality evaluation index
Cutting or Packing Problems	1D-Packing		Mechanical manufacturing, Building industryetc.	Bar material, wire stock and section steel cutting	Material utilization or scrap rate
	2D-Packing	Regular Packing	Paper industry, Glass industry, Printing Industry, Microelectronics industry, Building industryetc.	Paper, glass, and stone cutting; Microelectronic unit arrangement; Sheet metal blanking	Filling rate or fill height
		Irregular Packing	Mechanical manufacturing, Shipbuilding industry, Aviation, Automotive industry, Clothing industry, Leather processing, Furniture manufacturing, Building industryetc.	CNC machining; Sheet, wood, slate, cloth, and leather cutting	Filling rate or packing height value
	3D-Packing	Regular Packing	Transportation industry, Logistics industryetc.	Express shipment; Ship cabin layout	Filling density
		Irregular Packing	3D-printing, Aviationetc.	3D printing space layout; Spacecraft cabin layout	Filling density

Table 11 Classification Of Packing Problems And Their Applications (Guo et al., 2022)

Whether in 2D or 3D, the packing problem for concrete rubble fragments falls into the irregular problem category, due to their unique shapes. Packing algorithms do not necessarily take the structural performance of the packed shapes into account, though. To achieve this, some algorithms have been adopted to verify the stability of the arrangement during assembly. These methods are referred to as stacking algorithms in this thesis. All 2D irregular packing algorithms which do not fulfil structural requirements are referred to as nesting algorithms.

Due to the horizontal fabrication of the Cyclopean Spolia Walls, structural stability is not as crucial during the production process as it is for vertical productions. Therefore, nesting algorithms can be considered. These could reduce the computational power, enable the placement of any shape and in return reduce the database size. Therefore, the first phase of the structural experiments compares two-dimensional nesting algorithms with two-dimensional stacking algorithms. Thus, the following two sections discuss 2D nesting and stacking algorithms to explain the logic behind the algorithms used in this thesis.

– Due to the horizontal fabrication of the Cyclopean Spolia Walls, structural stability is not as crucial during the production process as it is for vertical productions. –

2.3.1. Nesting Algorithms

2D nesting algorithms are also known as plate algorithms, due to their deployment in steel plate-cutting processes (Steel Projects, n.d.). They aim to minimise gaps in arrangements of two-dimensional shapes

within a confined outline, but their performance and accessibility varies greatly. This thesis solely relies on open-source software, which can range from plugins for Grasshopper in Rhino3D, like OpenNest (*OpenNest - Parametric House*, 2020) or the open-source program DeepNest (Deepnest, 2025). The latter was chosen for the main experiments because it offered the widest settings and achieved more densely packed arrangements than OpenNest. Its underlying principle is explained below.

DeepNest

The DeepNest algorithm solves irregular 2D packing problems based on the open-source SVGNest tool. It is based on the orbital approach by Burke et al. (2007). The main concept is the No-Fit Polygon (NFP) method, whose aim is to arrange shapes inside an outline without overlaps. The NFP describes all possible placements of a revolving shape B around a fixed shape A, touching it at all times, but not intersecting. This is achieved with the 'orbital sliding method' (Burke et al., 2007), where B is “slid” along A’s edges (see Figure 36). The shape of the NFP is formed with a reference point on B, which is traced during the process. Once the NFPs are calculated for all shape pairs, DeepNest uses them to determine where a new part can be placed (see Figure 36). This is done in zones along the NFP where no overlap occurs.

As in SVGNest, DeepNest places larger shapes before smaller ones. This increases the chance of efficiently using the space, because small parts can fill gaps that large parts leave behind.

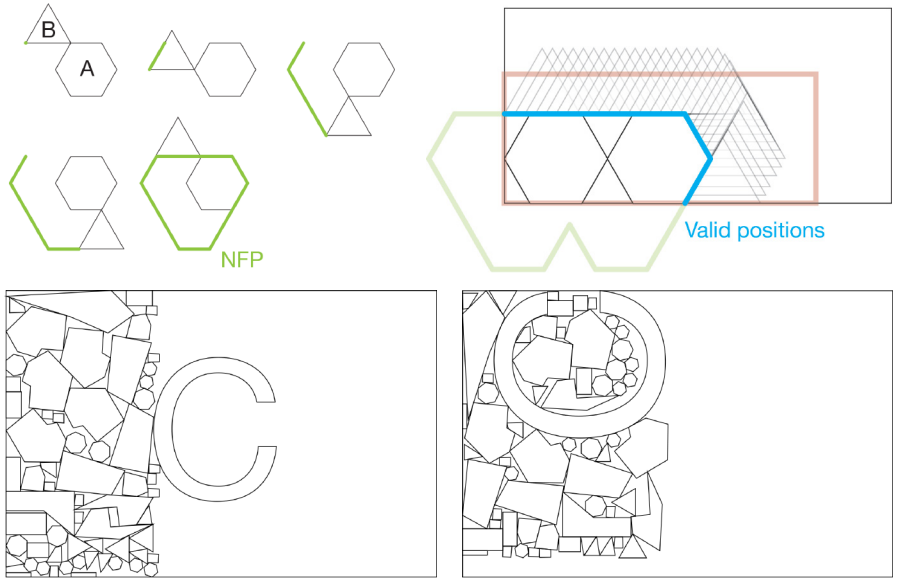

Figure 36 No-Fit Polygon (Top Left) Valid Positions For Shapes in DeepNest (Top Right), Shape Placement Order (Botton) (https://github.com/Jack000/SVGnest?tab=readme-ov-file)

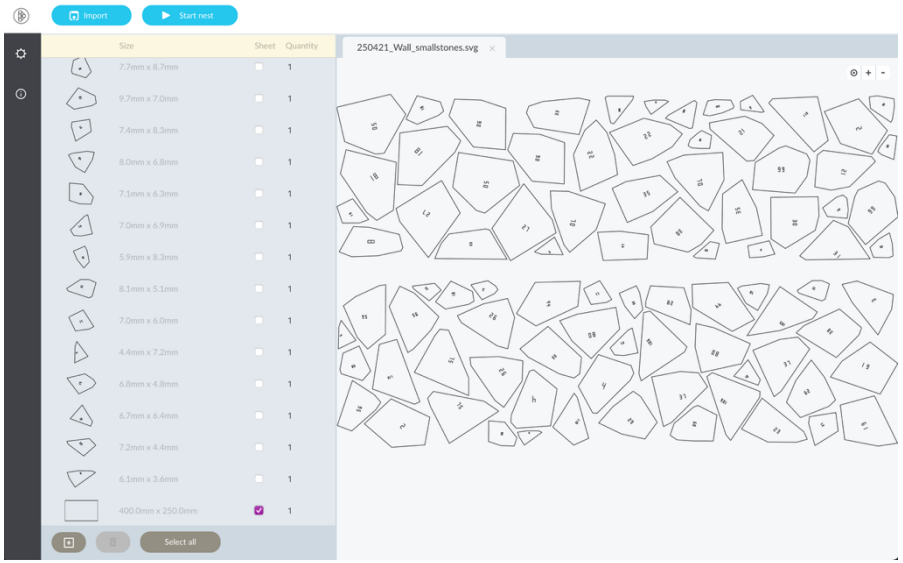

Table 12 Screenshot From DeepNest With Rubble Shapes And Wall Size

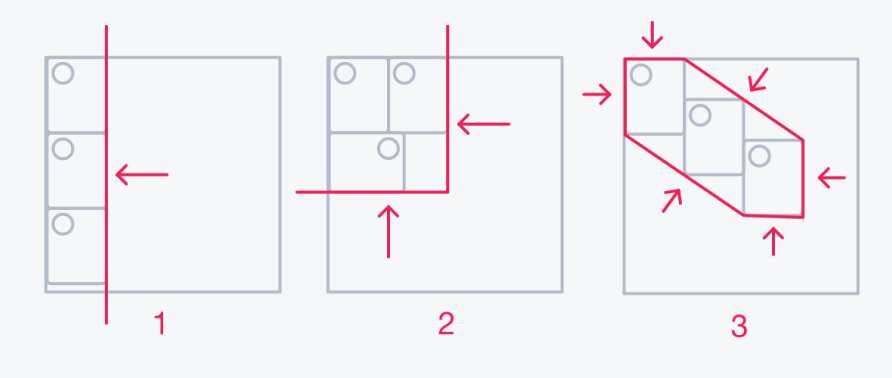

Table 13 Nesting Optimization Types (1: Gravity, 2: Bounding Box, 3: Squeeze) (DeepNest, 2025)

DeepNest offers three types of optimizations; Gravity, Bounding Box and Squeeze (DeepNest, 2025). Gravity aims to reduce the overall width of the nested layout towards the right, which preserves leftover material from rectangular sheets. Bounding Box minimizes the dimensions of the overall bounding box. This is ideal if only a part of the sheet is used and the goal is to use as much material as possible inside a rectangular shape, based on the top left corner. The Squeeze optimization reduces the total area occupied by the parts, regardless of the overall shape of the assembly. It is more suited to irregularly shapes sheets or when the goal is to fully utilize the entire sheet (DeepNest, 2025). This optimization has thus been chosen for the experiments, because it places the shapes evenly across the wall geometry. Additionally, it opens the possibilities for any type of inclusions in the future, like windows or doors.

2.3.2. Stacking Algorithms

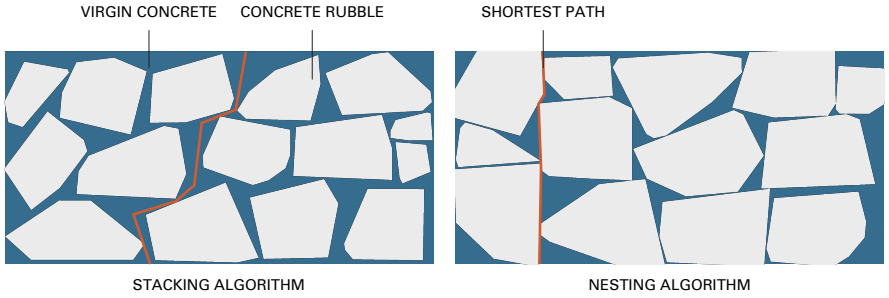

Figure 37 Shortest Path Through Mortar, Stacking vs. Nesting

The shortest vertical path through the mortar of a stone wall (vertical alignment) represents a potential failure point and is drawn in orange above (Almeida et al., 2021). Figure 37 therefore shows one of the main differences between stacking algorithms for dry stacked stone arrangement in comparison to nesting algorithms. A nesting algorithm can potentially produce an arrangement where the stones do not interlock at all and the shortest path's length is not much longer than the wall height. Stacking algorithms, amongst other variables, focus on interlocking the stones, to eliminate this issue. In addition to the guarantee of a stable final assembly, they also have to take the stability of the arrangement during the construction process into account.

Such an approach was used by Johns et al. (2023). for example. They stacked irregular stones and debris with live 3D scans into stable dry stacked structures (see Figure 38). These three-dimensional stacking algorithms are computationally intensive however. Due to the complexity of the shapes, they can take several minutes of calculation per element and require high-end tools (Johns et al., 2020)

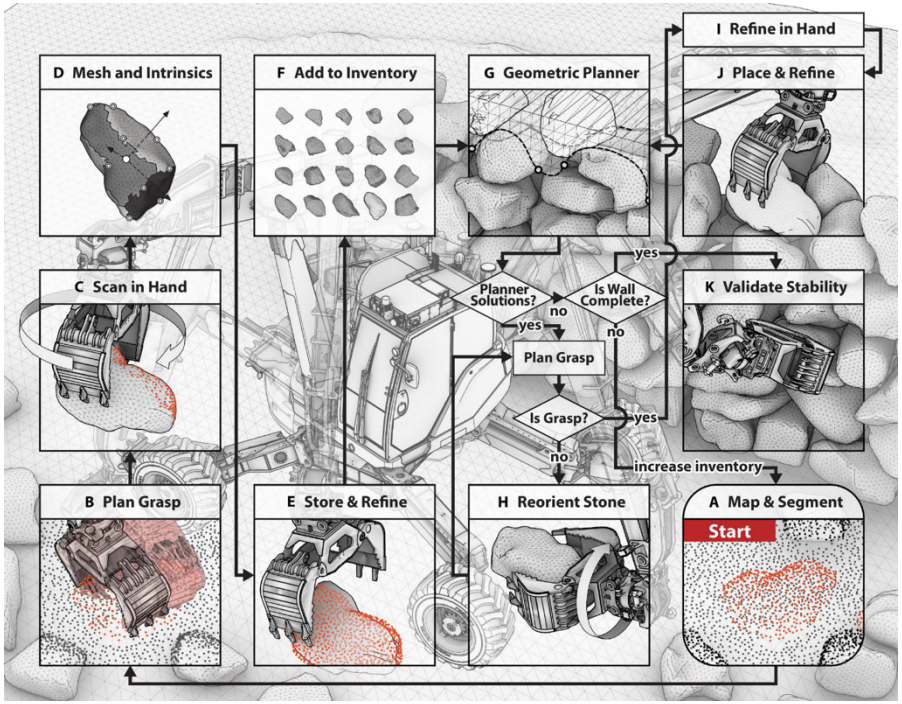

Figure 38 Autonomous Dry Stone 3D Scanning And Placement Process (Johns et al., 2023)

The Cyclopean Spolia project therefore focuses on two-dimensional approaches, to simplify the process. A 2D stacking algorithm with a focus on concrete rubble shapes was developed during the CORE course at TU Delft (Hany et al., 2024). It uses a predetermined tessellation to place the stones, which enables design choices to be made about the height of the rows and the size of the rubble stones. The algorithm combines a 2D stacking and a 2D nesting approach. Large rubble elements are stacked first and small rubble elements fill the gaps to limit the use of filler material. As the algorithm was based on the assumption of a large rubble database, it only works with a large number of stones (at least 10x), which does not fit the precast process planned in this thesis. Furthermore, the assembly relied heavily on the use of sticky mortar to stabilise the arrangement, which would not be feasible at 1:1 scale.

Another 2D stacking algorithm for rubble was developed by Grangeot et al. (2024). It is based on the Stable Packing 2D algorithm by Wang et al. (2024) and required only 8 seconds per stone placement during their setup. As this speed can significantly increase the production process, the algorithm is tested for horizontal precast processes in 3.6 Test Phase 1 - Algorithms and described in the following section.

Stable Packing 2D

The Stable Packing 2D algorithm was initially developed by Wang et al. (2024) for the creation of stable arrangement with irregular stone elements for dry-stacked masonry walls. The tool combines a geometric image convolution approach with heuristic structural verification method. It enables construction scenarios which are based on two dimensional scans of irregular elements. The algorithm begins with the input of binary images, which represent the stone outlines. Each shape is simplified and rotated to an optimal default orientation. This orientation is determined by maximising the stone's shape factor (SF), which is defined by dividing the area of the stone by the area of its minimum bounding rectangle. A perfectly rectangular stone therefore has an SF of 1 (see below). By choosing high shape factor values, the algorithm achieves efficient use of material and improves the stone interlocking.

$$\mathrm{SF}(M_m, S_m) = \frac{A_{S_m}}{A_{B_{M_m S_m}}}$$

Table 14 Shape Factor (Almeida et al., 2016)

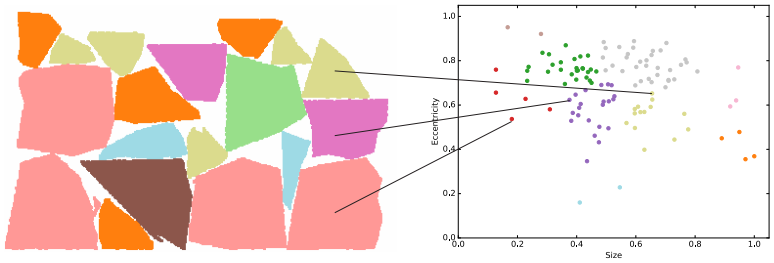

Table 15 Wall Arrangement And Cluster Generated With Stable Packing 2D

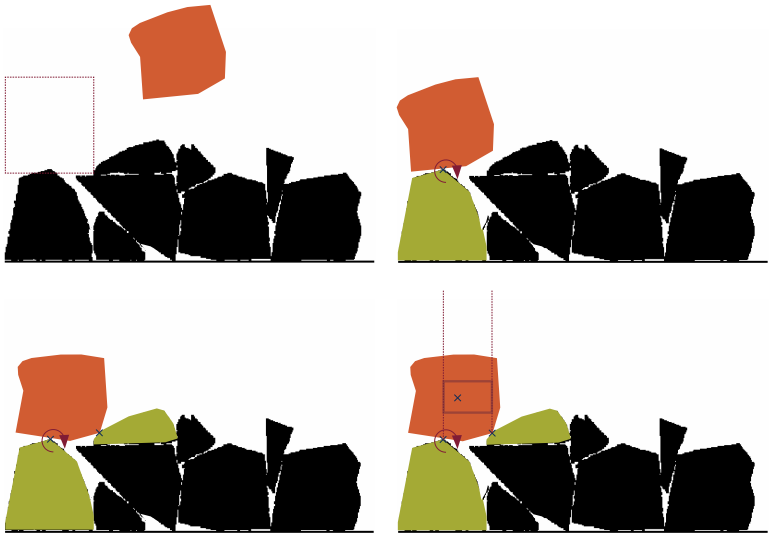

Figure 39 Geometry Placement Ensuring Two Contact Points With The Centre Of Mass In Between Them, Stable Packing 2D

After their rotation, the stones are clustered based on eccentricity and size. These groups reduce the search complexity and ensure that a diverse candidates are sampled. The wall itself is also defined as a pixel-based shape. For each iteration, a small batch of candidate stones gets randomly selected. These candidates are placed on the wall landscape with 2D convolution, which evaluates whether a stone fits into a local void, does not intersecting with an existing stone and ensures contact with the geometry below (see Figure 39).

The placement is evaluated against multiple criteria defined by Almeida et al. (2021). They include stone size and shape scores (FDP and FFP), the alignment with horizontal courses (FAH), vertical interlocking (FAV), and lateral stability. The algorithm ranks these options and subsequently derives a single performance score. The stability of the stone is evaluated by identifying whether the stone's centre of mass is supported by at least two points. If the condition is not satisfied, the stone is rotated until a stabilising orientation is found and the stone gets placed. Otherwise, the stone is discarded and another one tested (see Figure 39). This iterative process continues until the wall's height is reached or the algorithm failed to find a suitable stone.

To conclude, packing algorithms can have varied levels of complexity and can rely on different sizes of databases. A comparison of their structural performance for horizontal precast methods can be found in chapter 3.6, Test Phase 1 - Algorithms on page 70.

2.4. Precast Concrete Walls

2.4.1. Introduction

For concrete's strength values, engineers distinguish between Realcrete and Labcrete, due to the difference between on-site results to laboratory cube strength results (Torrent, 2013),. Precast concrete can be defined as "concrete which has been prepared for casting, cast and cured in a location which is not its final destination" (Elliott, 2019). Due to the controlled conditions in the factory, prefabricated elements offer the advantage that the strengths can be more predictable (Levitt, 2008, p. 155). However, in contrast to cast-in-situ concrete, they also need to be designed for their structural performance during fabrication, transport and assembly (Levitt, 2008, p.65). The production processes are distinguished between machine- and labour-intensive processes (Levitt, 2008, p.1). The first is linked to mass produced products like, pipes, extruded beams, or roofing tiles. All products requiring more custom approaches and manual labour fall into the second category. A more differentiated definition comes from Frohm et al. (2008), who separate automation as levels of mechanisation (LoAm) and computerisation (LoAc). Computerisation automates cognitive tasks and mechanisation automates human muscle power. The development of a process design with an automation potential for both is the aim of this thesis. Its development is laid out in Section 4, System Design and draws from the findings of this literature review.

2.4.2. Processes

Most prefabricated production processes show approaches of mechanization from LoAm 5 to 7 (see Figure 40 below). However, a broad implementation cannot yet be seen in precast concrete, due to the complexity of the mixture design and the processing (Reichenbach & Kromoser, 2021). They argue that customization would require a higher level of computerization (Figure 41), which is still lacking from most prefabrication plants. Nevertheless, the researchers see potential for customisation of mass precast products, which aligns with the aim for CS Walls. To understand how the industrial production methods for concrete walls work, the current processes are are discussed below.

LoAm	Description	Work	Equipment	Example
1	Totally manual	Manual	None	Muscle power
2	Static hand tool	Manual	Static tool	Screwdriver
3	Flexible hand tool	Manual	Flexible tool	Adjustable spanner
4	Automated hand tool	Manual	Automated tool	Hydraulic bolt driver
5	Static machine/workstation	Automatic	Machine designed for a special task	Lathe
6	Flexible machine/workstation	Automatic	Machine reconfigurable for different tasks	CNC-machine
7	Totally automatic	Automatic	All deviations or problems solved by machine	Autonomous systems

Figure 40 Levels Of Automation In Mechanization (Frohm et al., 2008)

LoAc	Description	Information	Control	Example
1	Totally manual	Manual	Manual	The user's earlier experience and knowledge
2	Decision giving	Proposed solutions	Manual with proposed approach	Work order
3	Teaching	Instructions	Manual according to instructions	Checklist, manuals
4	Questioning	Technology questions the execution	Manual with proposed recommendations from technology	Verification before action
5	Supervision	Technology supervises and calls for attention	Manual with supervision of technology	Alarms
6	Intervene	Automatic	Manual but technology takes over and corrects action	Thermostat
7	Totally automatic	Automatic	Automatic – user never involved	Autonomous systems

Figure 41 Levels Of Automation In Cognitive Tasks (Frohm et al., 2008)

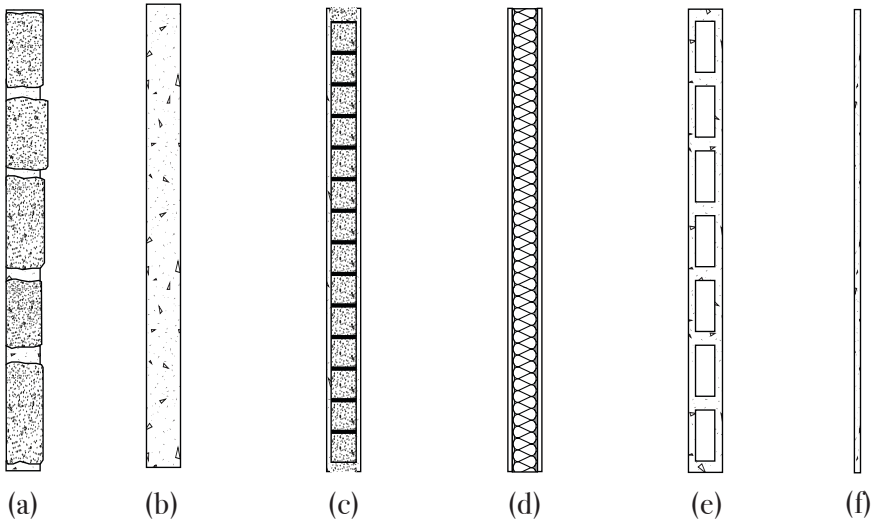

Figure 42 Typical Precast Wall Types, compared to a CS Wall: (a) Cyclopean Spolia Walls, (b) Solid Walls, (c), Composite Walls, (d) Sandwich Walls, (e) Lightweight Walls, (f) Facade Panels

Precast walls come in multiple forms. They range from solid walls, composite elements (combined with cast-in-situ concrete), sandwich walls (eg. concrete - insulation - concrete), lightened walls to cladding elements (Dutch Standards Institute, 2012). The Cyclopean Spolia Wall System discussed here, is produced in a similar way to solid walls (see Figure 42).

Prefabrication formwork systems can be categorized into horizontal, vertical and volumetric formworks (Pan & Pan, 2016). Volumetric moulds are used for three dimensional concrete shapes, like stairs for example. Vertical formworks have the advantage that they are space efficient and are be used for solid slabs for example. Walls, are mostly produced with horizontal processes, which can be classified into three categories, based on their formwork. Processes without a formwork describe digital processes, like extrusion or 3d printing. The two others are mobile and stationary processes. This section discusses conveyor systems, which are a form of mobile formworks and bench productions with tilting tables, which are a form of stationary formworks (Reichenbach & Kromoser, 2021). Even though more specialized processes exist (eg. injection in press mold or adaptive casting) these two offer the highest potential to mass-produce Cyclopean Spolia Walls.

Conveyor Systems

This form of mobile formworks is based on a conveyor belt system with multiple stations. The concrete is poured stationary and the formwork moves through the each production step (pouring, vibrating, curing etc.), which enhanced production capacity (Pan & Pan, 2016). The first

systems moved in a line and were called flow-line systems. Nowadays, carousel systems are mostly used, due to space efficiency (Reichenbach & Kromoser, 2021). An example can be seen in Figure 43.

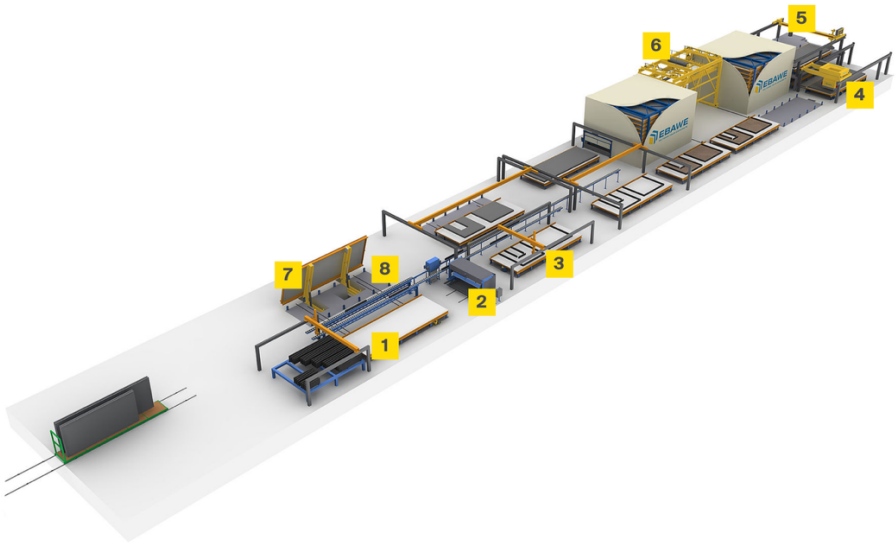

Figure 43 Carousel System (https://www.ebawe.de/en/products/carousel-plant-for-solid-precast-elements)

Reichenbach & Kromoser (2021) categorise the different production steps based on their level of automation in Figure 44, which is based on the production of double wall elements. This shows that most carousel systems have a high level of automation, with LoAm and LoAc of around 5 to 7. However, manual labour is still required for the positioning of reinforcement, inspection and storage. Reichenbach & Kromoser (2021) argue that the productivity of this mobile system depends on the most time-consuming process of the line.

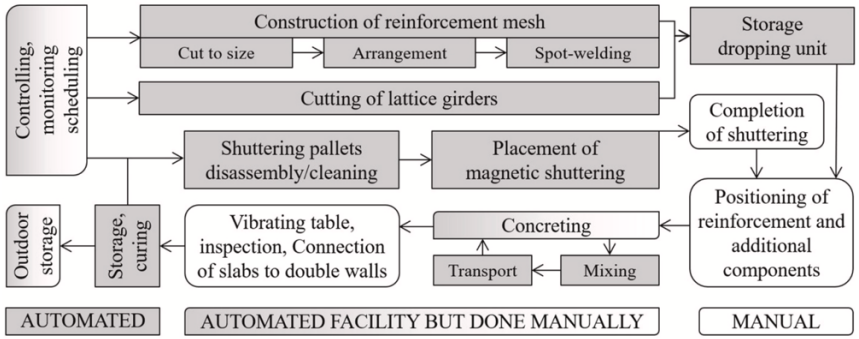

Figure 44 Process Diagram Of A Carousel Conveyor Prefabrication Plant (Reichenbach & Kromoser, 2021)

Stationary Tables

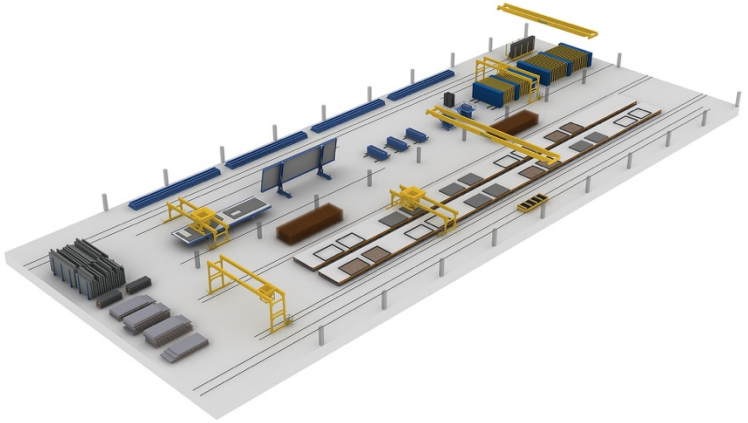

Figure 45 Concrete Precast Plant With Stationary Tables And Mobile Concrete Hoppers (https://www.ebawe.de/en/products/stationary-production-plants)

The traditional method for precast walls is the bench production with stationary tables. Here, each production step of the carousel system is executed in one location (Pan & Pan, 2016). The levels of automation

are lower than for mobile formworks and lie between LoAm 1 and LoAm 4 and are highest in the concrete mixing processes.

Figure 46 Tilting Table (https://www.gulfprecast.ae/products/wall-panels/

An important factor in prefabrication is the reduced strength at demoulding, which usually happens around 18 hours after casting the concrete (Elliott, 2019). Therefore, systems can be fitted with a tilting table (Figure 46), which helps for the lifting of the wall and also reduces bending forces in the fresh concrete.

Even though the LoAms of mobile methods are higher, stationary methods offer the availability of overhead cranes above the formwork and have a higher flexibility to introduce new production steps. Therefore, first tests for CS Walls will probably happen with bench production methods on a tilting table.

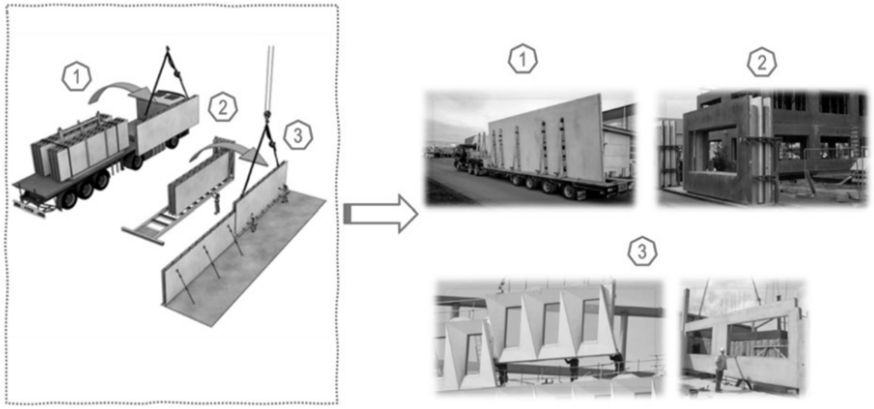

Figure 47 From Factory To Construction Site: (1) Vertical Tranportation, (2) Storage, (3) Handling And Installation (Martins et. al., 2023)

The transport process is similar in all prefabrication methods. As shown in Figure 47, the walls get transported vertically and then stored on site, until they get installed by crane (Martins et al., 2023). As prefabrication factories are expensive to run (Elliott, 2019), sometimes it is economical to build a temporary facility close to the site to minimize hauling costs.

2.4.3. Moulds

The main aim of a mould for precast concrete is the maintenance of the required geometry and keeping it to the desired tolerances. With extensive use, moulds grow in size and can generate unwanted positive tolerances. This lifetime depends on the material used for moulds (Levitt, 2008 p.66 - 73):

Steel (- 1000 uses)

Processes with large numbers of elements often use steel as a mould material. "It is the first choice [...], due to its high strength, abrasion resistance and good temperature stability compared to timber and plastics" (Levitt, 2008). The durability can lead to lifetimes of several thousand uses per mould.

Timber (5-100 uses)

Timber is a highly versatile material with multiple types of wood available and suitable for bespoke moulds with more customization. Its surface imperfections can directly impact the concrete surface, which can be desired for aesthetical reasons. The material can lack dimensional stability however, due to warping and size changes caused by moisture, aging or absorption of release agents. High-quality moulds depend on the carpenter's skills and the material needs to be stored under controlled humidity to prevent damage and maintain its dimensional stability. Timber moulds require regular checks, but can be reused up to 100 times.

Concrete (1000+ uses)

Concrete moulds offer a high level of precision and superior dimensional stability. It has a superior resistance to temperature and changes in moisture than other materials. These moulds need to be designed with a high cement content (350-400 kg/m3) and low w/c ratios. The moulds require months of curing and grinding for precise dimensions. Properly maintained however, they can withstand thousands of uses and are the most durable material for moulds. This is why they are mostly used for large-scale, high-precision structures like tunnels for example.

Plastics (10-1000 uses)

The properties of plastic moulds depend highly on the type of plastic used. They are mostly used to achieve complex forms, due to their flexibility in shape. To prevent bowing and to maintain the dimensions during the curing and pouring of the concrete, plastics require reinforcements like timber, steel or chipboard backing. Polymers like glass-reinforced polyester (GRP) can achieve up to 1000 uses. Thermoplastics suffer abrasion by aggregates however and are limited to 10-15 uses.

Aluminium (1000+ uses)

Aluminium moulds are mostly used for lightweight applications like roofing tiles. The advantages are its low weight, durability and corrosion resistance, bimetallic reactions can occur with the rebar however.

Composites

Some moulds might require a composite of materials.

Based on this, an adjustable steel mould would be the right choice for the prefabrication of CS walls, due to its longevity. The production of standard elements with steel moulds can achieve a tolerance as low as +-3mm or less (Elliott, 2019). Flexible wooden moulds can be used for custom forms or for openings within the walls. To prevent the concrete from sticking to the mould, release agents are used for most applications, where the amount of agent applied is crucial for the quality of the concrete. Typically, a rate of 15-30 m2/l is applied with airless spays or wet rags. Alternatively, a brush is used for application and the excess agent is scraped off by a rag. Moulds are also regularly painted to increase their lifetime (Levitt, 2008, p. 73 - 74).

2.4.4. Detailing

In comparison to in-situ concrete, the design of the connections between the individual precast elements is a crucial factor for a safe design (Elliott, 2019, p. 229). Internal effects are more influential to precast concrete, due its finite size and the joints between the elements. There are a variety of connections developed for all different types of load-cases for precast concrete panels (Freedman, 1999).

The wall can crack due to shrinkage of the material or strains due to changes in temperature or loads. Therefore, the joints between the elements is crucial to prevent failure of the structure. They have to be designed in a way, which prevents the elements from damage when they move (see Figure 48) (Elliott, 2019).

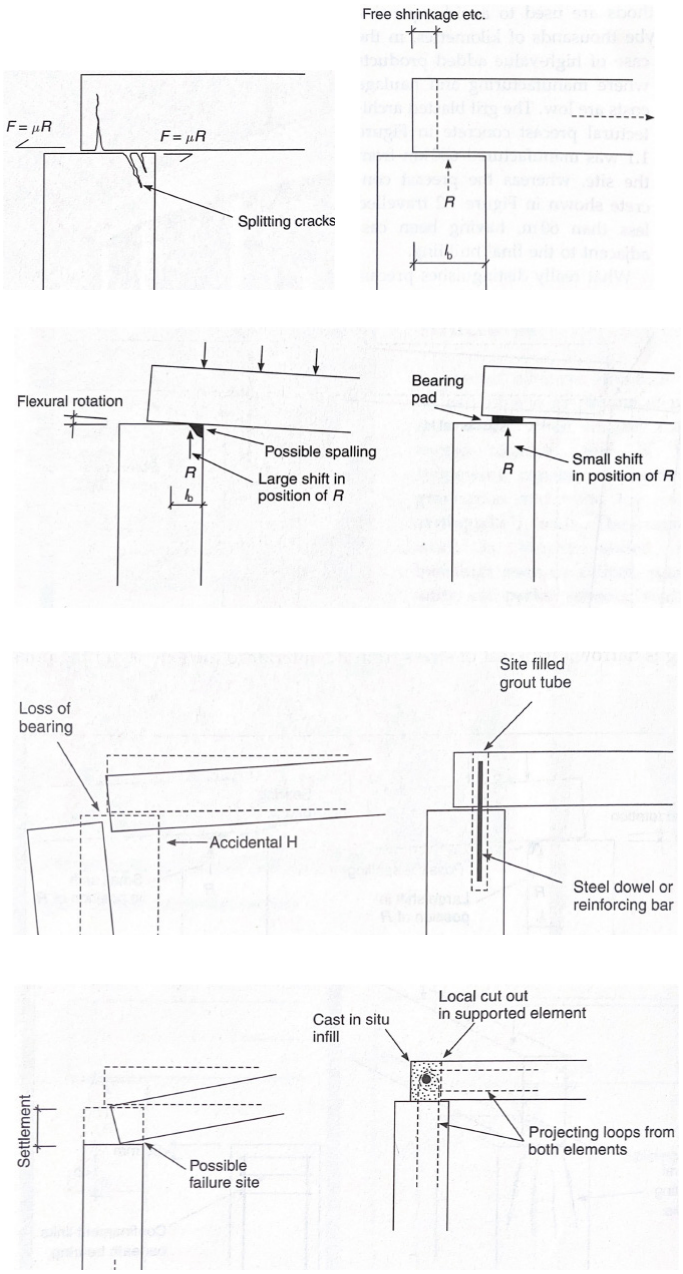

Figure 48 Potential Connection Failures according to Elliott (2019, p.2-4)

2.5. Cement and Aggregate Behaviour

Table 49 Concrete Ingredients

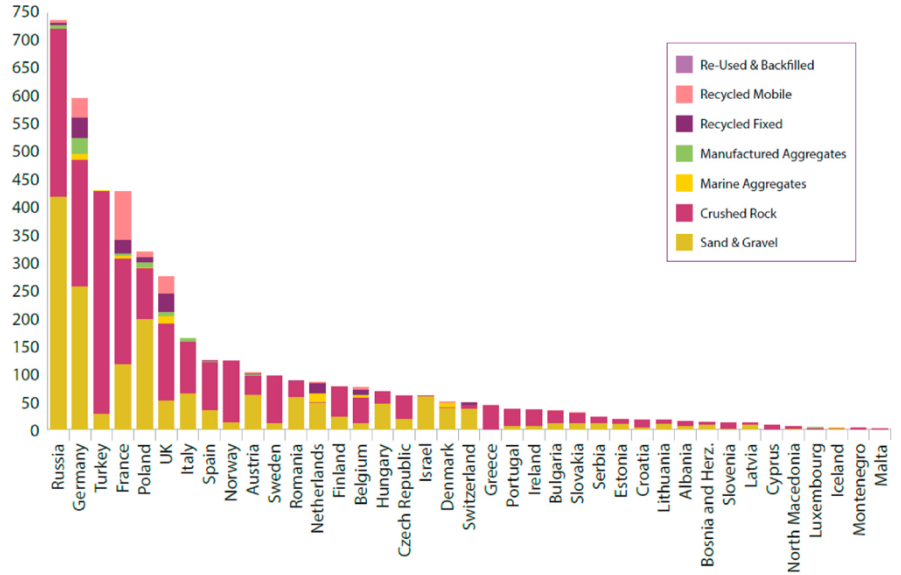

Table 50 Aggregates Production 2019 Per Country In Millions Of Tonnes (UEPG, 2020)

2.5.1. Aggregates

The inclusion of large concrete rubble elements into new concrete can be compared to the use of mega-sized aggregates. Therefore, it is important to understand the influence coarse aggregates have on concrete and which testing methods exist to assess bond strength and interfacial fracture properties.

The aggregate sector is Europe's largest non-energy extractive industry in terms of tonnage produced (UEPG, 2021). Coarse aggregates are defined with a diameter between 4.75mm to 150mm (ACI, 2012) and typically occupy around three-quarters of the concrete volume. Larger aggregates are called lump aggregates (Lin & Wu, 2025) or cyclopean concrete (Holt, 2013). These are discussed in Section 2.5.2 Cyclopean Concrete.

The choice of coarse aggregate significantly influences the mechanical properties of the concrete and its overall performance. Traditional coarse aggregates are natural stones, like Basalt, Diabase, Granite, Quartz, Magnetite or Limestone (listed from highest compressive strength to lowest). However, alternative coarse aggregates are used as well. These range from industrial byproducts like sintered fly ash or blast furnace slag to expanded clay or river gravel (van Mier, 1997). Furthermore, concrete construction waste material has been used as an aggregate, to produce 'recycled concrete' with coarse Recycled Concrete Aggregates (RCA) (Marinković & Carević, 2019).

Fine aggregates are usually comprised of sand. However, there are also approaches to use fine Recycled Concrete Aggregates (fRCA), which offer an alternative to the increasingly scarce resources for fine aggregates (Nedeljković et al., 2021). Similar to most concrete recycling

methods, Nedeljković et al. (2021) argue that the performance of the new product is influenced by the unknown design history of the concrete resources. This leads to an increase of cement use, due to contamination and high water absorption, which prevents the intended environmental advantages. This is why a Life Cycle Assessment is conducted for Cyclopean Spolia Walls in chapter 5.3, to determine the actual carbon emission savings.

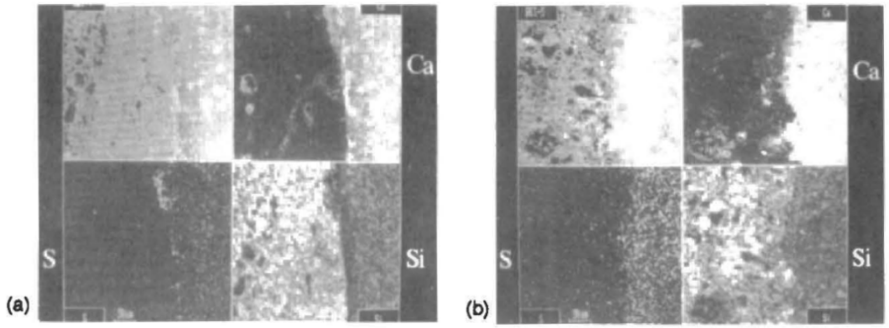

Table 51 a) sharp boundary between hard aggregates and cement paste (b) no sharp boundary between porous aggregate with cement paste (Zhang and Gjørv, 1989)

Maximum size in concrete, in. (mm)	Percentage of cleanly separated coarse aggregate fractions				
	Cobbles 6 to 3 in. (150 to 75 mm)	Coarse 3 to 1-1/2 in. (75 to 37.5 mm)	Medium 1-1/2 to 3/4 in. (37.5 to 19 mm)	Fine	
				3/4 to 3/8 in. (19 to 9.5 mm)	3/8 in. to No. 4 (9.5 to 4.75 mm)
6 (150)	20 to 30	20 to 32	20 to 30	12 to 20	8 to 15
3 (75)		20 to 40	20 to 40	15 to 25	10 to 15
1-1/2 (37.5)			40 to 55	30 to 35	15 to 25
3/4 (19)				30 to 70	20 to 45

Table 16 Coarse Aggregate that has produced workable concrete (ACI, 2012)

General knowledge on aggregates, based on van Mier (1997):

Natural aggregates usually have a low porosity and therefore show lower water absorption. Therefore, they are considered stronger and have a wider range of physical and mechanical properties They are often used in high-performance concrete, due to their good bond with the cement matrix. Lightweight aggregates like industrial byproducts have a high porosity and therefore a lower density. They absorb more water than high-density aggregates, which might necessitate pre-soaking of the aggregates or an adjustment of the water/cement ration (c/w). The porosity can therefore affect the cement-aggregate interface density. The choice of aggregate also influences the concrete's workability. This is the plasticity of the material during the first two hours after mixing the cement. Whereas angular particles increase interlock, smoother aggregates usually enhance the workability. The workability is also affected by the grading of the aggregates, so the particle size distribution. A finer grading requires a higher water demand for the same workability as a coarser grading. Grading also influences the properties of hardened concrete.

High-strength concrete requires strong aggregates, so usually natural stones, and optimized grading for minimized porosity. To achieve this low porosity, silica fume is often added. However, if the interface between aggregate and concrete is too dense, the crack path can pass through the aggregate, which increases the brittleness of the concrete.

Mostly, the interface between aggregate and cement paste is the weakest region. Eigenstresses, due to drying shrinkage for example, can lead to microcracks around the aggregates even before loads are applied.

The test of aggregate behaviour in concrete is not an easy task. Numerical simulation is often used in parallel with physical tests on the Macro and Micro level. On the Macro Scale, the region between the aggregate and the cement matrix, the interfacial transition zone (ITZ), can be tested on shear strength (Figure 52) and tensile or flexural bond strength (Figure 53). These can be combined with micro-indentation tests to determine microstructural differences in toughness around aggregates (Figure 54). Both types of tests are needed for a complete picture. The choice of aggregate is crucial for the desired qualities of the concrete. Their strength, surface and porosity have a major influence on the end product.

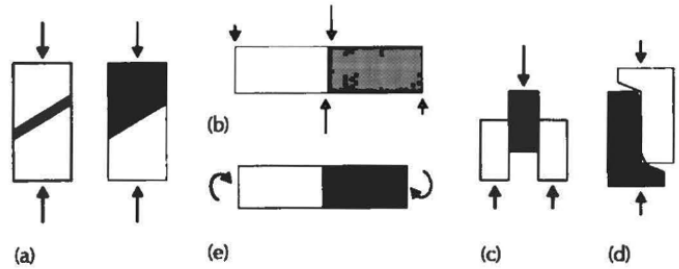

Figure 52 composite shear strength tests (a) specimen used by Taylor and Broms (b) four-point-shear beam, (c) push-through cube, (d) compact shear specimen and (e) cylinder subjected to torsion (van Mier, 1997)

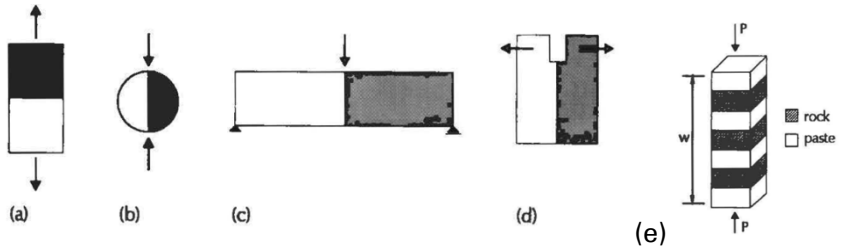

Figure 53 composite bond strength tests: (a) uniaxial tensile test, (b) splitting tensile test, (c) three-point-bend test, and (d) wedge splitting test (van Mier, 1997) (e) compressive prism for stiffness determination (Alexander & Mindess)

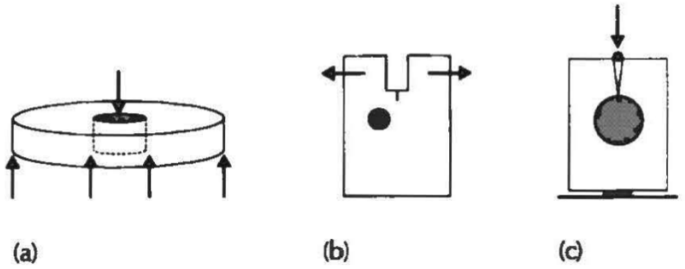

Figure 54 single particle composite tests for mechanical properties and crack growth (a) shear test designed by Mitsui et al., M(b) single-particle geometry of Vervuun et al.,s. and (c) two-phase composite model adopted by Lee et al

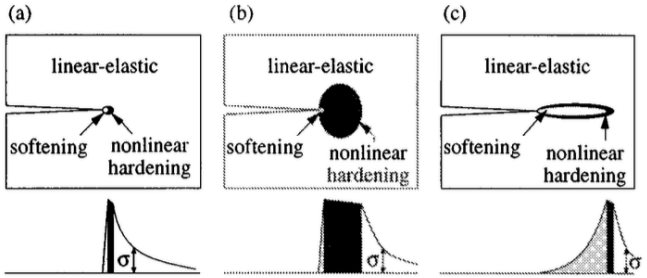

Figure 55 (Bazant (1985) brittle, ductile, semibrittle

2.5.2. Cyclopean Concrete

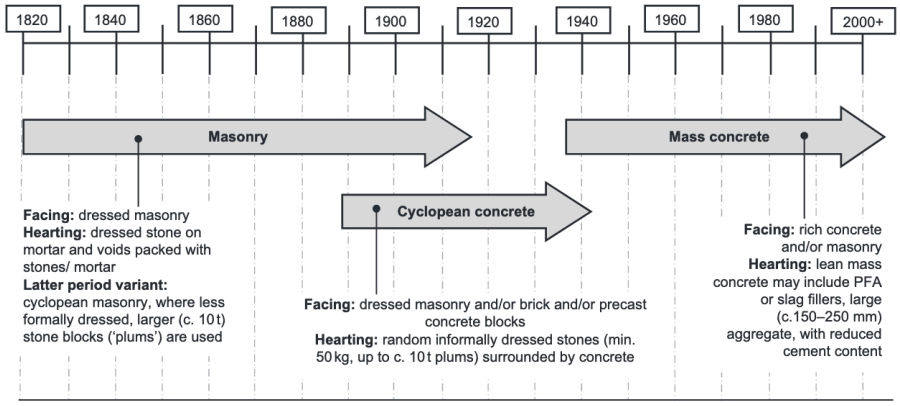

Table 56 Nomenclature for British Masonry and Concrete Dams (Holt, 2013)

This section introduces cyclopean concrete. It is the name-giving method for this thesis, as it involves large aggregate sizes in concrete. There is not much research about it, but these historic structures can serve as an example of the feasibility of a strong ITZ between large boulders and concrete. Furthermore, lump concrete is introduced.

Cyclopean Concrete is the method of embedding large stones (plums) into concrete structures. Even though larger sizes sometimes get used, the maximum practical size for coarse aggregates is a diameter of 150mm (ACI, 2012). Cyclopean Concrete structures use more than ten times the size of these aggregates. As aggregate size is usually limited by the distance between rebar, Cyclopean Concrete is mostly seen in megastructures like historic dams. It was a common technique before the 1950s, but since then, most dams have been built out of mass concrete without larger infill aggregates (Holt, 2013).

Table 57 The Unfinished Dol-y-Mynach Dam shows the construction Method of Cyclopean Concrete (https://industrialtour.co.uk/wp-content/uploads/2024/03/dol-y-mynach-dam-hollow-centre.jpeg)

Due to the difficulty to take representative samples from structures with such large aggregates, Maltidis & Stempniewski (2013) developed a finite element method (FEM) to assess crack behaviour for seismic loads in Cyclopean Concrete structures. They assign 60% of the mechanical strength of the mortar to the ITZ, which will serve as a reference for Cyclopean Spolia.

Current examples for Cyclopean Spolia are rare. The foundations of the Education City Stadium in Qatar serves as an example, but has a much smaller stone size than the historic dams. The boulders from the 45'000m3 of excavation on site were cut down to 200 mm to 400 mm coarse aggregates and then integrated into the concrete (Al-Hamrani et al., 2021). According to their life cycle analysis, this reduced greenhouse gas emissions by 32%.

Another method is Recycled Lump-Aggregate Concrete (RLAC). It consists of aggregate sizes which surpass the standard sizes and research suggests promising results. It mixes large-sized demolished concrete lumps with fresh recycled aggregate concrete (Lin & Wu, 2025). An example which incorporates rebar can be seen in Table 59.

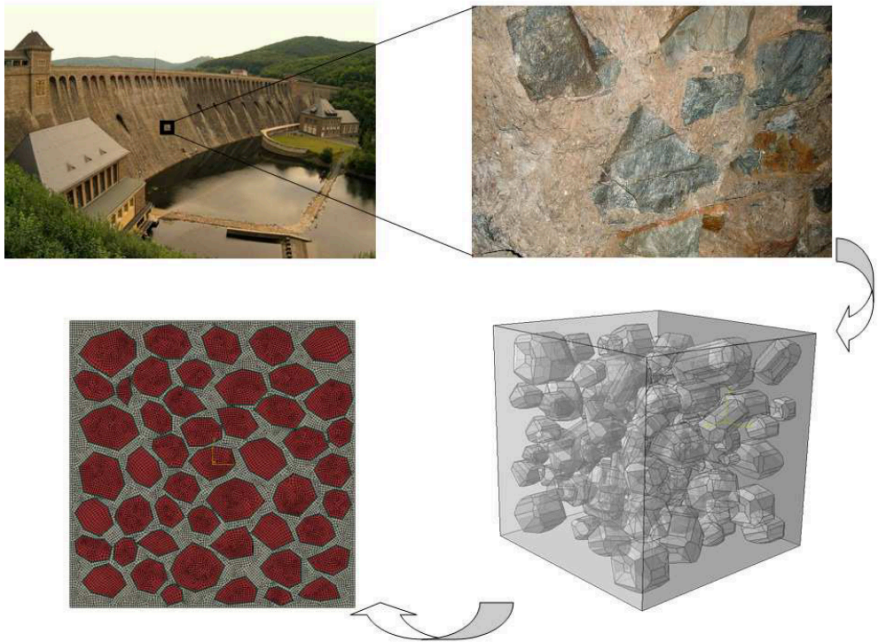

Table 58 Seismic Analysis Of An Old Cyclopean Concrete Dam Using FEM (Maltidis & Stempniewski, 2013)

Overall, cyclopean concrete proves that the aggregate size does not need to be limited to workable sizes, when building with large volumes. When designed in a smart way, even rebar can be integrated with giant aggregates.

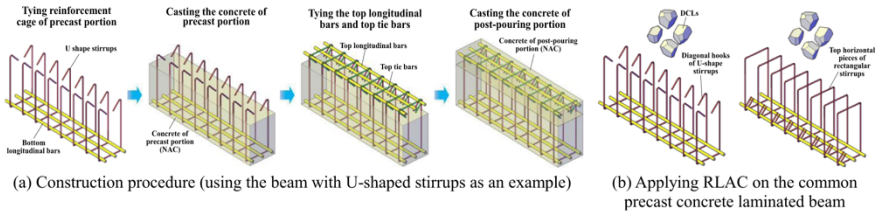

(a) Construction procedure (using the beam with U-shaped stirrups as an example) (b) Applying RLAC on the common precast concrete laminated beam

Fig. 2. Common precast concrete laminated beams.

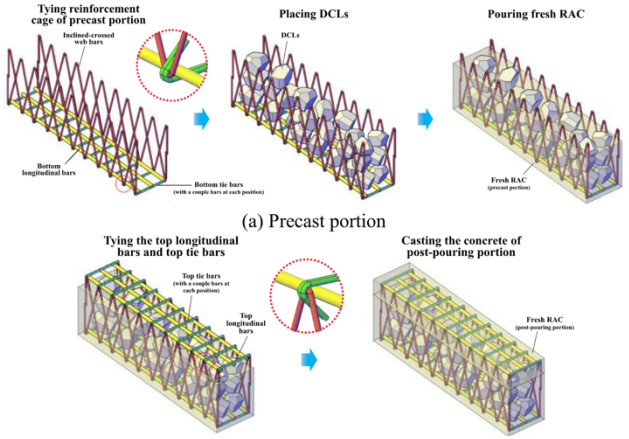

Table 59 Construction Procedure Of An RLAC Beam (Lin & Wu, 2025)

2.6. Answer to Research Questions

What are the current methods to reclaim concrete rubble without crushing it?

In recent years, several methods have emerged which save rubble from landfill or downcycling. These can be categorised as PRECS (Piecewise Reuse of Extracted Concrete in new Structures) and are able to retain the structural potential of concrete waste (Küpfer et al., 2023). Instead of grinding the rubble down, it is treated as a structural or decorative material. Methods range from stacking rubble with mortar in a masonry-like system, either horizontally (Oreb et al., 2024) or vertically (Grangeot et al., 2024), to carving shapes out of rubble (Clifford and McGee, 2018). Furthermore, the literature review showed that digital tools are essential to the management of irregular rubble shapes without extensive manual labour.
Overall, there is a growing number of workflows that reclaim rubble, but it remains a niche method.

What are the key technical, material and design challenges that require further exploration in load-bearing concrete rubble research?

Even though the reclaimed concrete rubble shows great potential, several challenges remain before it can become a standard building method. One major issue is the lack of extensive full-scale tests, which ensure the strength of the material and its failure modes, especially as it is difficult to assess the remaining strength of rubble fragments. Oreb et al. (2024) tackled this by using a weak mortar, so the wall would fail at the joint, not in the rubble. This method adds predictability but limits the use of the material's full strength. The predictability of the ITZ bond between the rubble and the mortar also has to be explored.
This thesis focuses on the challenge of the scalability rubble walls. Existing processes are either time-intensive or require manual labour. No rubble wall has been produced horizontally yet, which is why a horizontal precast method is investigated here.

What are the key factors necessary to prefabricate Cyclopean Spolia Walls?

The literature review showed that the creation of a standard precast rubble wall product would need to undergo multiple steps. To enable digital processes, the existing research emphasized the importance of algorithms to arrange the irregular rubble fragments. This approach can also enable automation processes during the precast process, which is important to achieve the customisation of standard products (Reichenbach & Kromoser, 2021), needed for CS Walls. The prefabrication workflow needs to be designed from the material sources to the assembly on site and focus on a formwork type. Furthermore, the walls have to structurally withstand the demoulding, transport and assembly process (Elliott, 2019). Due to the need of joining individual modules on site, precast walls need sophisticated connection details, to ensure their safety.
The factors mentioned above will be demonstrated exemplary in the workflow of the experiments (3. Structural Tests) and in the system design (4. System Design).

Structural Tests

Summary

The experiments investigated how different arrangements of concrete rubble influence the structural performance of horizontally prefabricated concrete walls. Informed by the literature review, the aim was to test whether different placement strategies and infill ratios could facilitate the construction of precast load-bearing concrete rubble walls. All tests were conducted at a 1:10 scale to compare the impact of the algorithms used to arrange the rubble, varying fragment diameters, and different virgin concrete infill volumes. The testing process used consistent materials, curing conditions, and sample dimensions to ensure comparability. Two main experimental phases give insight into the mechanical behaviour of Cyclopean Spolia Walls and test how digital tools might support precast methods.

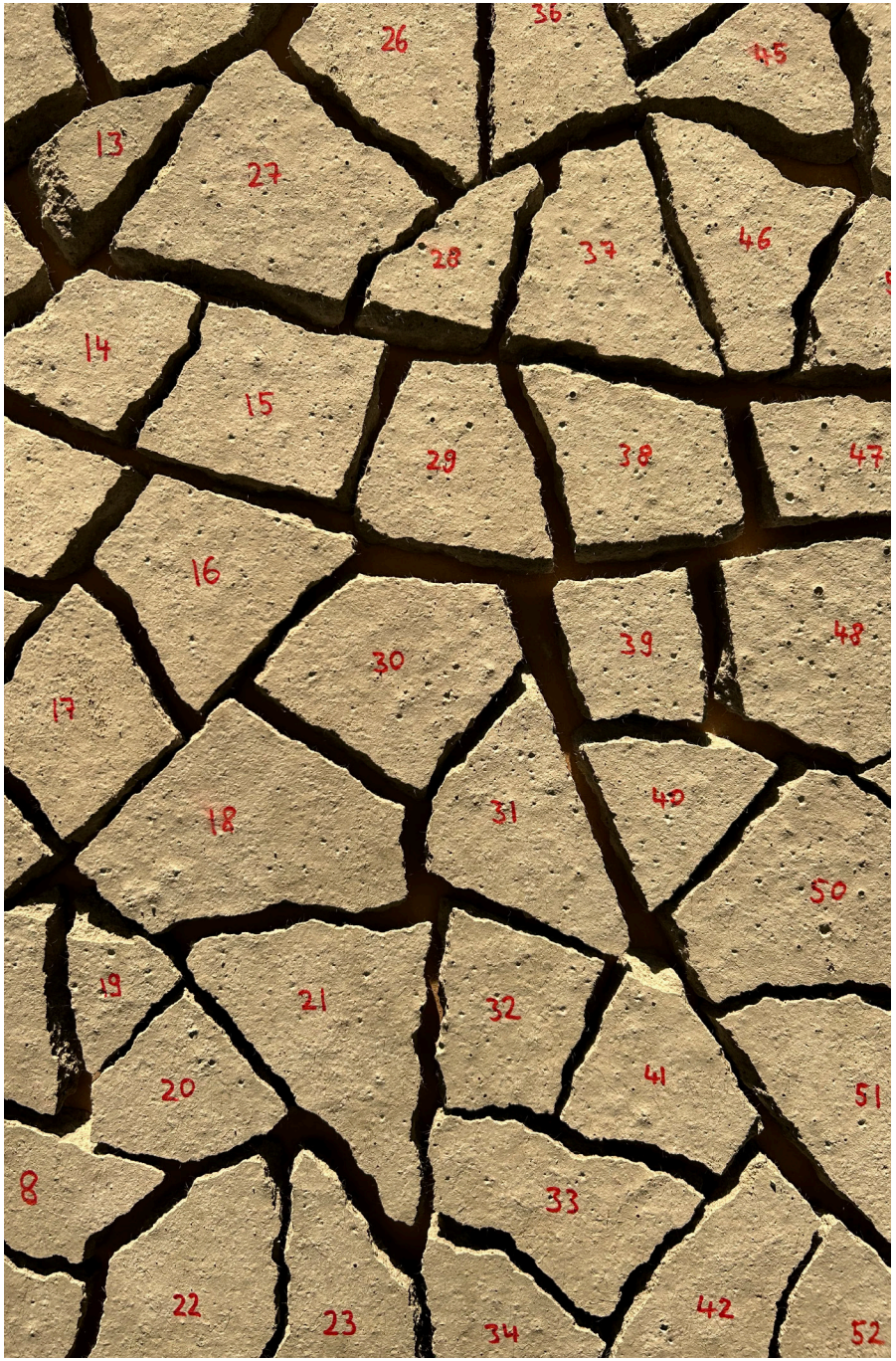

3.1. Introduction

The literature review shows a slowly growing interest in load-bearing concrete rubble. Several workflows were developed in 2024, which successfully reclaimed rubble into building products with both horizontal and vertical arrangements. However, only two projects conducted structural tests. Oreb et al. (2024) and Grangeot, Bastien-Masse, & Fivet (2024) confirmed that concrete rubble can be used in load-bearing wall systems. These results serve as the basis for assessing the general feasibility of Cyclopean Spolia Walls as structural elements. However, as the precast method discussed in this thesis enables a new way of arranging stones, it raises new questions regarding the structural performance of these arrangements. Therefore, experiments were conducted to compare these methods and draw conclusions for the development of the prefabrication workflow.

To determine the workflow, the literature reviewed revealed that research like the Autonomous Dry Stacking project (Johns et al. 2020), Cyclopean Cannibalism (Clifford & McGee, 2018), RR-CMU (Marshall & Grangeot, 2024) and Structural Concrete Rubble Arrangements (Grangeot, Bastien-Masse, & Fivet, 2024) used computational tools to build with irregular concrete waste fragments. In terms of scanning and algorithmic placement, the projects demonstrated that 2d scanning and 2d digital processing methods proved to be both successful and accessible. As existing methods rely on large databases, a 2d nesting algorithm is tested to reduce the number of data points needed.

Therefore, the first experiments explore if horizontal precast methods can enable the use of nesting algorithms for structural purposes and how they compare to existing stacking algorithms.

The following test phase then tests how different arrangement types affect structural behaviour.

The materials for the tests were selected based on the knowledge gained from the concrete research and the insights from rubble projects. The tests should provide an initial insight into the behaviour of a horizontally precast composite made from rubble and virgin concrete.

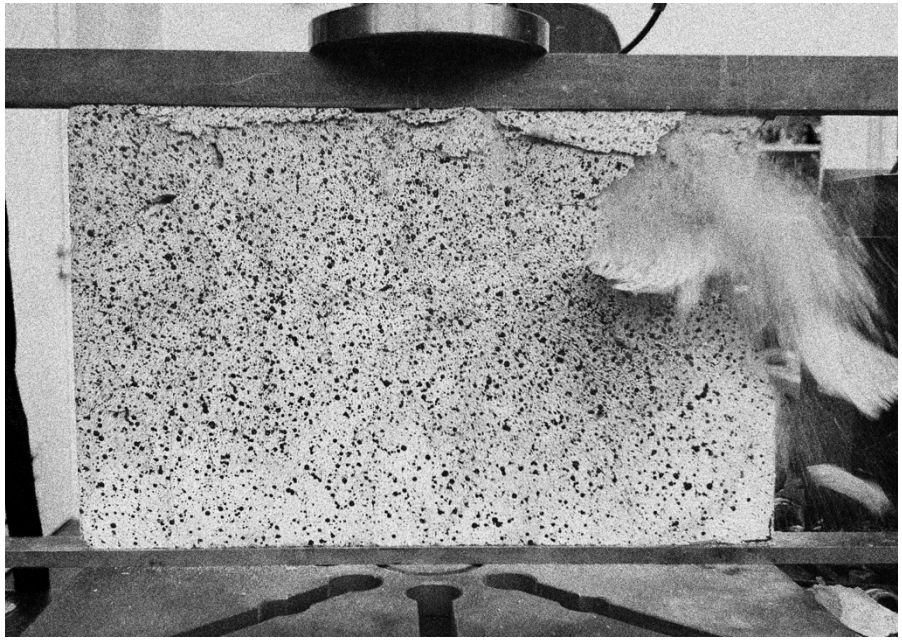

Figure 60 Failure Moment Of Sample N3, Algorithm Tests

3.2. Testing Variables

To understand how a prefabrication process can produce load-bearing walls from concrete rubble, it is essential to understand the impact of the rubble arrangement on the wall's final structural performance. The placement of the stones can be done manually or with the help of algorithms, which arrange previously scanned stones (Grangeot, Wang, Beyer, et al., 2024b; Johns et al., 2020; Wang et al., 2024). However, the performance of algorithms for horizontal precast processes has yet to be explored. Therefore, in the first experiment phase, called Algorithm Tests, the image convolution-based stacking algorithm by Wang et al. (2024) was compared to the DeepNest algorithm (Deepnest, 2025). This comparison then informed the digital workflow of a second round of experiments, called Arrangement Tests. This phase compared rubble diameters, infill-to-rubble ratios, and manual arrangements with non-reinforced concrete walls. To provide an overview, all testing variables are shown in Table 17. More details on how the variables were compared in the first and second experiments can be found in Figure 73 on page 70 and Figure 88 on page 77.

Variable	Tested		
Database Size	10x	1.1x	
Rubble Diameter	250 - 750mm	750mm - 1500mm	
Small Stones as Infill	Yes	No	
Virgin Concrete Infill Ratio	0.2	0.3	1
Arrangement Source	Nesting	Stacking	Manual

Table 17 Variables For Structural Testing

3.3. Boundary Conditions

3.3.1. Sample Sizes

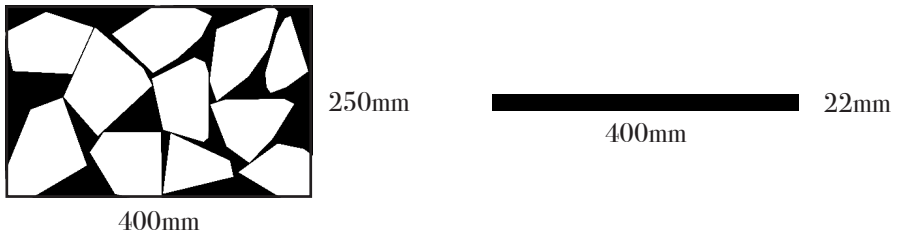

Figure 61 Sample Dimensions (1:10)

Due to the scope and resources available for this thesis, the tests were carried out at a 1:10 scale. For comparability, the samples needed to share the same dimensions, which are shown in Figure 61 above. The sample width of 400mm is defined by the maximum width of the Zwick 100kN Universal Testing Machine (UTM) used for the experiments. The thickness of 22mm represents a 22cm thick wall, which is an average value for precast concrete walls (Thomas Gruppe, n.d.-a). The height of 250mm was defined by the area in a 3m high precast wall, which offers space for concrete rubble to be inserted (see Section 4 System Design). The wall thus has a slenderness ratio of 1:18.

3.3.2. Material

The rubble and the infill for the algorithm and arrangement tests were produced with the same mortar mix to ensure comparability of the results. As the experiments were scaled to 1:10, a cement mortar was chosen, which contains only fine aggregates and no coarse aggregates. In a 1:10 sample, full-scale coarse aggregates would not fit into the cavities between the rubble and would not accurately represent the materials. Therefore, the samples were produced with the Weber Vloeibare ZandCement (*Weber Vloeibare zandcement®*, 2025) screed concrete. It is a mix of cement, quartz sand, and additives that improve fluidity and adhesion strength. With a grain size of 1 - 4mm, the fine aggregates of the cement mortar represent a full-scale concrete mix with medium-sized aggregates of up to 37.5mm (ACI, 2012). The screed concrete was chosen over other cement mortars due to its superior workability, which helped form air-tight walls with its fluidity.

400mm * 22mm = 8800mm2

8800mm2 * 16 MPa = 141kN

100 kN / 141 kN = 70%

The universal testing machine is limited to 100kN. Therefore, a concrete with a comparatively low final compressive strength of 16MPa was chosen (Table 18). With a sample area of 88 cm², the UTM would have reached its 100 kN limit once the concrete had reached 70% of its full strength (as shown in the calculation above). However, due to the tests occurring only 7 days after casting, the concrete would not have reached its full capacity. Additionally, the wall's strength was assumed to be mainly determined by the bond at the rubble and infill interface transition zone (ITZ), which would be lower than the infill's strength (van Mier, 1997).

The preliminary test round utilised gypsum as a rubble material with a low compressive strength of 2 MPa (Table 19) to simulate weak CCDW elements.

Product Image	
Material Name	Weber Vloeibare Zandcement
Manufacturer	Weber Beamix
Application	Flooring
Color	Gray
Form	Plastic bag (20 kg) – dry mortar
Processing Time	30 – 45 min
Aggregates	Fine Only (Quartz Sand)
Fine Aggregate Diameter	1 - 4 mm
min. Processing Temperature	> 5 °C
Compressive Strength	> 16 N/mm²
Flexural Strength	> 4 N/mm²
Surface Tensile Strength	> 0.5 N/mm²
Shrinkage	< 0.04 %
Density	2100 kg/m³
w/c ratio for experiments	1/7.1

Table 18 Properties Of Cement Used For The Experiments (Weber Vloeibare zandcement, 2025)

Property	Value
Product Image	
Material Name	Knauf Rotband Pleistergips
Manufacturer	Knauf
Application	Plastering Walls and Ceilings
Color	Beige
Form	Plastic bag (20 kg)
Processing Time	30 – 45 min
Aggregates	None
Compressive Strength	> 2 N/mm²
Flexural Strength	> 1 N/mm²
Density	1000 kg/m³
w/c ratio for experiments	1/1.18

Table 19 Properties Of Gypsum Used For The Preliminary Experiment (Knauf, 2023)

3.3.3. Curing

The samples were produced and cured inside the Green Shed at the Green Village Field Lab on the TU Delft campus (see Figure 62). The building protects the materials from the weather, but offers no control over the indoor environment. The humidity and temperature were therefore inconsistent during the curing process. To ensure comparability, the samples for each experiment phase were poured and cured simultaneously.

As the experiment stages built upon each other, the samples were produced in multiple stages. Hence, the timeframe did not allow a 28-day curing time (Eurocode, 2004) to ensure that the concrete reached its minimum compressive strength of 16MPa (*Weber Vloeibare zandcement®*, 2025). The wall samples were cured for 7 days, and the rubble between 9 and 14 days before the tests. As the rubble was produced earlier and with the same w/c ratio of 1/7, it was intentionally stronger than the infill concrete on the testing day.

To determine the strength of the rubble and infill concrete, additional standardised 40x40x40mm samples were taken during the pouring process. Their compressive strength was also tested during the experiments.

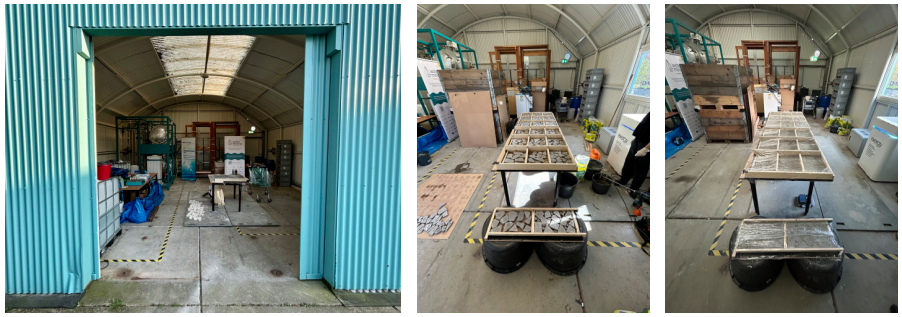

Figure 62 The Green Shed At The Green Village, Stone Arrangements, Samples Curing

3.3.4. Rubble

Rubble sourced from a waste centre typically comes from various construction sites, and the underlying building part is unknown. To ensure comparability between the test results, the rubble was produced manually with the same concrete mix and water-to-cement ratio (see Table 18). Additionally, real rubble elements with a thickness of around

22mm are difficult to source from waste centres. For reproducibility, all rubble elements have been produced with a uniform thickness of 22mm (+/- 1mm tolerance). To create the rubble, the concrete mix was poured into a flat rectangular formwork and broken by hand into the desired diameters after curing. To more closely resemble the edge structure of construction demolition waste, the rubble was produced while the concrete was still humid. Initial experiments by the author demonstrated that a 24-hour curing time yielded the best results. The edges could be rounded off by hand, approximating the geometry of damaged edges from transport of the rubble, and the concrete was still breakable by hand. To improve the bond, the fragments were submerged in water for 24 hours before the samples were cast, and the surface was dried before placing them in the formwork. This induced a saturated surface dry (SSD) condition, where the concrete's pores are filled with water, but the surface remains dry (see Figure 63). This increases the bond because it ensures that the rubble does not influence the w/c ratio of the infill cement at the ITZ. An oven-dry surface would otherwise locally soak water out of the mix, and a wet surface would add water to the mix (Yiğit Hunce et al., 2016).

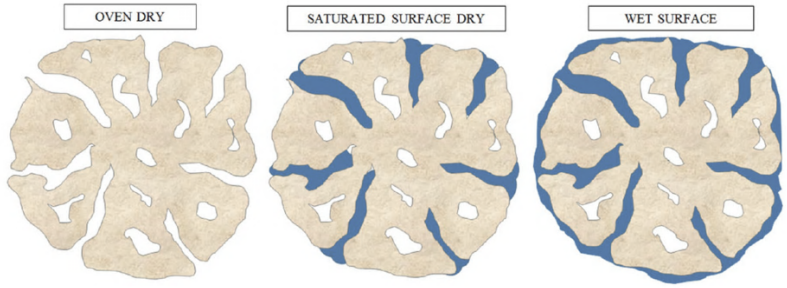

Figure 63 Saturated Surface Dry State Of A Material (Hunce et. al, 2016)

3.3.5. Sample Production

The samples for both experiments were produced with the same overall process. In total, four wooden frames were constructed to enable the simultaneous production of 26 walls. The shared process is listed and explained step by step, with references to Figure 64 and Figure 65.

Shared Production Steps

I. construction of a wooden formwork
II. pouring concrete (22mm thickness)
III. cure concrete for at least 24h
IV. demould concrete
V. break concrete
VI. label rubble
VII. scan rubble
VIII. save all scans in a database
IX. detect contours
X. digitally arrange rubble within the wall contour
XI. submerge rubble in water 24h before casting
XII. oil formwork and arrange saturated surface dry rubble
XIII. fill the gaps with concrete
XIV. demould the walls after at least 4 days
XV. spray speckle pattern

First, a wooden formwork was built to serve both the rubble and the sample production. To cast flat slabs with a uniform thickness of 22 mm, the formwork was filled with a layer of concrete. After the concrete was poured, the samples were cured for at least 24 hours before they were

demoulded. While still in this semi-hardened state, the rubble was manually broken into pieces with the desired diameter. Each fragment was then labelled and scanned to record its geometry. The scans were executed in 2D with a regular smartphone camera on a tripod, with the rubble on a dark surface. These photos were stored in a database, and their contour were detected digitally with OpenCV. As no automated process was found to scan rubble in mass with Segment Anything, the OpenCV method was used for this thesis. The scanning served as the base for the digital arrangement of the fragments. The capturing of the rubble contours and the arrangement process differed with the wall type. These are explained in detail in the following chapters.

24 hours before casting, all rubble pieces were submerged in water. This ensured a saturated surface dry condition to improve bond performance. Then, dividers were added to the formwork to provide a mould for the 400x250mm samples and a release agent was added. The rubble was arranged according to the plan, and the gaps between the pieces were filled with fresh concrete to complete the wall casting. After at least 4 days, the wall specimens were carefully demoulded. To enable digital image correlation (DIC) during testing, a high-contrast speckle pattern was applied to the surface of each sample. The bottom side of the slabs was therefore sprayed with white paint, and small black speckles were applied with the help of a sieve. To ensure that the samples did not exhibit internal cracks or damage before the tests, they were handled with care and transported in a layer of bubble wrap.

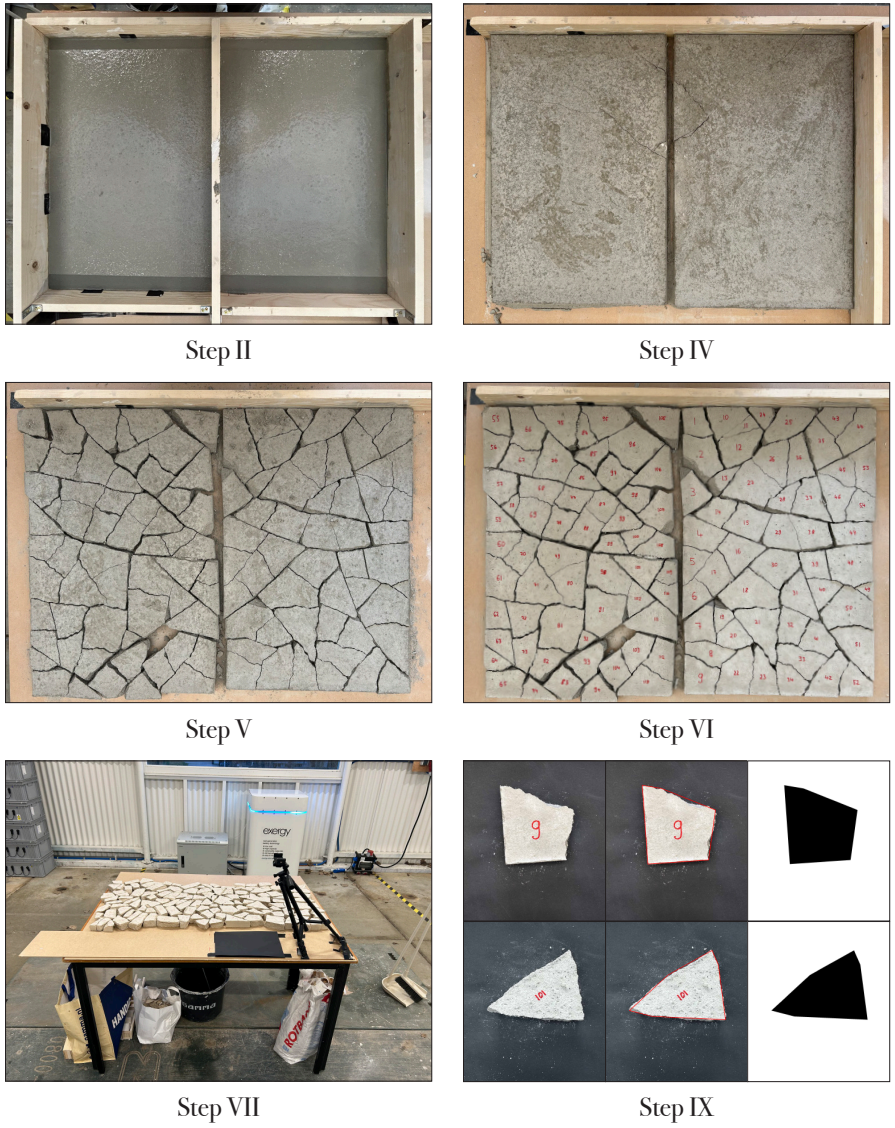

Figure 64 Sample Production Steps II - IX

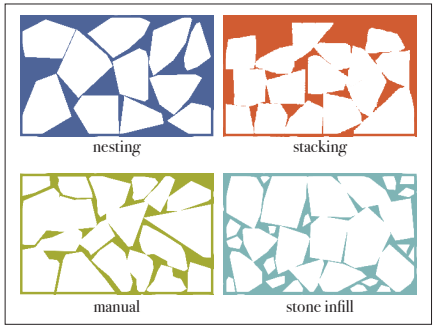

Step X

Step XI

Step XIII

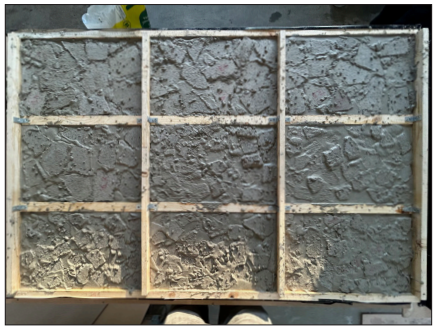

Step XIII

Step XIV

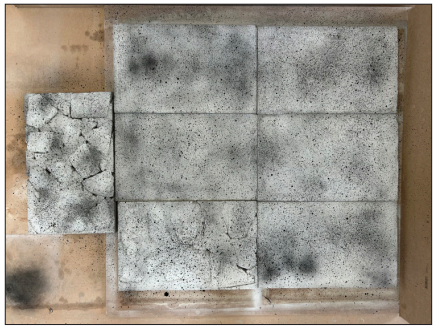

Step XV

Figure 65 Sample Production Steps X - XV

3.4. Data Collection

To compare the structural performance of the samples, a universal testing machine (UTM) was used to measure their behaviour under a compressive load. Three main data points were collected for every sample during the tests: the stress-strain curves, photographic documentation before and after testing and a video of the test for deformation and strain analyses with digital image correlation (DIC). These methods provided insights into the mechanical behaviour of the walls and are described below.

3.4.1. Axial Compression Tests

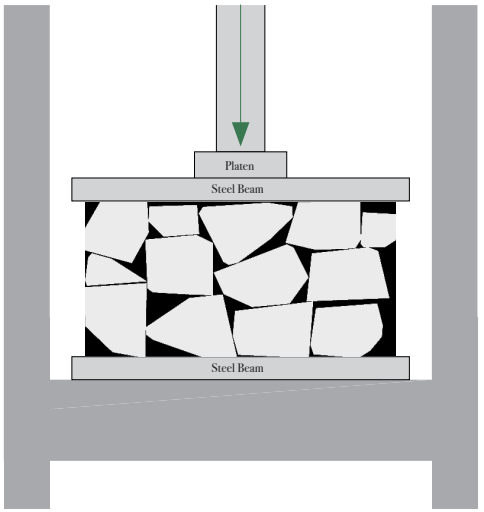

Figure 66 Compression Tests With The Universal Testing Machine Zwick Z100 (max. load 100kN)

As this thesis assesses a primary use case for the load-bearing Cyclopean Spolia Walls in regions without seismic risks, the wall is

designed to resist axial compression as its primary load. Therefore, in-plane compression tests were chosen for the experiments. They were carried out using a Zwick Z100 universal testing machine with a maximum load capacity of 100 kN. Each wall specimen was positioned centrally between the compression platens and loaded at a constant displacement rate. To spread the loads evenly across the samples, a 40 mm x 40 mm x 60 mm steel beam was placed on top of the walls.
The machine recorded force and displacement data throughout the test. These values yielded stress-strain curves, which were evaluated based on the load-bearing capacity and failure behaviour of the different wall assemblies. The resulting curves were used to compare the structural performance of the various rubble arrangements. Furthermore, the setup allowed for the documentation of the wall during its failure, which enabled constant photographic documentation and DIC. The Preliminary and Algorithm Tests were subjected to a displacement rate of 0.05 mm/second. Due to the large number of samples for the arrangement tests, the displacement rate was increased to 0.1 mm/second.

3.4.2. Photographic Documentation

The front side of each sample was photographed before and after the compression test. This describes the deformation of the wall and the development of cracks. The photos allow a direct comparison to identify crack locations, failure zones and differences in surface damage. This qualitative data supported the DIC results and the stress-strain behaviour.

Figure 67 Wall 8 Before And After Compressive Failure

3.4.3. Digital Image Correlation

A high-contrast speckle pattern was applied on the bottom flat side of each wall. This enabled the use of a DIC method, which gave insight into surface deformations and strain distributions during loading. The image correlation was carried out with the μDIC Python plugin (Olufsen et al., 2020), which was slightly modified to achieve the desired goal (the full code can be found in the appendix). The speckle pattern was applied with a white base paint and black spray dots. The pattern size and camera distance were calculated using the equations by Schaldenbrand (2021) and Schreier et al. (2009). The images were captured with a static phone camera setup, whose parameters are described in Table 20 and Figure 68.

Parameter	*Value*
Camera	iPhone 14
Sensor	12 MP
Sensor Size	4000 × 3000 px
Pixel Size	3 µm
Focal Length (f_0)	24 mm
Object Width (w)	400 mm
View Field Width (w_view)	500 mm
Sw	10.35 mm
OD	1183 mm
Length	0.4 m
Pixels	1080 px
Field of View (FOV)	0.16 m2
Image displacement accuracy	0.01
Image speckle dimension	3
Object speckle dimension	1.1 mm
Object displacement accuracy	0.0005 m

Table 20 DIC Setup Parameters Based On Schaldenbrand (2021

$$w_{speckle} = \frac{OD - f_0}{f_0} \cdot S_{w.S}$$

$$\frac{w}{Sw} = \frac{OD - f_0}{f_0}$$

Equation 1

Where:

- ***f0*** is the focal length of the lens
- ***OD*** is the distance between the object and the sensor
- ***w*** is the dimensions of the physical object, in this case its width
- ***Sw*** is the corresponding dimension on the sensor. This is normally expressed as number of pixels multiplied by the size of a pixel on the sensor, which is available in the camera parameters.

Figure 68 Digital Image Correlation Setup Equation (Schaldenbrand, 2021)

The following chapters explain the experiment setups in detail. They describe the rubble arrangements, present the findings and discuss the results. Each chapter begins with the same overview of the test setup, the variables, the dates and the sample production method.

3.5. Preliminary Tests

3.5.1. Test Setup

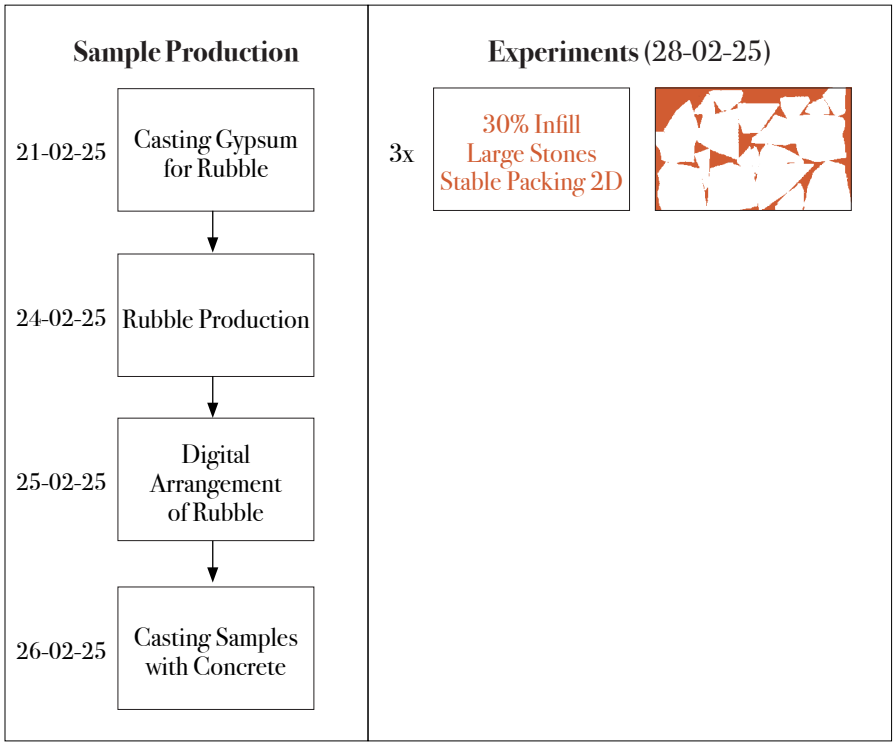

Figure 69 Experiment Setup Preliminary Tests

Objectives:

I. get familiar with the rubble production
II. test the formworks
III. set up the algorithm-to-wall workflow
IV. explore stronger infill than rubble
V. explore application methods of the speckle pattern
VI. explore the behaviour of the walls in the UTM
VII. test the data collection and analysis

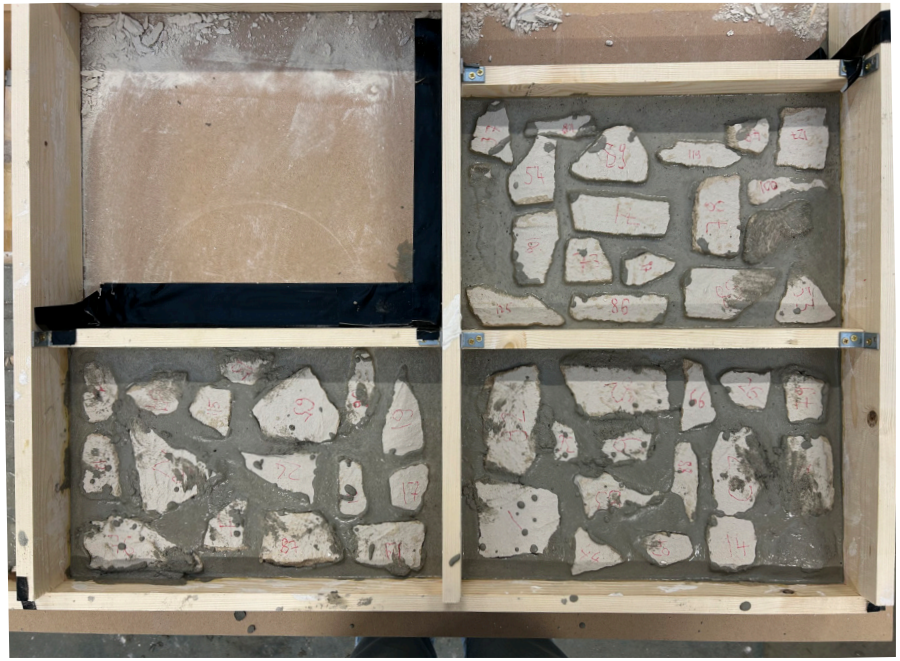

Figure 70 Preliminary Test Walls Using Stable Packing 2D

Before the main experiments were carried out, a preliminary test round was conducted to get familiar with the setup, materials, and procedure. Thus, three samples were arranged with the Stable Packing 2d algorithm by Wang et al. (2024) with the aim of exploring the behaviour of sample walls with stronger infill compressive strength than rubble compressive strength. This simulated a scenario where a weak concrete rubble element is paired with a stronger virgin concrete. Therefore, gypsum was used for the rubble with a compressive strength of only 2MPa (Knauf, 2023), combined with the 16 MPa concrete used in all other experiments. The specifications for both materials are listed in Table 18 and Table 19. As the primary aim of the experiments was to test the setup, the materials were not fully cured to their maximum strength. Due to time constraints, the specimens were demoulded two days after casting to spray the speckle pattern and transport them to the testing facility. However, the samples showed a weak bond between the gypsum and the rubble, which led to immediate cracks and failure of the walls during transport. To test the process, one wall was still sprayed with a speckle pattern and a compression test was executed.

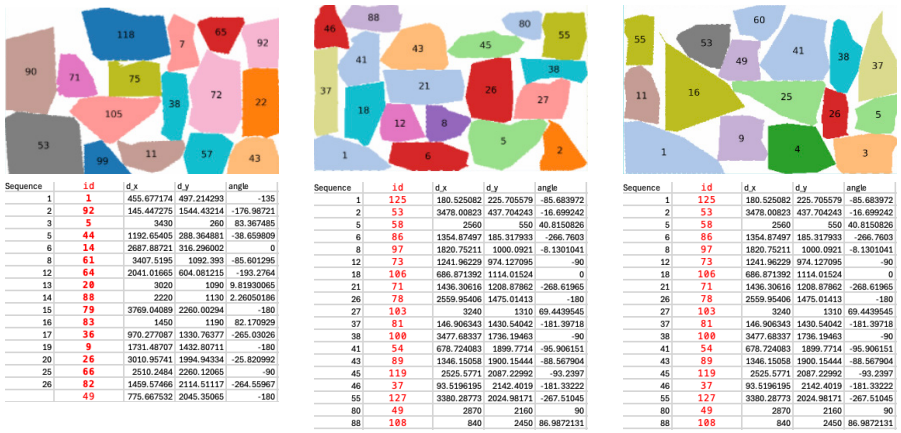

Sequence	id	d_x	d_y	angle
1	1	455.677174	497.214293	-135
2	92	145.447275	1544.43214	-176.98721
3	5	3430	260	83.367485
5	44	1192.65405	288.364881	-38.659809
6	14	2687.88721	316.296002	0
8	61	3407.5195	1092.393	-85.601295
12	64	2041.01665	604.081215	-193.2764
13	20	3020	1090	9.81930065
14	88	2220	1130	2.26050186
15	79	3769.04089	2260.00294	-180
16	83	1450	1190	82.170929
17	36	970.277087	1330.76377	-265.03026
19	9	1731.48707	1432.80711	-180
20	26	3010.95741	1994.94334	-25.820992
25	66	2510.2484	2260.12065	-90
26	82	1459.57466	2114.51117	-264.55967
	49	775.667532	2045.35065	-180

Sequence	id	d_x	d_y	angle
1	125	180.525082	225.705579	-85.683972
2	53	3478.00823	437.704243	-16.699242
5	58	2560	550	40.8150826
6	86	1354.87497	185.317933	-266.7603
8	97	1820.75211	1000.0921	-8.1301041
12	73	1241.96229	974.127095	-90
18	106	686.871392	1114.01524	0
21	71	1436.30616	1208.87862	-268.61965
26	78	2559.95406	1475.01413	-180
27	103	3240	1310	69.4439545
37	81	146.906343	1430.54042	-181.39718
38	100	3477.68337	1736.19463	-90
41	54	678.724083	1899.7714	-95.906151
43	89	1346.15058	1900.15444	-88.567904
45	119	2525.5771	2087.22992	-93.2397
46	37	93.5196195	2142.4019	-181.33222
55	127	3380.28773	2024.98171	-267.51045
80	49	2870	2160	90
88	108	840	2450	86.9872131

Sequence	id	d_x	d_y	angle
1	125	180.525082	225.705579	-85.683972
2	53	3478.00823	437.704243	-16.699242
5	58	2560	550	40.8150826
6	86	1354.87497	185.317933	-266.7603
8	97	1820.75211	1000.0921	-8.1301041
12	73	1241.96229	974.127095	-90
18	106	686.871392	1114.01524	0
21	71	1436.30616	1208.87862	-268.61965
26	78	2559.95406	1475.01413	-180
27	103	3240	1310	69.4439545
37	81	146.906343	1430.54042	-181.39718
38	100	3477.68337	1736.19463	-90
41	54	678.724083	1899.7714	-95.906151
43	89	1346.15058	1900.15444	-88.567904
45	119	2525.5771	2087.22992	-93.2397
46	37	93.5196195	2142.4019	-181.33222
55	127	3380.28773	2024.98171	-267.51045
80	49	2870	2160	90
88	108	840	2450	86.9872131

Figure 71 Test Wall Arrangements By Stable Packing 2D

3.5.2. Findings

The preliminary tests provided valuable insights into the choice of materials and the test setup. Firstly, the bond between the gypsum rubble and the concrete infill was insufficient. Cracks developed at the ITZ between the two materials during demoulding and handling. The bond strength was therefore too weak for the tests. This was mainly caused by early demoulding, which confirmed the need to cure the concrete for at least 4 days before removing the formwork. As a result, it was decided to produce the rubble for the following tests out of concrete. Furthermore, it encouraged some further research on improving the bond. This led to the decision to submerge the rubble underwater to achieve a saturated surface dry state before casting (Yiğit Hunce et al., 2016). Additionally, the gypsum rubble did not cure well inside the Green Shed. Compared to reference samples cured in a controlled indoor environment, the rubble showed a significantly lower compressive strength. This highlighted the sensitivity of gypsum to the environmental conditions found during the sample production and supported the decision to switch to concrete rubble for further experiments.

Furthermore, the experiments showed that the Stable Stacking 2D algorithm relies on a high accuracy for the rubble scans. The distortion of the 2D photos lead to some stones being a millimetre smaller in real life than on the scan. As the stability is assured through two contact points, these could not always be achieved with that tolerance. In result, the distortion value was adapted to achieve a higher accuracy.

Despite these issues, the test setup proved to work well. The compression tests, speckle pattern application, DIC measurement, and photographic documentation all produced reliable data, validating the overall testing workflow. The preliminary tests offered valuable insight for the Phase 1 and Phase 2 tests.

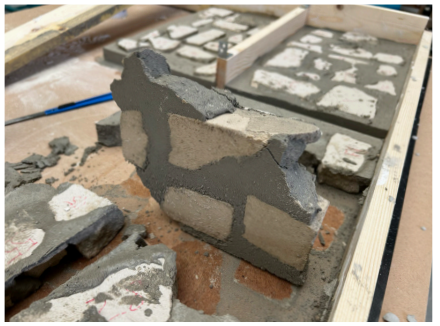

Figure 72 Breakage During Handling

Cast Date	Test Date	Age	Specimen	Code	Material	Area	F_{max}	F_{max}	σ	dL at F_{max}	F_{Break}	dL at break
		days				mm2	N	kN	Mpa	mm	N	mm
26.02.25	28.02.25	2	Specimen 1	00.0	Cyclopean Spolia	3500	2269	2.3	0.65	1.73	453.7435	3.9459887
26.02.25	28.02.25	2	Specimen 2	00.1I	Concrete	1600	1266	1.3	0.79	1.92	253.1635	4.7406673
26.02.25	28.02.25	2	Specimen 3	00.2I	Concrete	1600	1476	1.5	0.92	1.28	295.2584	4.2171559
26.02.25	28.02.25	2	Specimen 4	00.3I	Concrete	1600	1376	1.4	0.86	2.03	275.2395	4.8614883
21.02.25	28.02.25	7	Specimen 6	00.1G_35	Gypsum	2494	1035	1.0	0.42	1.63		
21.02.25	28.02.25	7	Specimen 7	00.2G_48	Gypsum	2298	1149	1.1	0.50	2.19		
21.02.25	28.02.25	7	Specimen 8	00.3G_30	Gypsum	2148	1239	1.2	0.58	1.66		
19.02.25	28.02.25	9	Specimen 9	mh_04	Gypsum	1600	4938	4.9	3.09	2.60		
19.02.25	28.02.25	9	Specimen 10	mh_05 failure	Gypsum	1600	256	0.3	0.16	0.28	244.6989	0.2831455
19.02.25	28.02.25	9	Specimen 11	mh_05	Gypsum	1600	5629	5.6	3.52	1.82		
19.02.25	21.02.25	2	Specimen01	mh_01	Gypsum	1600	3782	3.8	2.36	n.d.		
19.02.25	21.02.25	2	Specimen02	mh_02	Gypsum	1600	3880	3.9	2.43	n.d.		
19.02.25	21.02.25	2	Specimen03	mh_03	Gypsum	1600	3862	3.9	2.41	n.d.		

Table 21 Results Preliminary Test

3.6. Test Phase 1 - Algorithms

3.6.1. Test Setup

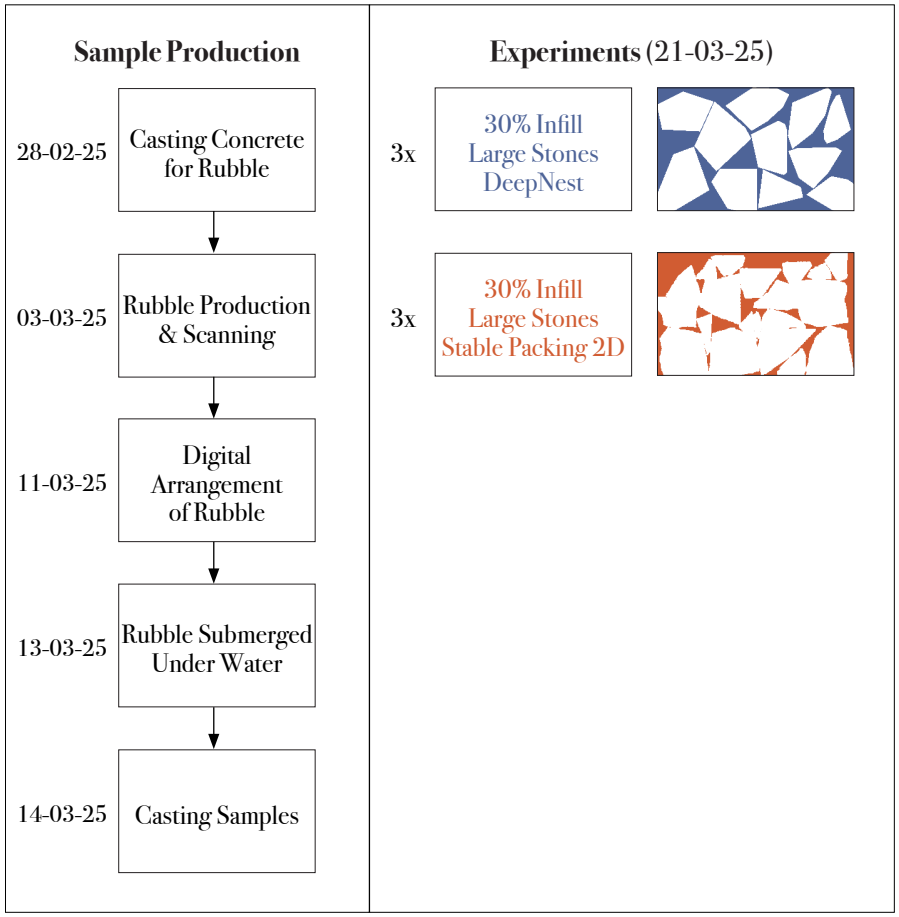

Figure 73 Experiment Setup Phase 1 - Algorithms

Wall Number	Arrangement	Arrrangement Type	smallest Rubble Size	largest Rubble Size	Database multiplier	Database Size	Infill %	Stones placed
S1		Stable Packing 2D	35 mm	150 mm	5.9	113	28%	19
S2		Stable Packing 2D	35 mm	150 mm	5.9	94	31%	16
S3		Stable Packing 2D	35 mm	150 mm	5.2	78	32%	15
N1		DeepNest	35 mm	150 mm	1.8	20	35%	11
N2		DeepNest	35 mm	150 mm	1.7	20	31%	12
N3		DeepNest	35 mm	75 mm	1.5	20	30%	13

Table 22 Algorithm Tests Wall Setup

Objectives:

I. compare nesting and stacking algorithms

II. decide which algorithm to use for the Arrangement Tests

The main advantage of horizontal prefabrication processes is the lack of structural constraints when placing geometry. As the walls are only loaded once the gaps are filled with the composite load-bearing material, they do not rely on their stability and interlocking during the construction process. The first testing phase therefore aimed to determine how the placement of the stones affects the final structural performance when a filler of similar strength to the rubble is used. Three walls with structural rubble arrangements were compared to three walls with scattered rubble. To produce them, a stacking and a nesting algorithm were used. The stacking algorithm Stable Packing 2D includes structural constraints, whereas the nesting algorithm DeepNest solely places the rubble within a form. Both arrangement approaches are explained below.

Stacking Algorithm

To assess structural stacking arrangements, the Stable Packing 2D algorithm by Wang et al. (2024) was used to generate three rubble assemblies for the Preliminary and Algorithm Test phase, respectively (a detailed explanation of the underlying algorithm can be found in 2.3.2 Stacking Algorithms). This section explains the generation of the walls for the algorithm tests.

As the algorithm incorporates strict structural constraints and therefore only places stones which fulfil those, a large quantity of samples is beneficial. Hence, the stacking walls were generated first, to ensure that the algorithm had access to the entire dataset of 113 rubble contours. The code was provided with binary images of the rubble and generated five stable walls during each run (see Figure 74). The generation of one wall took an average of 12 minutes, resulting in approximately one hour of calculation time per run. The wall assemblies were assessed on their lowest limit angle and their infill ratio. As one of the boundary conditions for these experiments was an infill ratio of 30% (+-3%), walls with ratios above 33% were excluded. For example, in Sample S1, the 4th option was chosen due to its low infill ratio, with 28% whitespace. Its lowest limit angle value was disregarded, as it only affected one rubble piece in the top corner (see Figure 74). After S1 was chosen, the rubble used was removed from the database, and the code was rerun.

After the three walls had been selected (see Figure 75), the assembly sequence and stone IDs were extracted and used to locate and position the rubble within the formwork.

On average, the algorithm placed 17 stones with a 30% infill rate. One can see from the arrangements in Figure 75, that S1 shows a larger quantity of small stones than S2 and S3. As the algorithm runs through each stone shape group, the small stone diameters are used up first and are no longer available for the walls generated later. Additionally, with the program's bottom-left to top-right placement, the walls showed that it finds fewer stones towards the end, due to the increased spatial constraints. If there are not enough small stones available, the top part of the wall is filled inconsistently, resulting in mortar hotspots (see S2 and S3 in Figure 76). A potential workaround would be to scan more small stones, as the algorithm already uses stone groups to ensure heterogenous choices.

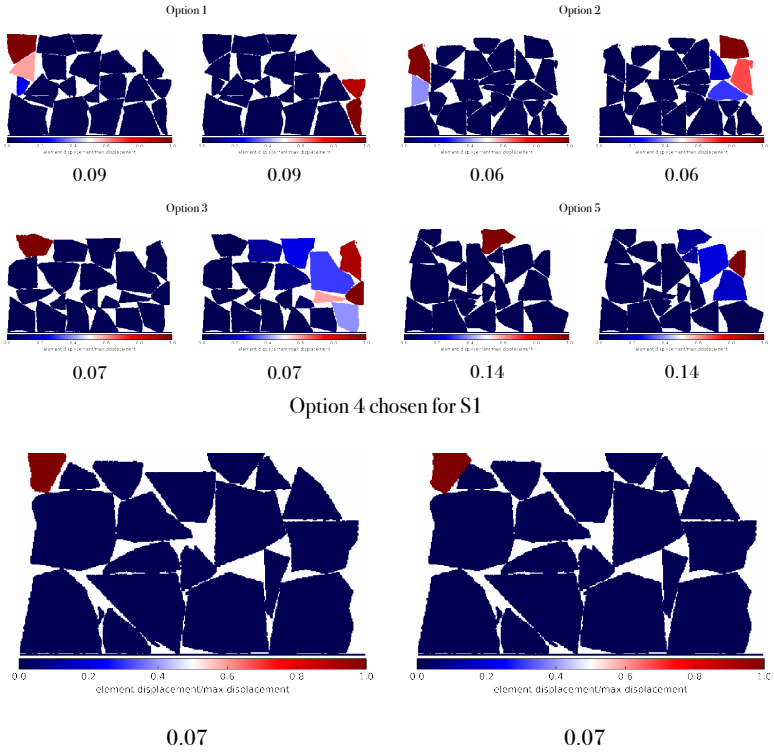

Figure 74 Wall S1 Stone Arrangement Options Generated By Stable Packing 2D

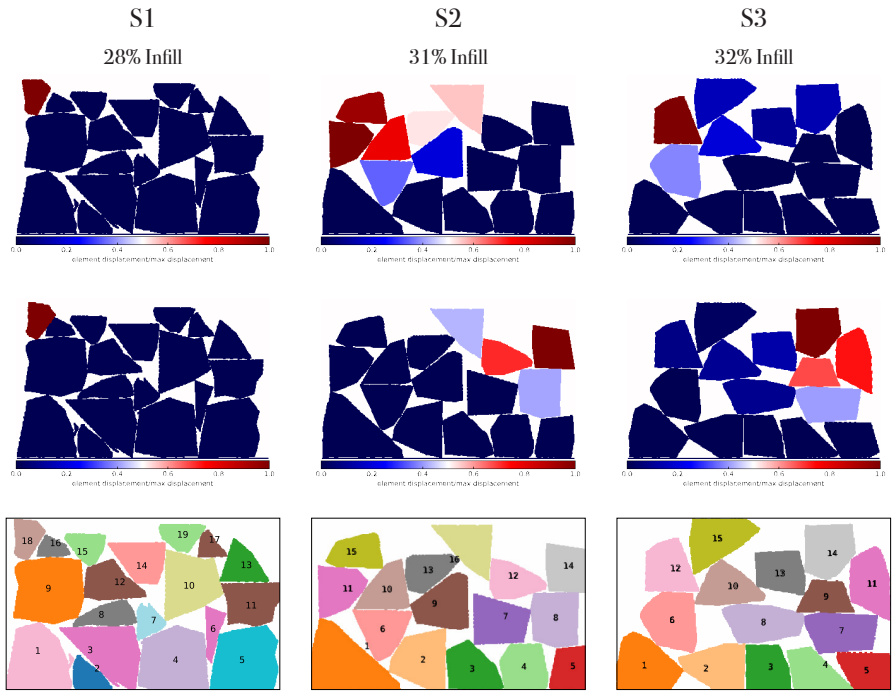

id	d_x	d_y	angle
91	478	440	-259°
19	1193	219	-137°
51	1486	591	-55°
48	2399	452	6°
96	3400	451	-93°
11	2944	896	-2°
58	2033	1012	-116°
13	1473	1098	-96°
81	633	1457	6°
76	2610	1543	-259°
88	3494	1284	-172°
108	1491	1552	-91°
102	3355	1795	-83°
6	1934	1876	-311°
24	1165	2070	-217°
92	678	2044	-148°
49	2899	2065	-218°
109	322	2195	-246°
64	2499	2223	-47°

id	d_x	d_y	angle
21	506	405	-175°
72	1589	470	16°
34	2284	336	-5°
87	3027	350	-189°
39	3708	330	-276°
40	1033	894	-22°
32	2664	1010	-168°
97	3465	1052	0°
41	1905	1253	-80°
99	1084	1459	40°
20	409	1468	-129°
86	2867	1584	-246°
84	1667	1727	-13°
104	3641	1745	-270°
100	673	1983	-86°
59	2256	2086	-182°

id	d_x	d_y	angle
107	427	378	41°
93	1459	371	-177°
55	2151	349	-185°
63	2814	288	-188°
77	3584	311	-97°
57	807	1026	-1°
68	3198	871	-93°
8	2083	996	-86°
89	2979	1345	-90°
45	1594	1499	-99°
73	3612	1562	-279°
54	766	1760	-94°
1	2343	1716	-187°
83	3014	2029	-139°
3	1452	2171	-38°

Figure 75 Three Walls Selected For Testing

Nesting Algorithm

The open-source nesting algorithm DeepNest was used to arrange the shapes within a defined wall geometry (a detailed explanation of the underlying algorithm can be found in 2.3.1 Nesting Algorithms)

The advantage of nesting algorithms designed for 2d horizontal arrangements is the absence of structural constraints when placing geometry. This reduces the number of additional stones required in the database to fill the space of a wall. Therefore, these algorithms could enable any batch of concrete to arrive at the prefabrication plant and be placed within a wall. This would reduce the storage required and resolve the issue of needing to provide access to each stone within an extensive database at all times. To simulate this process, the databases were significantly reduced for the nesting algorithm, compared to the stacking algorithm. Whereas the latter had access to a rubble database with 5- 6 times the number of stones needed for a wall, this factor was reduced to 1.5 to generate the nesting walls for the algorithm tests.

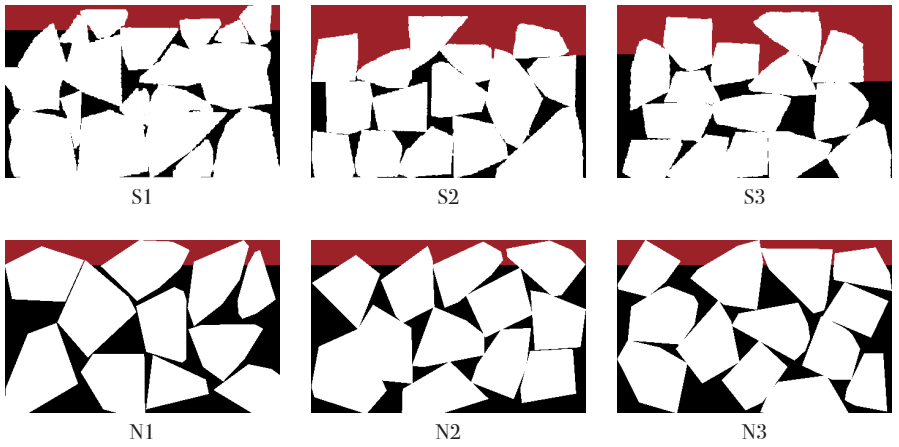

Figure 76 Infill Hotspots At The Top For Stacking vs Nesting

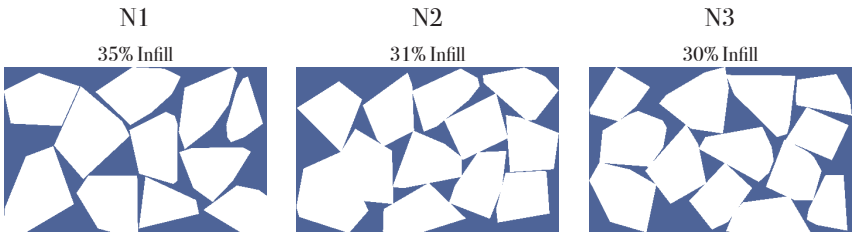

Figure 77 DeepNest Walls Selected For Testing

As DeepNest only accepts svg-files as data input, a Python script was written to transfer the points from the OpenCV contour detection into svg curves. The algorithm was provided with 20 contours to create each wall. On average, it placed 12 stones with an infill rate of 32% (see Table 22). The tolerance recommended by Marshall & Grangeot (2024) translates to 2mm in a 1:10 scale. However, the algorithm did not produce infills lower than 33% with that tolerance. Therefore, the distance between the rubble was set to 1 mm. As outlined in the literature review, the Squeeze optimisation utilises most of each sheet and enables irregular shapes, such as the inclusion of windows (DeepNest, 2025). Therefore, it was chosen as the optimisation setting for all arrangements. The nesting algorithm therefore achieved more evenly distributed arrangements and fewer mortar hotspots on the top than the stacking arrangements. The algorithm was also used for several arrangements in Phase 2 (3.6.2), where the database was further reduced.

3.6.2. Findings

	Max Stress	Min Stress	Avg Stress	SD Stress	SD Stress %	Max Strain at Failure	Min Strain at Failure	Avg Strain at Failure	SD Strain at Failure	SD Strain at Failure (%)
Stacking	7.3 MPa	4.7 MPa	5.7 MPa	1.2 MPa	21%	3.3%	1.3%	2.4%	0.8%	35%
Nesting	7.2 MPa	6.5 MPa	6.8 MPa	0.3 MPa	4%	1.4%	1.1%	1.2%	0.1%	11%
Infill	7.1 MPa	4.9 MPa	6.2 MPa	0.9 MPa	15%	12.9%	6.4%	10.5%	2.5%	24%
Rubble	29.3 MPa	21.2 MPa	24.7 MPa	3.3 MPa	13%	12.9%	9.0%	10.7%	1.5%	14%

Figure 78 Stress And Strain Per Algorithm Group

Rubble and Infill

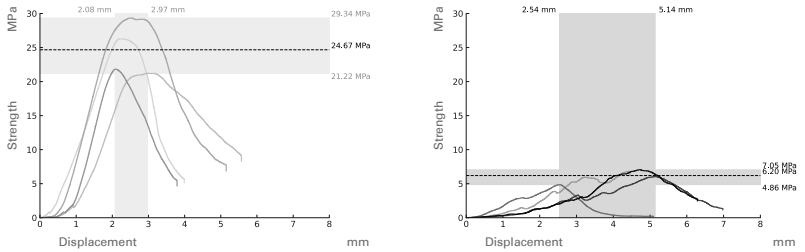

Figure 79 Stress-Strain Curve Rubble (left) and Infill (right)

The Rubble group represents four material samples, taken while the rubble was poured. The left graph in Figure 79 shows their stress-strain profile. With 25 MPa, they demonstrated the highest average maximum compressive strength among all tested materials. The right graph represents four specimens from the infill group, taken on the day the wall samples were cast. They exhibited a significantly lower compressive strength of 6.2 MPa and higher deformation. Furthermore, the spread of deformation is also higher, and the flatter curve shows a less brittle behaviour compared to the rubble.

Stacking Algorithm

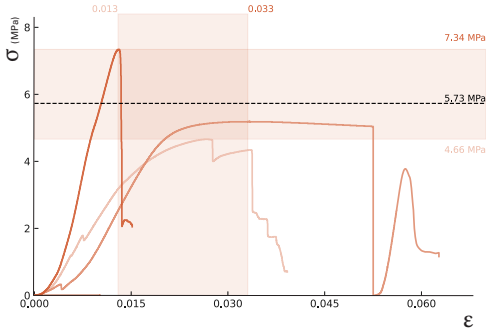

Figure 80 Stacking Stress-Strain Results

The walls arranged with the stacking algorithm exhibited a significant variability in strength. S1 demonstrated the highest strength with 7.34 MPa, and S3 the lowest with 4.66 MPa. Walls S3 and S2 were tested with a 4 mm-thick steel profile beam to spread the load evenly. The beam deformed by 1mm during the loading of S3, but started deforming completely during the loading of S2. The replacement steel beam did not distribute the load evenly, resulting in a decreased contact area. Therefore, it was exchanged with the 40x40mm full steel beam used for the rest of the experiments.

Figure 81 S2 Load Test: Bent Steel Profile (left) Point Load (right)

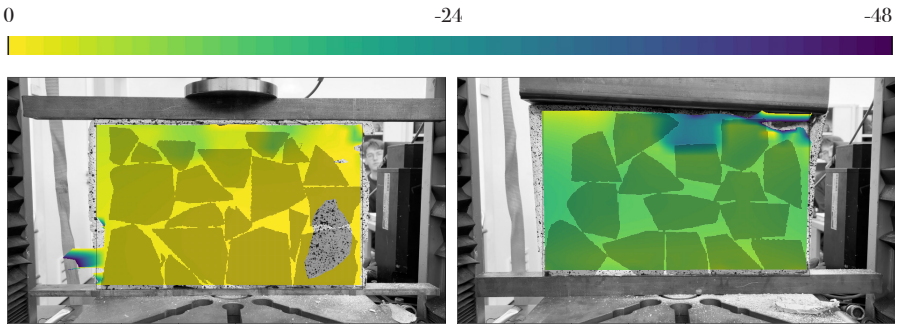

Figure 82 Displacement S1 (left) and S3 (right)

The DIC displacement images for Walls S1 and S3 show the deformation and strain within the top part of the wall. Figure 82 clearly shows an increased deformation of the wall before failure and a more ductile behaviour than S1, which is confirmed by the stress-strain curve. For both walls, the deformation is concentrated in the infill areas at the top, where the mortar hotspots lie. As the only wall in all experiments, the beam for S3 skewed towards the bottom right. As this beam deformed during the next test of S2, it cannot be determined whether the deformation was due to the arrangement of the spreader beam.

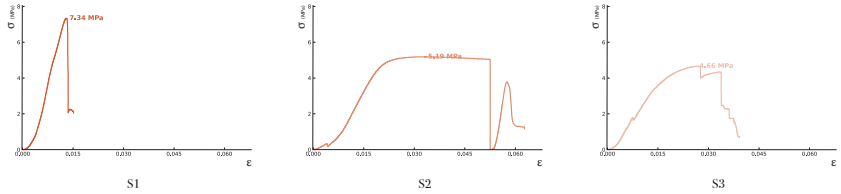

Figure 83 Stress-Strain S1-3

Nesting Algorithm

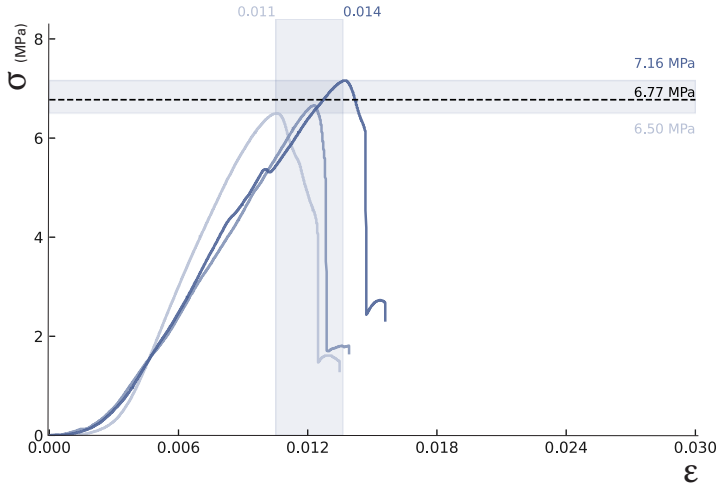

Figure 84 Nesting Stress-Strain Results

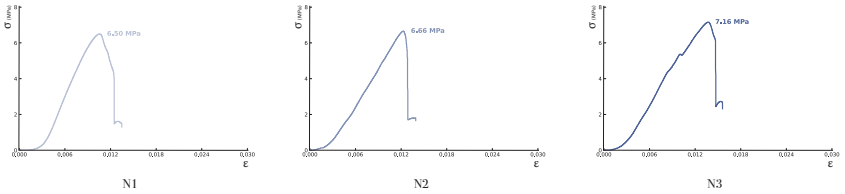

Figure 85 Stress-Strain N1-3

The Nesting algorithm demonstrated consistent performance across the wall samples, with a standard deviation of 11%. All three walls show a clear quasibrittle behaviour with a steep initial slope and an immediate drop after failure. All specimens exhibited cracks at the ITZ, extending through the infill and the rubble, as shown in Figure 86. The videos suggest that the cracks are initiated within the infill on the top and that the ITZ fails second.

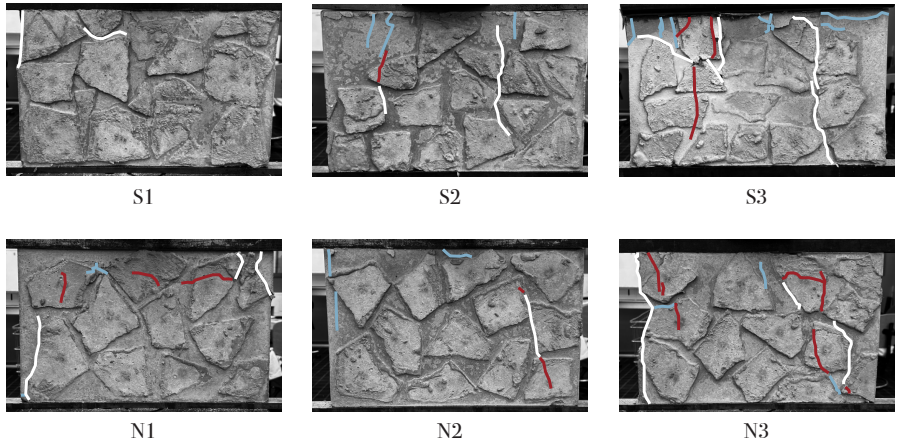

Figure 86 Cracks After Failure (White: At ITZ, Blue: Through Infill, Red: Through Rubble)

3.6.3. Discussion

The overall setup demonstrated a higher rubble strength than the infill, which was consistent with defining the wall's strength by the infill, similar to the strategy employed for the rubble masonry walls . The higher performance of the rubble was expected, as it was cast 14 days before the infill concrete and therefore had 21 days to cure. It outperformed the numbers provided by the manufacturer by 9MPa, even though the mixture had not yet cured for 28 days. This underlines the importance of the material tests on the day of testing the walls. The low deformation and comparatively low variability show the consistency anticipated by the mortar mix. The lower strength of the infill mortar was also expected due to its shorter 7-day curing time.

With the number of samples tested during the algorithm test, the results can only give an indication. Despite the technical issues during the loading of the stacking walls, the tests suggested that the nesting arrangements did not perform significantly worse than the stacking arrangements. Although they do not enforce structural constraints like the stacking algorithm, they were still able to achieve repeatable strength and deformation values in the three samples. This is especially notable considering that the algorithm operated on smaller rubble databases and did not prioritise interlocking.

The results for S3 and S2 should be treated with caution. With the insufficient strength of the spreader beam, they are not directly comparable to S1. The failure of S2 is not representative, as the replacement beam did not distribute the loads evenly. Whether the large deformation on the left of S3 is linked to the beam or the arrangement cannot be determined with certainty. The large mortar hotspot at the point of failure suggests that the arrangement was the cause.

The small stones available were depleted during the bottom-up placement sequence. As a result, infill concentrations increased in upper wall regions, introducing weaker zones in S2 and S3. S1 showed fewer mortar hotspots on the top. This could have contributed to the more brittle nature of S1 and its higher strength compared to S3.

The variability in these results suggests that while stacking can be structurally sound, its performance is sensitive to the availability of appropriately sized rubble pieces and their spatial distribution.

Figure 87 One Part Of The Stones Scanned For The Algorithm Tests

3.7. Test Phase 2 - Arrangements

3.7.1. Test Setup

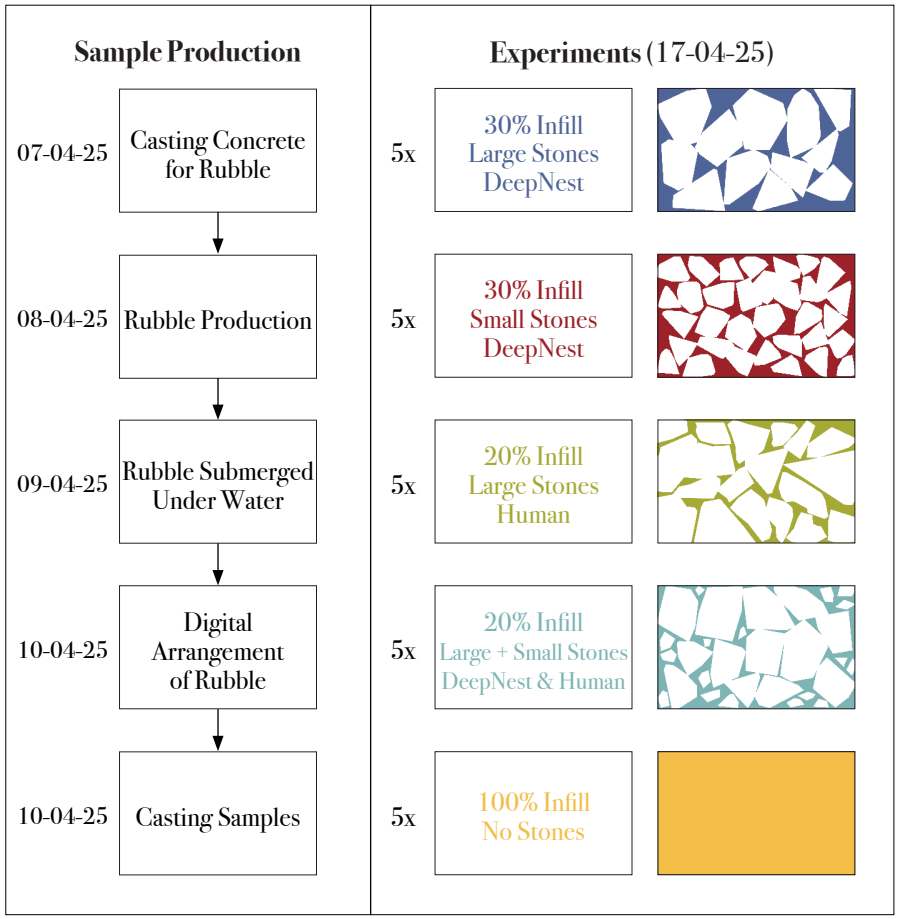

Figure 88 Experiment Setup Phase 2 - Arrangements

Wall Number	Arrangement	Arrrangement Type	smallest Rubble Size	largest Rubble Size	Database multiplier	Database Size	Infill %	Stones placed	Computing Time (minutes)
1		Large Stones	75 mm	150 mm	1.2	14	28%	12	07:18
2		Large Stones	75 mm	150 mm	1.4	14	30%	10	09:36
3		Large Stones	75 mm	150 mm	1.4	14	29%	10	10:24
4		Large Stones	75 mm	150 mm	1.4	14	32%	10	02:24
5		Large Stones	75 mm	150 mm	1.1	14	30%	13	07:04
6		Small Stones	25 mm	75 mm	1.1	40	33%	35	10:47
7		Small Stones	25 mm	75 mm	1.4	40	32%	29	02:51
8		Small Stones	25 mm	75 mm	1.3	40	33%	30	17:08
9		Small Stones	25 mm	75 mm	1.3	40	33%	30	08:12
10		Small Stones	25 mm	75 mm	1.1	40	34%	35	08:43
11		Manual	75 mm	150 mm	1.0	20	19%	20	n/a
12		Manual	75 mm	150 mm	1.0	17	22%	17	n/a
13		Manual	75 mm	150 mm	1.0	17	18%	17	n/a
14		Manual	75 mm	150 mm	1.0	19	22%	19	n/a
15		Manual	75 mm	150 mm	1.0	19	22%	19	n/a
16		Stone Infill	10 mm	150 mm	0.5	14	20%	30	04:56
17		Stone Infill	10 mm	150 mm	0.5	14	20%	30	17:29
18		Stone Infill	10 mm	150 mm	0.5	14	20%	31	07:12
19		Stone Infill	10 mm	150 mm	0.5	14	18%	26	02:39
20		Stone Infill	10 mm	150 mm	0.5	14	21%	29	12:04
21 - 25		No Rubble	0 mm	0 mm	n/a	n/a	100%	0	n/a

Figure 89 Wall Setup Phase 2 - Arrangements

Objectives:

I. Compare the influence of rubble diameters
II. Compare infill types
III. Assess Freedom of Rubble Placement
IV. Benchmark with unreinforced wall

The first test phase demonstrated that nesting algorithms have the potential to generate walls that are strong enough for load-bearing applications. Thus, the second phase assessed multiple arrangement types, which could be produced with small databases. The multipliers were therefore reduced to a maximum of 1.1 times the expected number of stones needed. The experiments then examined nesting arrangements with two different rubble diameters, which were compared to manual arrangements, a non-reinforced wall and the introduction of small rubble stones as infill materials. The findings from the first test phase indicate that the nesting algorithm does not exhibit a significant disadvantage compared to the stacking algorithm. Therefore, arrangements with the Stable Packing 2D algorithm are not included in this testing phase. To increase the sample size compared to the first phase, every wall arrangement was produced and tested five times (see Figure 90 below).

-- The experiments examined nesting arrangements with two different rubble diameters, which were compared to manual arrangements, a non-reinforced wall and the introduction of small rubble stones as infill materials. --

The following section explains the production of each arrangement and why it was included in the test.

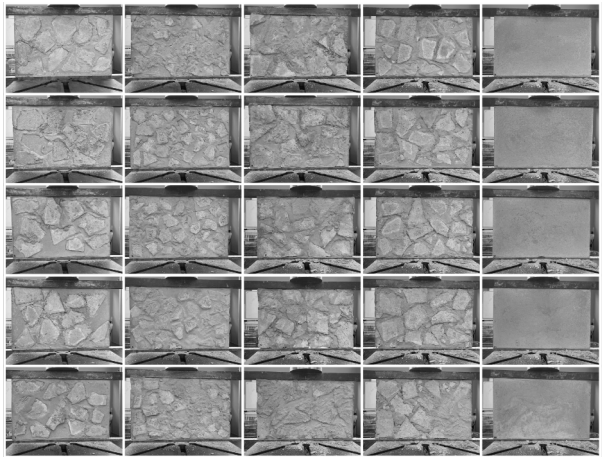

Figure 90 Wall Specimens

Large Stones

The first arrangement was produced in a similar way to the nesting arrangement of the algorithm test. The new variable in this testing phase was the diameter of the rubble. Therefore, the first arrangement only included rubble with a diameter between 75 mm and 150 mm. With this diameter, the wall arrangements fit a maximum of 13 rubble elements. In this round, the database size was further reduced to 14 stones, corresponding to approximately 1.1 times the maximum amount of rubble needed to fill the wall. This reduction was made after testing the algorithm's performance with several database sizes, which had no significant impact on its performance. The computation times were recorded, ranging from under 3 minutes to over 17 minutes (see Figure 89). The average time for all was 8 minutes and 30 seconds.

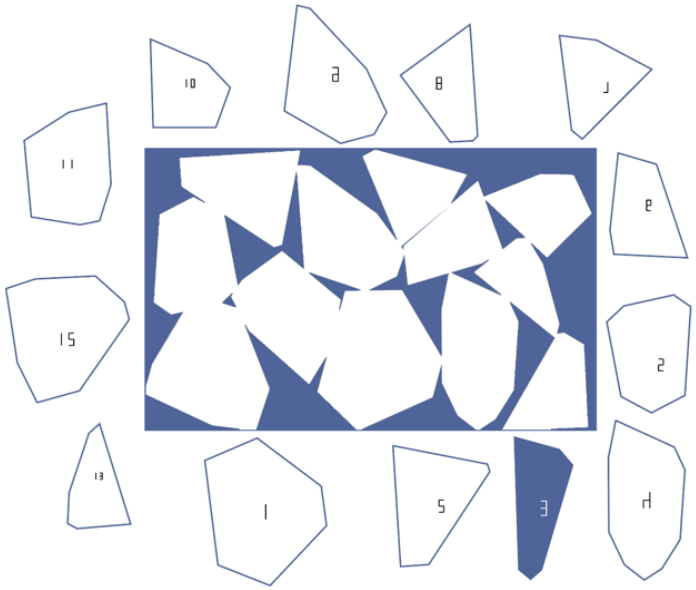

Figure 91 Nesting Process W1, 1.1 Multiplier, All Stones Were Placed Except For The Blue One

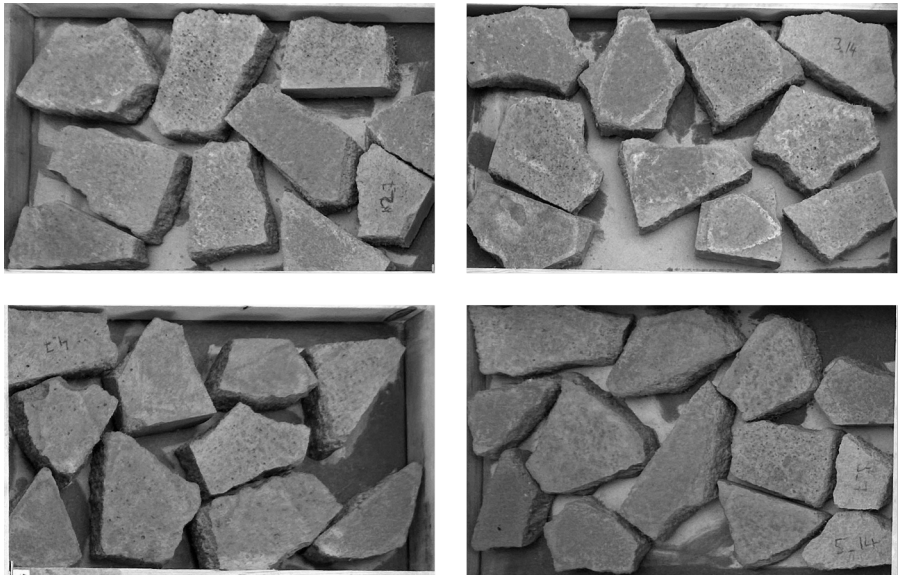

Figure 92 Nesting Large Stones Samples 2-5

Small Stones

Rubble with a diameter between 75 cm and 150 cm weighs between 210 kg and 850 kg, which poses a challenge for transport and handling. Therefore, CS Walls with smaller stone diameters were assessed and compared to those with larger rubble diameters. The sizes chosen are between 25 and 75cm, which translates to 25 - 75mm for the 1:10 experiments. The arrangement and production process are similar to the previous walls. The largest number of stones placed was 36 stones, which was translated to a 40-stone database with a 1.1 multiplier (see Figure 89, p. 77). The average number of stones placed was 32.

Although the lower weight is an advantage for smaller stones, the overall handling time is increased, as more rubble needs to be scanned, transported, and placed.

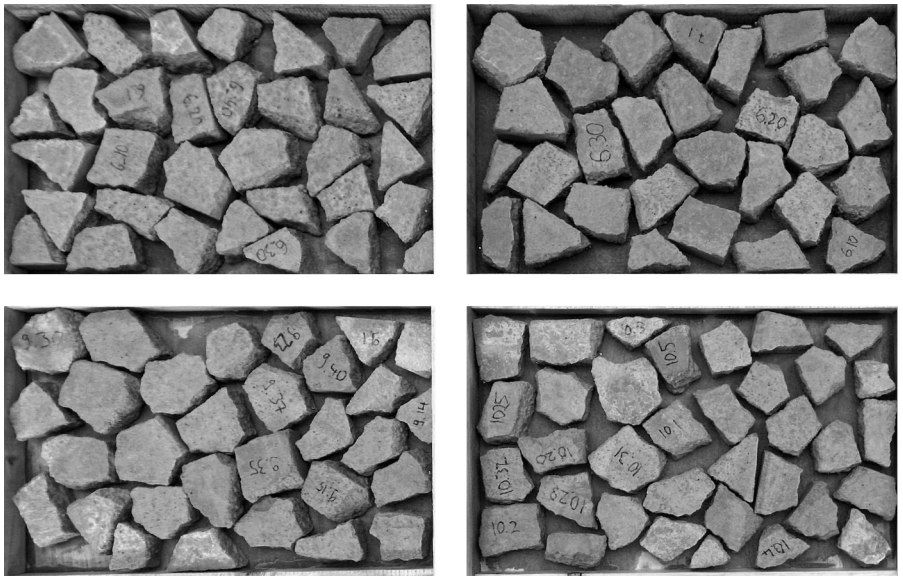

Figure 93 Nesting Small Stones Samples 7-10

Manual Arrangement

As neither the Stable Packing 2d nor the DeepNest produced walls with an infill rate below 28% in the database provided during this research, a manual process was implemented to create walls with a lower infill rate. This process showed that with an average of 20% virgin concrete infill, a human arrangement achieved a denser packing than the algorithms tested here. Additionally, the packing of the stones was realised by picking only one stone at a time, without the possibility to scan multiple shapes. The stones were picked up and immediately placed, which therefore translates to a multiplier of 1. The results of these arrangements are shown below in Figure 94. The rubble size for these arrangements ranges from 75mm to 150mm. This enabled the direct comparison of the wall performance to the Large Stones group and the Stones Infill group, which also use the same diameters.

-- As neither the Stable Packing 2d nor the DeepNest produced walls with an infill rate below 28%, a manual process was implemented to create walls with a lower infill rate. --

A tight fit between the stones was necessary to realise the low infill ratio. This left no tolerances and led to difficulties filling the virgin concrete in the gaps. This resulted in an insufficient infill between some stones. For future tests, a higher flowability of the virgin concrete is advised to realise an air-tight composite material.

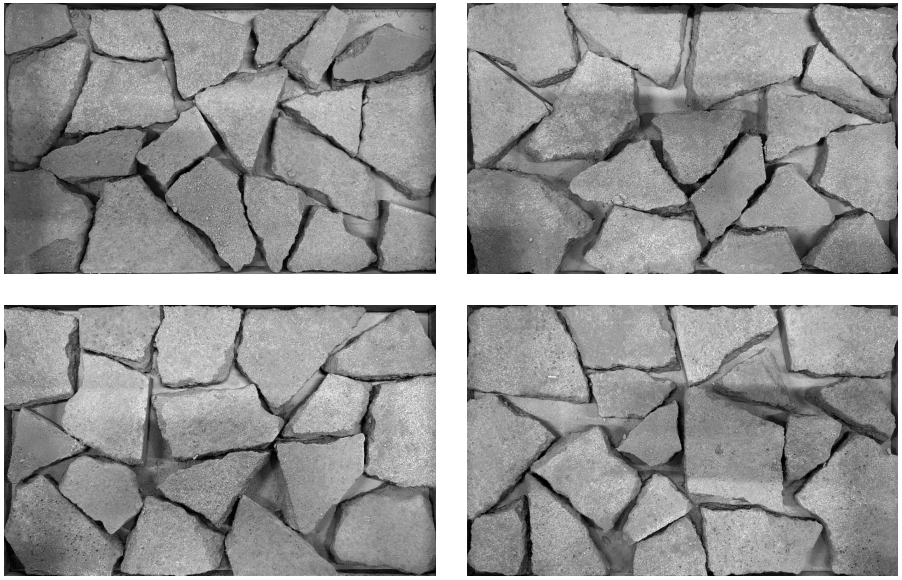

Figure 94 Manually Arranged Samples 11 - 14 (Arrangement Tests)

Stone Infill

This arrangement combined the procedure from the Large Stones group with a manual infill of smaller rubble in the gaps. The main rubble elements, with diameters from 75 mm to 150 mm, were arranged using the nesting algorithm. After these were placed, rubble pieces with a diameter of less than 25 mm were inserted into the remaining gaps to reduce the amount of virgin concrete required. The infill ratio reached an average of 20%, comparable to the manual arrangement. Similar to this group, the gaps were also more difficult to fill.

The inclusion of small stones can be handled algorithmically in theory. The scans at this scale proved unreliable, however, because the stones' diameters approached their thickness. The 2d contour, therefore, does not accurately represent the actual shape. For this reason, the small

stone infill was done by hand. While this introduced more variability and manual labour, it also demonstrated the potential of combining algorithmic and manual processes to achieve higher packing density and expressive outcomes. Visually, the addition of smaller stones introduced more variation to the wall texture and gave the surface a more animated appearance. This hybrid design could emphasise the spolia narrative within architectural applications, as it enables the inclusion of a broader range of fragments.

Visually, the addition of smaller stones introduced more variation to the wall texture and gave the surface a more animated appearance.

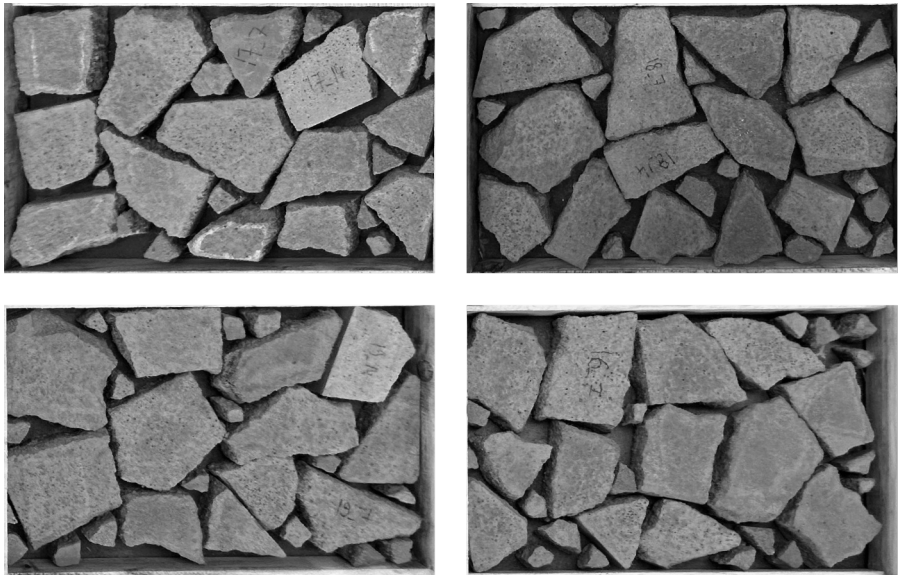

Figure 95 Stone Infill Samples 15 - 19 (Arrangement Tests)

No Rubble

To benchmark the performance of the Cyclopean Spolia Walls, a control group of solid concrete samples without integrated rubble was produced. These walls share the same dimensions as the other samples (400 × 250 × 22 mm) and were also cast with the same mortar. This group serves as a reference to understand the structural behaviour of a homogeneous wall of this scaled-down size. The results of this group also allow insights into the structural contribution of the rubble. A comparison of the stress-strain curves and failure patterns reveals the potential effectiveness of the rubble strategies. As the rubble is stronger than the infill, this helps to determine whether it acts as an inert filler or contributes to the wall's performance.

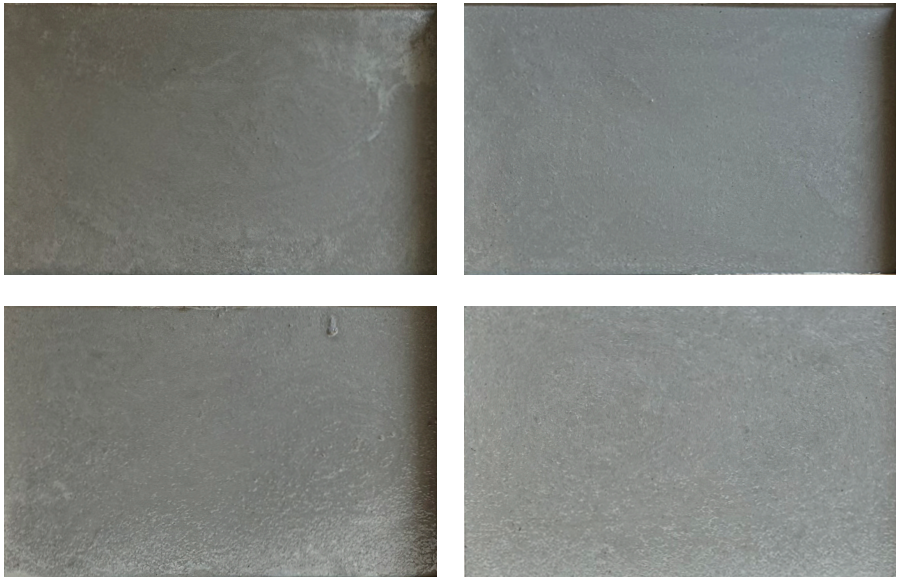

Figure 96 No Rubble Samples 22-25

3.7.2. Findings

The findings first analyse the stress-strain curves to examine general trends within the group results. The following sections then investigate the complete dataset for each sample. This includes arrangements, individual stress-strain curves, crack identification, DIC strain images and DIC displacement images.

Stress-Strain & Group Results

	Max Stress	Min Stress	Avg Stress	SD Stress	SD Stress %	Max Strain at Failure	Min Strain at Failure	Avg Strain at Failure	SD Strain at Failure	SD Strain at Failure (%)
Large Stones	7.4 MPa	4.4 MPa	6.0 MPa	1.1 MPa	18%	1.8%	0.8%	1.3%	0.4%	30%
Small Stones	6.7 MPa	5.0 MPa	5.8 MPa	0.6 MPa	10%	1.3%	0.9%	1.1%	0.1%	11%
Human	5.3 MPa	3.8 MPa	4.6 MPa	0.6 MPa	13%	1.8%	1.0%	1.5%	0.3%	20%
Stone Infill	7.3 MPa	3.9 MPa	6.0 MPa	1.2 MPa	20%	1.5%	0.8%	1.2%	0.2%	20%
No Rubble	7.0 MPa	4.8 MPa	6.2 MPa	0.8 MPa	13%	1.3%	0.7%	1.0%	0.2%	18%
Rubble	13.0 MPa	8.6 MPa	10.7 MPa	1.8 MPa	17%	5.7%	4.5%	5.0%	0.4%	8%
Infill	8.3 MPa	6.2 MPa	7.4 MPa	0.6 MPa	8%	6.8%	4.0%	5.1%	0.9%	17%

Table 23 Stress And Strain Per Arrangement Group

Together with Table 23, the charts displayed in Figure 97 show the stress-strain curves of the compression tests. The saturation of the curve indicates the performance of the specimen in relation to its group, where the sample with the highest peak stress displays the highest saturation. In Figure 97, the individual curves are placed on top of each other. The coloured horizontal region shows the maximum and minimum ultimate stress of each group. The vertical region displays the strain at these points and indicates when the maximum was reached.

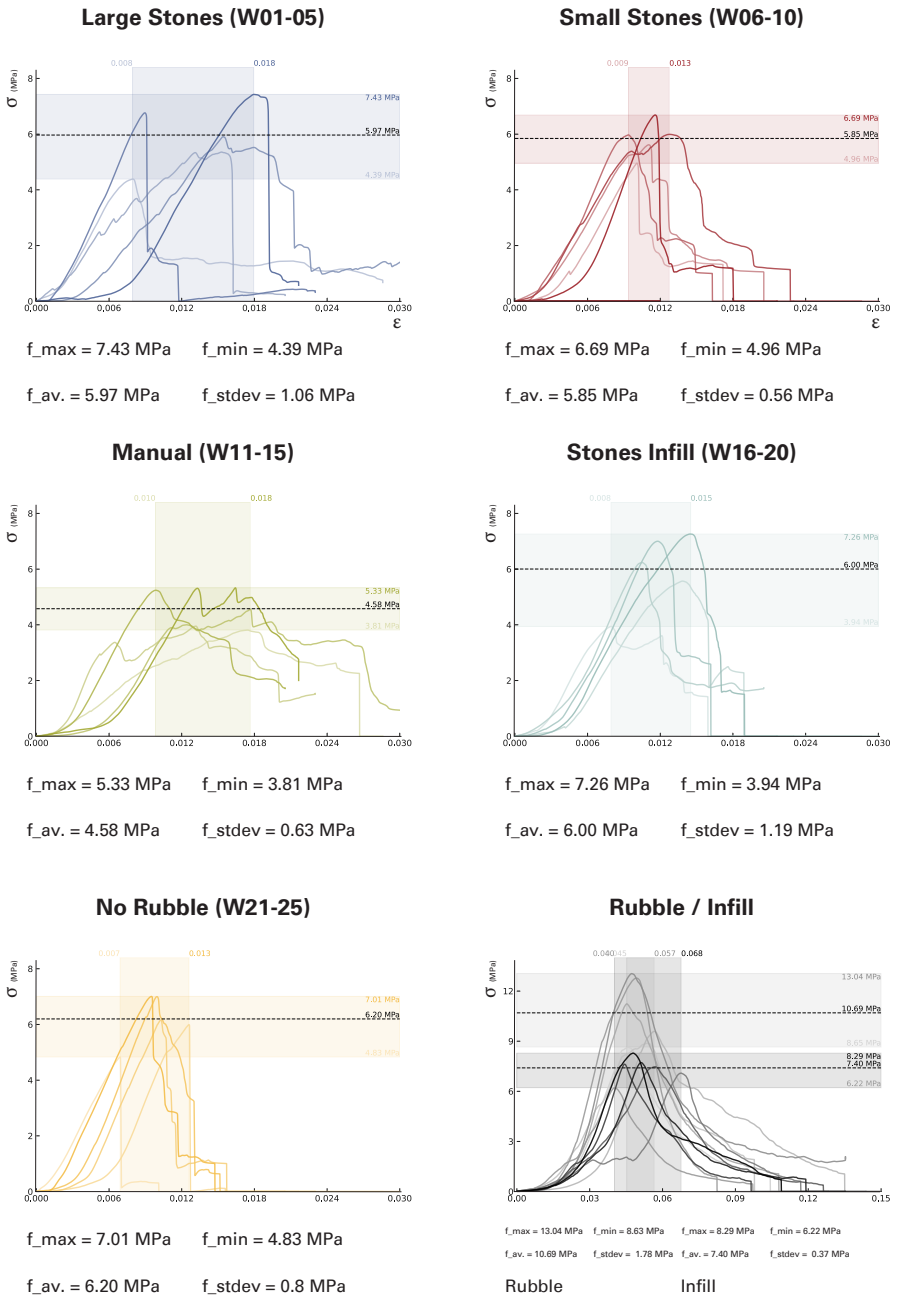

Figure 97 Stress-Strain Curves For All Groups

The results show that the rubble was the strongest material in the composite, with an average strength of nearly 11 MPa, about 5% higher than that of the infill material.

The walls without rubble represent unreinforced concrete walls and are the baseline for the other wall groups. The average peak stress of 6.20 MPa therefore serves as a comparative value. Its standard deviation of stress is relatively low, at 13%. The average strain at failure was 1% and represents the lowest value among all groups. The steep initial slope indicates a high modulus of elasticity. The steep decline of the force after the fracture point demonstrates the brittle nature of the mortar.

With an average strength of 6.0 MPa and a peak value of 7.4 MPa, the Large Stones group displayed a robust performance. However, the standard deviation and the graphs show that the range between the samples was relatively high compared to the others. The peak stress of sample W4 is 40% lower than the highest stress, which occurred in W5. The average strain was 1.3, slightly higher than Stone Infill, indicating a less brittle behaviour. With 1.3%, the Large Stones group is the only group which shows a higher average strain at maximum load than the other groups.

The Small Stones group, with rubble diameters between 25–75 mm and thus more stones in the composite, showed a slightly lower average strength of 5.8 MPa and a maximum of 6.7 MPa. Nevertheless, with 10% it demonstrated the lowest standard deviation of all groups and the lowest range of peak strengths. These values are even lower than the control walls without rubble. The average strain was 1.1% and exhibited a relatively small spread. The curve shapes consistently show a steep rise, indicating a quasibrittle material and the post-peak behaviour confirms that. The drop is not as sudden as in the no-rubble walls, though.

The walls assembled manually exhibited the lowest average compressive strength of 4.6 MPa. The standard deviation for strength is relatively low, at 13% compared to the other groups. Furthermore, these arrangements exhibited the highest peak strain values, similar to those of the Large Stones group, which indicates a more ductile behaviour. The curve shapes of the manual arrangements were the only ones to consistently show a wavy pattern with multiple peaks. This behaviour could only be slightly observed for W2 (Large Stones) and W19 (Stones Infill), even though these curves do not show such flat slopes.

Lastly, the Stone Infill group demonstrated the highest average peak stresses among the rubble arrangements. With a compressive strength of 6.0 MPa, the walls nearly match the No Rubble reference group. Its maximum strength reached 7.3 MPa, but this group shows the highest stress variability of all groups with a standard deviation of 20%. This is primarily due to the outlier W19, which also exhibits a distinct curve shape compared to the other stones.

Overall, clear quasibrittle behaviour comparable to that of the No Rubble group could only be observed for individual walls in the Large Stones, Small Stones, and Stones Infill Groups. Otherwise, most of the arrangement walls showed less brittle behaviour than the control group.

As the arrangement methods generate a multitude of stone configurations, an individual analysis of the data captured for the walls is necessary. The following section therefore assesses the visual displacement, visual strain, crack patterns and the stress-strain curves and analyses them according to the arrangement of the samples.

Large Stones Arrangements
W1 - W5

Method: DeepNest

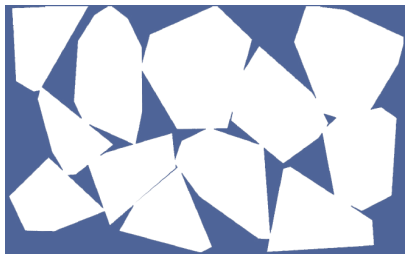

W1

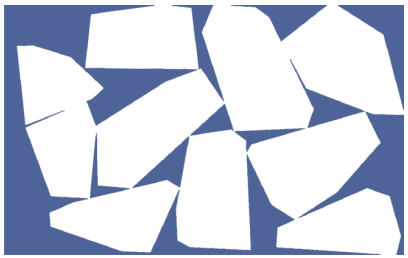

W2

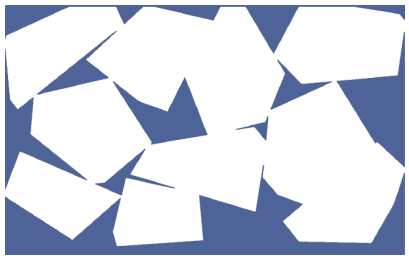

W3

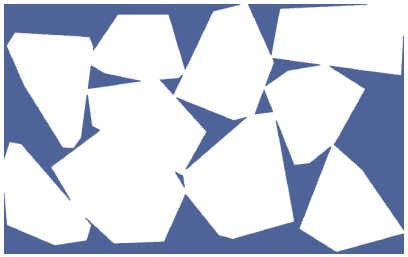

W4

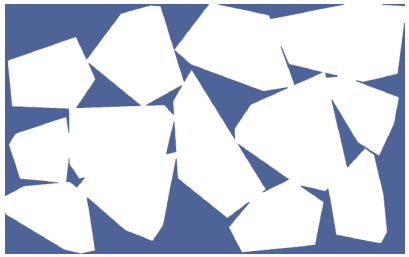

W5

Figure 98 Large Stones Arrangements

Large Stones Stress/Strain
W1 - W5

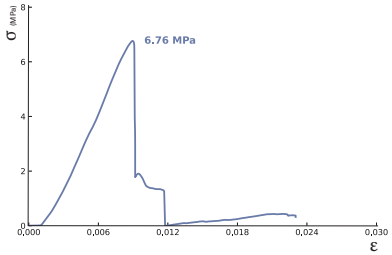

W1

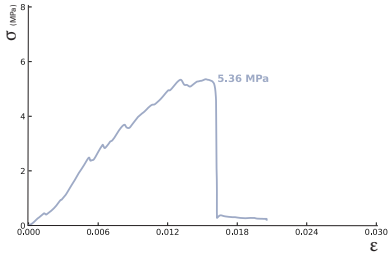

W2

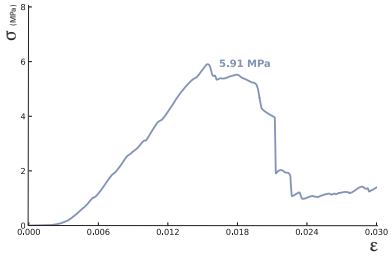

W3

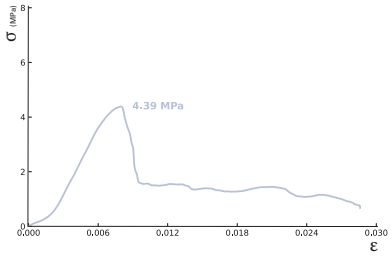

W4

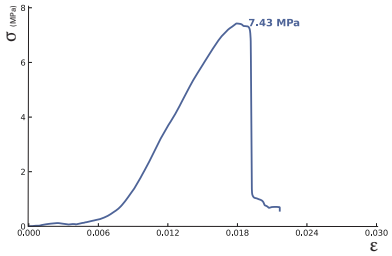

W5

Figure 99 Large Stones Stress-Strain Curves

Large Stones Cracks
W1 - W5

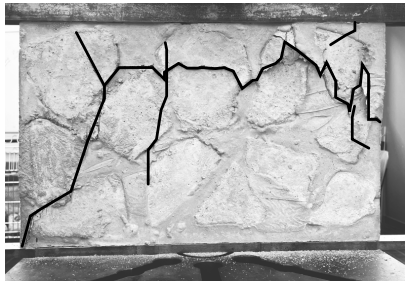

W1

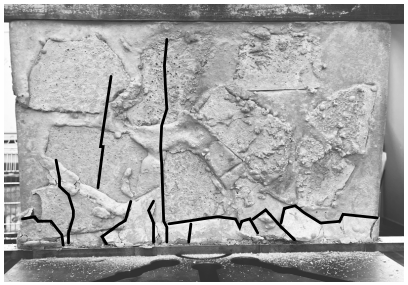

W2

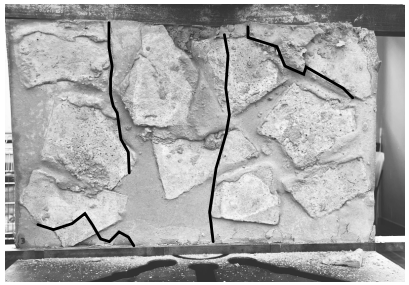

W3

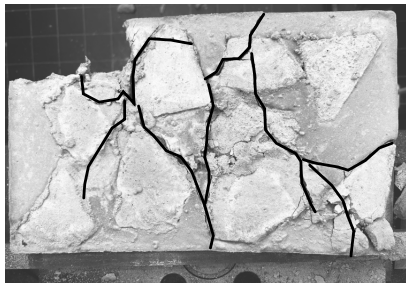

W4

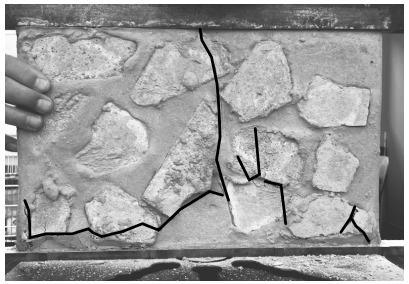

W5

Figure 100 Large Stones Crack Patterns

Large Stones Displacement
W1 - W5

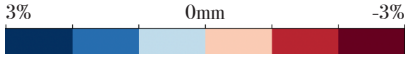

Displacement Legend

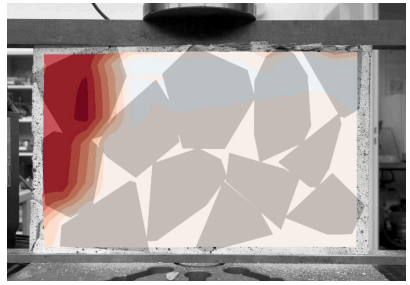

W1

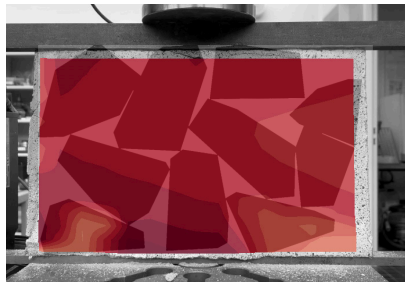

W2

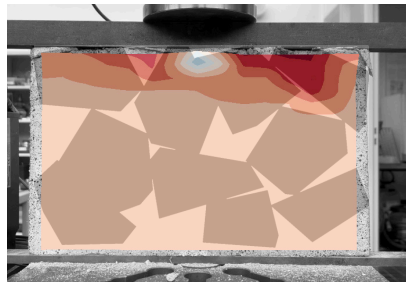

W3

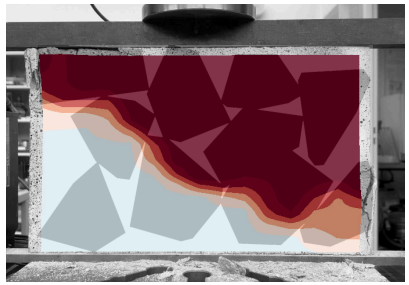

W4

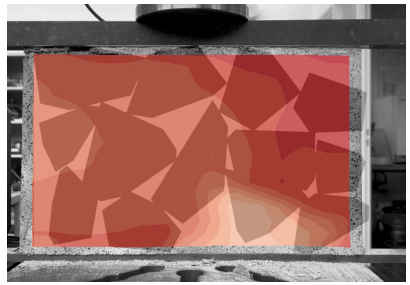

W5

Figure 101 Large Stones Displacement

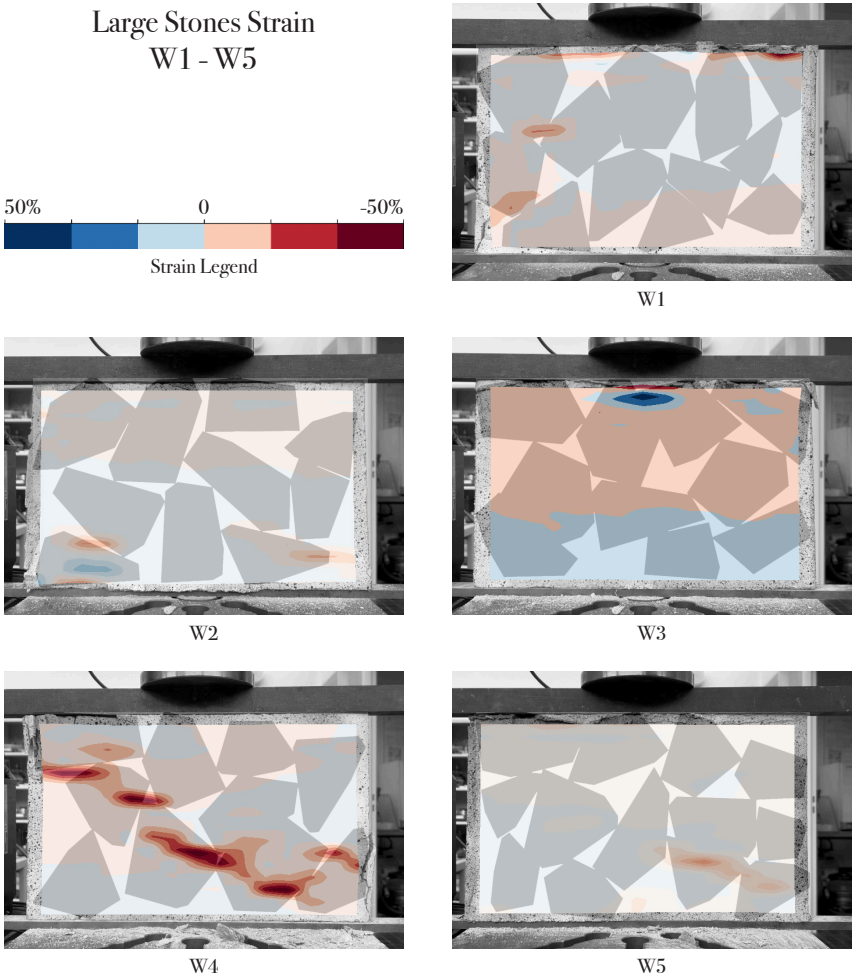

Figure 102 Large Stones Strain

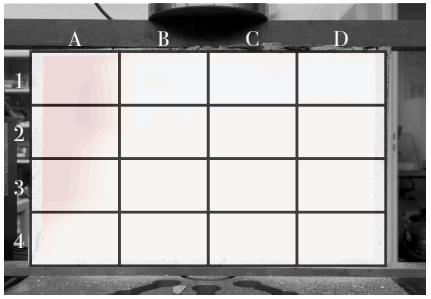

Figure 103 Regions Within The Samples Used Throughout The Analysis

Sample	Peak Stress	Peak Strain	Height
Large Stones W1	6.76 MPa	0.9%	250
Large Stones W2	5.36 MPa	1.5%	250
Large Stones W3	5.91 MPa	1.5%	250
Large Stones W4	4.39 MPa	0.8%	250
Large Stones W5	7.43 MPa	1.8%	250

Figure 104 Peak Stress and Strain Large Stones Group

The displacement maps for the Large Stones group show the diversity of stress-strain behaviour previously mentioned. There is no coherent breakage pattern visible throughout the arrangements.

W5 resisted the highest peak stress and was the only wall which showed an initial compaction phase in the curve. This was caused by the compaction of the mortar in zone 1. The wall was then evenly compacted by 2%, until it failed in D4, with vertical crack initiation through the rubble and ITZ. W5's DIC maps show the most uniform displacement of all the walls.

W1 had the second highest strength. The failure was initiated by a crack that propagated at the ITZ of a stone in A3, which had only one contact

point and subsequently slid down, when the ITZ bond failed. The crack went through the shortest vertical path.

W3 shows the only wavy post-failure curve in the diagrams, which indicates further settling. It was primarily dominated by strains in row 1 and exhibited a strong displacement of the material there, which ultimately led to its failure at the ITZ in D1.

W2 showed similar uniform displacements to W5, and in contrast to the other walls, the highest strain values were observed in region 4. For W2, the crack initiation was vertical and at an ITZ in B4. It propagated through a rubble stone in C2 before failure. The final failure happened in A4 through two rubble stones.

W4, on the other hand, demonstrated the lowest strength and underwent a horizontal slide, characterised by a high strain of up to -50% between the rubble. The crack did not follow the shortest path.

Small Stones

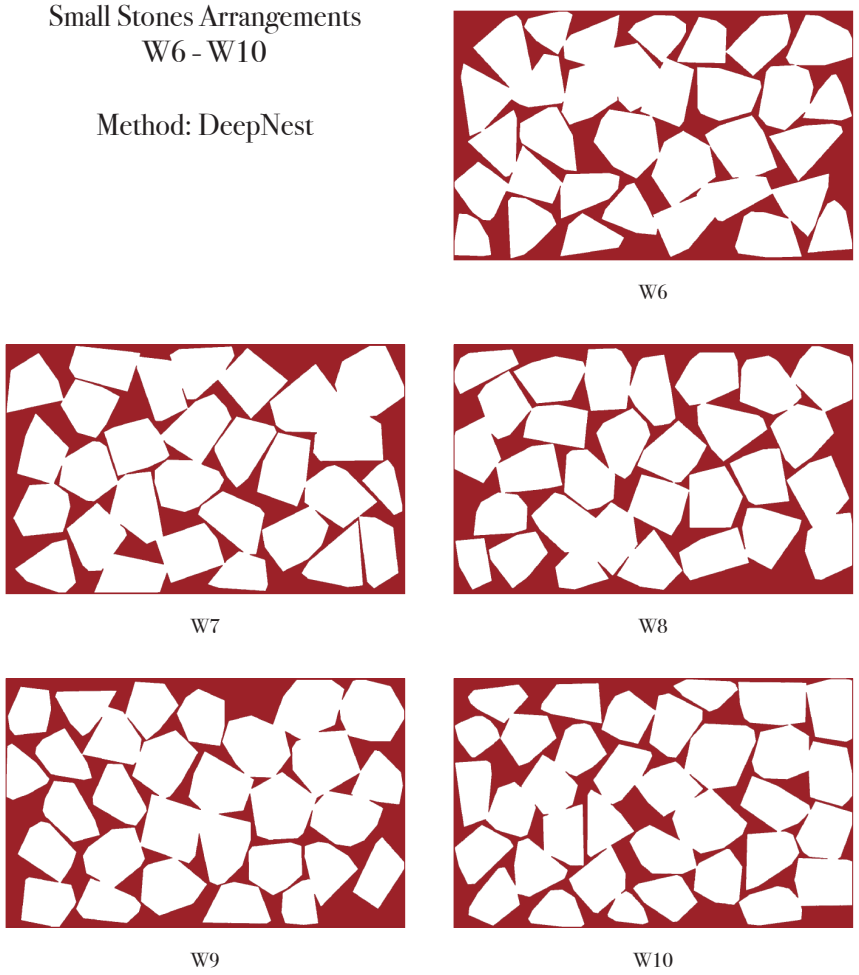

Figure 105 Small Stones Arrangements

Small Stones Stress/Strain
W6 - W10

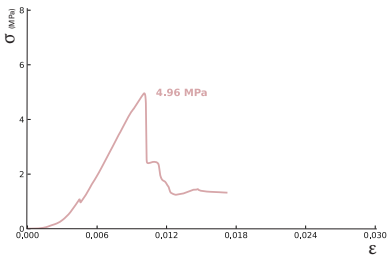

W6

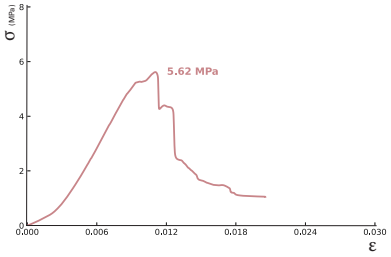

W7

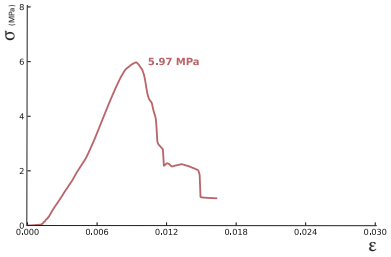

W8

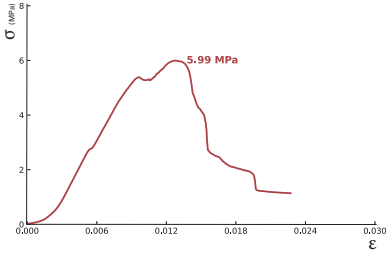

W9

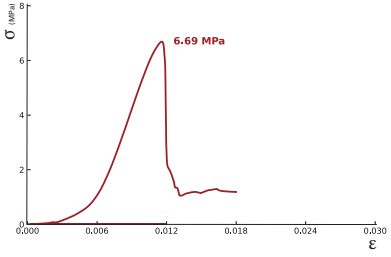

W10

Figure 106 Small Stones Stress-Strain Curves

Small Stones Cracks
W6 - W10

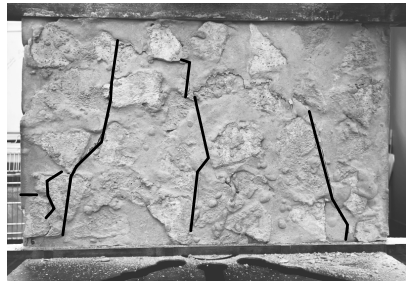

W6

W7 n/a

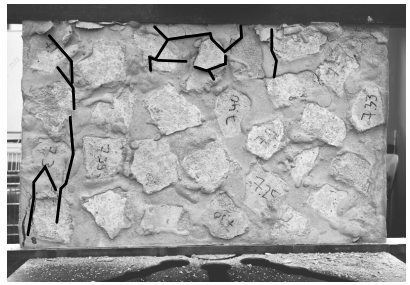

W8

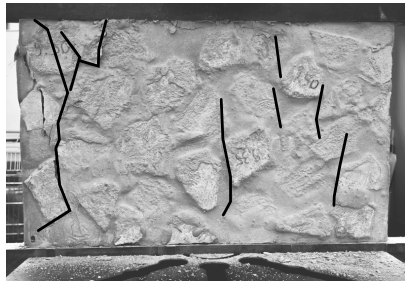

W9

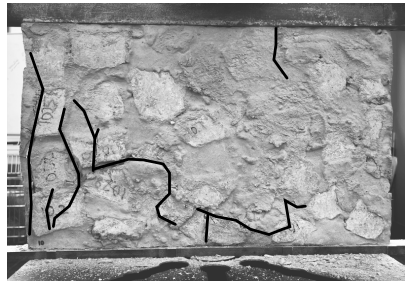

W10

Figure 107 Small Stones Cracks

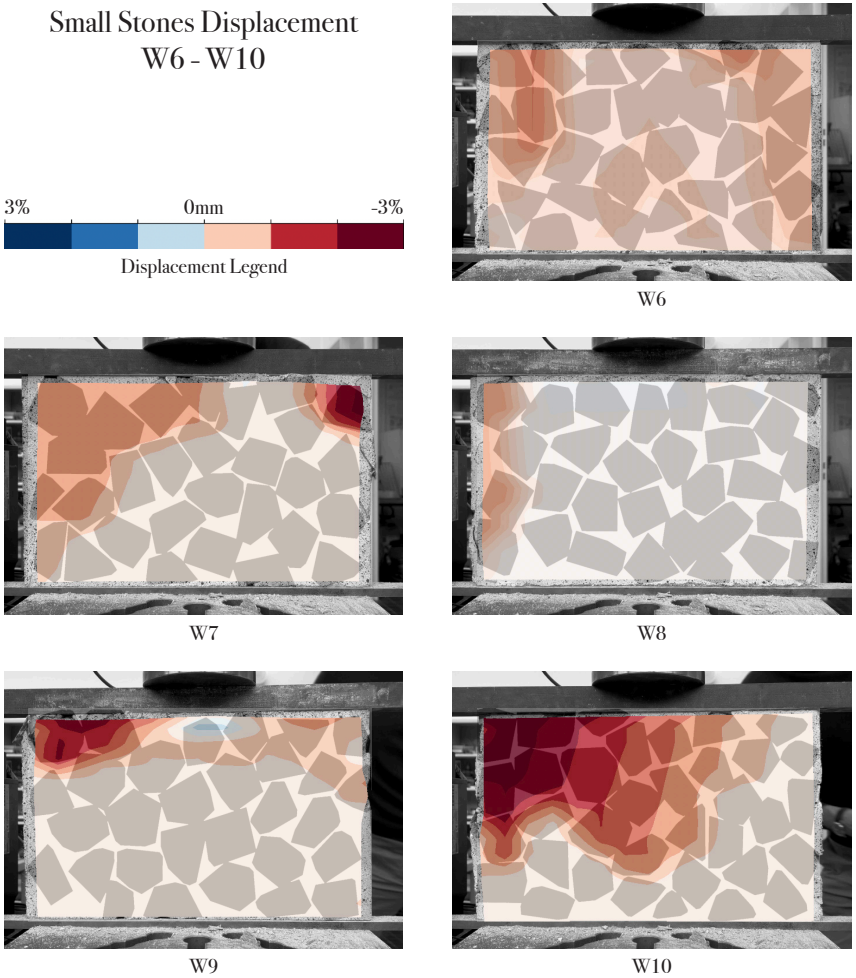

Figure 108 Small Stones Displacement

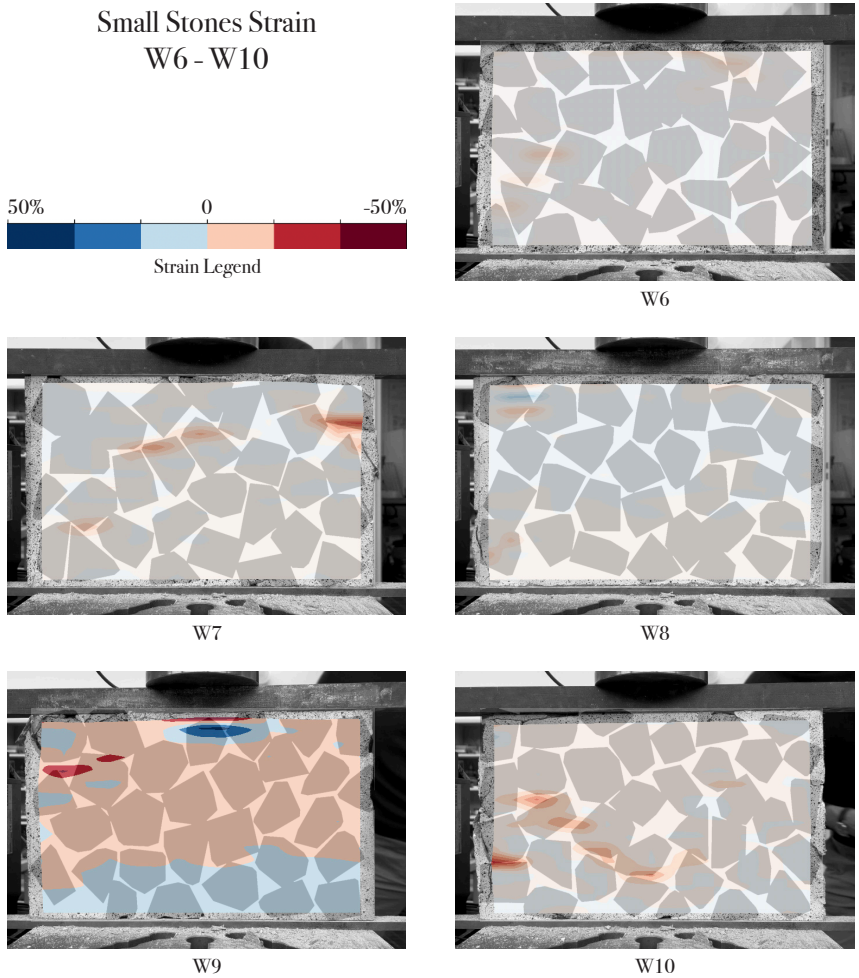

Figure 109 Small Stones Strain

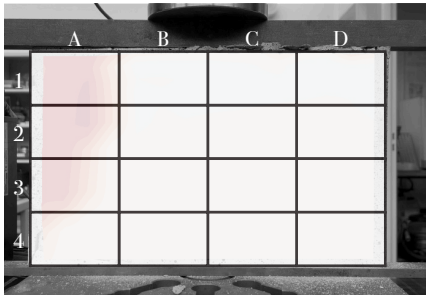

Figure 110 Regions Within The Samples Used Throughout The Analysis

Sample	Peak Stress	Peak Strain	Height
Small Stones W6	4.96 MPa	1.0%	250
Small Stones W7	5.62 MPa	1.1%	250
Small Stones W8	5.97 MPa	0.9%	250
Small Stones W9	5.99 MPa	1.3%	250
Small Stones W10	6.69 MPa	1.2%	250

Figure 111 Peak Stress and Strain Small Stones Group

The small stones group shows the least variability in peak stress and in peak strain. The displacement and strain maps reveal multiple regions of failure.

W10, which resisted the highest peak stress, demonstrates displacements of more than 3% in approximately one-quarter of the wall, with strain peaks of around 20%. Its failure was initiated by a horizontal crack at the ITZ, where the infill and rubble separated. W9 and W8 showed a similar peak stress, and both failed due to strains in region A, which caused cracks through the ITZs at the shortest vertical path. W7 misses a photo for the final crack propagation, as it fell from the UTM while unloading. It failed due to an ITZ crack in D1, resulting from a stone with only one contact point. Post failure, large cracks propagate vertically through Zone B. W6 shows less displacement and stresses than the other samples. It failed due to a vertical crack through the rubble and ITZ.

All samples failed due to stones in either zone A or D, in contrast to the Large Stones group, which exhibited sliding in different regions of the geometry. The walls all show quasibrittle behaviour. Additionally, none of the samples had an area of more than 30% slip away, unlike what was observed in the Large Stones arrangements. The slips are confined to the smaller regions. Similar to the previous group, the cracks primarily form at the ITZ and subsequently propagate through the rubble.

Manual Arrangements
W11 - W15

Method: Manual

W11

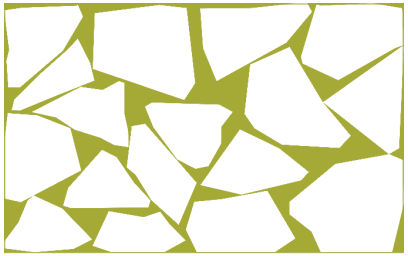

W12

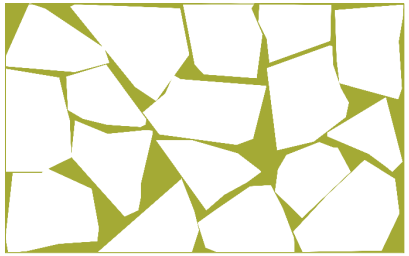

W13

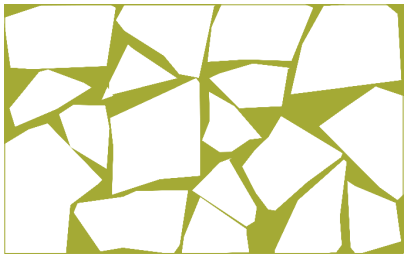

W14

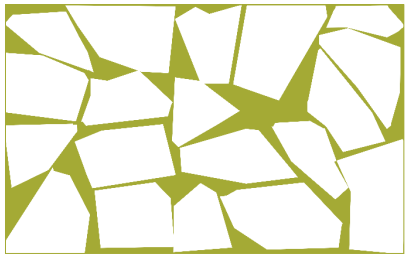

W15

Figure 112 Manual Arrangements

Manual Arrangement Stress/Strain
W11 - W15

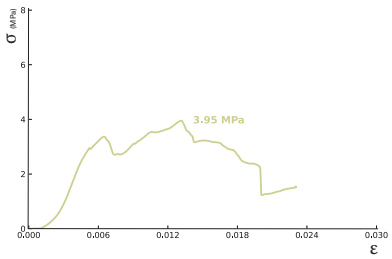

W11

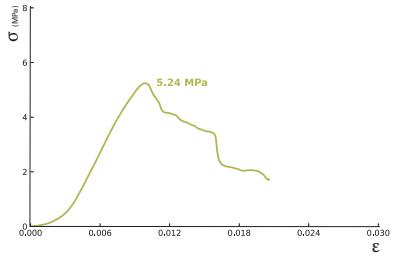

W12

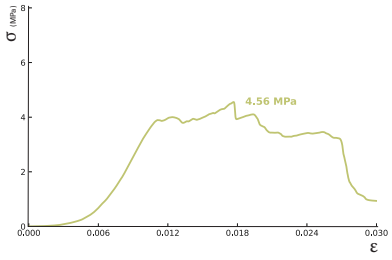

W13

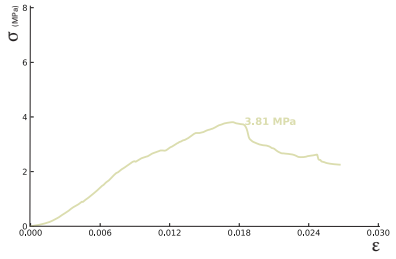

W14

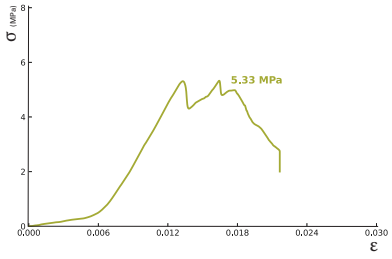

W15

Figure 113 Manual Arrangements Stress-Strain Curves

Manual Arrangement Cracks
W11 - W15

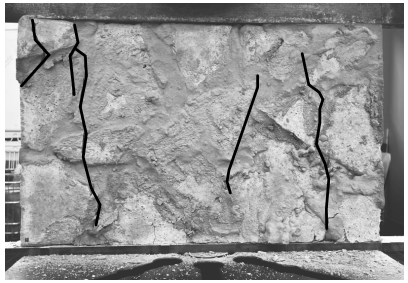

W11

W12

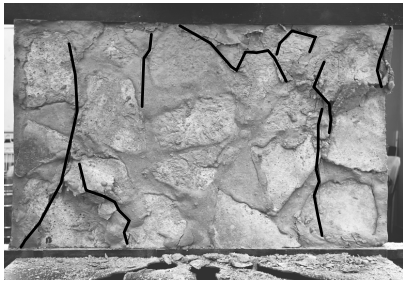

W13

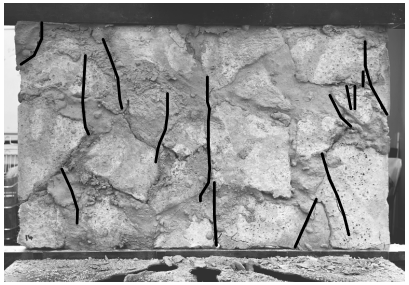

W14

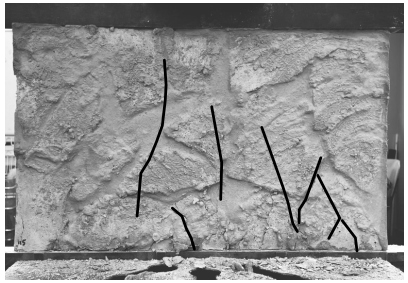

W15

Figure 114 Manual Arrangements Cracks

Manual Arrangement Displacement
W11 - W15

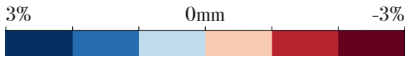

Displacement Legend

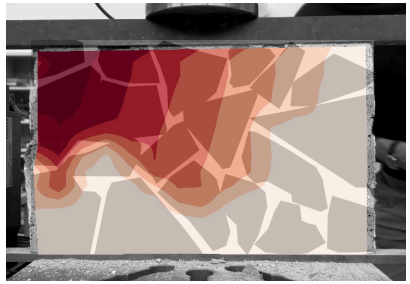

W11

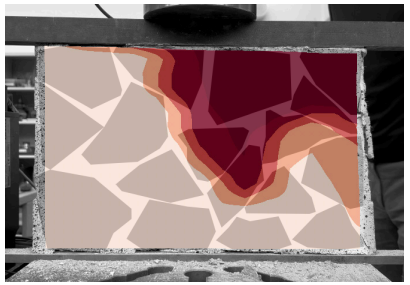

W12

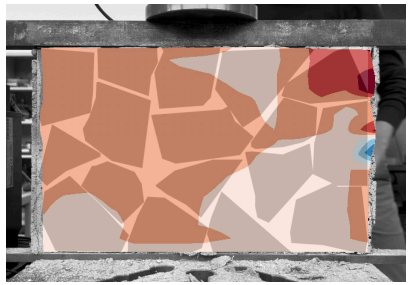

W13

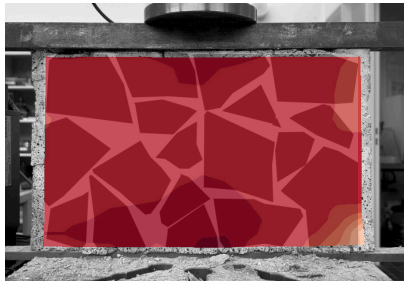

W14

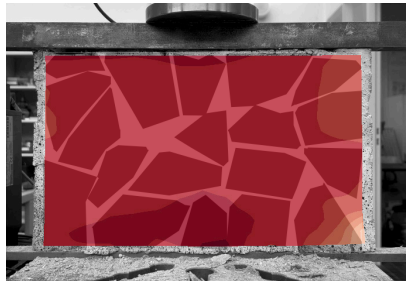

W15

Figure 115 Manual Arrangements Displacements

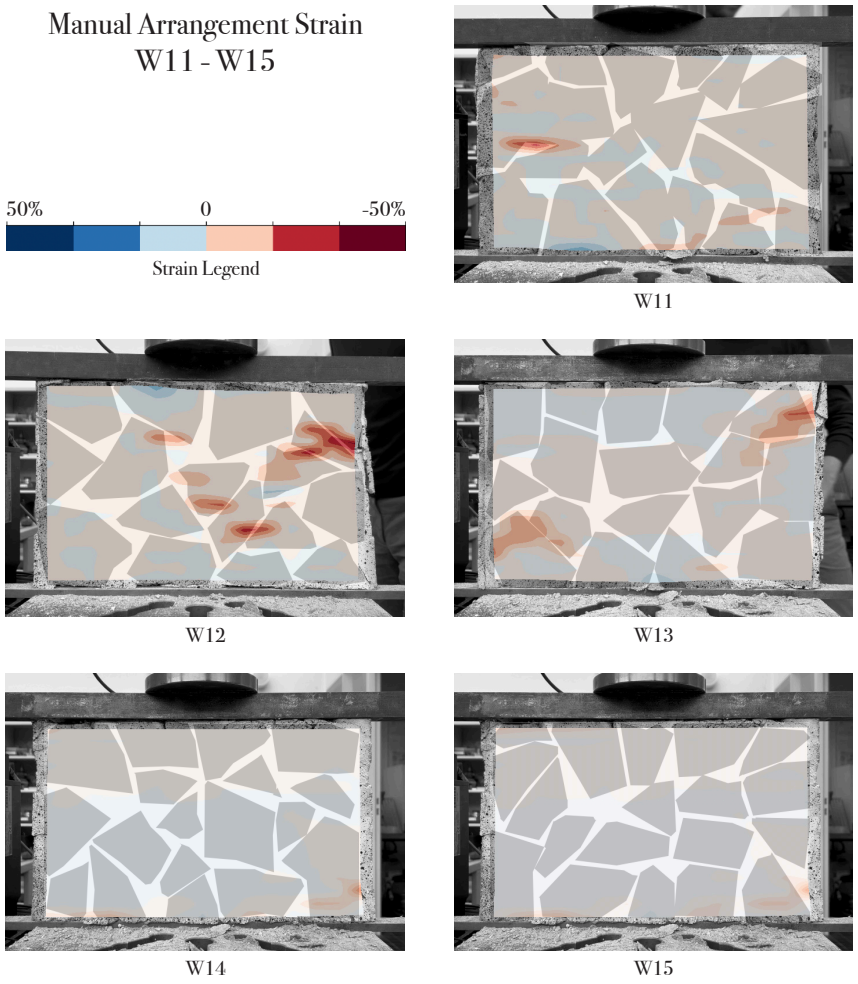

Figure 116 Manual Arrangements Strain

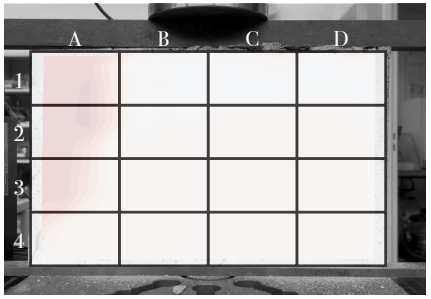

Figure 117 Regions Within The Samples Used Throughout The Analysis

Sample	Peak Stress	Peak Strain	Height
Manual W11	3.95 MPa	1.3%	250
Manual W12	5.24 MPa	1.0%	250
Manual W13	4.56 MPa	1.8%	250
Manual W14	3.81 MPa	1.7%	250
Manual W15	5.33 MPa	1.6%	250

Figure 118 Peak Stress and Strain Small Stones Group

Due to the tight arrangement, the gaps between the stones were too small in some places for the fluidity of the infill concrete. As shown in Figure 119, some cavities were not completely filled. This is crucial for analysing the manual arrangement data.

The curves of all samples (except for W14) start with a steep slope, similar to the other quasibrittle groups. Then, all samples start a gradual post-peak decline and show compaction behaviour. For W11, W13, and W14, this does not result in a clear failure point. The curves indicate where the rubble breaks through the infill and then compacts again, thereby packing the rubble tighter. The displacements were therefore extremely high compared to the other groups. Even though their peak strength was reached at around a similar strain as the previous groups,

they resisted the forces for a longer time. The group still had an average strength of around 3 MPa at 20% strain, at a displacement when the other groups had all already failed. W13 even reached 28% of strain with a remaining strength of around 3 MPa.

In addition to the atypical behaviour of the group, two walls outperformed the others. W15 and W12 had the highest peak stresses, at 5.2 MPa and 5.3 MPa, respectively. Their curves showed the steepest initial slopes, indicating a higher modulus of elasticity. In contrast, W14 had the weakest strength and the most horizontal slope of all samples. Its bottom side is portrayed in Figure 119 below, in comparison with W15. It can be seen that it shows more unfilled gaps than the strongest wall.

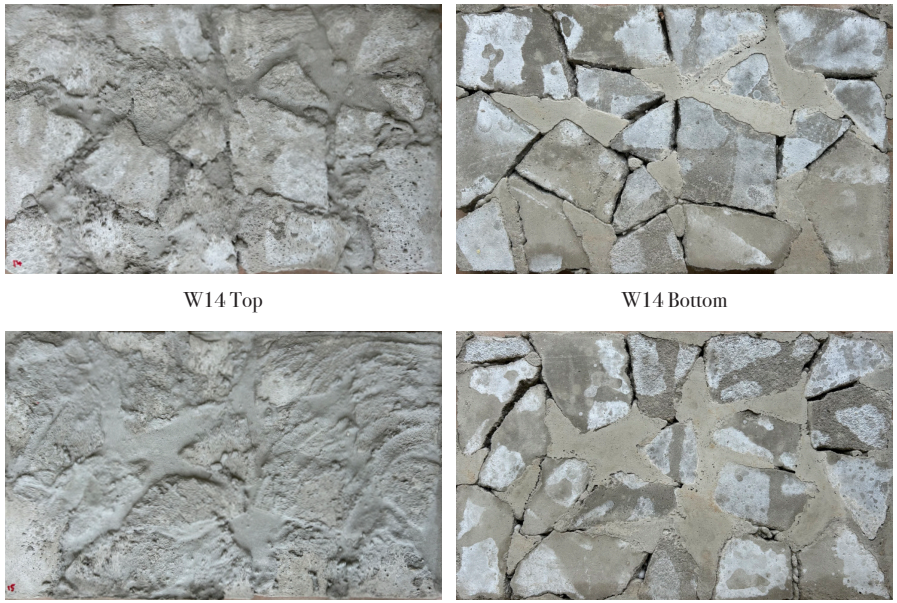

W14 Top | W14 Bottom

W15 Top | W15 Bottom

Figure 119 Unfilled Gaps Due To Tight Arrangement

W11-W13 show concentrated strains in the DIC maps at the interfaces of stones.

It was observed during the experiments that the walls lost overall stability and the bond between the stones weakened during loading. In contrast to the previous groups, the walls did not crack at distinct points or initiate with a single crack, which ultimately led to failure. They rather disintegrated and had no stability left after the test. This led to W12 falling out of the machine during unloading.

Stone Infill

Stone Infill Arrangements
W16 - W20

Method: DeepNest + Manual
Stone Infill

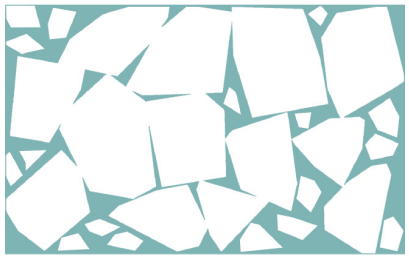

W16

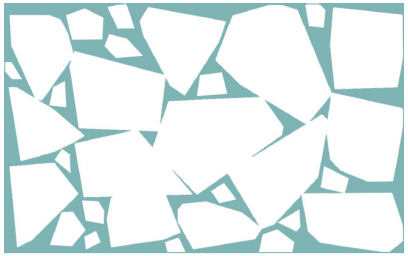

W17

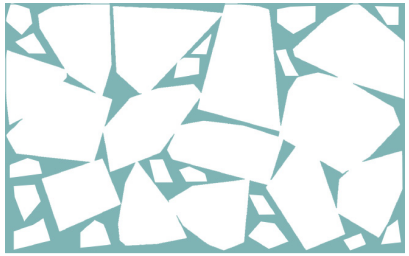

W18

W19

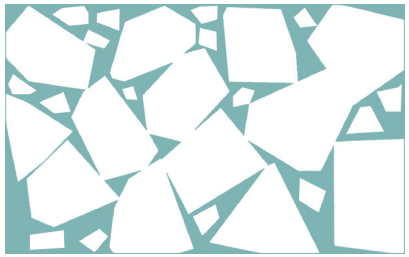

W20

Figure 120 Stone Infill Arrangements

Stone Infill Stress/Strain
W16 - W20

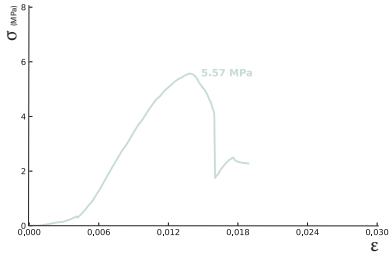

W16

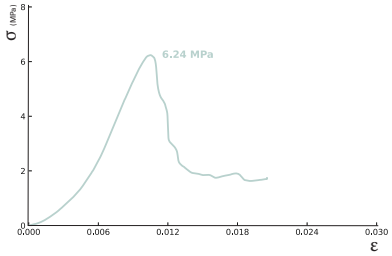

W17

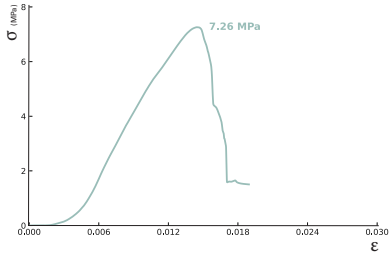

W18

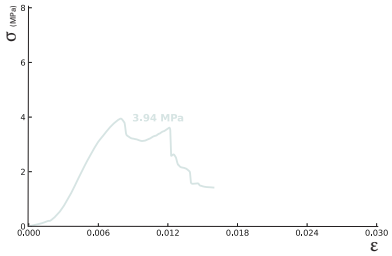

W19

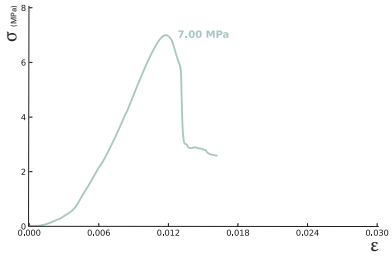

W20

Figure 121Stone Infill Stress-Strain Curves

Stone Infill Cracks
W16 - W20

W16

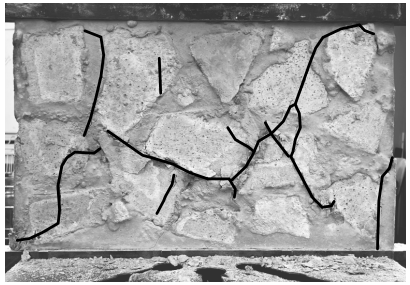

W17

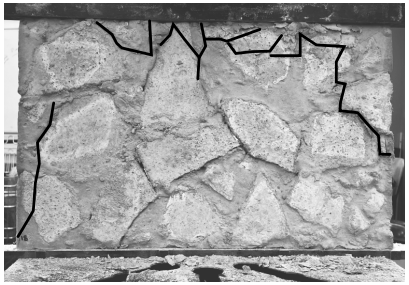

W18

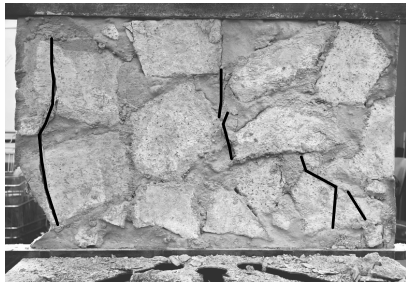

W19

W20

Figure 122 Stone Infill Cracks

Stone Infill Displacement
W16 - W20

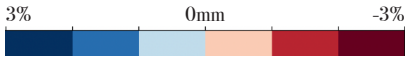

Displacement Legend

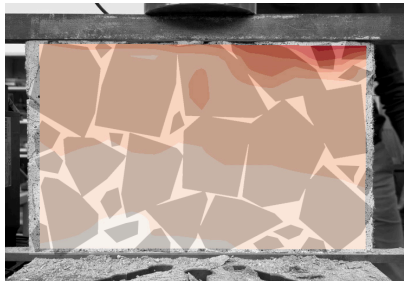

W16

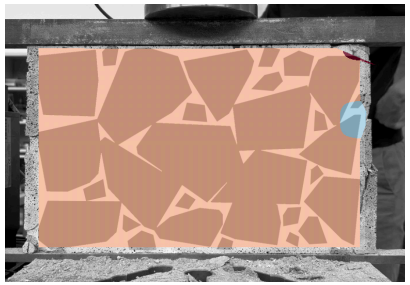

W17

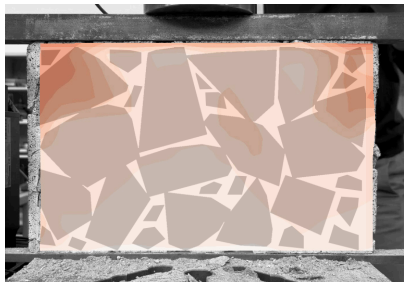

W18

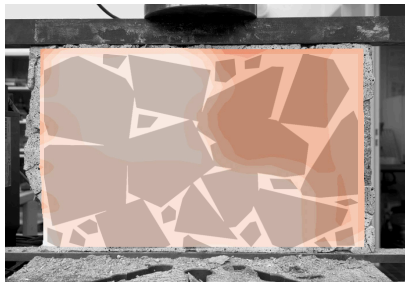

W19

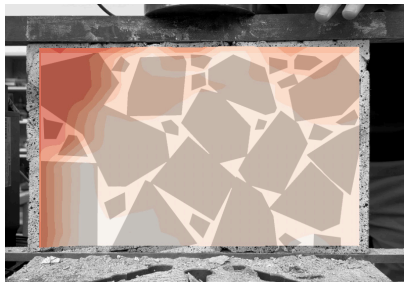

W20

Figure 123 Stone Infill Displacement

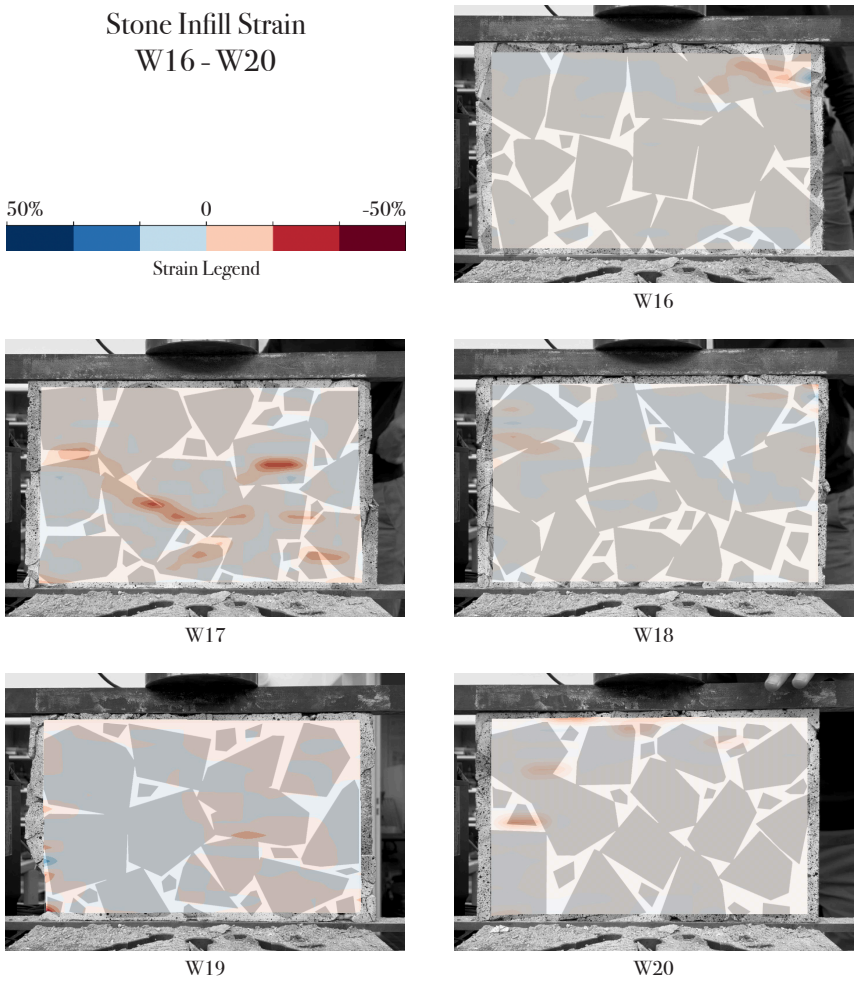

Figure 124 Stone Infill Strain

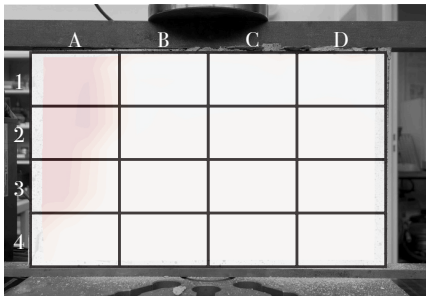

Figure 125 Regions Within The Samples Used Throughout The Analysis

Sample	Peak Stress	Peak Strain	Height
Stone Infill W16	5.57 MPa	1.4%	250
Stone Infill W17	6.24 MPa	1.0%	250
Stone Infill W18	7.26 MPa	1.5%	250
Stone Infill W19	3.94 MPa	0.8%	250
Stone Infill W20	7.00 MPa	1.2%	250

Figure 126 Peak Stress and Strain Stone Infill Group

The stone infill group exhibited a similar average peak strength to the Large Stones group and approached the strength of the control group. The post-peak behaviour is also similar and does not show compaction like the manual infill group did. Nevertheless, due to the low infill area of 10%, the cavities between the stones were tight, which also led to inconsistent infill (Figure 127 compares the strongest and weakest samples). All displacements happened in zones A and D of region 1.

W18 demonstrated the highest strength, with a peak stress of 7.3 MPa, the second strongest arrangement tested overall. It failed in D1, after a crack initiation through an ITZ and a rubble piece.
W20 also showed a high strength and failed in Region A, resulting from a high strain above the rubble in the corner. A crack through this rubble then initiated the failure (see Figure 128 below).

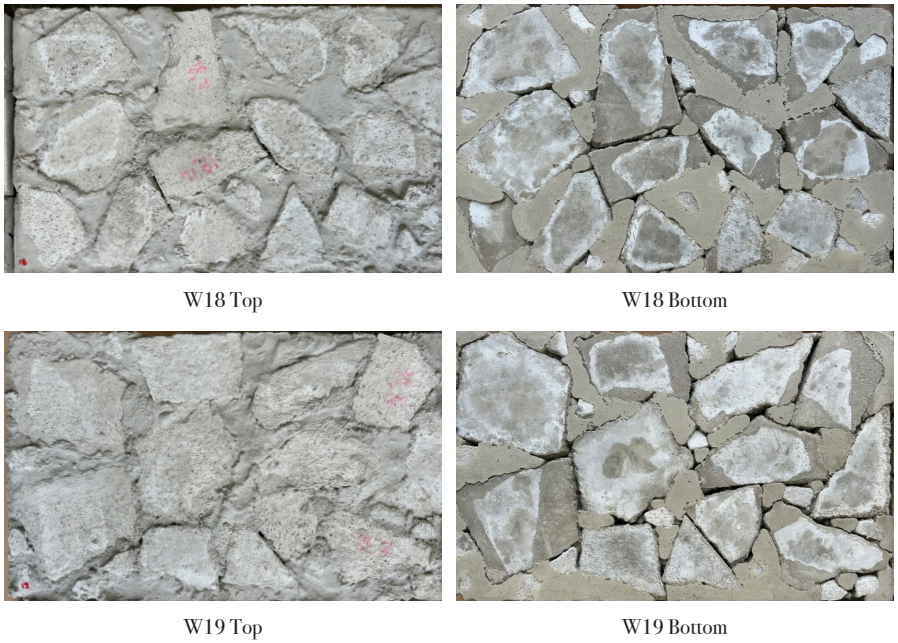

W18 Top | W18 Bottom

W19 Top | W19 Bottom

Figure 127 Unfilled Gaps Due To Tight Arrangement (W18 & W19)

Figure 128 Zoom In W20: 1mm distance between wall and ground (left), crack through rubble

W17 was subject to high displacements in zones A and D, which are not represented by the images, because the DIC system neglects the outer centimetre of the sample at times. Before failure, high stresses were visible throughout zone 3, which led to a horizontal crack through the ITZ.
W16 failed through high stresses in D1, which was a corner only filled with small stones. It did not show a large crack through the wall, as it only failed locally.
W19 was the weakest sample and an extreme outlier. It showed an extremely low gap fill, which led to an initial compaction from Zone C1 to zone D4. The failure happened with a crack through the rubble in region A.
Overall, the group has an average strength of 6.5 MPa without the outlier, which makes it the strongest group tested.

No Rubble

No Rubble Arrangements
W20 - W25

Method: No Rubble

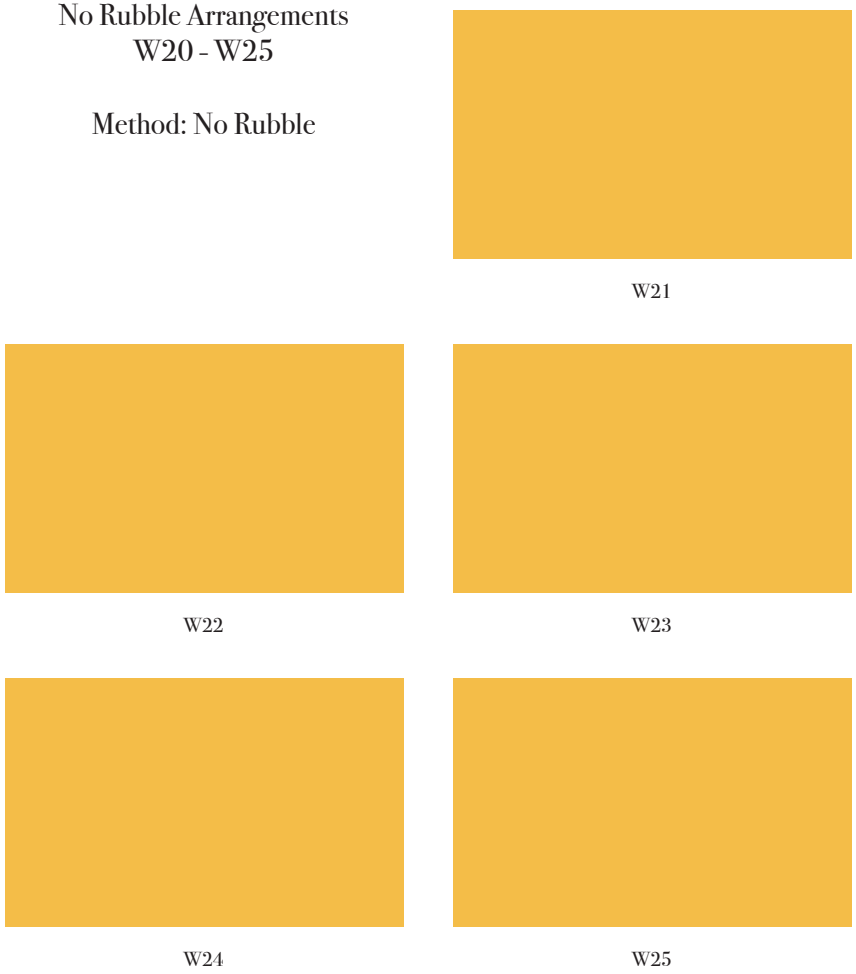

W21

W22

W23

W24

W25

Figure 129 No Rubble Walls

No Rubble Stress/Strain
W21 - W25

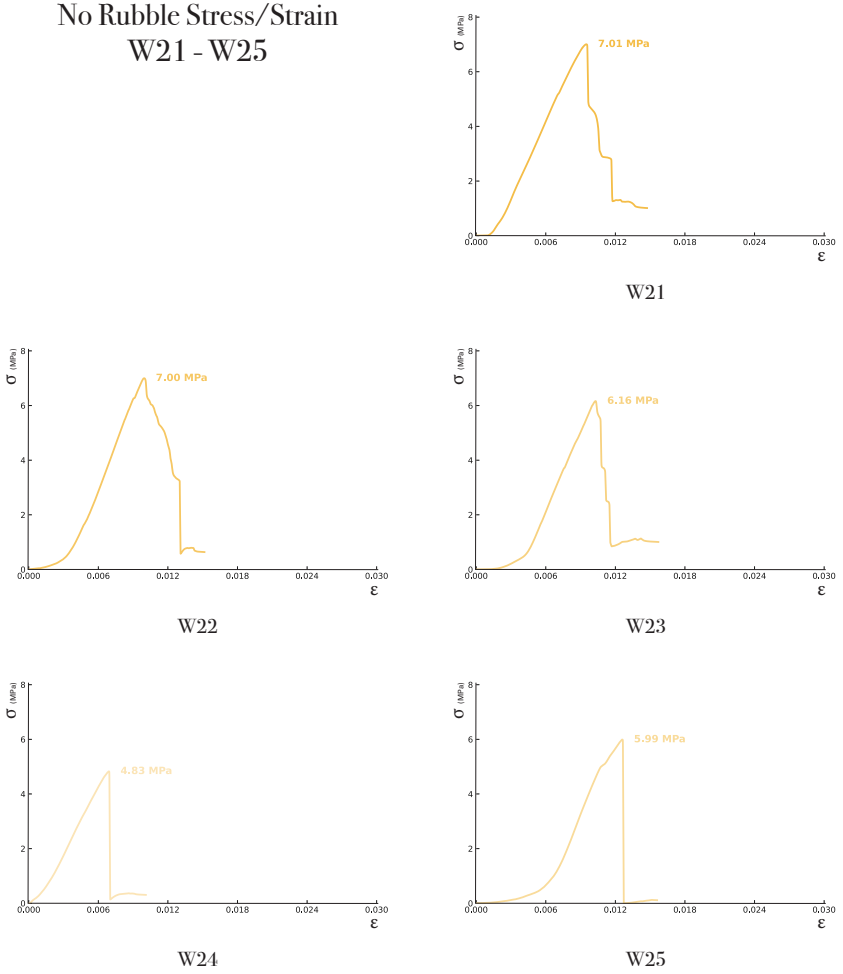

W21

W22

W23

W24

W25

Figure 130 No Rubble Stress-Strain Curves

No Rubble Cracks
W21 - W25

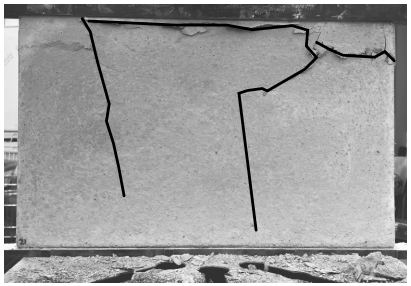

W21

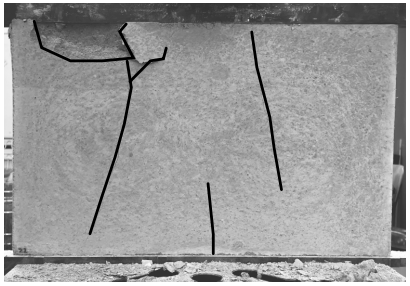

W22

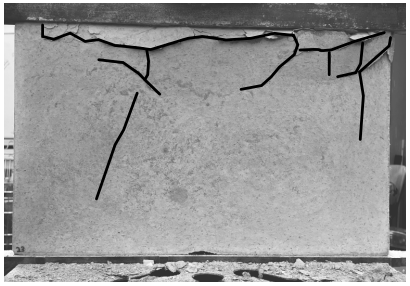

W23

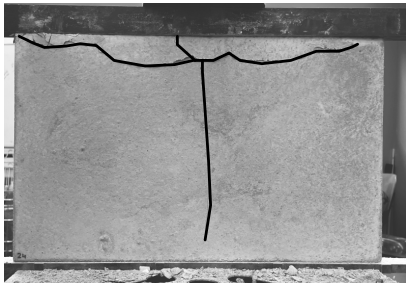

W24

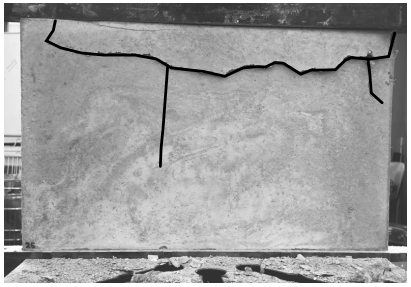

W25

Figure 131 No Rubble Cracks

No Rubble Displacement
W21 - W25

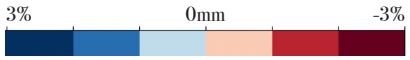

Displacement Legend

W21

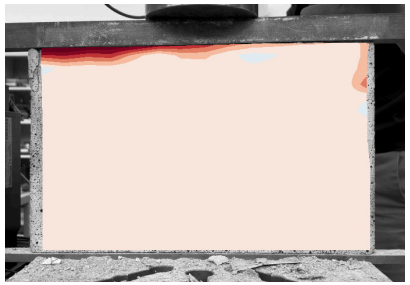

W22

W23

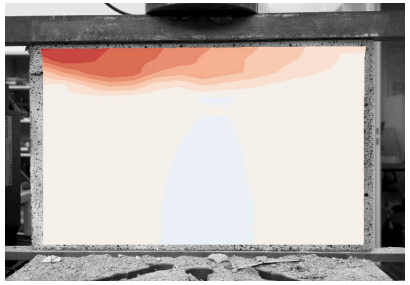

W24

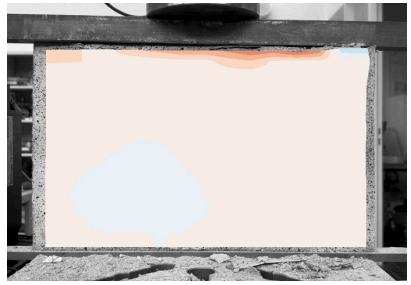

W25

Figure 132 No Rubble Displacement

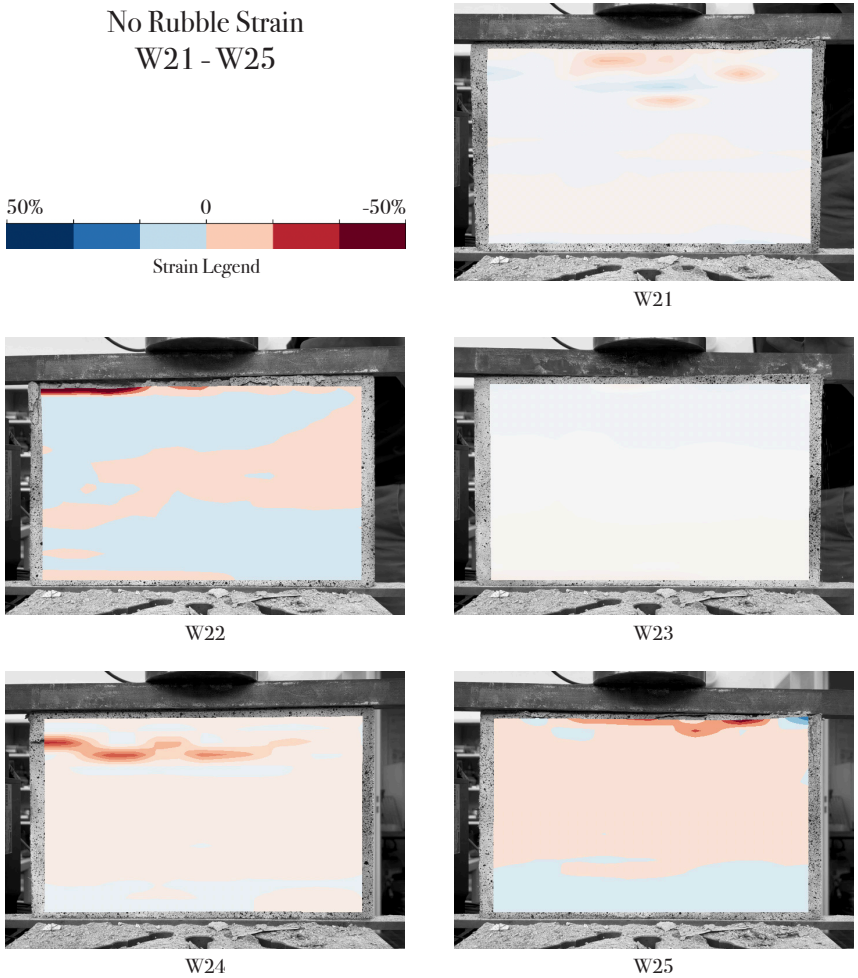

Figure 133 No Rubble Strain

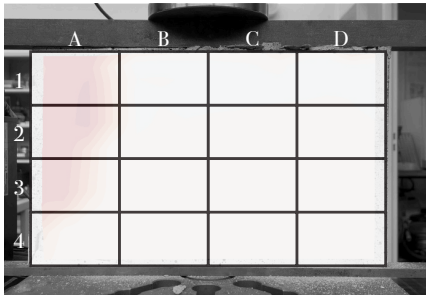

Figure 134 Regions Within The Samples Used Throughout The Analysis

Sample	Peak Stress	Peak Strain	Height
No Rubble W21	7.01 MPa	0.9%	250
No Rubble W22	7.00 MPa	1.0%	250
No Rubble W23	6.16 MPa	1.0%	250
No Rubble W24	4.83 MPa	0.7%	250
No Rubble W25	5.99 MPa	1.3%	250

Figure 135 Peak Stress and Strain Stone Infill Group

The control group without rubble showed the highest average compressive strength and the lowest peak strain. All samples showed a sharp failure after the peak load and minimal deformation.

Every sample shows the highest stresses in zone 1, which led to failure initiated by horizontal cracks between zone 1 and 2.

W24 can be considered an outlier, with a maximum peak stress of 4.8 MPa.

3.8. Discussion

The findings revealed a variety of behavioural patterns for the tested arrangement types. As the boundary condition of each group was the process of the arrangement, the walls therefore included a variety of rubble shapes and placements. Consequently, the findings section examined both individual samples and group results. These results are discussed below.

Rubble and Infill Interaction

The material tests confirmed that the older concrete rubble fragments demonstrated a higher compressive strength than the infill mortar. A critical factor in the failure behaviour of the rubble/infill composites was also the presence of the interfacial transition zones (ITZ) between the two materials. Across all groups, crack initiation frequently occurred along these interfaces, which confirmed that the ITZ often acts as the weakest link in the composite (Oreb et al., 2024; van Mier, 1997). In many samples, the stress concentration in the ITZ triggered failure before the full strength of either the rubble or mortar was reached.

No Rubble Walls

With its stiff, strong, and brittle behaviour, the control group without rubble behaved as expected for unreinforced mortar of this slenderness ratio. The steep initial slopes of the stress–strain curves correspond to a high modulus of elasticity, and the sharp post-peak drops confirm brittle failure. The wall samples showed a slightly lower peak strength than the cube samples. According to Mier (1997, p. 70), a higher slenderness ratio of the specimen leads to steeper slopes, which was also observed in comparison of the stress-strain curves. Evenly loaded confined cube samples stabilise the post-peak behaviour, which explains the difference in the result.

Overall, the low variability of the results confirms the predictability of monolithic concrete behaviour at laboratory settings, and the stress-strain curves can be taken as a baseline for comparison.

Large Stones

The Large Stones group demonstrated solid performance, with a high average peak strength. However, it also showed the widest spread in results, which suggests structural inconsistency. With a stone diameter of 75mm to 150mm, only a maximum of 13 stones fit into each sample wall. With that limited number of stones, the area of the individual infill cavities was higher, which led to localised weak points. This can explain why the DIC showed varying positions of maximum stress and different failure patterns. These included diagonal slides, vertical cracks and local compactions.

The W1, for example, illustrated a potential failure mechanism that could have been prevented with a stacking algorithm. As shown in Figure 136, the area that introduced the failure was dominated by a stone with only one contact point, which led to an unstable load path through the rubble, according to . Without mortar surrounding it, this place would have immediately collapsed. It is interesting to note, however, that the other samples did not exhibit a failure due to such an obvious placement fault. Additionally, the group showed several

instances of crack propagation through the rubble. This could suggest that the strain was so high that the rubble broke before the crack found a path through the ITZ or the weaker infill. Based on this, a failure could potentially also have occurred with stacked rubble.

Together with the high performance of the group compared to the control group, this suggests that a nesting algorithm could still be a viable option for placing large stones inside walls when they are enclosed with mortar. However, if the rubble chosen is restricted to large diameters, a larger variability of failure modes must be taken into account, which leads to uneven performance and requires appropriate safety factors.

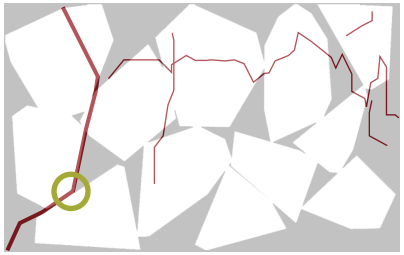

Figure 136 Crack Pattern Of W1, (Thick Red: Crack At Failure, Thin Red: Crack Propagation, Green Circle: Single Contact Point)

Small Stones

The Small Stones group presented the most consistent behaviour across all groups. Its low standard deviation of 10% and the uniform stress–strain curves make this the most structurally reliable arrangement type. The results suggest that the increased number of stones per wall resulted in a more evenly distributed interface. The higher spread of cavities for the mortar infill therefore led to fewer localised weaknesses and spread the risk of structural placement mistakes. Furthermore, crack initiation occurred equally through the infill and the rubble, which suggests a homogeneous composite.

Although the strength was slightly lower than that of the Large Stones group, the homogeneity and predictability of performance suggest that smaller rubble enhances the predictability of the wall's failure mode. Furthermore, the smaller stones are easier to handle, due to their lower weight. However, the trade-off lies in higher labour intensity for scanning and placing the fragments, as more individual stones are necessary.

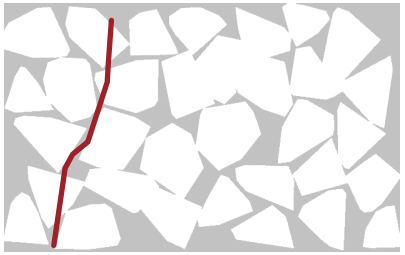

Figure 137 Crack Initiation Through Infill And Rubble, W6

Manual Arrangement

The manually arranged group exhibited the lowest peak strength and showed a unique failure behaviour compared to all groups, which can be attributed to a slight ductile behaviour. Its stress–strain curves revealed post-peak resistance and a wavy shape. This indicates progressive failure and energy absorption. Combined with the results from the DIC maps, the videos, and the cracks, this indicates poor compaction and a lower bond. This low bond can mainly be attributed

to the tight-fitting rubble configurations, where the 10% infill made it difficult to fill the cavities with the mortar used.
Additionally, the cracks did not propagate from a single point but rather spread across the wall. This type of failure is softer and less reliable, but offers more visual warning before collapse than the other arrangements. This could be an advantage of walls with low mortar strength.
Two arrangements with a higher gap infill than the other manual samples outperformed the average, though, suggesting that with a more fluid concrete, tighter arrangements could still be feasible. The tight arrangements could be tested again with a more fluid mortar. Nevertheless, the tight gaps would restrict the aggregate size in real-world applications and probably require manual labour to ensure an airtight wall.

Stone Infill

Despite a similar infill ratio to the manual infills, the Stone Infill group achieved one of the highest average peak strengths. As the cavities were filled with smaller stones, it suggests that the rubble compensated the reduced virgin concrete gap infill. However, the group also exhibited one extreme outlier, which was probably caused by the inconsistent virgin concrete infill. Experiments with more samples in the future could confirm this.
The DIC strain maps revealed that failure consistently occurred after areas with lower gap infill compacted, leaving stiffer areas disproportionately stressed. The hybrid placement tested here still needs to be proven with actual rubble, as it is unknown whether the small shapes used in this arrangement accurately represent the actual rubble found in waste centres.
Still, the group's performance validates the hybrid arrangement, as a strategy for decreased infill ratio, as some results show a superior outcome compared to the control group.

Summary

Overall, the results of the experiments demonstrated a consistent performance of the walls, despite their variety of rubble arrangements. With the highest standard deviation of 20% for the Stone Infill and most groups showing around 10%, the experiments have a lower variability than the walls tested by Oreb et al. (2024) for example.
The arrangement tests aimed to compare the performance of rubble diameters and virgin concrete infill. In addition, they also provided insight into the homogeneity of the composite created. With the quasibrittle failure modes, the results showed a good bond between the rubble and the infill for the experiments (Mier, 1997, p. 104), which indicates the homogeneity targeted by the horizontal fabrication process. This homogeneous behaviour suggests that the rules for masonry stacking may not be the most determining factor in the stability of precast CS Walls.
The weakest peak stress among the rubble wall samples still reached 70% of the average peak stress of the control group. If a virgin concrete with a lower strength than the weakest rubble is used, its properties could therefore be taken as a benchmark to determine the wall's strength.

However, the structural tests were conducted on 1:10 samples with saturated surface dry rubble, which increased the bond strength. In his book on concrete fracture testing, Mier (1997, p. 207) points out that scaled tests do not always represent the behaviour of full-scale materials. As the strain and displacement data showed that the ITZ frequently governed failure, this factor is crucial for real-size applications. Capinteri & Ferro (1995) show that the tensile strength decreases with the sample size. Whether the bond of these experiments can therefore be implemented during a 1:1 construction process needs to be determined in more detail through material research and confirmed with full-scale structural tests.

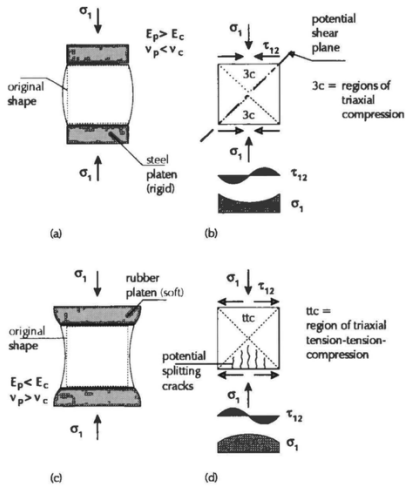

Figure 138 Differences In Crack Behaviour Caused By The Test Platen (van Mier, 1997, p. 73)

The tests also showed that zones 1 and 4 were often subjected to local stresses. After controlling the videos, it was observed that these issues were sometimes caused by a slight uneven surface, as seen in W20, for example (see Figure 128 on page 98). Although these were not the primary causes of the fracture, a rubber layer could have mitigated the impact of these production imperfections (see Figure 138).

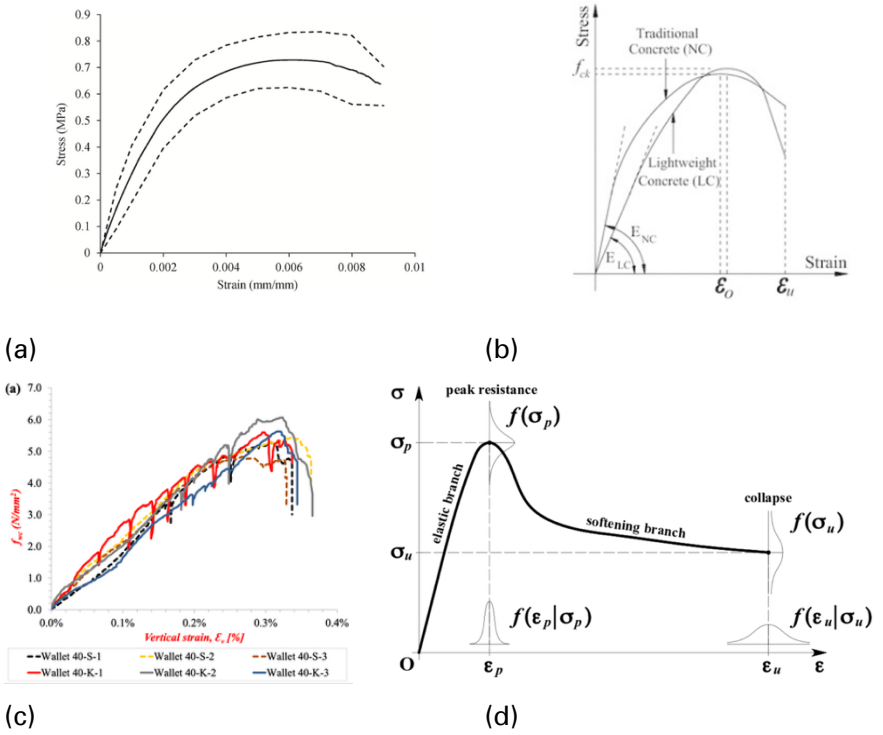

Figure 139 Stress-Strain Curves For Different Load-Bearing Wall Materials: (a) Rammed Earth (Average And Standard Deviation) (Gil-Martin et al., 2022) (b) Concrete And Lightweight Concrete (El Zareef, 2017) (c) Unreinforced Multi-Leaf Stone Masonry Walls (Amer et. al., 2023), (d) Brick Masonry (Parisi, 2012)

To find a pattern, the results for the CS Walls tested can be compared to stress-strain behaviours of existing load-bearing wall materials and composites (see Figure 139 above). The No Rubble control group, the

Large Stones group and the Stones Infill group show similar slopes to lightweight concrete walls (El Zareef, 2017). The Small Stones group showed a stress-strain curve comparable to that of brick masonry or traditional concrete, whereas the Manual group resembled the compaction behaviour of multi-leaf stone masonry walls (Amer et al., 2023). As expected, none of the walls exhibited ductile behaviour, similar to a rammed earth wall (Gil-Martín et al., 2022), for example.

Although the average strengths of the groups are comparable, they exhibit different failure modes. The Small Stones group demonstrated a slightly lower average strength and requires more labour, but has a more predictable failure pattern, whereas the stronger Large Stone group demonstrated less predictability. The hybrid method, which combines small and large stones, looked promising, especially when the infill is well distributed. Therefore, these characteristics must be taken into account when choosing the stone arrangement.

3.9. Conclusion

Based on the three testing phases, the results demonstrate that a horizontal precast method for Cyclopean Spolia Walls can lead to structurally viable, load-bearing elements. The tests showed that the arrangements have different structural advantages, but all performed better than expected. They demonstrated that low-tech digital tools, based on small databases, can result in structurally sound arrangements when combined with a strong mortar and a good bond.

Among the groups tested, the Stone Infill configuration proved to be the most promising. It achieved high strength values and stable results while maintaining a low virgin concrete infill ratio. It demonstrated that the combination of large structural rubble with small stone infill is more effective than achieving low infill ratios through overly tight arrangements.

The Large Stones group highlighted certain constraints in design flexibility. With fewer elements and larger mortar gaps between them, this arrangement resulted in greater variability in strength and failure modes. Stacking algorithms could mitigate this by optimising contact points and alignment to improve the ultimate failure strength. The Algorithm Tests revealed a potential drawback of the stacking arrangements used here. The walls showed mortar hotspots at the top, where no stones were found to fill the gaps. This weakened the performance and could only be fixed with an extensive database. These findings suggest that while stacking algorithms can improve the axial compressive strength of horizontally precast walls, they may not be strictly necessary for use cases where structural failure is not solely governed by material strength, but by other critical failure modes.

Furthermore, several indicators showed rubble and infill work as a composite, which is more reliant on the bond between the material than on the arrangement. Cracks consistently propagated through both rubble and infill, as well as along their interface, which suggests that the stones are structurally integrated into the wall system. Despite this, the performance was still largely governed by the strength of the ITZ, suggesting further tests on the bond quality between rubble and virgin concrete for CS Walls.

In summary, the 1:10 results suggest that Cyclopean Spolia walls have the potential to meet structural requirements for load-bearing walls when properly designed. These have to be confirmed by full scale tests, to validate the findings.

3.10. Answer to Research Questions

> How can digital tools facilitate the scalability of load-bearing rubble walls?

The structural tests showed that low-tech digital tools like 2D scanning and nesting algorithms could enable scalable workflows for concrete rubble arrangements. If paired with a horizontal precast process and a strong ITZ bond strength, these tools could facilitate the adoption of rubble walls.

Nesting algorithms, without structural constraints, achieved a consistent compressive strength and significantly reduced the rubble database needed. This also allows the fragments to be placed more freely in horizontal precast walls, which could enable flexible just-in-time production and design freedom. Digital tools thus simplify the adoption of reclaimed rubble for walls, by reducing labour, material preparation, and design limitations.

> How does the arrangement and the diameter of concrete rubble affect the structural performance of load-bearing walls under compression?

The structural tests showed that the rubble diameter and their arrangement only have a slight impact on the wall's peak compressive strength, but show a greater impact for the failure behaviour and their reliability. Small rubble distributed loads more evenly, which resulted in a more reliable strength and failure behaviour. Large rubble fragments increased the variability, due to larger cavities. Tight manual packing reduced strength because the cavities hindered an even infill distribution. Walls combining large rubble with small stone infill achieved strong, stable results. The experiments showed that well-balanced rubble placement and consistent infill improve performance, and that overall homogeneity and the ITZ bond are more critical than the stone size and their arrangement.

System Design

Summary

This chapter translates the experimental findings into a scalable prefabrication system for Cyclopean Spolia Walls. It defines structural limits, explores potential applications, and outlines key design aspects for both architecture and construction. The system design introduces two lifting strategies, detailed wall connections, and proposes standard wall sizes based on transport restrictions. It also explains how digital tools and simplified databases enable an efficient horizontal production process. Finally, the full prefabrication workflow is illustrated. It demonstrates how Cyclopean Spolia Walls could be integrated into current building practices.

Previous Page: Figure 140 Potential Use Cases For Cyclopean Spolia Walls (Mix Of AI And Collage)

4.1. Architectural References

Les Bleuets, Paul Bossard (1962), Paris (Alonso et al., 2019)

Table 24 Les Bleuets Paris After Renovation By RVA (https://www.baunetzwissen.de/beton/objekte/wohnen-mfh/sanierung-der-rsidence-les-bleuets-bei-paris-9880081)

At Les Bleuets in Créteil, Paul Bossard built a manifest of imperfection. To create a contrasting new expression for precast concrete construction, Bossard embedded hand-placed slate stones into the concrete. This approach transformed the technical panels into surfaces full of life, with a hint of critique of the rigidity of the mass housing the project represents. He used on-site casting methods and gave the workers the freedom to place the stones to their liking, which created a large variability of arrangements. The method echoes Cyclopean Spolia Walls, which question perfection and bring unforeseen texture into otherwise plain walls. Bossard's result was a sculptural façade that challenged the homogeneity of the mass prefabricated systems from his time.

Les Bleuets was renovated in 2018, but the concrete/slate composite has stood the test of time. Les Bleuets stands as a rare case where a concrete panel system integrated planned inconsistencies, both technically and visually.

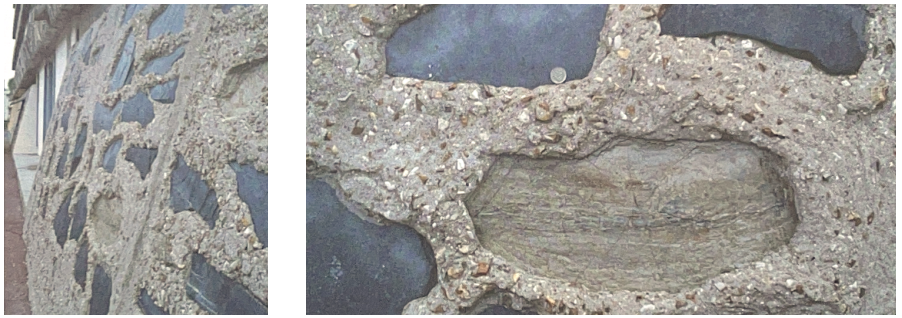

Table 25 Concrete Elements With Embedded Slate Debris (Alonso et al., 2019)

Casa 1413, H ARQUITECTES (2017), Spain

The Casa 1413 by H ARQUITECTES integrates the site's conditions into the main structural wall. The stones from an original natural stone wall and the sandstone found during the excavation, are used to construct a new load-bearing wall (H ARQUITECTES, n.d.). To achieve this, they use a formwork and alternate between stone layers and mortar (see Figure 141). For aesthetic reasons, they pep the outer layer of the exterior wall until the stones appear on the surface. The interior of the wall is left with the finish of the formwork wall itself.

Figure 141 Casa 1413 Facade (https://www.harquitectes.com/wp-content/uploads/2023/03/1413-harquitectes-casa-ullastret-01.jpeg)

Figure 142 Wall Construction Process Casa 1413 (https://www.harquitectes.com/wp-content/uploads/2023/03/1413-harquitectes-casa-ullastret-35.jpg)

Social Housing 2104, H ARQUITECTES (2022), Palma de Mallorca

In Mallorca, H ARQUITECTES resurrected a building from its debris back to life on the same site. Its former debris is visibly reintegrated into the main structural walls of the new building. With a precast process similar to Cyclopean Spolia, they reclaimed the existing stones and embedded them into new concrete. Off-site, they built wooden formworks, which were filled with the stones. To create a solid new material, they filled it up with concrete and cut the cured blocks into modular individual building elements. Through this process, they create a natural-stone-like texture and aesthetic, as a reminiscence of the building's past.

Figure 144 New Building

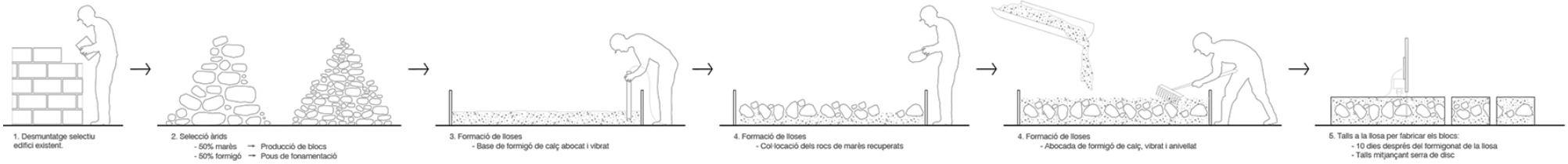

Figure 143 Wall Construction Process Social Housing 2104 (https://www.harquitectes.com/en/proyectos/ibavi-2104/)

4.2. CS Wall Application Scenarios

This chapter explores potential application scenarios for Cyclopean Spolia Walls, which serve as the foundation for the system design. To inform the boundaries for the applications, the potential structural limits of CS Walls are discussed below.

4.2.1. Structural Limits

More than 60% of the volume of Cyclopean Spolia Walls is made up of concrete rubble. These fragments come from a variety of buildings, which means that their original mixture and age could differ significantly. To accurately predict the structural performance of these elements, one would need to know the strength of the weakest rubble piece in the composite and the bonding strength at the ITZ. To test each individual fragment of a wall would be too time-intensive. Therefore, in a future process, a conservative estimate has to be made to evaluate the lower boundary of the rubble strength. This 'worst-case-scenario' can be set up based on historical data of concrete mixtures used in the region and the maximum age that the rubble could have. Together with 1:1 structural tests and potential shear bond tests (Nazir & Rashid, 2018; van Mier, 1997) this could determine the strength more reliably.

As 1:1 structural tests were beyond the scope of this thesis, the wall strength was estimated based on the 1:10 tests and compared to existing tests on load-bearing rubble from the literature. The results showed that the performance of the Cyclopean Spolia Wall, arranged with nesting algorithms, achieves a slightly lower compressive strength than that of the infill material. If the walls whose gaps were not completely filled are disregarded, the weakest peak stress of rubble walls tested still demonstrated 70% of the average peak stress of the unreinforced wall. On average, the control group was only 4% stronger than the average peak strength of the CS Walls. Therefore, the test walls showed a similar compressive strength behaviour to the material used for the infill. However, the compressive strength of the individual materials is not enough to predict composite behaviour. As the shear bond strength between concrete and rubble could be less strong in real-life circumstances, due to water transport (no SSD) or microcracks (Yazdi et al., 2020), these values cannot be directly transferred to 1:1 setups.

Therefore, the System Design is based on values from the available literature. The CCDW masonry walls by Oreb et al. (2024) demonstrated a compressive strength between 5 and 10 MPa. In addition to this, the data gathered by Grangeot, Bastien-Masse, & Fivet (2024) showed no failure of their rubble/mortar composite wall, when it was subjected to stresses of 2 MPa. As their data suggested a similar mechanical behaviour to a masonry wall, they conservatively assume a compressive strength of 3 to 8 MPa.

- [...] in contrast to the methods used by Oreb et al. (2024) and Grangeot, Bastien-Masse, & Fivet (2024), the final strength of the horizontal precast process relies more on the ITZ bond between rubble and mortar, than on stone interlocking -

However, in contrast to the methods used by Oreb et al. (2024) and Grangeot, Bastien-Masse, & Fivet (2024), the final strength of the horizontal precast process relies more on the ITZ bond between rubble and mortar than on stone interlocking. Therefore, another method to predict their final strength would be to base it on the strength of the

weakest member and derive the ITZ strength from it. In their analysis of a cyclopean concrete dam, Maltidis & Stempniewski (2013) developed a numerical model to analyse its remaining strength on a Representative Volume Element (RVE). They assigned 60% of the mortar strength to the ITZ within the RVE. For Cyclopean Spolia, this would result in 7.2 MPa if a C12/15 concrete is used as infill.

Based on these insights, the final strength of CS Walls could lie between 2 MPa and 7.2 MPa. To proceed with the system design and LCA, a rounded average value of 5 MPa is assumed. However, this is speculative and needs to be confirmed through full-scale structural tests.

Similar to what was shown in Grangeot, Bastien-Masse, & Fivet's research (2024) for Switzerland, the walls could be used for a three-story residential building in the Netherlands or Germany, based on local code (Nen-En, 2006).

	Max Stress	Min Stress	Avg Stress	SD Stress	SD Stress %
Large Stones	7.4 MPa	4.4 MPa	6.0 MPa	1.1 MPa	18%
Small Stones	6.7 MPa	5.0 MPa	5.8 MPa	0.6 MPa	10%
Human	5.3 MPa	3.8 MPa	4.6 MPa	0.6 MPa	13%
Stone Infill	7.3 MPa	3.9 MPa	6.0 MPa	1.2 MPa	20%
No Rubble	7.0 MPa	4.8 MPa	6.2 MPa	0.8 MPa	13%
Rubble	13.0 MPa	8.6 MPa	10.7 MPa	1.8 MPa	17%
Infill	8.3 MPa	6.2 MPa	7.4 MPa	0.6 MPa	8%

Figure 145 Results From The Arrangement Tests

Figure 146 Potential Use Cases For Cyclopean Spolia Walls (Mix Of SORA And Collage)

4.2.2. Applications

In the Netherlands, Cyclopean Spolia Walls could be used as load-bearing walls for low-rise buildings (Nen-En, 2006), non-structural walls for partitions or also in landscaping or infrastructure projects, where low-strength walls are needed.

Based on the structural limitations, potential applications could be:
Load-bearing:

I. Main walls of low-rise buildings (housing, warehouses, etc.)
II. Retaining walls

Self-weight only:

III. Free-standing walls for landscaping
IV. Noise barriers for highways and train tracks
V. Interior acoustic, fire or separation walls

4.2.3. Case Study

To show how Cyclopean Spolia Walls could come to life, a wall system is developed and demonstrated with a case study building, that forms the base for the detail drawings and assembly. The structure is a 2-story residential building with external load-bearing walls and CS basement walls. The load-bearing Cyclopean Spolia Walls are 7m long and include two windows of 1.6m width each. A structural calculation is performed to determine the stress on the basement wall, which conservatively assumes that the space above the windows takes no loads. The calculations are based on the Dutch NEN-norms and can be found in the Appendix. They showed that a stress of 1.37 MPa acts on the wall, which is below the minimum strength of 5MPa presumed for CS walls. The case study building is further used to explain the prefabrication, transport and assembly details.

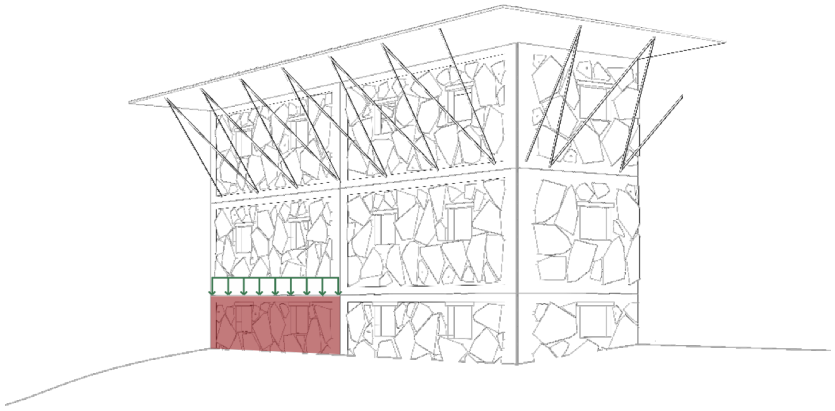

Figure 147 Cut Fragment Of The Case Study Building, The Stresses are Calculated For Red Wall

4.3. Wall Design

4.3.1. Architectural Design

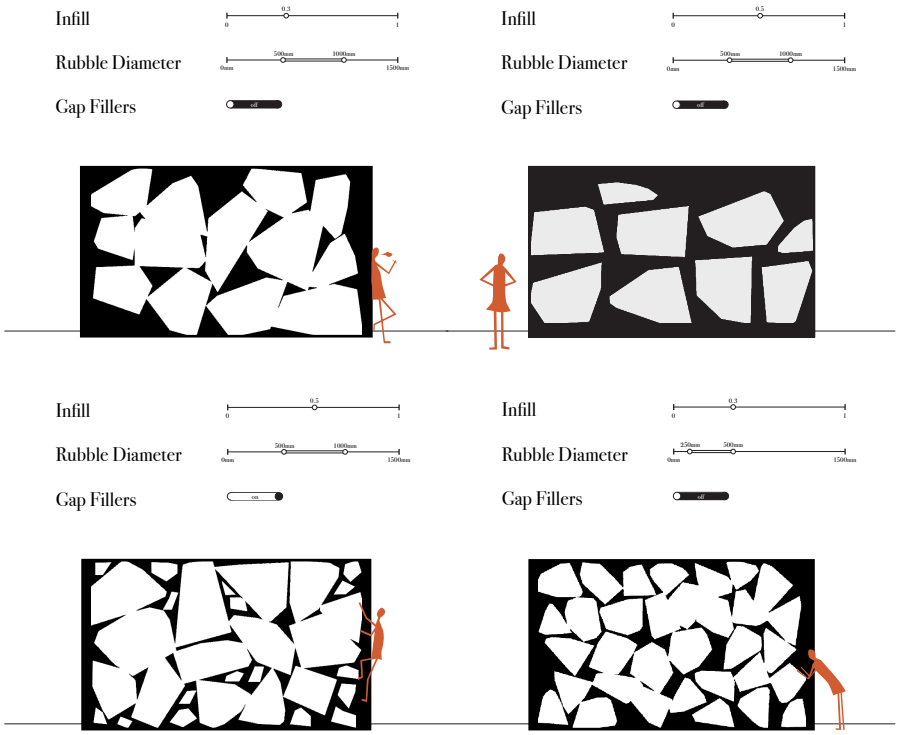

Figure 148 Arrangement Options For Cyclopean Spolia

Cyclopean Spolia offer a new architectural language for reclaimed concrete to designers. Their embedded rubble proposes a multitude of expressions. The walls can be made from debris from unknown projects, if sourced from the waste centre, but they can also be carefully chosen to represent a specific demolished building and its character.

Furthermore, the tests have shown that the fragment arrangements and the rubble diameter do not have a significant impact on the wall's strength. The demonstrator in Section 4.4 on page 123 shows potential arrangements, which could be realised with precast methods for Cyclopean Spolia.

In addition, the prototypes of Grangeot et al. (2024) from EPFL show how distinct and recognisable concrete elements could also be embedded into wall designs.

Figure 149 Prototype 01 (Grangeot et al., 2024)

Figure 150 Prototype 02 (Grangeot et al., 2024)

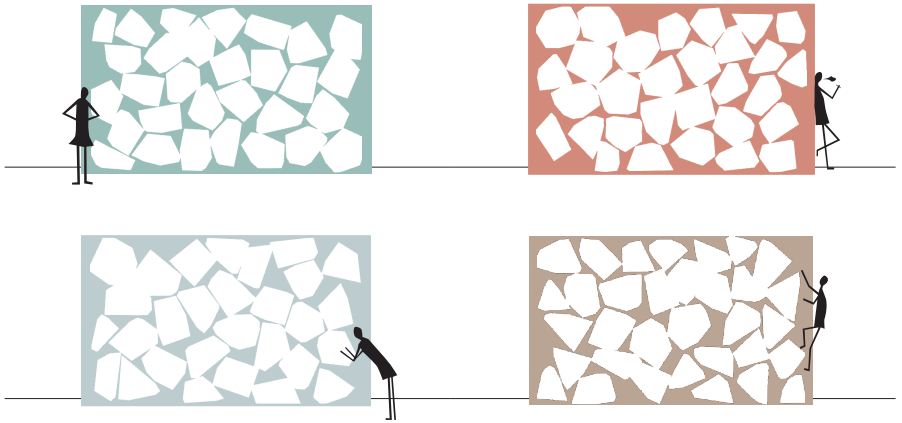

Figure 151 Coloured Infills

In addition to this, coloured infills could underline the contrast between the grey debris and the virgin concrete:

Due to the different thicknesses of the rubble, one face of the walls will demonstrate an almost flat surface, whereas the other face will show a pattern of multiple fragment heights. This opens the possibilities to display different faces, based on the desired expression and function of the wall. If the rough side is placed towards the insulation of the building, a loose-fill insulation would be recommended.

The thickness of the rubble used was not discussed during the experiments, but could also become an additional design variable. In relation to the infill thickness, this factor significantly influences the roughness of the wall's appearance, as can be seen in Figure 153 and Figure 153

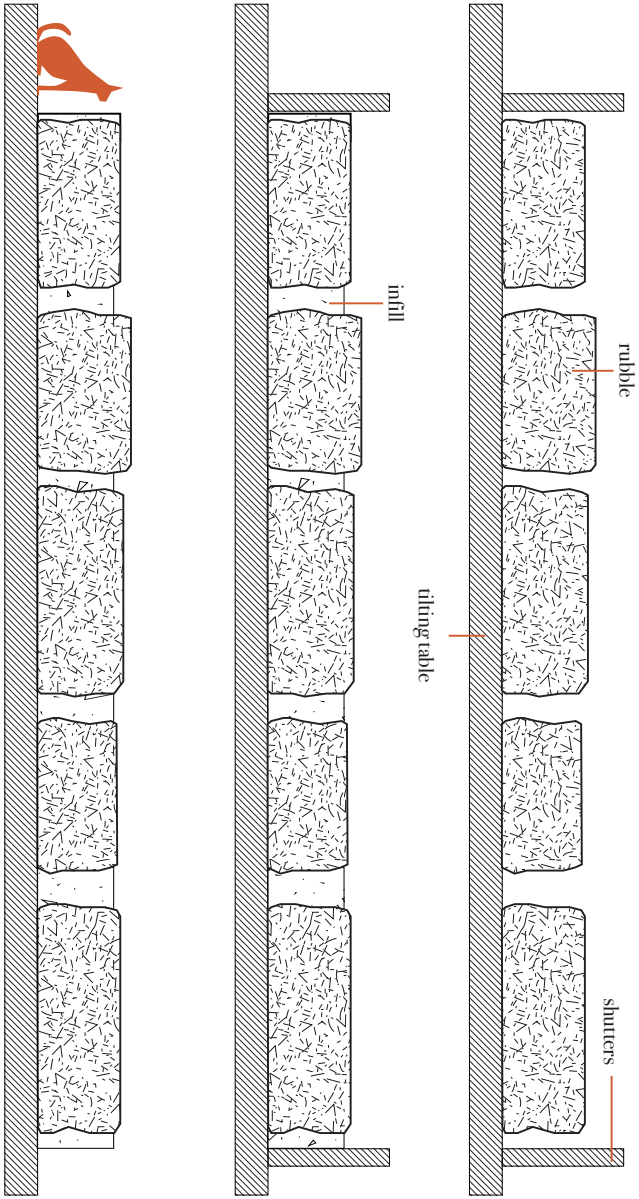

Figure 152 Wall Section Showing The Height Difference In Rubble

Figure 153 Thick Rubble vs Thin Rubble (AI & Collage)

4.3.2. Technical Design

Dimensions

The size for standardizes prefabricated walls is defined by the size of the precast table. The formwork can be adjusted based on the size required by the project. Wall sizes of up to 20 m in length and 6 m in height are possible, depending on the demand (Martins et al., 2023). However, the dimensions are mostly restricted by the transport process. The dimensions and weight restrictions for this thesis are based on the capacity of an open three-axle truck by EU standards (Council Directive 96/53/EC, 1996). The maximum dimensions for the trailers are 13.6 m in length and 3 m in height, with a maximum load capacity of 36 t (International Transport Forum, n.d.). Typical limits for weights are 20 t, according to Mackay-Sim (2011). On this basis, the following size restrictions are defined:

max length = 11m

max height = 3m

max thickness = 0.3m

The largest wall would therefore be 10m x 3m and weigh around 19.5 tonnes, with a concrete density of 2400 kg/m³ and a steel density of 8050 kg/m³. As this would enable a truck to only transport one of those walls at the same time and requires a large tilting table, the assumed wall size for the case study will be length taken for the calculation will be at 7m.

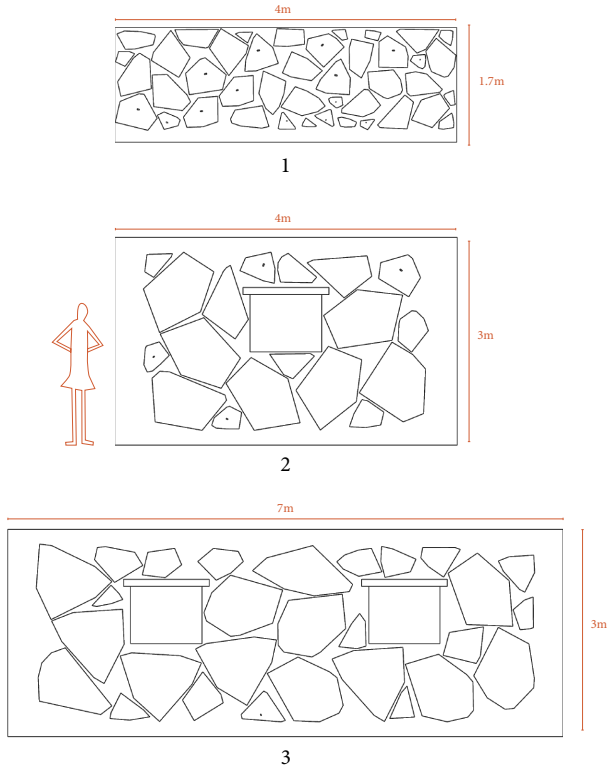

Figure 154 Possible Wall Sizes For CS Walls

Wall Design

The wall design has to provide space for the placement of the concrete rubble and ensure the transport and assembly of the walls. Precast walls are usually lifted by anchor points embedded into the top part of the wall. The strength of the design can be determined by the concrete or the anchor strength. For walls with a strength less of 15 MPa, the concrete is the determining factor. In these cases, additional v-shaped reinforcement is placed for transport (Mackay-Sim, 2011), as can be seen in Figure 155 below.

Figure 155 Lifting Of A Precast Wall By Embedded Anchor Points (https://www.precastconcretemagnet.com/news/precautions-for-lifting-precast-concrete-compo-76626504.html) And V-Shaped Hanger Bars (Mackay-Sim, 2011)

Subsequently, due to the low strength of Cyclopean Spolia Walls, two options of design for transport are introduced.

The first one places an outer ring of 20cm at the edge of each wall, reserved for virgin concrete. This facilitates the edge design without rubble interfering with the formwork and creates space to place rebar. As a V-shape is not possible, due to the rubble, a ring is introduced, which guides the forces around the fragments (see Figure 156 and Figure 157). The transport anchors are then attached to the reinforcement and embedded in the virgin concrete, together with the rubble. Even though this method requires more carbon intensive steel and offers less space for rubble placement, it enables the wall to integrate into existing modes of transport and equipment.

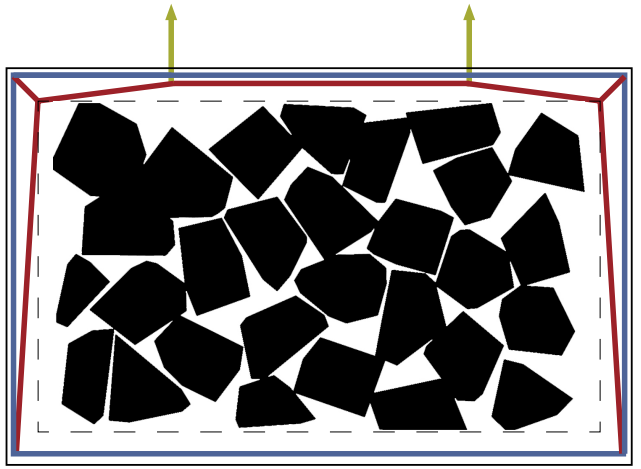

Figure 156 Forces Through The Outer Rebar Ring (compression, tension and external forces)

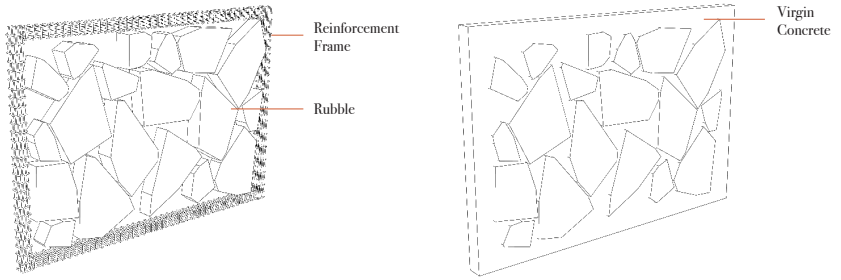

Figure 157 Wall Design With Reinforcement Frame

The second method is based on a transport 'beam', which is introduced on the bottom of the walls. This method of localized rebar leaves space in the entire wall to place rubble, but requires a new mode of transport. Instead of creating local tensile forces in the top of the wall, straps transfer the tensile forces to the bottom of the wall and the bending forces are absorbed by the rebar beam. Therefore, the rubble area only

experiences compression forces from below while lifting. As the wall is placed on shims, before it gets connected to the foundation, there is enough space to remove the straps when the wall is placed.

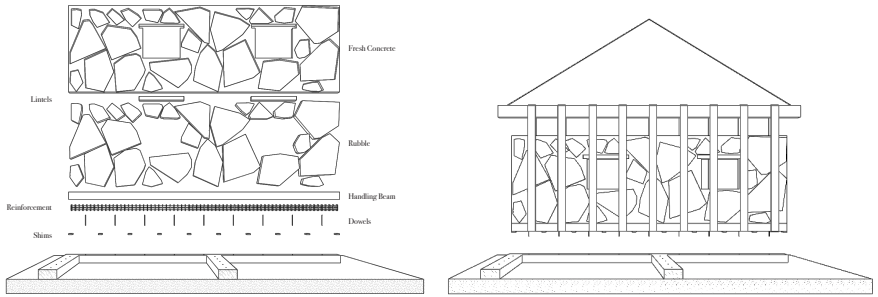

Figure 158 Wall Components With Handling Beam

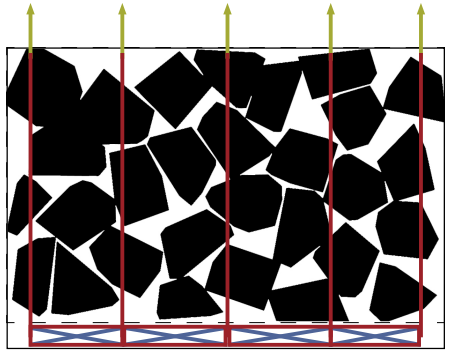

Figure 159 Transport Mode And Force Flow (compression, tension and external forces)

Both systems have their advantages and disadvantages and the following sections are based on CS Walls with a handling beam. However, a small edge ring without rubble is always needed, to ensure a tolerance for the rubble placement and place connection pieces, which are discussed in the next section.

Horizontal Connections Between The Walls

To create a monolithic building structure, the wall connections are crucial for the load transfer between the walls. Therefore, the elements are joined with in-situ concrete, which provides a load transfer between the walls. The wall edges are shaped in a u-form, which acts as a lost formwork on site. To join the walls, steel connecting loops are placed in the outer virgin concrete ring during prefabrication, before the concrete is poured. These are placed above each other on site and ensure a strong connection.

Furthermore, there is a 20mm gap left between the walls, to account for the 16mm tolerance recommended by NEN-EN 14992+A1 (Dutch Standards Institute, 2012) for walls between 3 m to 6 m length.

Connection to the foundation

In the prefabrication factory, the wall is equipped with shims and notches on the bottom edge. On site, dowels are introduced into the foundation. When the wall is placed, the wall slips onto the dowels and the shims act as placeholders for the grout (see Figure 160). To create a load-bearing layer with the foundation, the dowels are then bolted to the wall and the gaps in between the shims filled with grout. The shims are 30mm high, according to NEN-EN 14992+A1. D2 (Figure 166) shows a 1:5 detail section of a connection to the foundation.

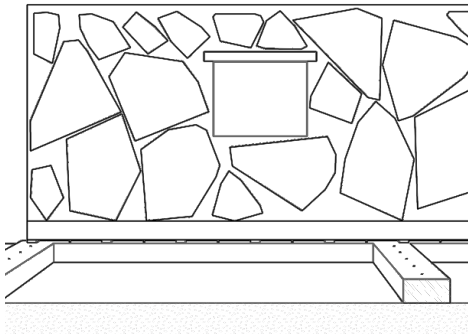

Figure 160 CS Wall With Shims Is Placed On Strip Foundation

Vertical Wall Connections and Connection To Floor slab

To place the floor slab, a notch and dowels are cast into the CS Wall edge in the factory. The floor slab is designed with a grout tube, which holds the dowel, once it is placed on the notch of the wall. To prevent spalling, due to flexural rotation (Elliott, 2019, p.2-4), bearing pads are introduced at the contact point. To fix the connection, the holes are filled with grout. The above wall gets placed on top and is also distanced with shims and connected with dowels into the wall below. Thus, a monolithic structural behaviour can be ensured. D1 (Figure 165) shows a 1:5 detail section of a vertical wall to wall connection with a floor slab. The drawings on the next pages demonstrate a residential application of a load-bearing external Cyclopean Spolia Wall. It shows that the surface can be turned towards the outside and towards the inside. The latter offers a high heat storage capacity of 486 kJ/m2K and a u-value of 0.229 with a cork facade cladding. If the wall is not plastered, the rubble can define the interior space of the building with its strong surface topography. With an internal insulation, the heat storage capacity of the structure decreases to 53 kJ/m2K with a u-value of 0.26 W/(m2K) (Ubakus, 2025). This option enables the rubble to define the building's facade and advertise the reclaimed material to the outside.

The 1:5 details are based on an internal CS Wall with external insulation.

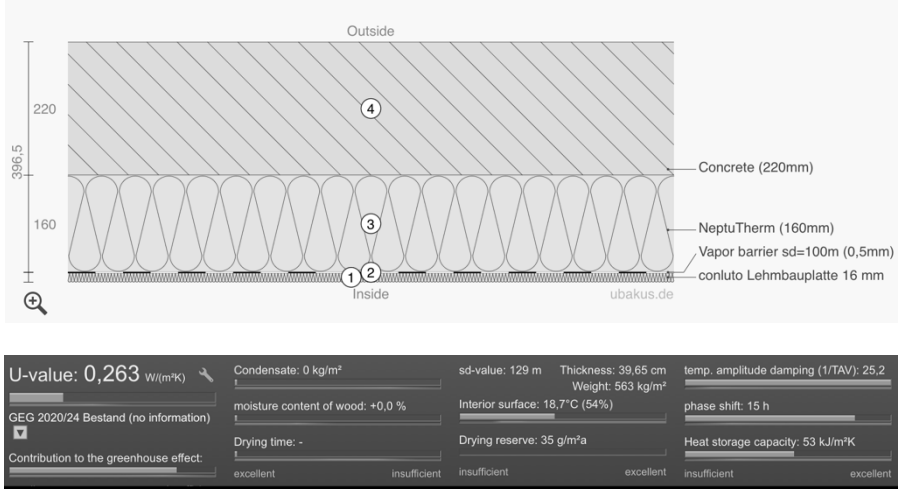

Figure 161 CS Wall, Insulated From The Inside (Ubakus, 2025)

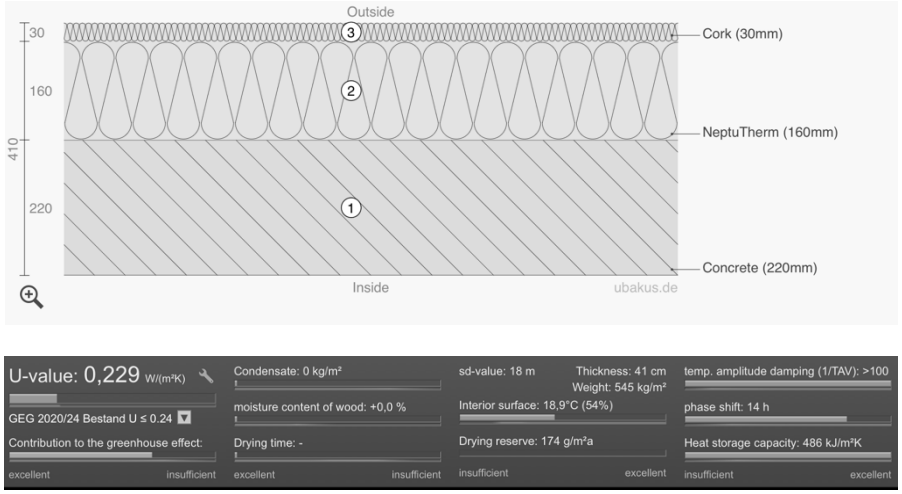

Figure 162 CS Wall Insulated From The Outside (Ubakus, 2025)

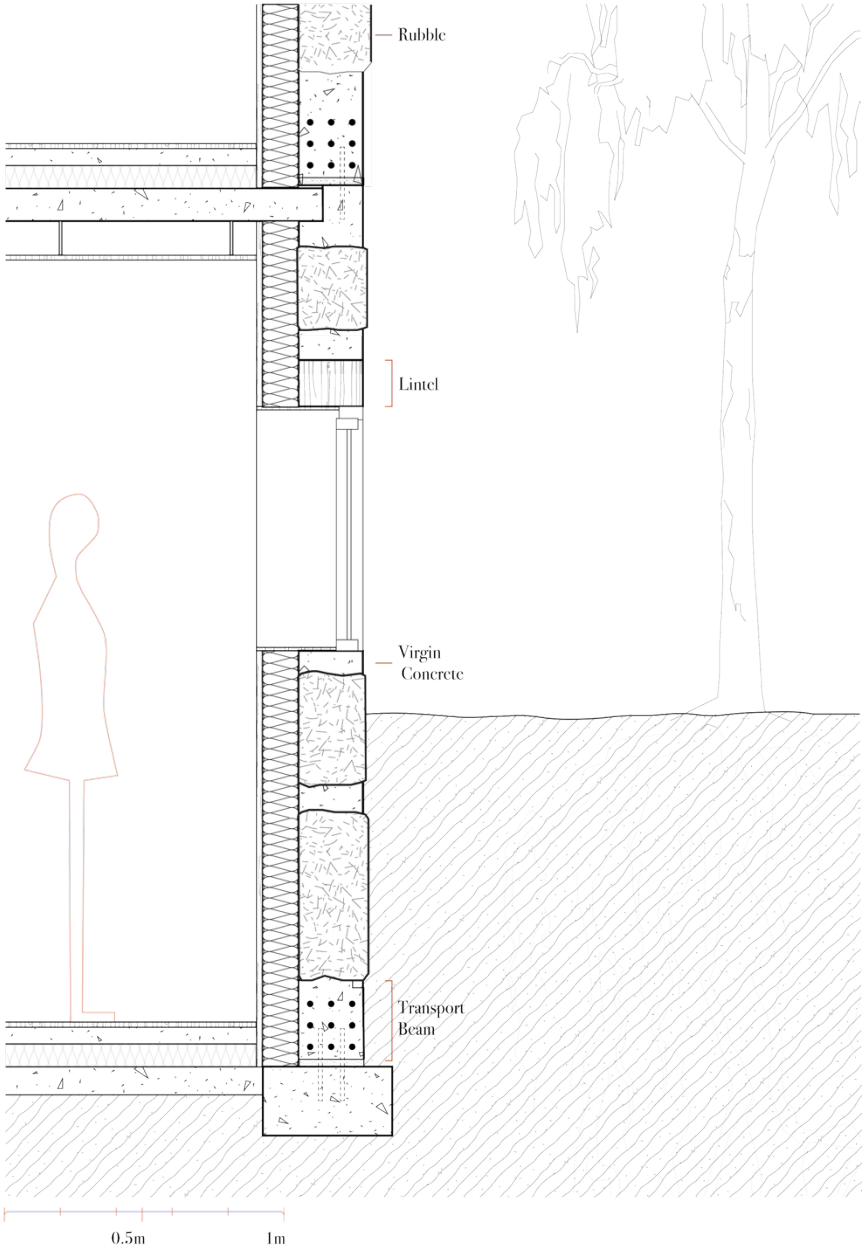

Figure 163 1:20 Section External Cyclopean Spolia Wall

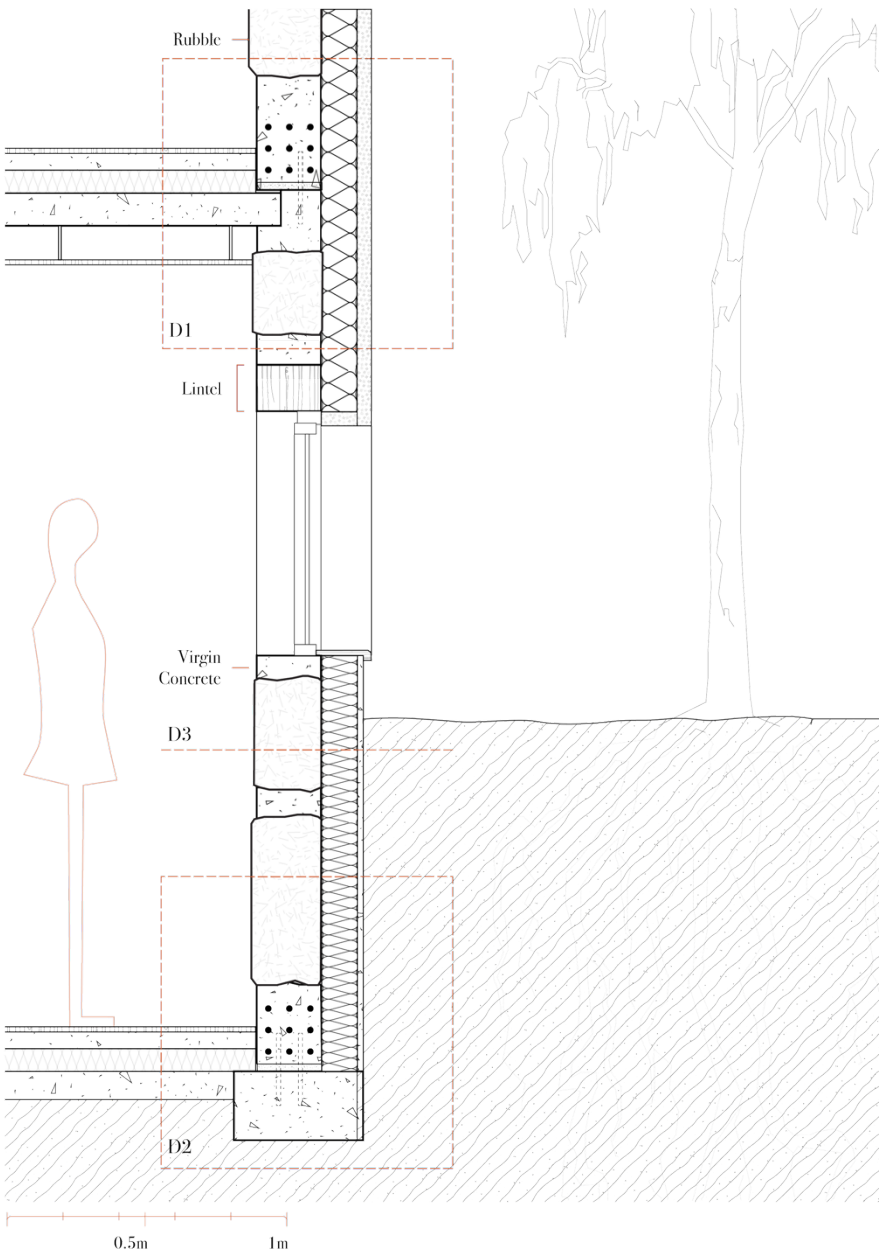

Figure 164 1:20 Section Internal Cyclopean Spolia Wall

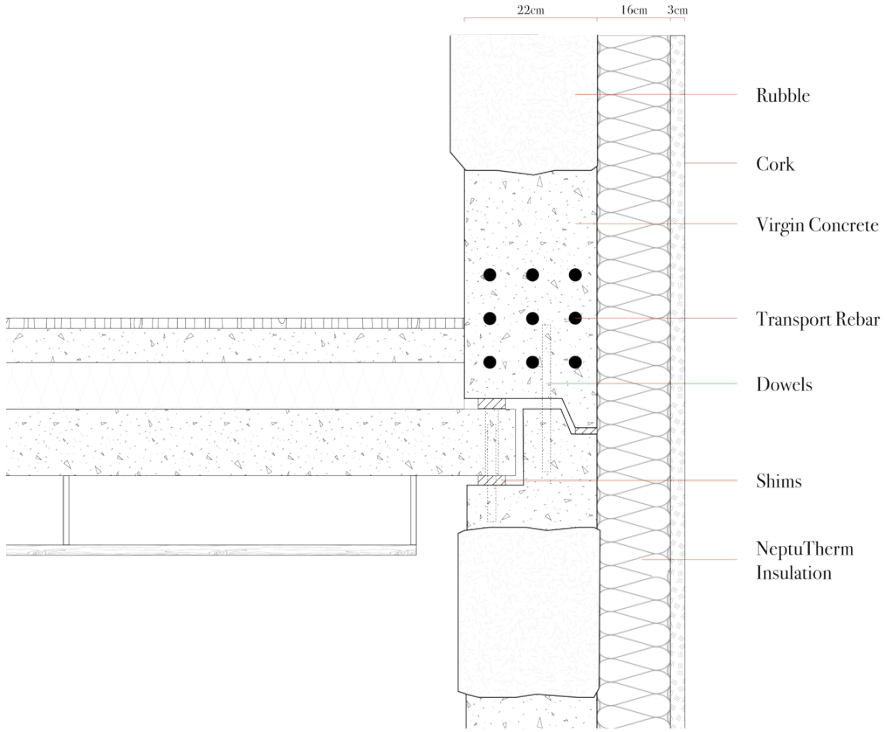

Figure 165 D1 - 1:5 Wall Detail Top Connection & Slab

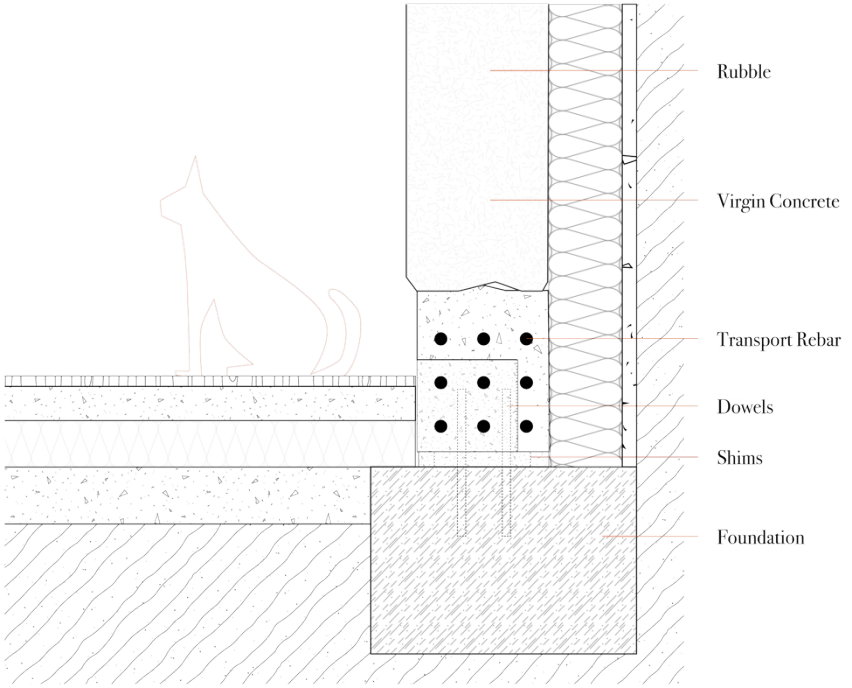

Figure 166 D2 - 1:5 Wall Detail Foundation Connection

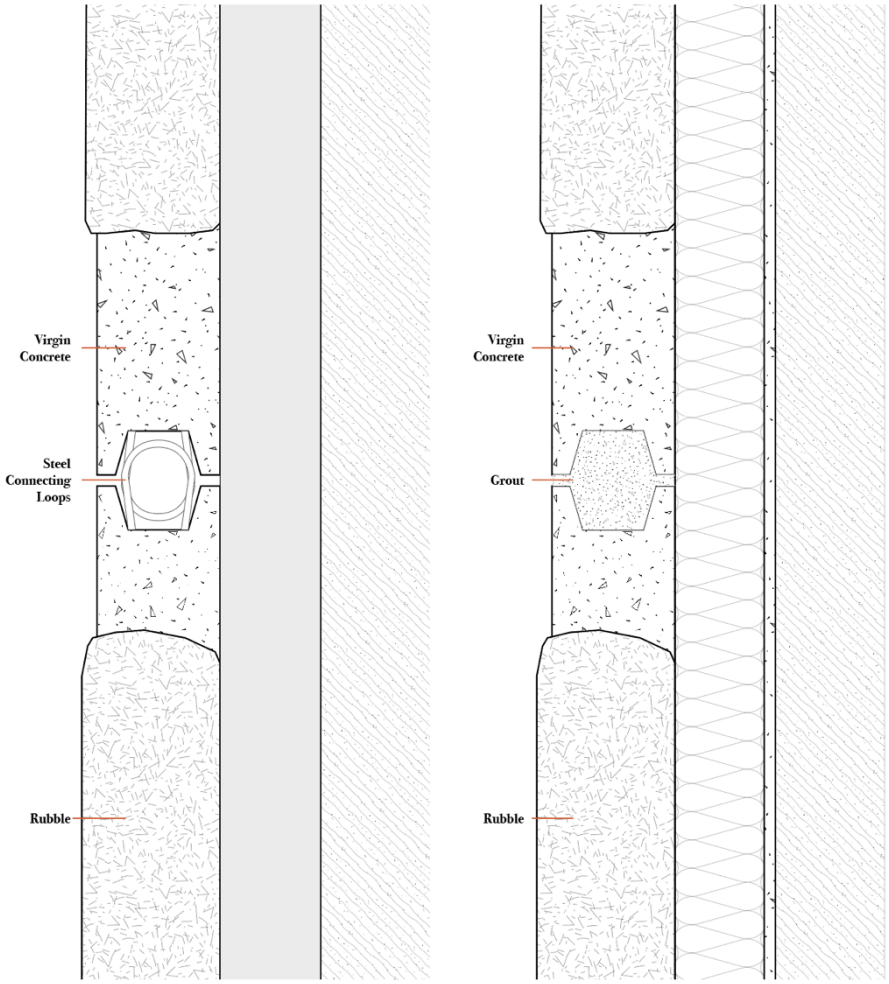

Figure 167 D3 - 1:5 Wall Connection Detail, Left: During Installation, Right: Final Installation Of The Wall

4.4. Demonstrator Design

4.4.1. Introduction

Figure 168 Polished Egg, Karin Sander, 1994 (https://www.karinsander.de/thumbs/work/chickens-egg-polished-raw-size-0/1994_ks_huhnereipoliertroh0_1994_karinsander-920x613-q80.jpg)

To showcase the aesthetic qualities and the variety of surface qualities Cyclopean Spolia Walls offer, six demonstrator walls were built (see Figure 173 and Figure 174). These clearly show the difference between the topography on the front surface and the smooth back surface. Additionally, the rubble arrangements tested in the experiments are presented (large, small, stone infill) and three new varieties are introduced. To represent the freedom of placement that horizontal precast offers, the first option is a rubble pattern. It shows a gradient from large to small stones. The second option demonstrates the potential of coloured concrete filler material, to increase the contrast between the reclaimed rubble and the virgin material. The sand tone gives the composite a warmer appearance, which would be suitable for interior application for example. The last option is a thought experiment. Some rubble from the broken experiment samples was reclaimed and reintroduced into a new Cyclopean Spolia Wall. This demonstrates a potential end of life scenario for rubble walls, entering a new cycle. Future research has to confirm its feasibility.

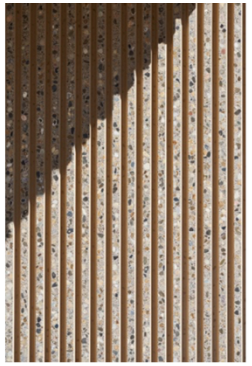

Figure 169 Concrete Surface Treatments (1) (https://carusostjohn.com/projects/stadtraum-hauptbahnhof/) (2) (https://www.bft-international.com) (3) (https://www.folkarchitects.com)

In the demonstrator, all walls are left raw to focus on the reclaimed rubble and its arrangement. This does not need to be the case, though. Figure 168 shows a polished egg by artist Karin Sander. It elevates a functional object of small worth on a plinth and gives it new value, solely with time and surface treatment. If reclaimed concrete rubble is seen as an aesthetic choice and the aim is to give new life to rubble, even luxurious terrazzo-like surface treatments could be applied on the flat side. If the use case is purely functional, less expensive surface treatments like paint or cladding are also an option.

4.4.2. Experiment Materials End Of Life

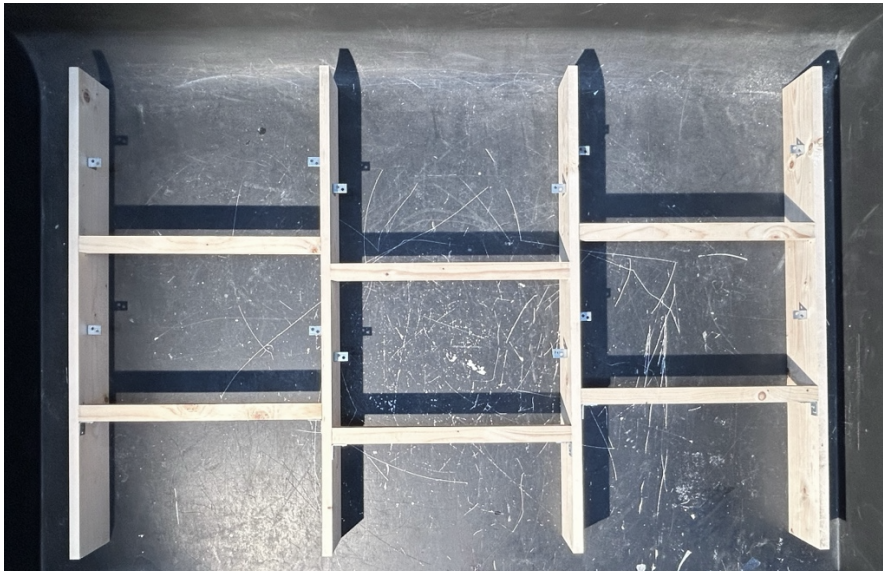

Figure 170 Raw Wooden Demonstrator Shelf Built From Sample Formwork

As the project aimed to reduce the waste created during the thesis, the demonstrator is built purely out of reclaimed materials from the experiments. The formworks used for casting the samples were sanded down and reassembled to serve as the shelf, which was mostly painted with the remaining spray from the DIC speckle pattern. All remaining rubble was either used for the demonstrator or as stand holders for an exhibition design on campus. The wood was reused in the architecture faculty for models. Even though some remains from the broken samples were introduced in the demonstrator, most of the specimens had to be disposed of, due to the heavy damage the compression tests caused.

4.4.3. Demonstrator Images

Figure 171 Demonstrator Shelf

Figure 172 Demonstrator Shelf With Cracked Experiment Samples (Bottom)

Figure 173 Rubble Arrangements Rough Surface, Left: Tested In Section 3, Right: Alternative Arrangements

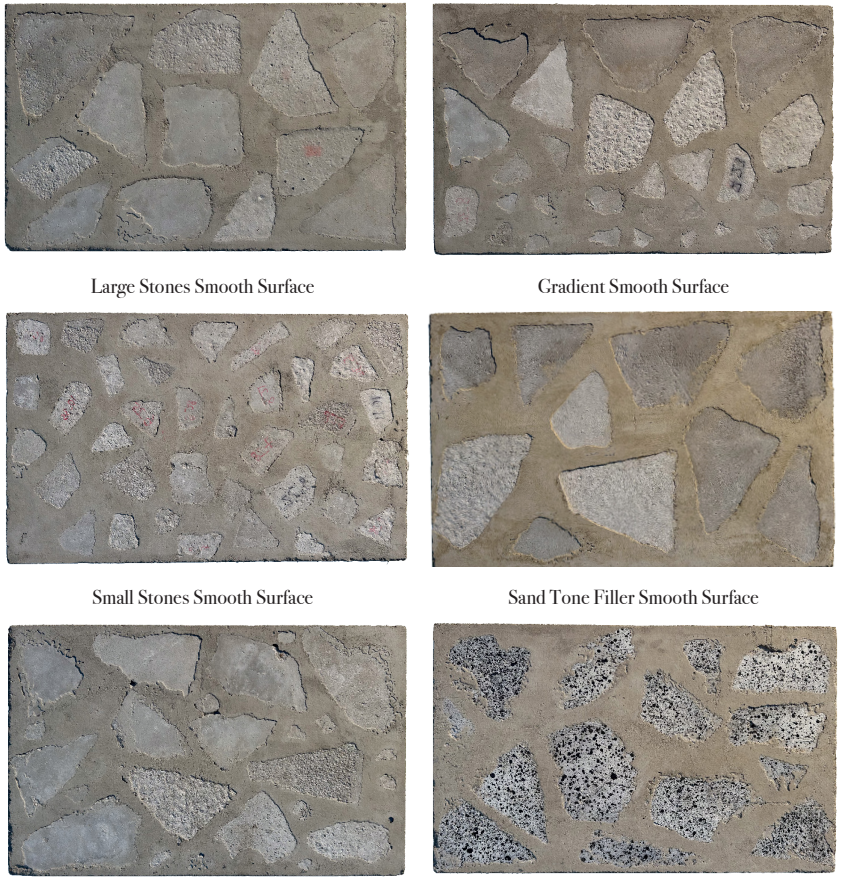

Figure 174 Rubble Arrangements Smooth Surface, Left: Tested In Section 3, Right: Alternative Arrangements

Figure 175 Demonstrator Shelf Front With Rough Surfaces

Figure 176 Demonstrator Shelf Back With Flat Surfaces

Figure 177 Demonstrator Shelf Close Up

Figure 178 Demonstrator Shelf Close Up

4.5. Construction Process

4.5.1. Objectives

The prefabrication process for Cyclopean Spolia draws from the knowledge gathered during the literature review, the two experiment phases and informal conversations with industry specialists. The tests were based on a preliminary process design, which was adapted and refined during the development of the thesis. The purpose of drawing out the process is to show a way how Cyclopean Spolia Walls could be brought to life. Based on the computerisation processes enabled by the workflow from the experiments, the aim is to pave the way for a high level of mechanisation throughout the prefabrication process. The levels of automation, described by Frohm et al. (2008), are thus used to assess the method. The full process developed during this thesis is explained in section 4.5.4 Prefabrication Process.
A detailed feasibility analysis, which includes economic factors, has to be tested in subsequent research within the field.

- The prefabrication process for Cyclopean Spolia draws from the knowledge gathered during the literature review, the two experiment phases and informal conversations with industry specialists. -

4.5.2. Automation

Figure 179 uses the diagram developed by Reichenbach & Kromoser (2021) as a base to assess a stationary precast wall process, which integrates the production of Cyclopean Spolia Walls. The stationary process is chosen, due to its independence from other processes within the factory. It can be customised more easily without interrupting chain processes, like in carousel systems.
The diagram indicates the steps on the tilting table with a thick black line. It shows that the rubble arrangement is integrated as an additional workflow, which starts with the wall design. The digital arrangement of the rubble enables an mechanisation of the rubble placement, if a calibrated overhead crane is present. The rubble is positioned before the regular placement of reinforcement and additional units (window frames, special edge formworks, etc.). This protects the more fragile units from damage. The concreting is shown as automated, but done manually. The digital arrangement delivers enough data for a potential automation of the cavity filling with a calibrated overhead concrete dispenser. This workflow was not tested during the experiments, though.
The diagram shows that Cyclopean Spolia Walls could be produced with little additional steps, which get integrated into proven precast processes. Furthermore, it shows the high level of automation, which can be obtained.

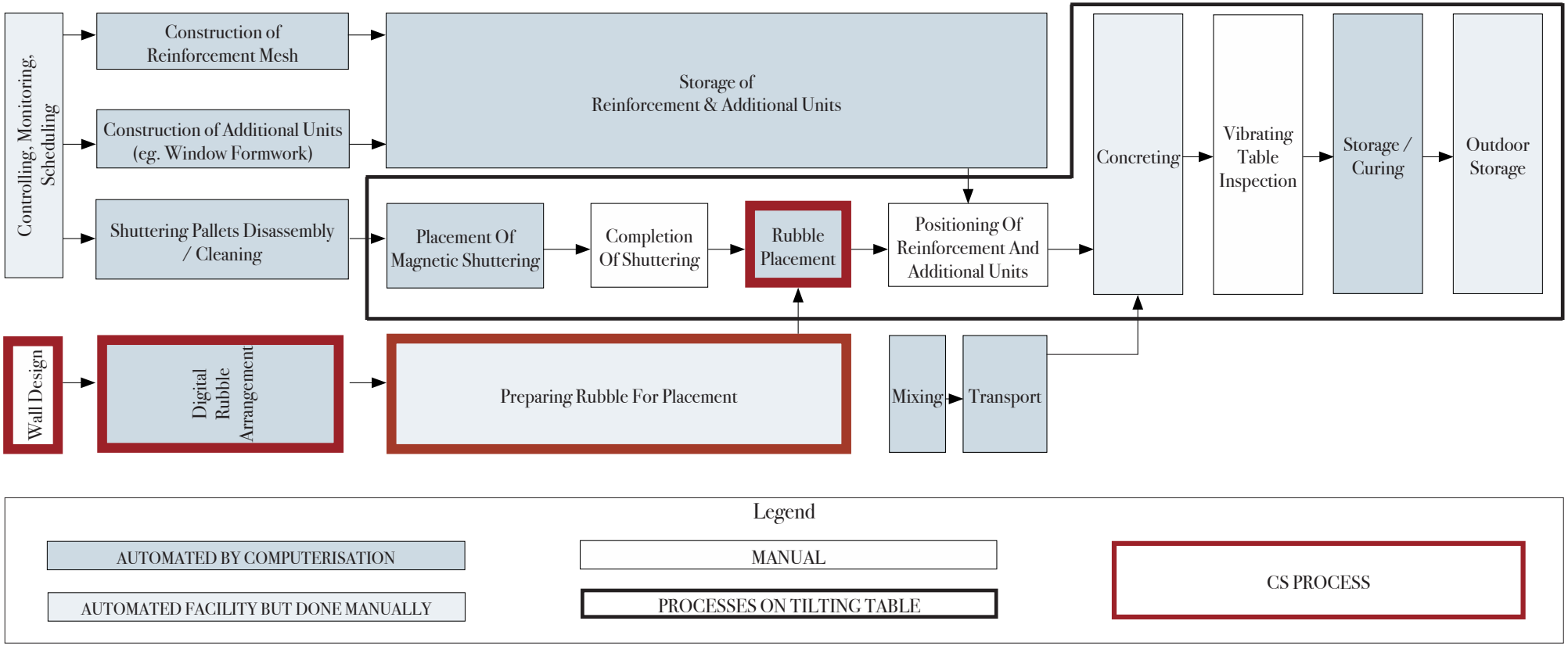

Figure 179 Process And Automation Of Cyclopean Spolia Prefabrication (Based On The Framework By Reichenbach & Kromoser (2021)

4.5.3. Databases

The reduction of the rubble database size required from the algorithm, is a crucial factor for the simplification of the process which precedes the prefabrication method. To arrange rubble with algorithms which restrict the placement of shapes, large amounts of stones have to be scanned and stored. Furthermore, once a wall is designed, individual stones need to be accessed from the storage, to be transported to the precast plant. This requires a sophisticated logistical system, where each stone is accessible at all time. The structural tests showed the potential to use arrangements created by nesting algorithms for CS Walls. They were able to match any shapes the fragments might have with an infill ratio of under 35% during the sample production. The results showed, that a strong infill material and a good bond can lead to a high performance of these arrangements. This opens the doors for small databases and therefore first-in-first-out (FIFO) storage systems (Sembiring et al., 2019).

Figure 180 First In First Out (FIFO) vs Last In First Out (LIFO)
(https://www.interlakemecalux.com/blog/fifo-lifo-inventory-management-systems)

4.5.4. Prefabrication Process

The following pages show the envisioned production process for Cyclopean Spolia Walls. Its development follows the path of the rubble, from the demolition of a building to its new life as a structural member of a new building.

Steps 1-6

The material supply for Cyclopean Spolia Walls begins with the demolition of a concrete building in the traditional destructive way. The option of reclaiming large pieces gives an incentive not to precrush the rubble on site. The rubble is then transported to a waste management facility. Until this point, the process is similar to most demolition projects.

From here on, the rubble is not crushed down, but transferred to a conveyor belt. Due to the wide variation in rubble sizes and their suitability for use in Cyclopean Spolia Walls, the first step is a sorting process. It involves the separation of the large rubble from smaller pieces with a 250 mm diameter sieve. The thickness of the remaining oversized fragments are then separated mechanically. Rubble with a height between 200 mm and 350 mm is selected for Cyclopean Spolia Walls, while all other pieces continue into the standard downcycling stream or are used in other applications.

The suitable rubble pieces undergo a scanning process with a photo from above to detect their 2D contour. Each stone is tagged with a QR-code for subsequent identification, placed into a thickness and diameter group and the contours are saved in a digital database.

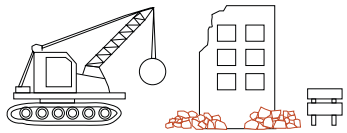

The base for the material supply is the demolition of a concrete building.

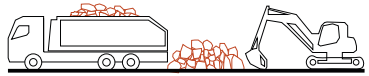

The rubble gets transported to a waste management site.

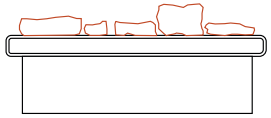

The rubble is transferred to a conveyor belt.

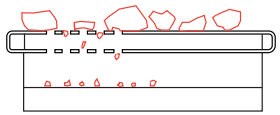

To find the rubble suitable for CS Walls, it goes over a 250mm sieve.

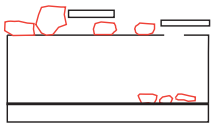

Rubble with a thickness between 200mm and 350mm is separated for Cyclopean Spolia Walls.

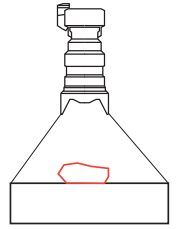

The contour of the rubble then gets scanned and the stones tagged.

Figure 181 Process, Step 1-6

Steps 7-12

The prepared stones are then transferred with a crane to a temporary storage shelf. The inventory follows a first-in-first-out (FIFO) principle (Sembiring et al., 2019) to improve accessibility and algorithm performance. This inventory is divided into four groups or more according to the rubble diameter and thickness. This enables design choices to be made for the stone arrangements.

At the next stage, the architect defines the wall geometry, including dimensions and openings. The rubble diameters and the infill type is chosen to adapt the aesthetical language to the project. Based on these parameters, the algorithm chooses how many rubble fragments are dispatched to the precast plant and calculates a possible arrangement.

Following the design process, the selected rubble elements are packaged and delivered to the stationary precast table. There, the formwork is adjusted to the desired wall dimensions.

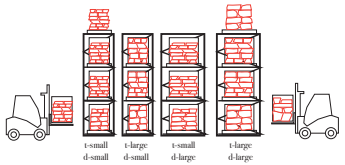

The rubble is temporarily stored in a FIFO system, grouped by thickness and diameter.

The desired wall size, arrangement, infill and window placement is chosen by the architect

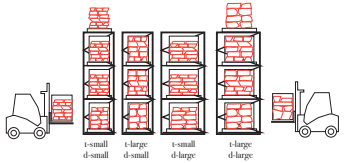

The algorithm determines the amount and type of rubble for the wall and chooses accessible batches accordingly

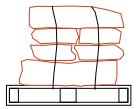

The rubble is packaged...

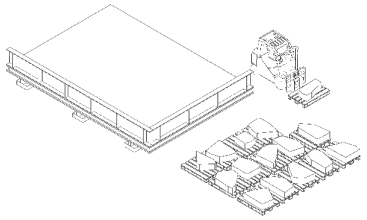

and transported to the stationary precast table, based on the wall requirements

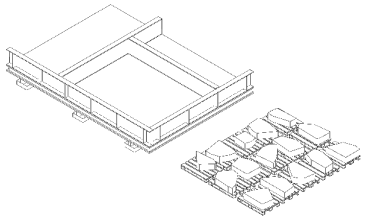

The formwork is adjusted to the desired size.

Figure 182 Process Drawings 7-12

Steps 13-18

To enable openings within the walls for the placement of windows and doors, lintels and interior formwork is placed. Rebar anchors are positioned for the handling beam and connection rings are arranged on the sides. Unless it is the top wall, dowels are placed in the top edge, for vertical wall connections.

Each tagged rubble stone is then picked up with an overhead crane and positioned in its designated location within the formwork, as defined by the algorithm. If damage occurs to a stone during transport, the algorithm rearranges the fragments and may replace the stone with a spare. To insure its availability, a batch of additional stones of each group are always stored close to the tilting table. The flexibility of rubble placement enables a fast reaction time if an error occurs.

Once all stones are in place, the gaps between them are filled with virgin concrete. This can happen manually or with an automated nozzle system, which is informed by the geometry from the algorithm.

The wall is left to cure overnight. Once cured, the precast table is tilted, and the wall is demoulded. It gets detached from the tilting table via small rebar anchors and lifted with loops, which are thread in between the shims. Finally, the completed Cyclopean Spolia Wall is transported to the construction site by truck.

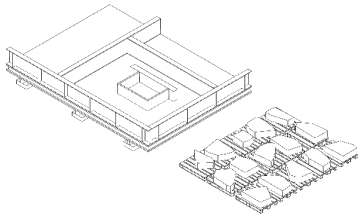

Reba and potential lintels and window formworks are placed.

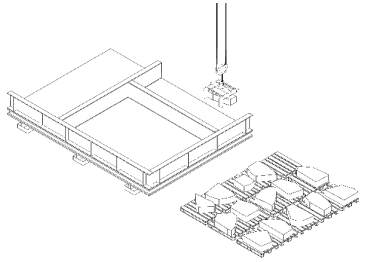

The rubble stones are picked up by crane and placed on the position determined by the algorithm.

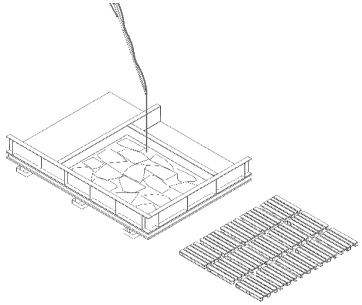

To fill the wall, virgin concrete is poured into the gaps with a nozzle (automated or manually)

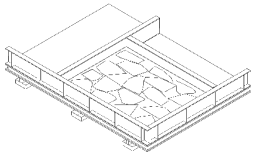

The wall is cured overnight.

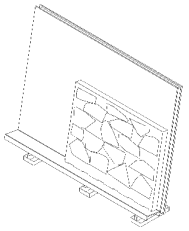

The table gets tilted and the wall demoulded.

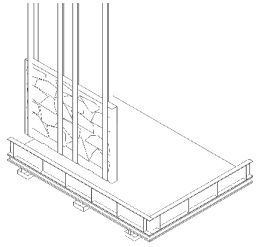

The wall is lifted and transported on site by truck.

Figure 183 Process 13-18

4.5.5. Transport and Assembly

Steps 19-24

On site, the wall gets positioned by crane onto the foundation, with the dowels sliding into cavities in the lower wall edges.

Until the floor is placed, the wall can fall sideways, so it has to be secured with at least two bracing props per panel.

Then, grout is filled in the gaps between the shims and in the cavities with the dowels. After the exterior wall is connected to the foundation, the interior walls are placed and the floor slab is connected. Now, the bracing props can be removed. As the next step, the walls of the subsequent floors are placed and lowered onto dowels inside the upper wall edge. The process is repeated until the case-study building has reached its final height of three stories.

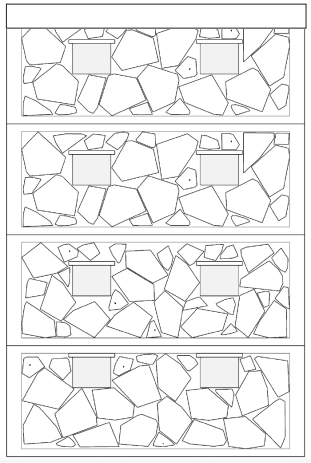

Figure 184 Final Height Of Case Study Building

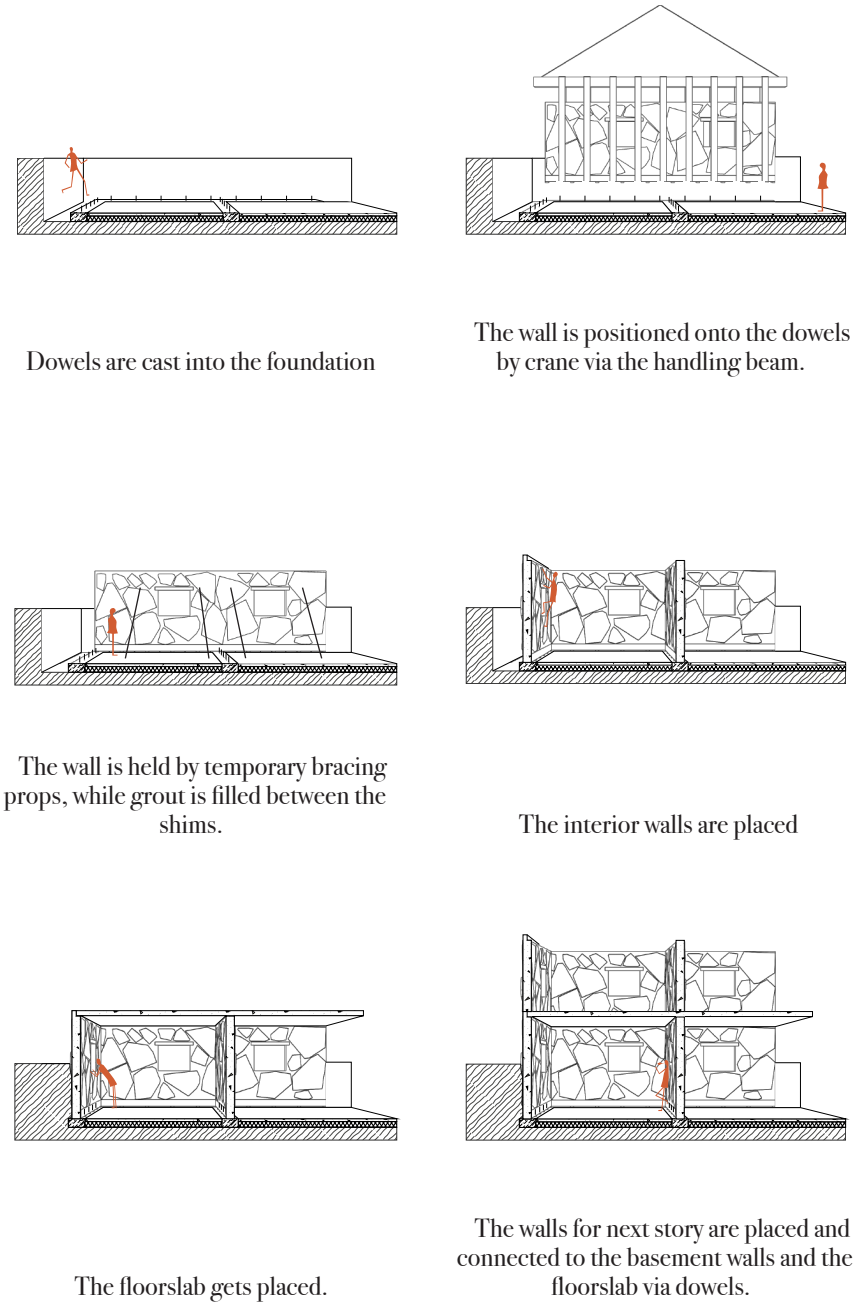

Figure 185 Steps 19-24

4.6. Process Actor Maps

4.6.1. Introduction

Th previous system and process design showed a path how rubble could be integrated into precast walls. It demonstrated that the workflow can be introduced into existing processes and be realized with established technologies. However, it still leaves open which step is executed by whom and at which site. Therefore, five scenarios are presented, which map the locations, stakeholders and the assets required for each process. This gives an overview of potential synergy effects from vertical integration, which could facilitate the adoption of Cyclopean Spolia. Through consolidation of process steps at specific locations and the reduction of stakeholders, transport can be reduced to minimize environmental impact and cost.

The maps are colour coded (see Figure 186), based on the process location and main actor and promoter of the CS Walls is indicated. Furthermore, the assets are divided into existing equipment, which the stakeholder already owns and new equipment they would need to be acquired. The size of the asset boxes indicate how heavy or light an asset is. Heavy represents complex and large machinery and light represents simple and small machinery.

The maps are linear in time, start with the demolition of a building and end with rubble integrated into a new building.

Figure 186 Process Actor Maps Legend

4.6.2. Analysis

The full map diagrams can be found in Section 4.6.3, on page 138. The maps focus on the integration of rubble into the walls and do not included the supply chains for formworks, rebar, virgin concrete etc.

Map 1: CS As Facilitator

In the first scenario, each step is done by separate expert firms, which adapt their existing workflow to Cyclopean Spolia. An external CS Firm organizes the design service, the sales and the communication between the supply, production and logistic firms. The waste is treated and sorted by a construction and demolition waste management company, who are already equipped with sorting and handling machines. The prefabrication is handled by a precast plant, which arranges some stationary tables for rubble placement.

This process is highly fragmented and therefore requires the most transport steps. Ideally, the prefabrication plant is close to the waste management firm, to reduce distances. The advantage of the fragmented steps is that every firm does what it can do best and that it only requires adaptation of existing processes and no new factory. This division of labour would be the most feasible for early testing stages for Cyclopean Spolia, as the initial investment is lower.

Map 2: Integration Into Waste Management

In the second map, the Cyclopean Spolia production is vertically integrated into the process of a waste management firm. They profit from cheap raw material supply, due to the availability of rubble at their

site. This eliminates the transport from the sorting station to the precast plant and creates a synergistic effect. The downside of this vertical integration is that a waste management firm has to acquire know how, equipment and a customer base for precast walls, which is not their core business (Lehtinen, 2010).

Map 3: Integration Into Prefabrication

The third map is similar to the second in its synergistic potential, due to vertical integration. It locates all sorting, storing and production steps within one prefabrication firm. This also eliminates the transport required between initial waste sorting and the casting of the walls. A manual pre-sorting of the rubble on the demolition site could facilitate the adoption of this workflow. Nevertheless, it embodies the same challenge and high investment as Map 2 for the main actor.

Map 4: Cyclopean Spolia Firm

The fourth map relies on a new firm, which integrates the entire value chain into its operations. To ensure that the building demolition is streamlined for CS rubble supply and to pre-sort the rubble, the firm integrates the demolition process into its process. A mobile scanning and tagging unit generates the database directly on-site, which eliminates an additional sorting location. The rubble can then be stored at the precast plant and directly integrated into CS Walls, which are then distributed and installed by the firm. This process cuts out a transport step and a sorting location, but it requires a strong initial investment and a high local market demand.

Map 5: On Site CS

To eliminate the transport of the rubble and the walls completely, Map 5 introduces a process which revolves around an on-site mobile factory unit. The CS Firm offers a service which integrates the rubble directly into the walls of the new building. The rubble is stored, scanned and placed in formworks close to the site in a temporary blow-up tent structure. Examples for this workflow is the process explored by Johns et al. (2023) (see Figure 38 on page 44) and the walls built in 2022 for the Social Housing 2104 by HARQUITECTES (see 0

Architectural References on page 109).

Conclusion

- Overall, the maps reveal the importance of combining the rubble supply with the CS Wall production process. -

Overall, the maps reveal the importance of combining the rubble supply with the CS Wall production process. Even though most machines are already available, they are currently separated between waste management sites and precast plants. The combination of these production steps can create synergy effects and reduce transport and storage expenses. Furthermore, a manual pre-sorting at the demolition site can reduce the heavy machinery needed for separating the rubble in the waste treatment plant. As a proof of concept, an On-Site Cyclopean Spolia process could be a starting point, as it requires the least steps.

4.6.3. Maps

Map 1: CS As Facilitator

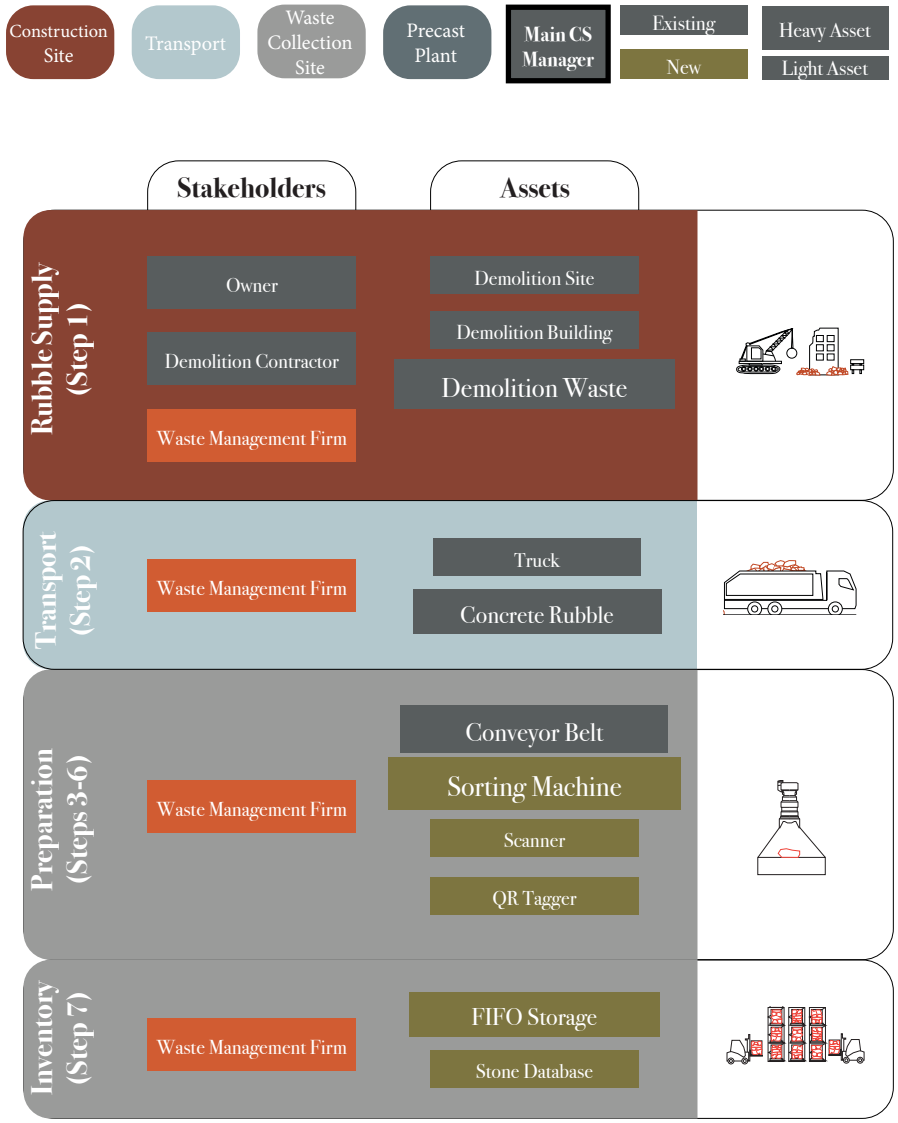

Figure 187 Map 1: CS As Facilitator

Map 2: Integration Into Waste Management

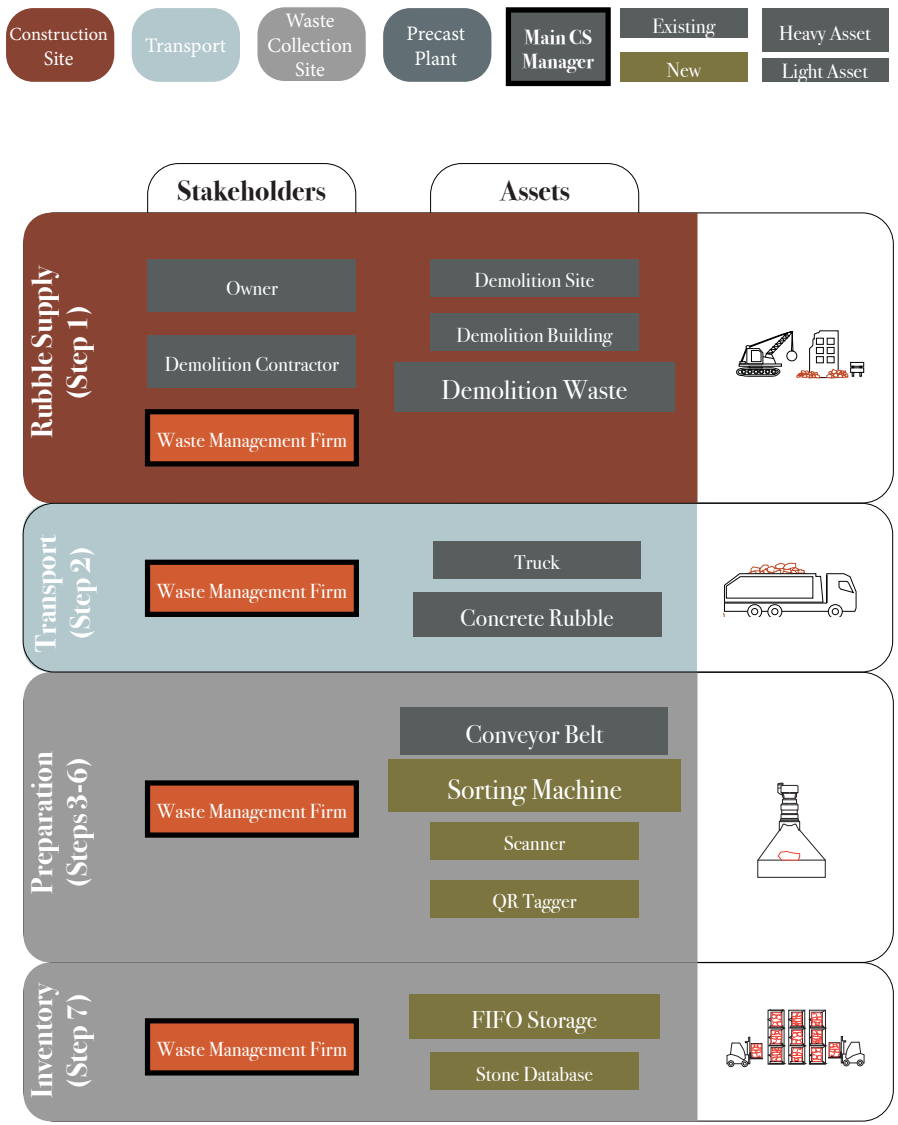

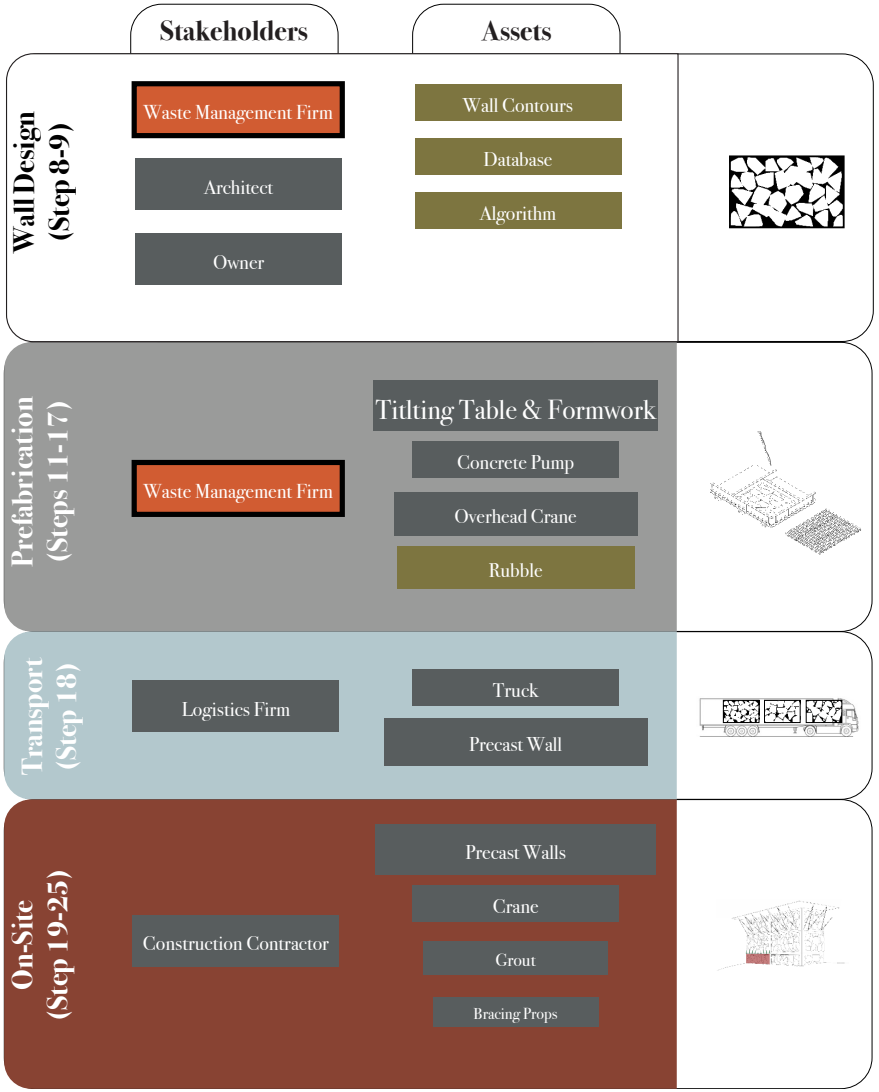

Figure 188 Map 2: Integration Into Waste Management

Map 3: Integration Into Prefabrication

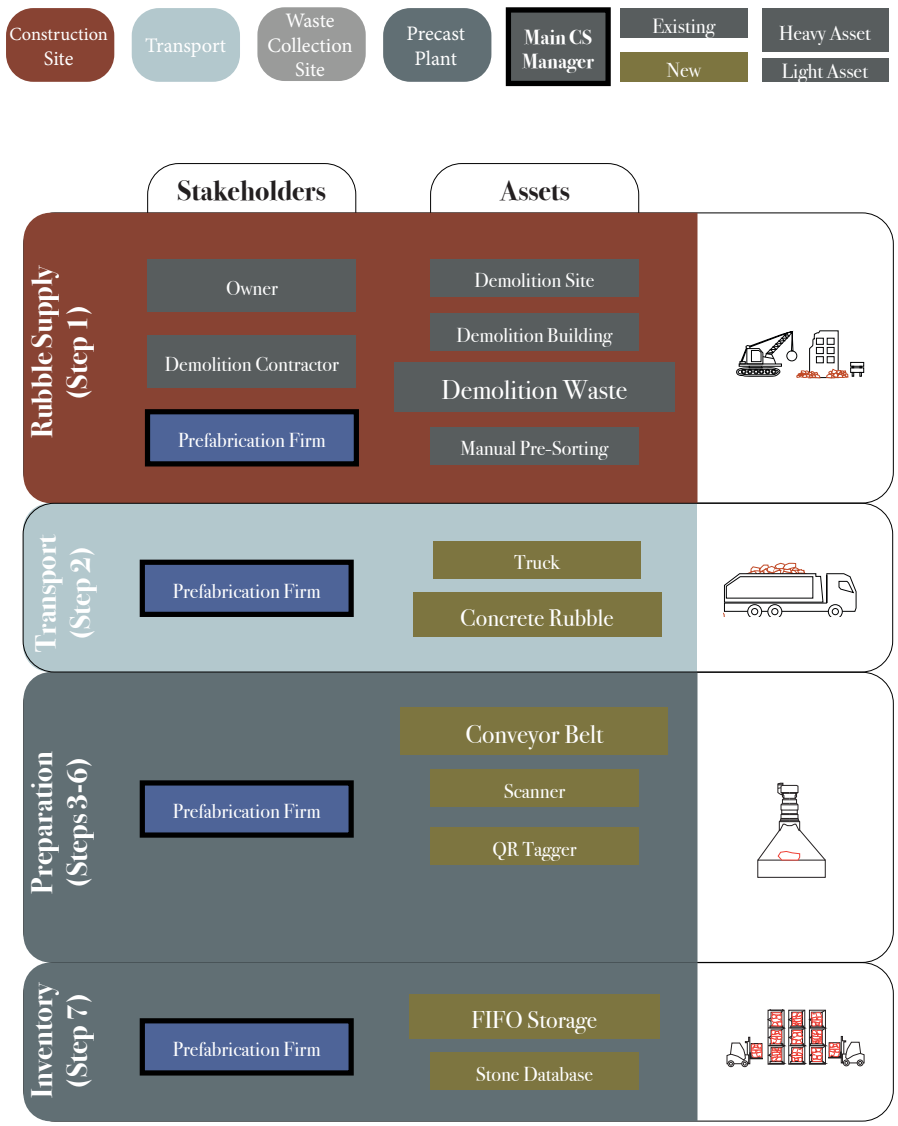

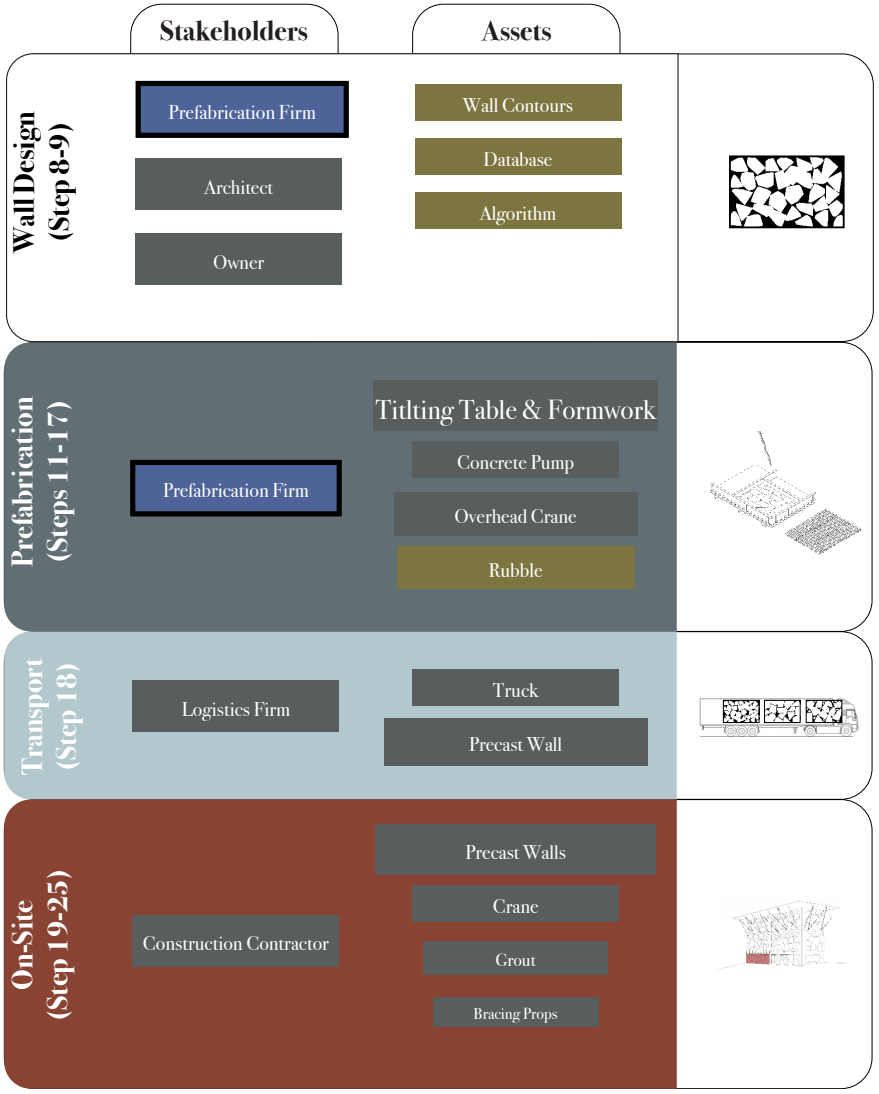

Figure 189 Map 3: Integration Into Prefabrication

Map 4: Cyclopean Spolia Firm

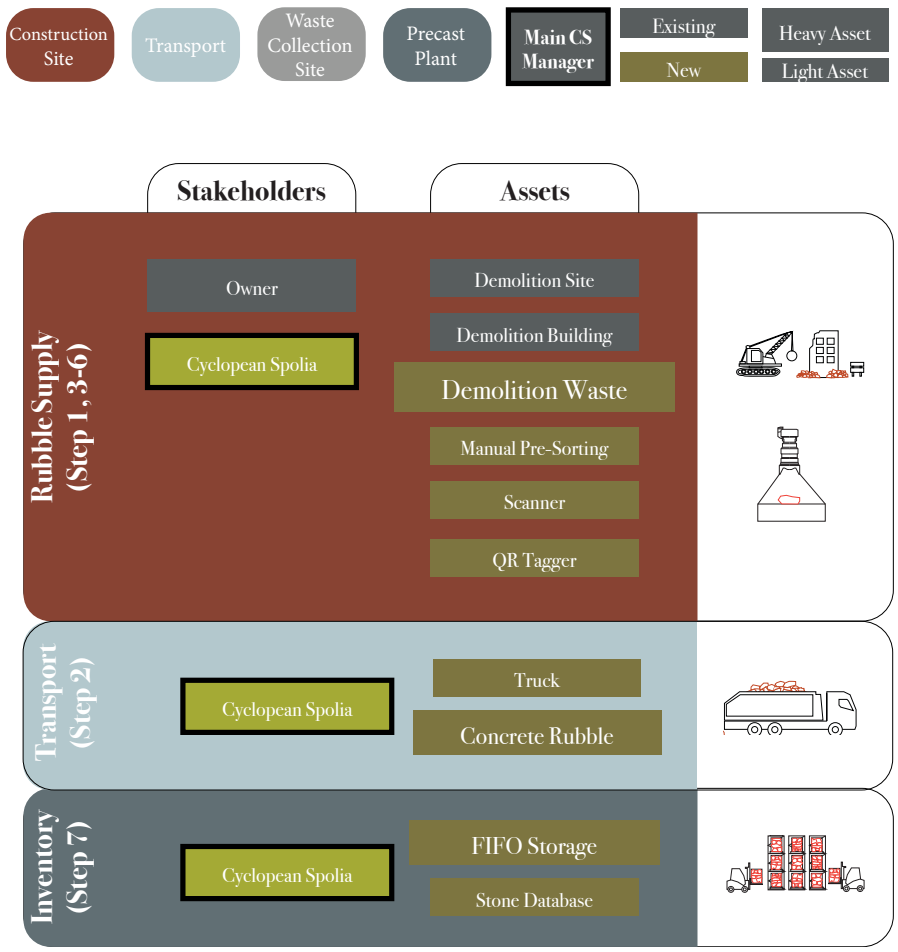

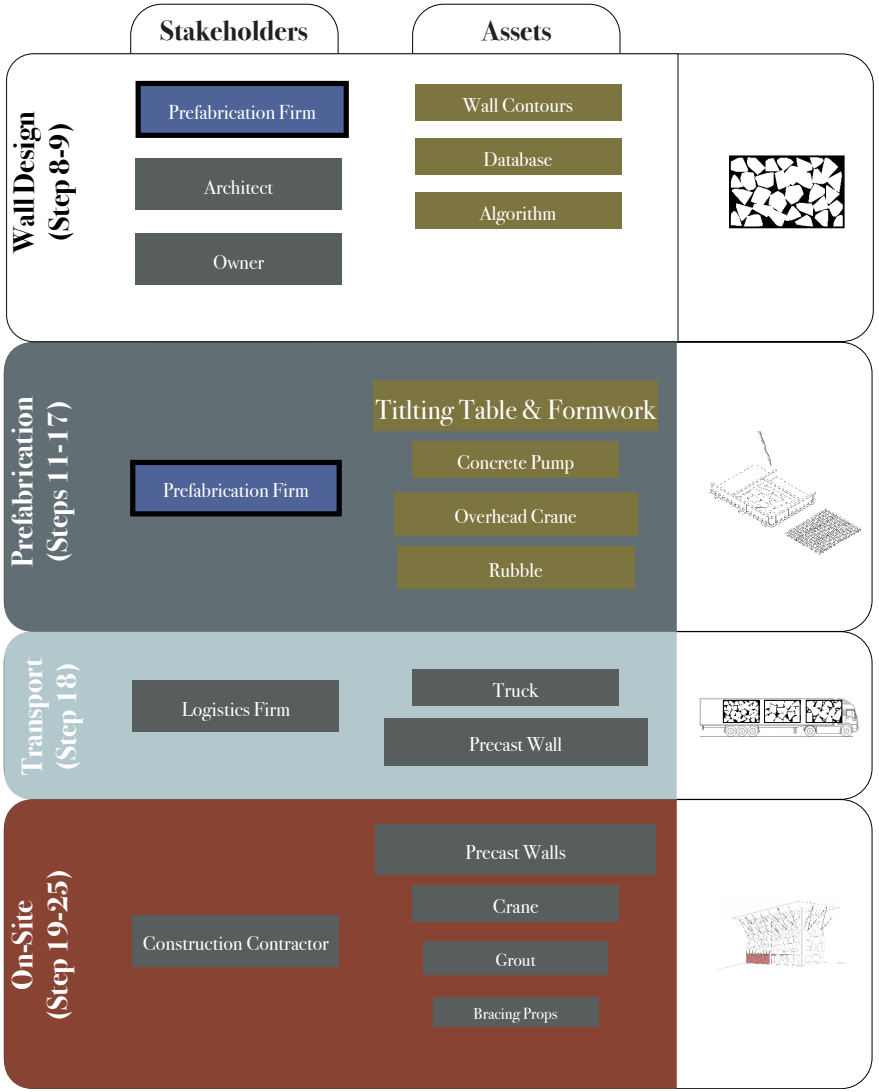

Figure 190 Map 4: Cyclopean Spolia Firm

Map 5: On Site CS

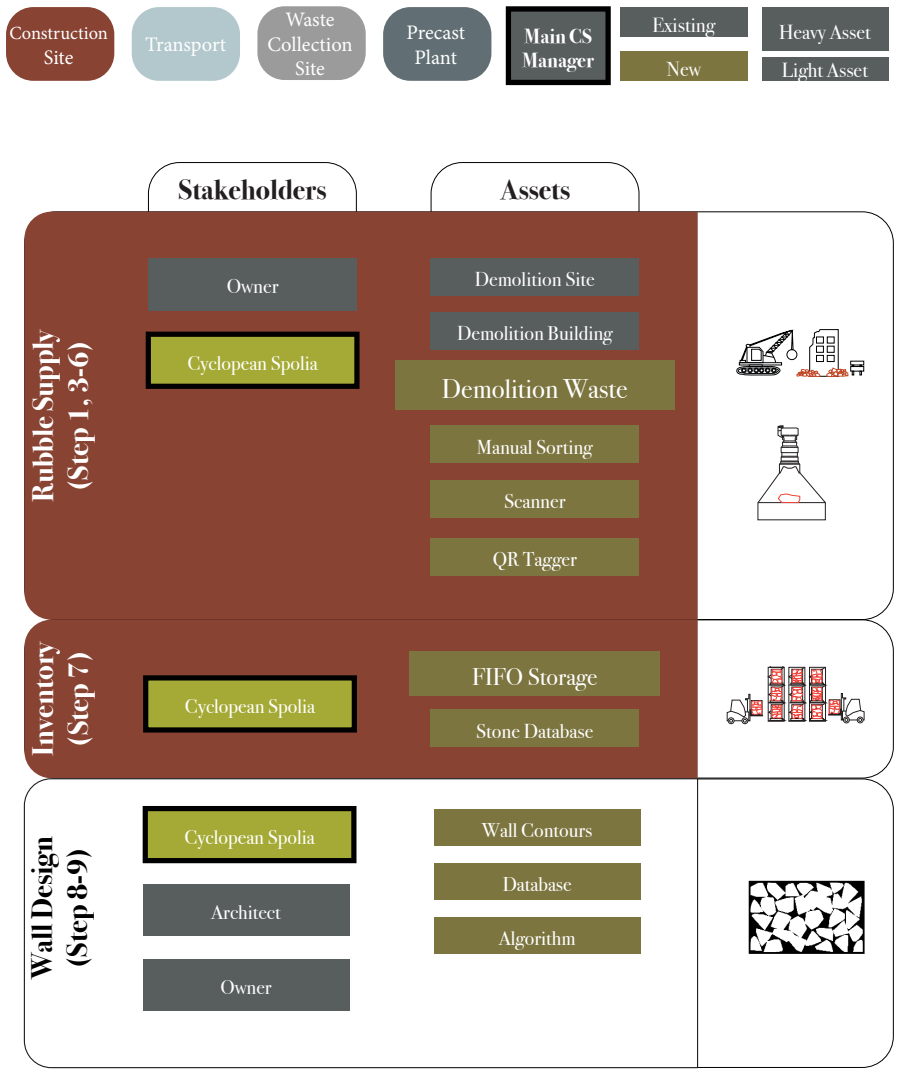

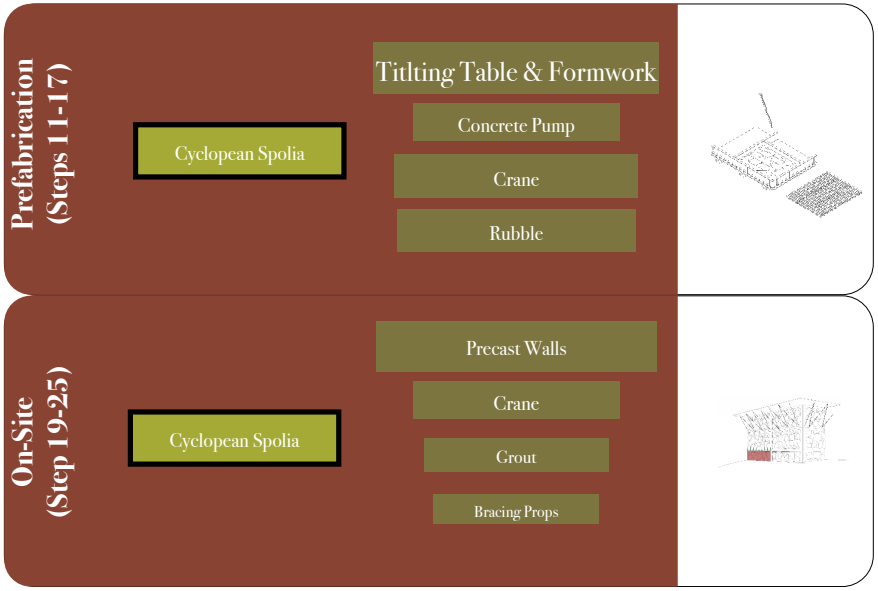

Figure 191 Map 5: On Site CS

4.7. Answer To Research Questions

How can a prefabrication process enhance the design freedom of load-bearing concrete rubble walls?

The structural tests and the system design demonstrated how a horizontal precast process can influence the options for rubble placement. As no structural integrity is required during the construction process, the rubble can be freely arranged. This also improves the scalability of the process, as storage and replacement of rubble is facilitated. The design freedom was showcased by the demonstrator walls, which showed the variety of arrangements enabled by the CS process.

How can Cyclopean Spolia Walls be designed to integrate into existing prefabrication and construction processes?

The process designed here is integrated into a stationary precast wall production module. Except for a new crane gripper, all equipment is already present in the factory. Multiple scenarios were laid out for the rubble supply, to incorporate it into current waste management streams. The technical wall design is based on common precast wall connections, which does not require new processes on site. Therefore, the process was designed for an easy adoption of Cyclopean Spolia within existing construction methods.

4.8. Conclusion

The System Design chapter showed a possible path towards the realization of Cyclopean Spolia Walls. The built architectural projects which were discussed, prove that similar approaches have successfully been implemented. Based on the assumed structural performance from the tests, future applications for CS Walls are vast. The wall design showed that the technical challenges prefabrication imposes upon rubble integrated walls can be overcome. The demonstrator revealed the surface finishes and possible rubble arrangements, to show the potential of rubble as a design feature.

- The process design was able to demonstrate how traditional precast methods could produce rubble walls within their existing workflows -

The process design was able to demonstrate how traditional precast methods could produce rubble walls within their existing workflows, which can be transported and assembled like regular prefabricated walls. The maps discussed several methods on the division of labour and the assets required for Cyclopean Spolia.
To conclude, the system design showed different paths and considerations which have to be taken into account to realize CS Walls. It showed a high potential for the integration of the process into existing workflows and for its design.

Environmental Impact

Summary

This section illuminates the environmental impact of Cyclopean Spolia Walls from three different perspectives. First, it discusses the waste reduction the process offers and how it could be developed. Then, to quantify the environmental impact, a cradle-to-gate analysis is conducted, which focuses on Global Warming Potential (GWP) and the total non-renewable energy (PENRT). The analysis compares different solid wall configurations as the functional unit. Lastly, the circularity of CS Walls is discussed, based on a framework by Zabek et al. (2023).

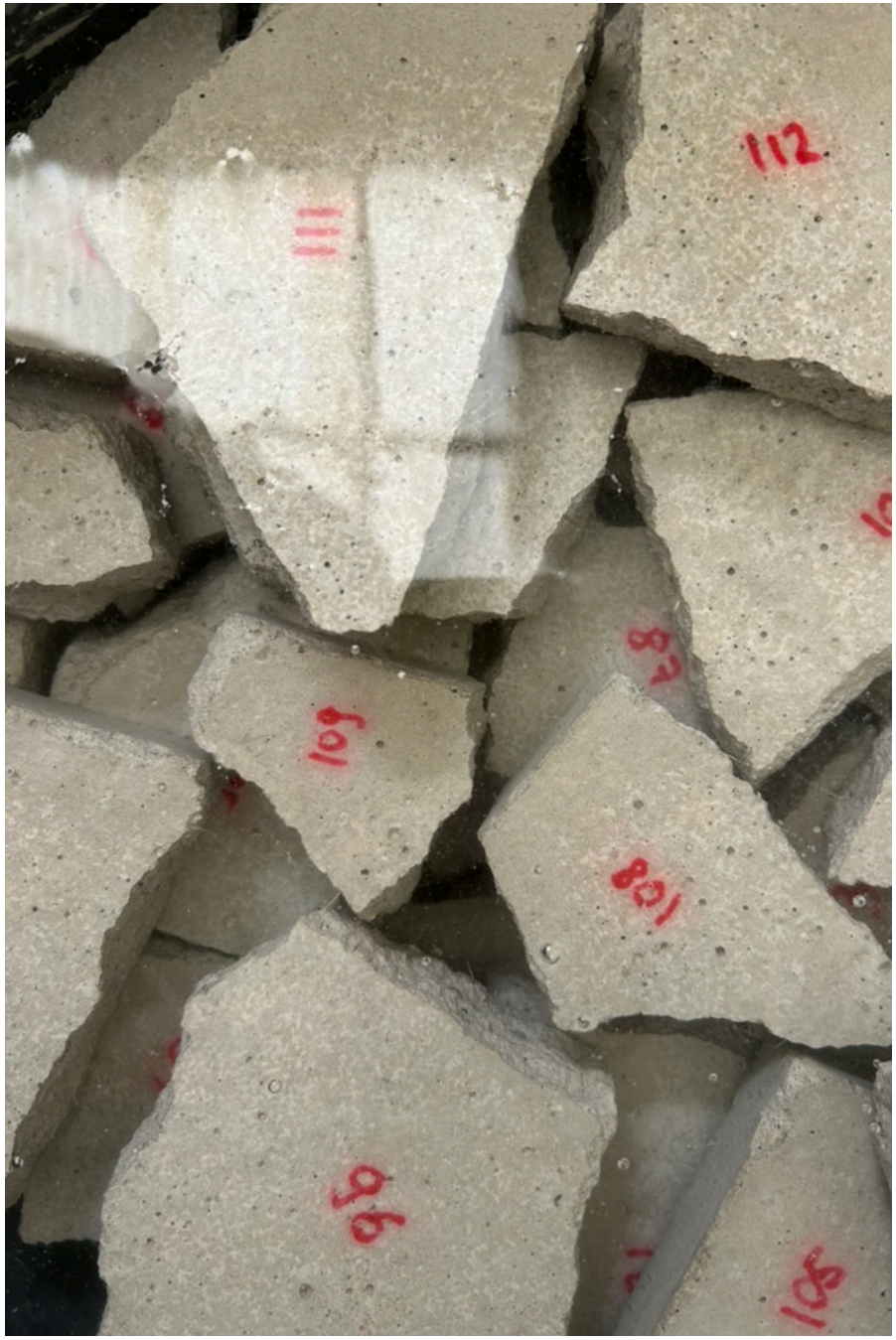

5.1. Introduction

CS Walls could lead to a new way of assessing concrete waste. As they propose a new stream of reclaiming the material, they offer new value perception to concrete rubble. This could save parts of it from entering a singular downcycling process and elevates its use case to structural applications. The first part of this chapter therefore focuses on the waste reduction which is facilitated by CS Walls.

In addition to the effect on waste, the reclaimed rubble fragments also have a positive environmental impact on the new wall in which they are integrated into. Due to their volume, they reduce the need for virgin concrete, which could lower their carbon footprint. To assess this numerically, the second chapter introduces a Life Cycle Analysis. It compares the infill ratios investigated during the experiments phase to multiple alternative solid wall systems.

However, the aspect of reclaiming a building piece is difficult to express in numbers. Therefore, the third section discusses the circularity of Cyclopean Spolia Walls in a qualitative approach.

5.2. Waste Reduction

After soil, concrete is the heaviest waste on earth and the second largest component of human waste by weight (*Database - Waste - Eurostat*, n.d.). According to Islam et al. (2019), around 60% of demolition waste is concrete (see Figure 192). Currently, concrete rubble in Europe is either downcycled or landfilled (Baldania & Bhogayata, 2023; Vermeulen, 2016).

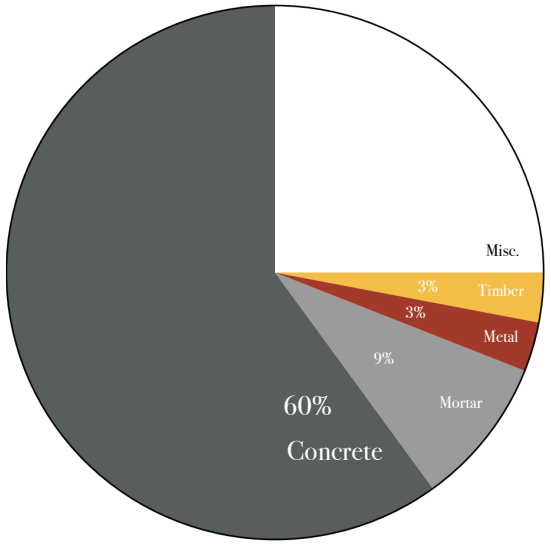

Figure 192 Average Waste Types In Demolished Buildings (Islam et al., 2019)

When there is no way around demolishing a building, the first aim should always be the reuse of full components, based on the circularity R-ladder (Cramer, 2022). The Cyclopean Spolia process has to be seen as the next step, for elements which cannot be reused in their entirety, or for projects where reuse was not planned for or not economically

feasible. CS Walls can then offer a higher quality waste stream for concrete rubble, compared to the existing options. As the demolition method does not need to be adapted, their supply introduces no new costs for the demolition contractor.
Nevertheless, the potential for a cheaper disposal of rubble could lead to an incentive for demolition companies to leave larger pieces intact. This would increase the percentage of rubble suitable for precast wall integration.

- When there is no way around demolishing a building, the first aim should always be the reuse of full components -

As the process cannot incorporate every shape of rubble, it only offers a value increase for parallel-sided fragments, which are mainly found in walls and floor slabs, according to FCRBE (2021). This thesis focused on a visible integration of rubble into walls, to communicate the reclaimed material in its surface, similar to Les Bleuets in Paris by Paul Bossard (1962). However, other shapes could also be integrated into concrete as lump aggregates, like in the paper by Lin & Wu (2025) or the Social Housing 2104, designed by HARQUITECTES (2022). These 'invisible' inclusions can further reduce the waste generated and increase the value given to concrete rubble.

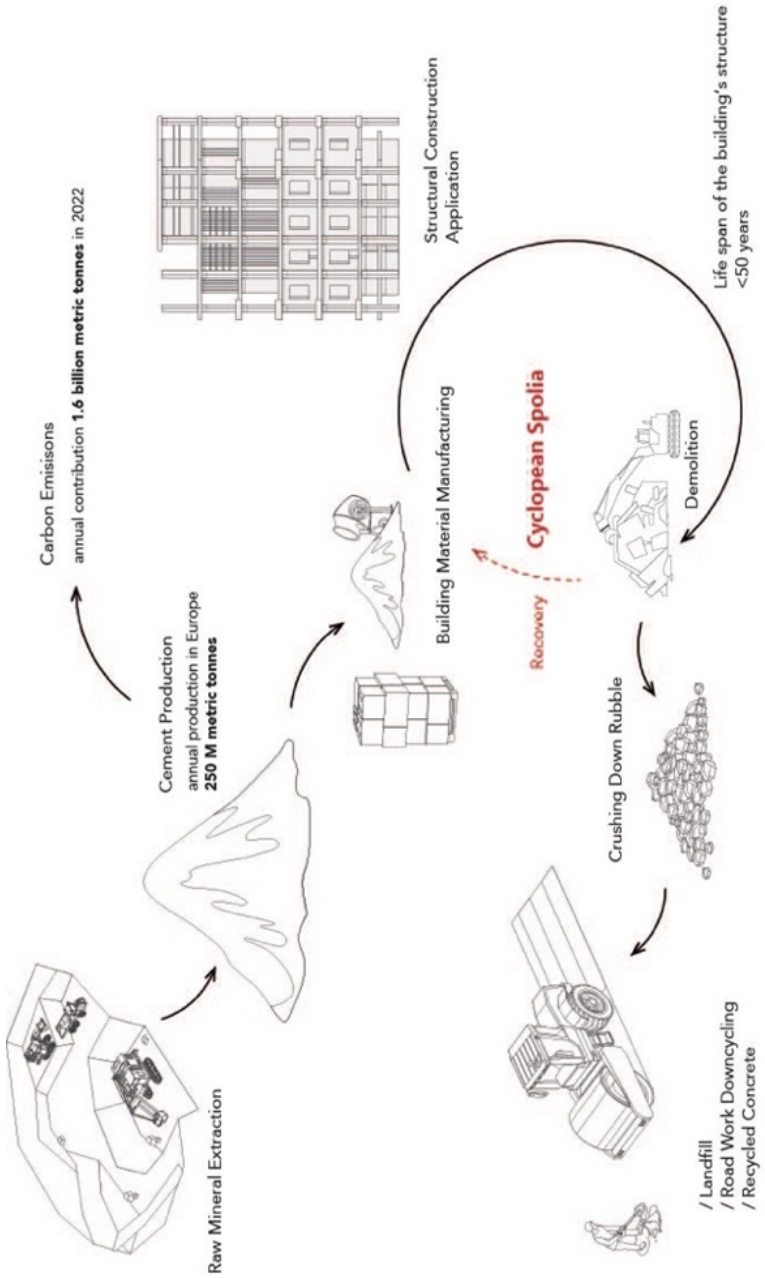

Figure 193 Cyclopean Spolia Diagram (adapted from Mosaic Walls (2024))

5.3. Cradle-To-Gate Assessment

To quantify the environmental impact of CS walls, a cradle-to-gate analysis is conducted. As there is currently no product, which directly compares to Cyclopean Spolia, different types of materials, commonly used for solid walls are assessed.

5.3.1. LCA Setup

The LCA setup defines the goal and the scope of the study, according to ISO 14044 (2006).

Cradle To Gate	Product Stage	A1	Raw material extraction
		A2	Transport to manufacturing site
		A3	Manufacturing
Cradle To Practical Completion	Construction Stage	A4	Transport to construction site
		A5	Installation / Assembly
	Use Stage	B1	Use
		B2	Maintenance
		B3	Repair
		B4	Replacement
		B5	Refurbishment
		B6	Operational energy use
		B7	Operational water use
Cradle To Grave	End of Life Stage	C1	Deconstruction & Demolition
		C2	Transport
		C3	Waste processing
		C4	Disposal
Cradle To Cradle	Circularity	D	Benefits and loads beyond system boundary

Figure 194 LCA Stages, In Orange: Stages Analysed For This Project (based on Klöpffer and Grahl, 2014)

"The goal and scope of an LCA shall be clearly defined and shall be consistent with the intended application. Due to the iterative nature of LCA, the scope may have to be refined during the study." (ISO 14044, 2006)

Goal

The introduction of concrete rubble into precast walls mainly influences the product stage of the walls. Therefore, the objective of this study is to investigate how it can reduce the carbon emissions of a solid wall system in stages A1-A3. It therefore verifies, whether the reduction of concrete waste from existing buildings can also reduce the carbon emissions of future buildings. The study is targeted to designers and future researchers, to inform of potential savings, which can be achieved with CS Walls and how they compare to other common structural systems.

Scope and Functional Unit

In this thesis, the primary function for a Cyclopean Spolia is defined as the main structural member of a low-rise building. Therefore, a case study of a three story multi-family residential building in Germany is assessed. The study illustrates the decision process for the material for a load-bearing solid external wall during the design of such a building. The functional unit is defined as:

"The provision of a load-bearing exterior wall system that supports a three-story low-rise multi-family building in Germany "

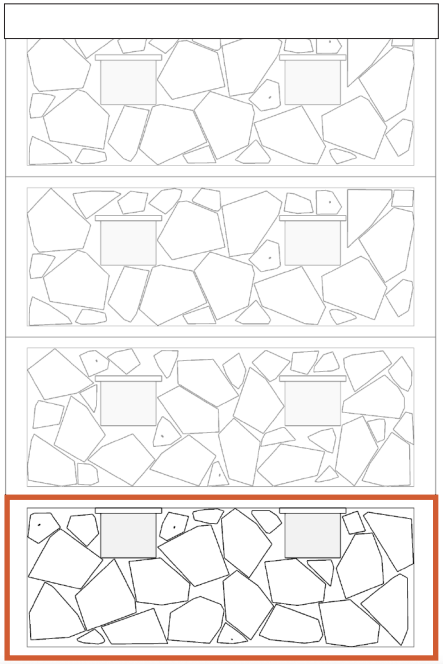

Figure 195 Diagram Of A Three Story Case Study Building, The LCA Is Calculated For Orange Wall

The regional EU standards ISO 14040 & ISO 14044 are used for the study and the EPDs accessed are based on EN15804 +A1 or EN15804 +A2.
For the calculations, 1 m2 of the lowest wall of the building is compared (see Figure 195). As System Boundaries, a Cradle to Gate study is conducted, including stage A1 to A3. A4 is disregarded, as transport distances highly depend on the individual project location. The units chosen for comparison are solid, load-bearing wall systems and exclude structural frame systems. To compare them to a Cyclopean Wall, which faces the exterior of the building, all systems have external structural members with internal insulation (DIN 4108-2, 2013). The choice of the main load-bearing material influences the wall thickness and the insulation thickness. All other wall materials (eg. insulation vapor barriers, paint etc.) are disregarded, as the values proved to be similar for each system. The study focuses on the Global Warming Potential (GWP) of the wall setups and on the total primary energy resources (PENRT). The case study is situated in Germany, as the Environmental Product Declarations (EPD) are more accessible than in the Netherlands.

5.3.2. Wall Systems Assessed

For the LCA, the virgin concrete infill of the rubble arrangement of the CS Walls is decisive. The structural test phase assessed 20% and 30% virgin concrete infill. Hence, these two configurations are measured on their carbon impact, with the previously assumed compressive strength of 5 MPa in 1:1 scale applications. To benchmark the CS Wall material, it is compared to common materials for residential multi-family houses. According to Zandonella Callegher et al. (2023), since 2010, brick, concrete and wood are the dominant materials for multifamily houses. Based on this, this study will assess the following materials:

I. Brick
II. C35/37 Concrete (Precast)
III. C35/37 Concrete (in-situ)
IV. C35/37 RCA Concrete (in-situ)
V. Rammed Earth

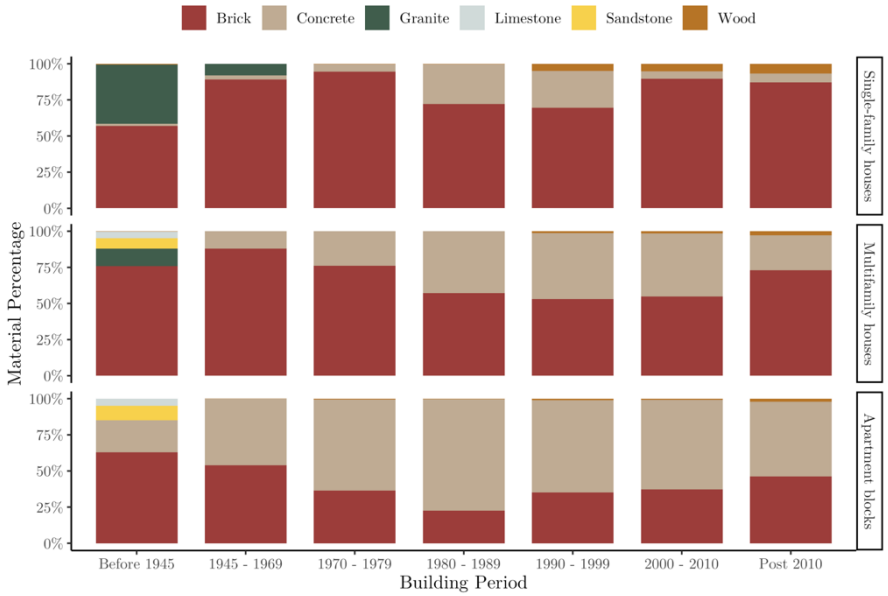

Figure 196 Wall Materials At EU27 Level According To Building Types And Construction Periods (Zandonella Callegher et al., 2023)

As wood constructions are usually executed as frames, they are disregarded here. The concrete types chosen are a precast wall, to compare to the construction method of CS Walls; an unreinforced in-situ concrete wall, to compare the lack of rebar; and an unreinforced RCA concrete wall, to include the current recycling stream of concrete rubble. Furthermore, a prefabricated rammed earth wall by ClayTec (n.d.) is assessed, to compare CS Walls to a similar low-carbon, low-strength product.

	Brick	Precast Wall	C30 Concrete	R-C30 Concrete	Rammed Earth	CS Wall 30%	CS Wall 20%
f_ck	12.00 MPa	30.00 MPa	30.00 MPa	30.00 MPa	2.00 MPa	5.00 MPa	5.00 MPa
safety factor	1.5	1.5	1.5	1.5	1.5	1.5	1.5
f_cd	8.00 MPa	20.00 MPa	20.00 MPa	20.00 MPa	1.33 MPa	3.33 MPa	3.33 MPa
GWP (C02e / m3)	**113 kg**	**398 kg**	**232 kg**	**226 kg**	**9 kg**	**105 kg**	**93 kg**
(CO2eq / m3) / f_d	14 kg	20 kg	12 kg	11 kg	7 kg	32 kg	28 kg
PENRT (MJ / m3)	**1180 MJ**	**3170 MJ**	**984 MJ**	**962 MJ**	**124 MJ**	**682 MJ**	**609 MJ**
(MJ / m3) / f_d	148 MJ	158 MJ	49 MJ	48 MJ	93 MJ	205 MJ	183 MJ

Table 26 LCA Materials

As shown in Table 26, the chosen materials exhibit a variety of compressive strengths. Hence, a direct comparison of their CO2 eq. emissions per m3 would undermine their performance variety. Figure 197 shows that such a method demonstrates a 10x higher carbon footprint of the C30/37 precast wall than the CS Wall. This approach disregards the superior structural performance of the precast wall compared to the unreinforced 5MPa CS Wall, though.

To counteract this bias, the results were benchmarked against each material's compressive strength, as shown in Figure 198. It demonstrates that a C30/37 unreinforced concrete wall actually emits less CO2eq per MPa than CS Walls do. Furthermore, despite the low compressive strength of rammed earth, the prefabricated clay wall still emits 80% less CO2 than the CS Wall.

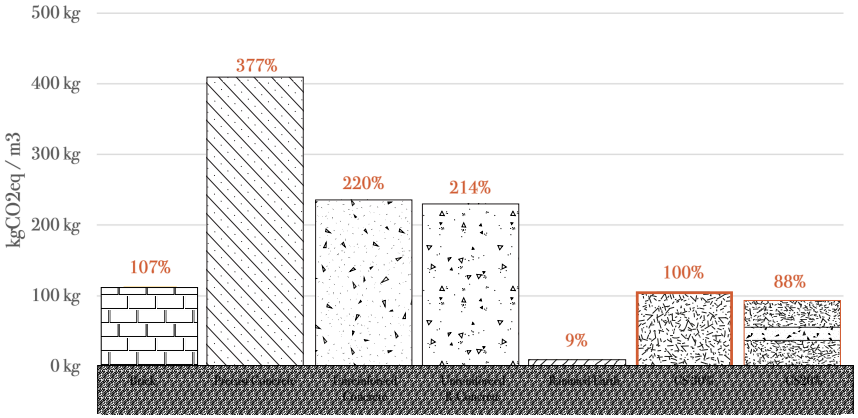

Figure 197 Comparison Of GWP Per m3 (A1-A3)

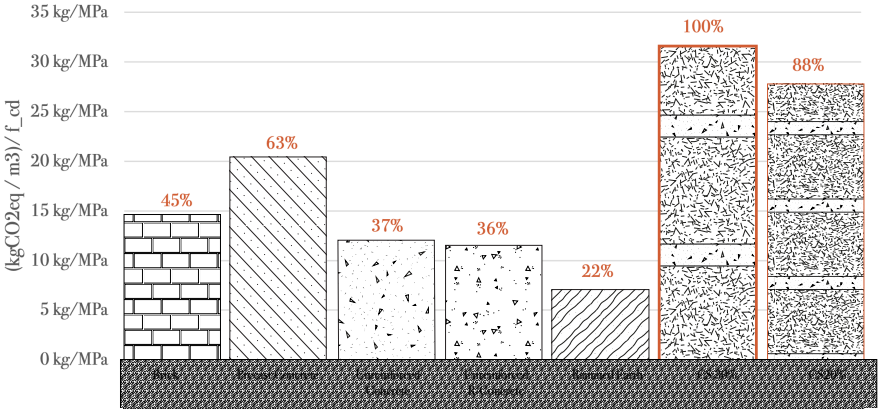

Figure 198 Comparison Of GWP Per Compressive Strength Unit MPa (A1-A3)

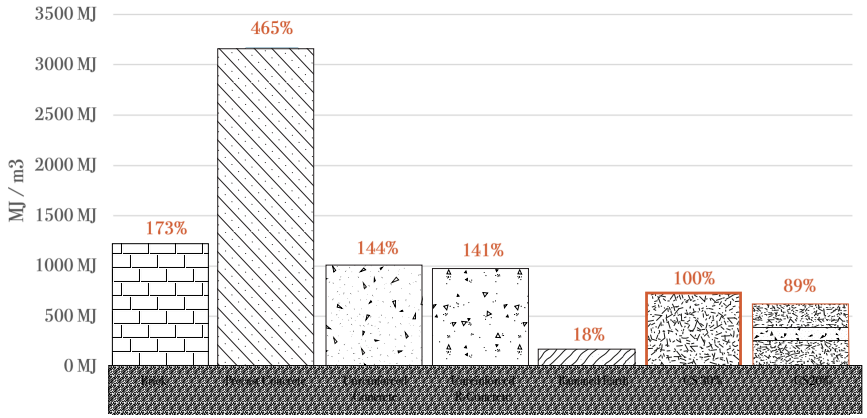

Figure 199 Comparison Of Energy Required Per m3 (A1-A3)

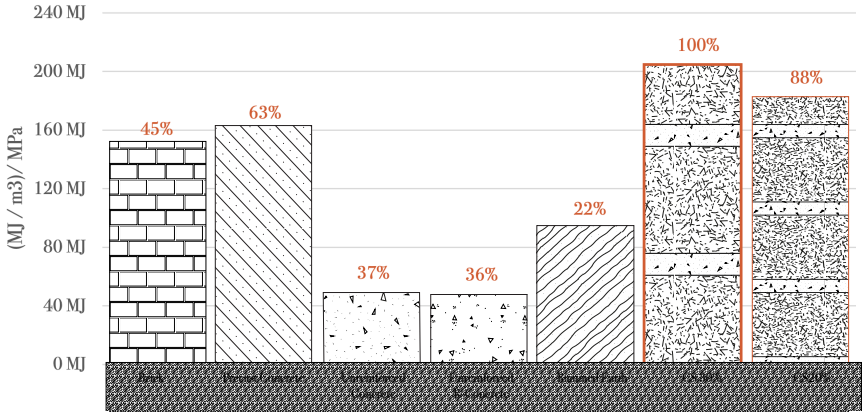

Figure 200 Comparison Of Energy Required Per Compressive Strength Unit MPa (A1-A3)

The chart in Figure 198 gives a good indication of the material carbon footprint, but is still not representative of the use case analysed for CS Walls, because the compressive strength is not always the primary factor which determines the wall thickness of a three-story multifamily house.

Therefore, the materials are not compared based on their volume or weight, but on the actual quantity used in the case study project. The walls are dimensioned based on EU and DIN norms, for a construction project in Germany, without any seismic loads. The individual materials and their dimensions are explained below.

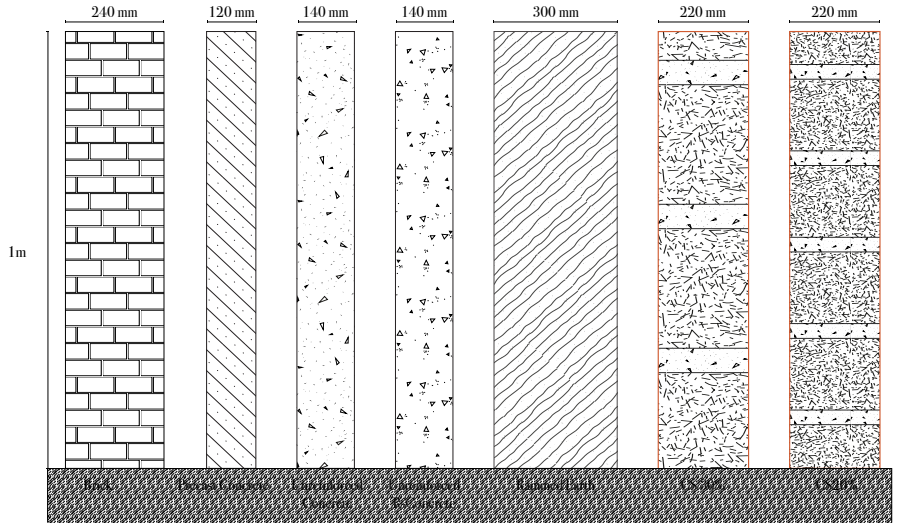

Figure 201 Case Study Wall Thicknesses

Brick

Bricks are still the main building material for single-family and multifamily houses in Europe, as shown in Figure 196 (Zandonella Callegher et al., 2023). For this LCA, a backing brick with 12MPa is analysed, which is commonly used for load-bearing walls. With 113kg CO2 eq. / m3 (Bundesverband der Deutschen Ziegelindustrie e.V., 2021), they show a smaller C02 footprint per volume than concrete (see Figure 197), but a significantly higher footprint than rammed earth. According to DIN 1053-1 (Jäger et al., 2002), a brick wall for a clear height above 275cm and a building height above two stories requires a minimum thickness of 240mm. These dimensions are therefore adopted for the calculations.

C30/37 Concrete (precast)

The fabrication of CS Walls is integrated into common precast wall processes. The product chosen is a solid, reinforced C30/37 concrete wall by the Thomas Gruppe in Germany, which manages nearly 50 factories in Central Europe (Thomas Gruppe, n.d.-b). With the wall's mix of concrete and steel, it shows the highest GWP per m3 of the materials assessed, based on their EPD (thomas gruppe - Geschäftsfeld Betonbauteile, 2020). According to them, 64% of the GWP lies in the cement. However, the product offers more use cases than CS Walls, due to its high compressive and tensile strength. Its reinforcement and the controlled precast environment also enables a relatively low thickness of 100mm, according to DIN 1045-1 (2009, p. 175). The slenderness ratio of $\lambda = 85$ raises this thickness to 120mm, due to the clear height of 3m of the case study (Mendler, 2023). For comparability, GWP values for cement in the precast wall were replaced by the EPD used for the unreinforced wall.

C30/37 In-Situ Concrete (unreinforced)

As the rubble in CS Walls prevents the use of regular rebar, the use-cases will be limited to compression-dominated loads. This also enables the use of unreinforced concrete walls. Walls, which can be built with bricks, can easily be built with unreinforced concrete (Mendler, 2023) This technique offers a way to reduce the use of carbon-intensive steel. Unreinforced concrete is described in DIN 1045-1:2008-08 and is specified with a minimum width of 140mm, only 20mm more than reinforced in-situ concrete (DIN 1045-1, 2009, p. 175). Due to the lack of steel and the missing steps within the pre cast factory, the unreinforced wall emits only 232kg CO2 eq. / m3. (InformationsZentrum Beton GmbH, 2013)

C30/37 In-Situ RCA Concrete (unreinforced)

The current best-case scenario for concrete waste management is the recycling of crushed rubble into aggregates (RCA). Therefore, this method is also compared to CS Walls, to show the benefit of reclaiming larger elements. For comparability to common concrete, it is also regarded as an unreinforced, in-situ wall with the same thickness of 140mm. As the carbon-intensive cement is not substituted with RCAs, the emissions per m3 are similar to common concrete (Betonwerk Büscher GmbH & Co. KG, 2024), as is demonstrated in Figure 197.

Rammed Earth

If locally sourced, rammed earth has one of the lowest carbon footprints of all building materials (Morel et al., 2021). Furthermore, it can only be loaded in compression where, depending on the mix, it has a strength of around 2MPa. The walls can even be prefabricated in sections up to 4m in length. Due to the low strength, the typical thickness is 300mm and thus the thickest wall compared here (ClayTec, n.d.). Its characteristics are thus comparable to CS Walls, with a lower carbon footprint per m3 (ÖKOBAUDAT, 2018), but a lower structural performance.

Figure 202 Prefabricated Rammed Earth Wall (https://claytec.de/produkt/mauerwerk-stampflehm/stampflehm-fertigwand/)

Cyclopean Spolia 30%

The prefabrication of the CS Walls is calculated based on the numbers of a C30/37 precast wall by *Thomas Bauteile* in Germany (thomas gruppe - Geschäftsfeld Betonbauteile, 2020). They state that 7% of the GWP is caused by the electricity used during the process and 5% by the transport of the preliminary products. For the raw materials, a C12/15 concrete is used for the 30% virgin concrete infill and the handling beam (InformationsZentrum Beton GmbH, 2023), which gets an additional 6% rebar steel per m3 (RIVA Stahl GmbH, 2021), based on the ratio from the precast wall. The carbon emissions for the rubble is mainly determined by the additional transport volume needed and the placement in the factory. As the amount cannot be determined accurately here, it is presumed as a cut-off criteria below 1%.

	Factor	GWP	MJ/m3
Electricity	7.0%	32 kg	222 MJ
Transport	5.0%	23 kg	158 MJ
C12 / 15 (CS30)	30%	39 kg	219 MJ
C12 / 15 (CS20)	20%	26 kg	146 MJ
Handling Beam	6.7%	9 kg	49 MJ
CS30 Total		**105 kg**	**682 MJ**
CS20 Total		**90 kg**	**575 MJ**

Table 27 CS Walls GWP & Energy Calculation, Based On Precast Walls, C12/15 Concrete And Reinforcement Steel

DIN 1045-1 states a minimum thickness of 200 for C12/15 concrete. Due to decreased amount of strength in the ITZ between rubble and infill, 10% is added to this for safety. This results in 220mm thick walls, which echoes the walls tested in 1:10.

Cyclopean Spolia 20%

The experiments showed that the integration of smaller stones or the tighter packing of larger stones can enable infills as low as 20%. To assess this impact, a second CS Wall with 20% infill is also included into the calculations.

5.3.3. Results & Discussion

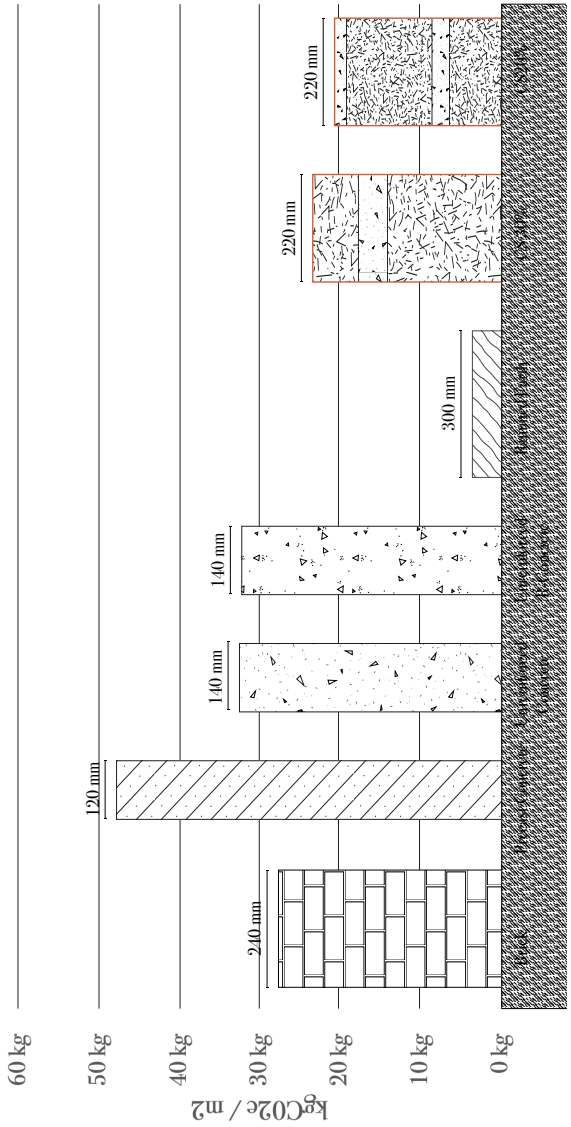

Figure GWP Per m2 Wall In The Case Study (A1-A3)

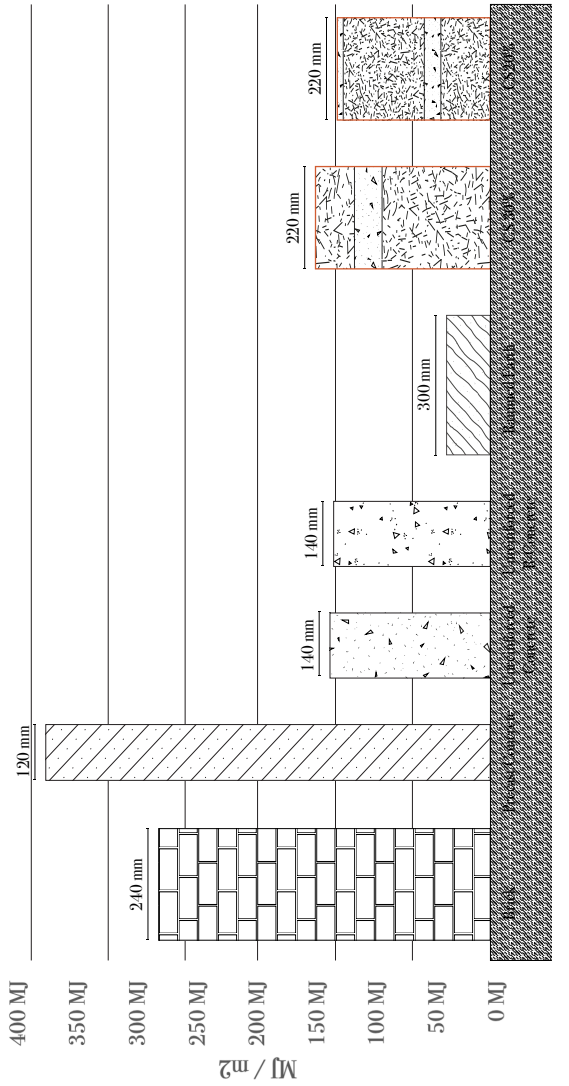

Figure 203 Energy Required Per m2 Wall In The Case Study (A1-A3)

A 30% infill could suggest that a CS wall only emits 30% of a common precast wall. The results show that this is not the case.
The dimensions of the walls largely influences the Global Warming Potential and the Primary Energy Non Renewable Total (PENRT) of the materials. Also, CS walls require the same amount of energy in the factory than common precast walls at least. Furthermore, places like the edges and the handling beam cannot be filled with rubble or contain rebar. Nevertheless, for modules A1 to A3, the precast concrete wall shows the overall highest footprint. Its EPD states that 64% of its GWP is influenced by the raw cement and metal (thomas gruppe - Geschäftsfeld Betonbauteile, 2020). This explains why the CS walls only emit about half the energy, despite the precast wall's slenderness.

- for modules A1 to A3, the precast concrete wall shows the overall highest footprint -

The unreinforced walls emit more kg CO2 eq. than CS30, but use less energy resources. The latter can be explained by the energy used in the factory to precast the CS walls. The RCA could only reduce the GWP and PENRT by 2%. Despite their thickness, the bricks only emit 17% more carbon than the CS30 wall, but use 90% more primary energy, close to the precast wall. Even though the rammed earth wall is nearly three times thicker than the precast wall and around 40% thicker than CS Walls, they emit the least kg CO2 eq. and have the lowest energy demand.
It has to be noted that this LCA did not deduct the energy from the CS Walls, which would otherwise be required to crush the concrete rubble. Future 1:1 structural tests could confirm higher strengths, especially for lateral, wind and impact forces, which could lead to more slender CS Walls. Alternative fillers, like geopolymers for example could further reduce the carbon emissions of the walls and should be investigated in future research.

5.4. Circularity

Multiple frameworks exist to assess the circularity of building products, like the R-Ladder strategy by Cramer (2022), the Cradle-To-Cradle method (Mc Donough & Braungart, 2002) or the Level(s) methodology introduced by the EU (Dodd et al., 2020). All aim at the transition of current linear economy to a circular economy (CE). To assess Cyclopean Spolia, parts of the AEGIR framework by Zabek et al. (2023) are discussed here. The authors combined all three previously mentioned systems. The principles they chose are all based on criteria that could be measured or described at the material or product level. Table 28 provides and overview of all key performance indicators (KPI) of the AEGIR framework. These were assessed based on what is known about CS Walls at the moment and seven principles chosen, which will be further discussed in this section (indicated with the green boxes). The GWP, 'Use of reused material' and 'Bill of quantities' were already illuminated in the Cradle-To-Gate section. The other principles either target unknown factors during the process (like use of renewable primary energy) or themes that do not apply to concrete (like compostability).

Principle	Unit
GWP	kg CO_2-eq.
Use of non-renewable primary energy (PENRE)	MJ
Use of renewable primary energy (PERE)	MJ
Use of renewable resources	kg
Use of recycled material	kg
Use of reused material	kg
Hazardous substances (HWD)	kg
Materials for recycling or reuse	kg
Durability / Lifespan / Maintenance / Warranty	years
Bill of quantities	misc.
Demountability / Reversibility (type of installation)	Qualitative
Financial concept for multiple life-cycles (take-back, leasing)	Qualitative
Modularity	Qualitative
Local material	kg
Low-Tech	Qualitative
Material purity	Qualitative
Compostability	Qualitative

Table 28 AEGIR Principles, The Green Boxes Are Assessed In The Circularity Section And The Green Text Was Assessed In The Cradle-To-Gate Section (based on Zabek et al., 2023)

5.4.1. AEGIR Principles

Materials For Recycling Or Reuse

The End-Of-Life (EoL) scenario of the rubble walls is still unclear at this point. For low-rise buildings, reversible connections could be designed, which would enable an EoL reuse scenario for entire walls. The current connections focus on the creation of monolithic structures and are therefore difficult to disassemble. A potential second life cycle as another rubble wall was introduced as a thought experiment in the demonstrator (see CS Rubble[2] in Figure 173 and Figure 174 on page 126) and would be consistent with the process developed here. Future tests have to show the feasibility of this approach. Smaller rubble could be recycled into RCAs.

Durability / Lifespan / Maintenance / Warranty

The durability of CS walls is a major topic for future research. It is assumed to be lower than virgin concrete walls, due to the different material properties of the materials used. Long-term tests have to show their expected lifespan and the maintenance required for the walls. Due to the interface between rubble and virgin concrete, frost could surface as a weakness of the walls, similar to repaired concrete (Łagoda & Gajda, 2021).

Demountability / Reversibility (Type Of Installation)

As already discussed in Material For Recycling Or Reuse, the current connections are irreversible, as is common for prefabricated walls. For low-rise buildings, reversible connections, similar to brick or rammed earth walls, should be developed in the future, to enable the reuse of the wall as a component.

Financial Concept For Multiple Life Cycles

The process actor maps did not include the business and ownership model for each scenario.

Even though wall leasing systems exist for temporary construction walls (TWS, 2025), this would be difficult to adopt, due to the long lifespan of concrete walls of over 50 years (thomas gruppe - Geschäftsfeld Betonbauteile, 2020). However, a future buyback option could be introduced for the rubble and for entire walls.

On the ownership side, cooperatives could be a path to ensure an interest for long-lasting systems, which also enable multiple life cycles.

Local Material

Due to their weight and size, precast walls are expensive to transport and their deployment range around the factory is thus limited. The local supply of the raw materials is therefore the most crucial factor. The supply of the rubble depends largely on the demolition activity of the area. If the CS plant is located close to urban centres with a high construction volume, a constant local supply could be guaranteed.

In Europe, limestone, the main raw material for cement, is mainly produced in Spain (21%), Italy (16%) and Germany (13%) (European Commission, 2021). However, most countries also have a local production and local concrete plants, which also ensures low transport.

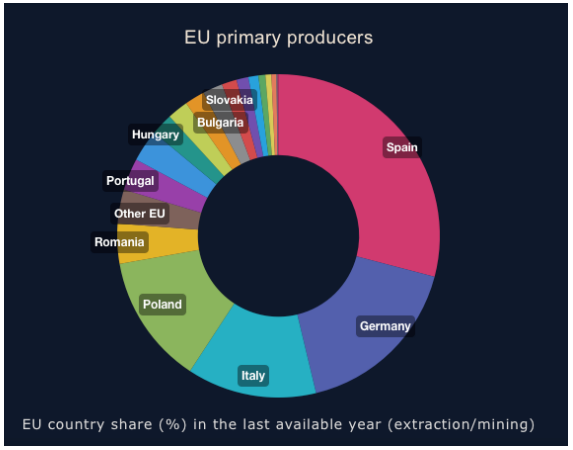

Figure 204 Limestone Production In Europe in 2021 (European Commission, 2021)

Low-Tech

The main aim of this thesis was to provide a scalable and low-tech solution for the integration of concrete rubble into load-bearing walls. With a simplified 2D scanning method and a common nesting algorithm, the complexity of the digital tools is minimised. The precast process is based on existing methods and the tools required are common. The heaviest machinery in the process is the sorting station, to identify suitable rubble fragments. This could however be substituted by a manual process, to simplify this step.

Material Purity

The largest part of CS Walls is made out of concrete. Only the edges contain some steel rebar for the connections and the handling beam. Hence, the separation of the waste streams at the EoL is facilitated.

5.5. Conclusion

The three sections complement each other in describing the environmental impact of CS Walls. The waste reduction is the main aim of the process, which it can effectively fulfil.

- Overall, the section showed that Cyclopean Spolia can contribute to a more circular approach in treating our concrete waste -

The cradle-to-gate analysis showed that the functional unit chosen majorly influences the performance comparison of the products. Whereas a volume-based calculation showed a major difference between the materials chosen, a case study based approach, which included the thickness of the walls, showed a more similar performance of CS walls to brick walls and unreinforced walls. Furthermore, the calculations showed that the GWP reduction of CS Walls compared to common precast walls is linearly based on the infill ratio, as some resource consumption is fixed in the process. Overall, the GWP could still be reduced by more than 50% compared to common precast walls. The circularity discussion was based on the framework by Zabek et al. (2023). Despite the good performance in modules A1-A3, it showed that other aspects of circularity are still undefined or weaknesses of Cyclopean Spolia. Even though principles like locality, low-tech or material purity are strong point for CS Walls, there is still room for improvement with regards to demountability and EoL. The life-span and financial concepts have to be researched in more depth in the future. Overall, the section showed that Cyclopean Spolia can contribute to a more circular approach in treating our concrete waste, when methods of component reuse are not feasible.

Discussion & Conclusion

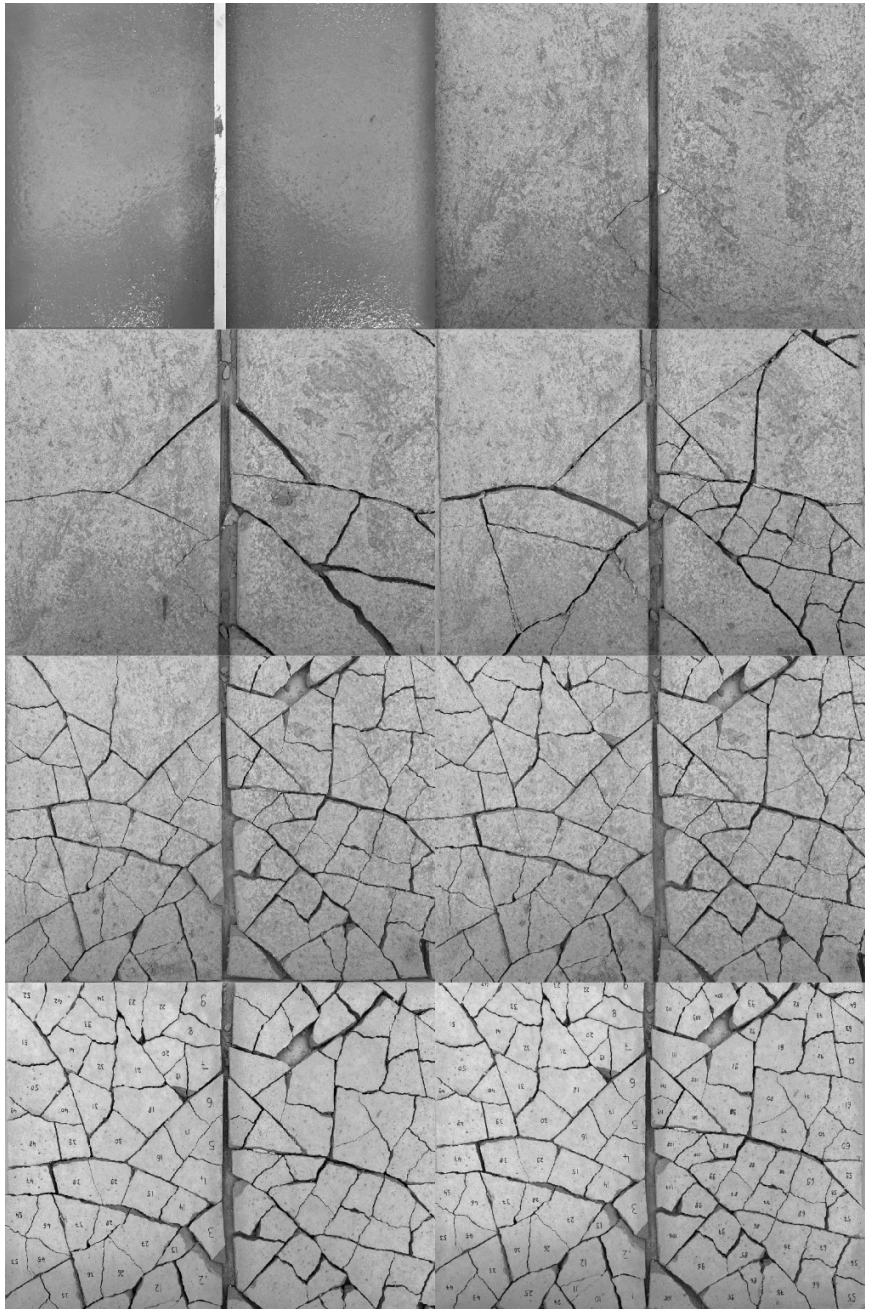

Summary

This Section combines the three research pillars. It draws a conclusion based on the findings of the entire thesis, maps the limitations and proposes further research. It also answers the main research question and discusses the approach taken in this thesis.

6.1. Discussion

Together with the literature review, the three pillars 'structural tests', 'system design', and 'environmental impact' illuminated Cyclopean Spolia Walls from multiple angles. Combined, they demonstrated that horizontally precast rubble walls can be considered a viable alternative to conventional solid-wall systems for the described use cases.

Even though the rubble arrangements tested in the experiment phases behaved slightly differently, with hybrid and small stone arrangements showing the most promising results, they demonstrated that a certain degree of freedom of placement can be achieved. This was key for the wall design aspect in the system design. It enables multiple wall expressions and gives architects the opportunity to influence the wall's expression. In addition to the design aspects, this placement freedom also enabled more flexibility in the precast process and reduced the complexity of storage. The analysis of existing prefabrication methods regarding their levels of automation and mechanisation (Frohm et al., 2008) improved the integration of CS Walls into existing processes. Based on the precast concepts by Elliot (2019), the walls were detailed with the integration into existing construction processes in mind. The use of well-established tilting-table processes, steel anchorage techniques, and in-situ concrete connections demonstrates that the technical hurdles associated with rubble walls can be overcome without the need for complex machinery.

With this in mind, the process design and actor maps highlighted the importance of complexity reduction for implementing CS Walls and the benefits of vertical integration in reducing transport. It showed that Cyclopean Spolia could be implemented in various ways to achieve multiple scales.

The environmental impact discussion confirmed that CS Walls show a significant advantage with regard to GWP and PENRT in cradle-to-gate calculations compared to standard precast C30 panels, as well as to unreinforced concrete and brick walls. As volume-based comparisons initially overstated CS Wall benefits, a case-study approach compared walls within a use-case scenario. The results demonstrate a competitive advantage for Cyclopean Spolia, which can offset the additional effort required to source and place the rubble.

However, the AEGIR circularity framework analysis revealed gaps that need to be addressed in future research to improve the circularity of the product.

Taken together, these three pillars develop CS Walls as a scalable, resource-efficient solution for low-rise load-bearing construction.

6.2. Limitations

This thesis was subject to the following limitations:

I. Although the materials used in the 1:10 scale tests represented the full-scale materials in terms of size, they do not accurately represent full-scale behaviour. 1:1 tests are needed.
II. The sample size of the experiments is relatively small, compared to the individuality of the configurations within each group.
III. The rubble used in the experiments was self-produced and might not represent the behaviour of debris from demolition sites.
IV. The discussion of the prefabrication process did not consider economic factors.

6.3. Answer to Main Research Question

> How can parallel-sided concrete rubble waste be reclaimed and integrated into load-bearing prefabricated concrete walls to improve structural performance, design freedom and scalability?

The horizontal prefabrication method proposed in this thesis enables a higher degree of concrete waste fragment placement inside rubble walls. This is enabled by the lack of structural integrity needed during the construction process and the full enclosure of the stones with concrete. The structural tests demonstrated that non-structural assemblies could be a viable option for rubble walls in low-rise buildings. With the integration of the method into existing precast processes and the reduction of complex equipment needed, it could significantly improve the scalability compared to other methods of building with rubble.

6.4. Further Research

This thesis provided a first insight into the scalability of Cyclopean Spolia Walls produced with a horizontal precast method. Several aspects require further investigation to provide a more complete image of the feasibility and scalability of CS Walls.

> 'Irrespective of how well concrete can tolerate the use of other sources of waste or coproduct materials, each application has to be fully performance-assessed before acceptability' (Levitt, 2008).

What Levitt describes in the above quote is that full-scale and long-term tests are essential for the implementation of new construction methods to ensure their safety. Therefore, it would be necessary to conduct full-scale experiments on these composites to validate the results of this thesis. The 1:10 samples allowed for efficient comparison of variables, but did not fully reflect full-scale behaviour. This would also provide insight into potential challenges associated with the prefabrication process and the pouring of concrete into the cavities.
Additionally, the strength of the bond at the ITZ between rubble and infill is a key factor in the performance of the walls. Dedicated bond tests are needed to investigate methods which enhance the bond strength between the infill and common edge surfaces found in rubble. The influence of rebar regarding transport, ageing and the precast process is also still to be investigated.

Furthermore, the comparison between stacking and nesting algorithms should be repeated with a larger sample size to draw a reliable conclusion. The tests in this thesis were based on three samples per group and were subject to technical challenges during the loading process. This would help assess whether their computational complexity and the larger database requirement are justified for precast applications.

Furthermore, tests on the transport and handling of the walls could be performed to assess their resistance to flexural bending and localised tension due to the anchors.

- The strength of the rubble itself also influences the structural performance of CS Walls -

The strength of the rubble itself also influences the structural performance of CS Walls. As the fragments are sourced from a variety of demolished structures, their mechanical properties vary. Further research is needed to determine the extent of residual strength remaining in rubble and to identify conservative assumptions that can be made to ensure adequate safety margins.

As mentioned by Grangeot et al. (2024), more accurate and large-scale scans of rubble in waste treatment plants should be conducted. This will help quantify typical geometries and confirm the amount of flat rubble present after demolition.

This thesis used a cement-based mortar for the tests. However, alternative strong binders with lower carbon emissions, such as geopolymers, could also be tested to reduce the environmental impact of the infill material.

The case study was based on a three-story building and thus took a conservative approach. Future research should investigate the potential to build higher with CS Walls, if 1:1 tests confirm the structural performance assumed here. This would also positively influence the environmental impact, as the product becomes more comparable to common precast walls. Regarding the LCA, the added energy consumption of the walls should be calculated in detail and compared to the energy required to crush the concrete otherwise.

Lastly, the economic feasibility of such a prefabrication process should be analysed in the future. This is crucial for the implementation of CS Walls as a competitive precast product, given the initial investment required.

6.5. Conclusion

The experiments showed that if rubble and infill form a strong composite, precast load-bearing concrete rubble walls can be achieved with low-tech methods. The results demonstrated how rubble diameter and arrangement influence the mechanical behaviour of load-bearing rubble walls, in terms of structural predictability and strength. These insights informed the development of a wall system designed to make Cyclopean Spolia Walls practically applicable. However, the strength of the bond between rubble and virgin concrete must be studied further, and the logistics of rubble sourcing and scanning at industrial scale remain to be verified. If full-scale mock-up tests confirm the findings of this thesis, the results could serve as a foundation for implementation.

The thesis set out to explore whether low-tech digital tools could generate structurally sound walls from concrete rubble. This goal has largely been achieved. The proposed workflow proved to be repeatable, accessible, and effective even when using small datasets. The combination of digital scanning, lightweight algorithms, and horizontal prefabrication, enabled structurally consistent outcomes without the need for high-end infrastructure. These findings not only validate the design methodology, but also open the door to scalable approaches to load-bearing rubble elements.

Beyond structural feasibility, the environmental analysis confirmed the positive impact of Cyclopean Spolia Walls. By embedding reclaimed rubble into precast elements, the process reduces the need for virgin concrete and preserves the material value of concrete waste fragments, that would otherwise be downcycled or landfilled. The integration of this waste stream into new architectural elements has the potential to reduce emissions associated with concrete production and extend the life cycle of existing material stocks. However, the circularity discussion showed some potential for improvement in regard to the reversibility of the wall connections. Some indicators still need further research, like the durability for example, to come to a full overview of the product's life cycle.

- Cyclopean Spolia reframes demolition debris as a design material. The results suggest that structural performance and storytelling could coexist in a prefabricated rubble wall system.

In addition to the reduced environmental impact, the walls carry a distinct visual identity. Their texture and composition capture the memory of past constructions and introduce variation into otherwise uniform wall assemblies. This aesthetic dimension supports a narrative of reclaimed materials and offers architects a way to embed stories into mass-produced building components. Even though the process introduces additional handling steps during prefabrication and at waste facilities, it also opens up new value streams and opportunities for design-driven circularity.

To conclude, Cyclopean Spolia reframes demolition debris as a design material. The results suggest that structural performance and storytelling could coexist in a prefabricated rubble wall system. If proven economically feasible, Cyclopean Spolia could be applied across a wide range of architectural, infrastructural, and landscape applications. This contemporary notion of spolia responds to the growing challenge of construction waste and proposes to turn demolition sites into quarries for architectural expression.

List Of Figures

List Of Tables

References

ACI. (2012). *Guide to Mass Concrete Reported by ACI Committee 207*.

Al-Hamrani, A., Kim, D., Kucukvar, M., & Onat, N. C. (2021). Circular economy application for a Green Stadium construction towards sustainable FIFA world cup Qatar 2022™. *Environmental Impact Assessment Review*, *87*, 106543. https://doi.org/10.1016/j.eiar.2020.106543

Almeida, C., Guedes, J. P., Arêde, A., & Costa, A. (2016). Geometric indices to quantify textures irregularity of stone masonry walls. *Construction and Building Materials*, *111*, 199–208. https://doi.org/10.1016/j.conbuildmat.2016.02.038

Almeida, C., Miranda Guedes, J., Arêde, A., & Costa, A. (2021). Compressive behaviour of old one-leaf stone masonry walls; the influence of patterns' regularity and constructive process. *Construction and Building Materials*, *311*, 125339. https://doi.org/10.1016/j.conbuildmat.2021.125339

Alonso, P., Palmarola, H., & Arkitektur- och designcentrum. (2019). *Flying panels: How concrete panels changed the world*. ArkDes ; Ediciones UC ; DOM Publishers.

Amer, O., Aita, D., Bompa, D. V., Mohamed, E. K., Torky, A., Hussein, Y. M., & Ali, A. H. (2023). Behavior of unreinforced multi-leaf stone masonry walls under axial compression: Experimental and numerical investigation. *Engineering Structures*, *293*, 116621. https://doi.org/10.1016/j.engstruct.2023.116621

Ansys. (n.d.). *EduPack* [Computer software].

Baldania, M., & Bhogayata, A. (2023). Utilization of concrete waste from demolition sites in pavement subgrade. *Materials Today: Proceedings*, *93*, 99–105. https://doi.org/10.1016/j.matpr.2023.07.029

Betonwerk Büscher GmbH & Co. KG. (2024). *EPD R-Concrete* (EPD No. EPD-Kiwa-EE-171735-EN).

Böhmer, S., Moser, G., Neubauer, C., Peltoniemi, M., Schachermayer, E., Tesar, M., Walter, B., & Winter, B. (2008). *Aggregates Case Study*. https://www.yumpu.com/en/document/read/7181959/aggregates-case-study-jrc-ipts-sustainable-production-and-

Borri, A., Corradi, M., Castori, G., & De Maria, A. (2015). A method for the analysis and classification of historic masonry. *Bulletin of Earthquake Engineering*, *13*(9), 2647–2665. https://doi.org/10.1007/s10518-015-9731-4

Brandon Clifford. (2021). *The Cannibal's Cookbook. Mining Myths of Cyclopean Constructions*. https://www.naibooksellers.nl/the-cannibal-s-cookbook-mining-myths-of-cyclopean-constructions.html?___store=english&___from_store=default

Bundesverband der Deutschen Ziegelindustrie e.V. (2021). *EPD Mauerziegel* (EPD No. EPD-BDZ-20210062-ICG1-DE). Institut Bauen und Umwelt e.V. (IBU).

Burke, E. K., Hellier, R. S. R., Kendall, G., & Whitwell, G. (2007). Complete and robust no-fit polygon generation for the irregular stock cutting problem. *European Journal of Operational Research*, *179*(1), 27–49. https://doi.org/10.1016/j.ejor.2006.03.011

Capinteri, A., & Ferro, G. (1995). Size effects on tensile fracture properties: A unified explanation based on disorder and fractality of concrete microstructure. *International Journal of Rock Mechanics and Mining Sciences & Geomechanics Abstracts*, *32*(4), A196–A197. https://doi.org/10.1016/0148-9062(95)97277-P

Certain Measures. (2015). *Mine The Scraps*. https://www.certainmeasures.com/projects/mine-the-scrap

ClayTec. (n.d.). *Stampflehm Fertigwand*. Retrieved 6 May 2025, from https://claytec.de/produkt/mauerwerk-stampflehm/stampflehm-fertigwand/

Clifford, B., & McGee, W. (2018). Cyclopean Cannibalism, 2017. In G. Retsin, M. Jimenez, M. Claypool, & V. Soler (Eds.), *Robotic Building* (pp. 32–33). DETAIL. https://doi.org/10.11129/9783955534257-005

Coelho, A., & De Brito, J. (2013). Conventional demolition versus deconstruction techniques in managing construction and demolition waste (CDW). In *Handbook of Recycled Concrete and Demolition Waste* (pp. 141–185). Elsevier. https://doi.org/10.1533/9780857096906.2.141

Collaud, A., Mongillo, M., Niederhäuser, E. L., Pathé, J., Redaelli, D., & Buri, H. (2023). Reuse of concrete for the construction of a retaining wall: A case study. *Journal of Physics: Conference Series*, *2600*(19), 192016. https://doi.org/10.1088/1742-6596/2600/19/192016

Council Directive 96/53/EC of 25 July 1996 Laying down for Certain Road Vehicles Circulating within the Community the Maximum Authorized Dimensions in National and International Traffic and the Maximum Authorized Weights in International Traffic., § L 235 (1996).

Cramer, J. (2022). *Building-a-circular-future-jacqueline-cramer-amsterdam-economic-board*.

Culjak, I., Abram, D., Pribanic, T., Dzapo, H., & Cifrek, M. (2012). A brief introduction to OpenCV. *2012 Proceedings of the 35th International Convention MIPRO*, 1725–1730. https://ieeexplore.ieee.org/document/6240859

Database—Waste—Eurostat. (n.d.). Retrieved 15 May 2025, from https://ec.europa.eu/eurostat/web/waste/database

DeepNest. (2025). *DeepNest* [MacOS].

Deepnest. (2025). *Deepnest—Open source nesting software*. https://deepnest.io/

DIN 1045-1. (2009). *DIN 1045-1*.

DIN 4108-2. (2013). *Mindestanforderungen an den Wärmeschutz*.

Dodd, N., Mauro Cordella, & Shane Donatello. (2020). *Level(s) – A common EU framework of core sustainability indicators for office and residential buildings*.

Dutch Standards Institute. (2012). *NEN-EN 14992+A1*.

El Zareef, M. A. (2017). Seismic damage assessment of multi-story lightweight concrete frame buildings reinforced with glass-fiber rods. *Bulletin of Earthquake Engineering*, *15*(4), 1451–1470. https://doi.org/10.1007/s10518-016-0027-0

Elhacham, E., Ben-Uri, L., Grozovski, J., Bar-On, Y. M., & Milo, R. (2020). Global human-made mass exceeds all living biomass. *Nature*, *588*(7838), 442–444. https://doi.org/10.1038/s41586-020-3010-5

Elliott, K. (2019). *Precast Concrete Structures*. CRC Press.

Ensamble Studio. (2023). *Missing Pieces | ensamble-studio*. https://www.ensamble.info/missingpieces

Eurocode. (2004). *Eurocode 2_en.1992.1.1.2004*.

European Commission. (2020, 20). *Circular Economy Principles for buildings design*.

European Commission. (2021). *RMIS - Raw materials' profiles*. RMIS - Raw Materials Information System. https://rmis.jrc.ec.europa.eu/rmp/Limestone

Eurostat. (2022). *Waste statistics*. https://ec.europa.eu/eurostat/statistics-explained/index.php?title=Waste_statistics

FCRBE. (2021). *Interreg FCRBE Reuse Toolkit: Concrete Rubble*. Interreg FCRBE.

Freedman, S. (1999). Loadbearing Architectural Precast Concrete Wall Panels. *PCI Journal*, *44*(5), 92–115. https://doi.org/10.15554/pcij.09011999.92.115

Frohm, J., Lindström, V., Stahre, J., & Winroth, M. (2008). *Levels of Automation in Manufacturing*.

Gálvez-Martos, Schoenberger, & Zeschmar-Lahl. (2018). *Construction and demolition waste best management practice in Europe*.

Gezondheitsraad. (2012). *Manual Lifting during work*.

Gil-Martín, L. M., Fernández-Ruiz, M. A., & Hernández-Montes, E. (2022). Mechanical characterization and elastic stiffness degradation of unstabilized rammed earth. *Journal of Building Engineering*, *56*, 104805. https://doi.org/10.1016/j.jobe.2022.104805

Grangeot, M., Bastien-Masse, M., & Fivet, C. (2024). *Upcycling concrete rubble into masonry walls: Design and assessment of two prototypes built with digitally augmented tools*.

Grangeot, M., Bastien-Masse, M., Parascho, S., & Fivet, C. (2024). Upcycling Concrete Rubble Into Masonry Walls: Design and Assessment of Two Prototypes Built With Digitally Augmented Tools. In J. A. O. Barros, V. M. C. F. Cunha, H. S. Sousa, J. C. Matos, & J. M. Sena-Cruz (Eds.), *4th fib International Conference on Concrete Sustainability (ICCS2024)* (Vol. 574, pp. 324–331). Springer Nature Switzerland. https://doi.org/10.1007/978-3-031-80724-4_40

Grangeot, M., Fivet, C., & Parascho, S. (2023). From concrete waste to walls: An investigation of reclamation and digital technologies for new load-bearing structures. *Journal of Physics: Conference Series*, *2600*(19), 192019. https://doi.org/10.1088/1742-6596/2600/19/192019

Grangeot, M., Wang, Q., Beyer, K., Fivet, C., & Parascho, S. (2024a). *Leveraging existing construction tools for upcycling concrete waste into slender walls*.

Grangeot, M., Wang, Q., Beyer, K., Fivet, C., & Parascho, S. (2024b). Structural Concrete Rubble Arrangements: A Framework for Upcycling Demolition Waste into Slender Masonry Walls for Buildings. In P. Eversmann, C. Gengnagel, J. Lienhard, M. Ramsgaard Thomsen, & J. Wurm (Eds.), *Scalable Disruptors* (pp. 15–27). Springer Nature Switzerland. https://doi.org/10.1007/978-3-031-68275-9_2

Guo, B., Zhang, Y., Hu, J., Li, J., Wu, F., Peng, Q., & Zhang, Q. (2022). Two-dimensional irregular packing problems: A review. *Frontiers in Mechanical Engineering*, *8*, 966691. https://doi.org/10.3389/fmech.2022.966691

Hany, L., Lalyko, T., van der Meulen, A., & von Kardorff, M. (2024). *Mosaic Walls*. TU Delft.

Holt, G. D. (2013). Unambiguous nomenclature for cyclopean British dam building history. *Dams and Reservoirs*, *23*(2), 78–84. https://doi.org/10.1680/dare.13.00026

Huuhka, S., Kaasalainen, T., Hakanen, J. H., & Lahdensivu, J. (2015). Reusing concrete panels from buildings for building: Potential in Finnish 1970s mass housing. *Resources, Conservation and Recycling*, *101*, 105–121. https://doi.org/10.1016/j.resconrec.2015.05.017

InformationsZentrum Beton GmbH. (2013). *EPD C30/37 Concrete* (EPD No. EPD-IZB-20130431-IBG2-DE). Institut Bauen und Umwelt e.V. (IBU).

InformationsZentrum Beton GmbH. (2023). *EPD C12/15 Concrete* (EPD No. EPD-IZB-20230418-IBA1-DE).

International Transport Forum. (n.d.). *PERMISSIBLE MAXIMUM WEIGHTS OF LORRIES IN EUROPE*.

Islam, R., Nazifa, T. H., Yuniarto, A., Shanawaz Uddin, A. S. M., Salmiati, S., & Shahid, S. (2019). An empirical study of construction and demolition waste generation and implication of recycling. *Waste Management*, *95*, 10–21. https://doi.org/10.1016/j.wasman.2019.05.049

ISO 14044. (2006). *ISO 14044:2006*. ISO. https://www.iso.org/standard/38498.html

Jäger, W., Pflücke, T., Waurig, R., Figge, D., & Meyer, U. (2002, July). *Ziegelmauerwerk nach DIN 1053—1*. Arbeitsgemeinschaft Mauerziegel im Bundesverband der Deutschen Ziegelindustrie e. V.,.

Johns, R. L., Wermelinger, M., Mascaro, R., Jud, D., Gramazio, F., Kohler, M., Chli, M., & Hutter, M. (2020). Autonomous dry stone: On-site planning and assembly of stone walls with a robotic excavator. *Construction Robotics*, *4*(3–4), 127–140. https://doi.org/10.1007/s41693-020-00037-6

Johns, R. L., Wermelinger, M., Mascaro, R., Jud, D., Hurkxkens, I., Vasey, L., Chli, M., Gramazio, F., Kohler, M., & Hutter, M. (2023). A framework for robotic excavation and dry stone construction using on-site materials. *Science Robotics*, *8*(84), eabp9758. https://doi.org/10.1126/scirobotics.abp9758

Keulemans, G. (2016). *The Geo-cultural Conditions of Kintsugi: The Journal of Modern Craft: Vol 9, No 1*. https://www.tandfonline.com/doi/abs/10.1080/17496772.2016.1183946

Khan, I. S., Ahmad, M. O., & Majava, J. (2021). Industry 4.0 and sustainable development: A systematic mapping of triple bottom line, Circular Economy and Sustainable Business Models perspectives. *Journal of Cleaner Production*, *297*, 126655. https://doi.org/10.1016/j.jclepro.2021.126655

Kinney, D. (2001). *Roman Architectural Spolia*.

Kirillov, A., Mintun, E., Ravi, N., Mao, H., Rolland, C., Gustafson, L., Xiao, T., Whitehead, S., Berg, A. C., Lo, W.-Y., Dollár, P., & Girshick, R. (2023). *Segment Anything* (No. arXiv:2304.02643). arXiv. https://doi.org/10.48550/arXiv.2304.02643

Knauf. (2023, March). *Knauf Haftputz*.

Küpfer, C., Bastien-Masse, M., & Fivet, C. (2023). Reuse of concrete components in new construction projects: Critical review of 77 circular precedents. *Journal of Cleaner Production*, *383*, 135235. https://doi.org/10.1016/j.jclepro.2022.135235

Küpfer, C., Bastien-Masse, M., Grangeot, M., Meier, C., Graulich, L., Pathé, J., & Fivet, C. (2024). From soon-to-be demolished mushroom column slabs to reused reinforced concrete saw-cut assemblies: The case of the rebuiLT pavilion. *IOP Conference Series: Earth and Environmental Science*, *1363*(1), 012052. https://doi.org/10.1088/1755-1315/1363/1/012052

Küpfer, C., & Fivet, C. (2023). Panorama of approaches to reuse concrete pieces: Identification and critical comparison. *Journal of Physics: Conference Series*, *2600*(19), 192006. https://doi.org/10.1088/1742-6596/2600/19/192006

Łagoda, G., & Gajda, T. (2021). Change of Mechanical Properties of Repair Mortars after Frost Resistance Rests. *Materials*, *14*(12), Article 12. https://doi.org/10.3390/ma14123199

Lehtinen, T. (2010). *Advantages and Disadvantages of Vertical Integration in the Implementation of Systemic Process Innovations: Case studies on implementing building information modeling (BIM) in the Finnish construction industry*.

Levitt, M. (2008). *Precast Concrete Materials, Manufacture, Properties and Usage, Second Edition*. CRC Press.

Lin, L., & Wu, B. (2025). Shear behavior of precast recycled lump-aggregate concrete laminated beams using inclined-crossed stirrups. *Engineering Structures*, *326*, 119502. https://doi.org/10.1016/j.engstruct.2024.119502

Llatas, C. (2013). Methods for estimating construction and demolition (C&D) waste. In *Handbook of Recycled Concrete and Demolition Waste* (pp. 25–52). Elsevier. https://doi.org/10.1533/9780857096906.1.25

Mackay-Sim, R. (2011). *DESIGN FOR EDGE LIFTING OF PRECAST CONCRETE PANELS*.

Maltidis, G., & Stempniewski, L. (2013). *Earthquake analysis of an old cyclopean concrete dam and its seismic retrofit with post-tensioning anchors.*

Marinković, S., & Carević, V. (2019). Comparative studies of the life cycle analysis between conventional and recycled aggregate concrete. In J. de Brito & F. Agrela (Eds.), *New Trends in Eco-efficient and Recycled Concrete* (pp. 257–

291). Woodhead Publishing. https://doi.org/10.1016/B978-0-08-102480-5.00010-5

Marinković, S., Radonjanin, V., Malešev, M., & Ignjatović, I. (2010). Comparative environmental assessment of natural and recycled aggregate concrete. *Waste Management*, *30*(11), 2255–2264. https://doi.org/10.1016/j.wasman.2010.04.012

Marshall, D. J. M., & Grangeot, M. (2024). *An Investigation into Machine Learning Matchmaking for Reused Rubble Concrete Masonry Units (RR-CMU)*.

Martins, R., Carmo, R. D., Costa, H., & Júlio, E. (2023). A review on precast structural concrete walls and connections. *Advances in Structural Engineering*, *26*(14), 2600–2620. https://doi.org/10.1177/13694332231191073

Mc Donough, W., & Braungart, M. (2002). *Cradle to Cradle: Remaking the Way We Make Things by William...* https://biblio.co.uk/9780865475878

Mendler, A. (2023). *Leitfaden-unbewehrte-Betonwaende-nach-DIN-1992-1-1*.

Morel, J.-C., Charef, R., Hamard, E., Fabbri, A., Beckett, C., & Bui, Q.-B. (2021). Earth as construction material in the circular economy context: Practitioner perspectives on barriers to overcome. *Philosophical Transactions of the Royal Society B: Biological Sciences*, *376*(1834), 20200182. https://doi.org/10.1098/rstb.2020.0182

Movomech. (n.d.). *Vacuhand Pro*.

Nazir, I., & Rashid, K. (2018). *Assessment of Bond Strength between Concrete and Repairing Cementitious Concrete in Tension and Shear*.

Nedeljković, M., Visser, J., Šavija, B., Valcke, S., & Schlangen, E. (2021). Use of fine recycled concrete aggregates in concrete: A critical review. *Journal of Building Engineering*, *38*, 102196. https://doi.org/10.1016/j.jobe.2021.102196

Nen-En, V. (2006). *Eurocode 6—NEN-1996*.

ÖKOBAUDAT. (2018). *EPD Stampflehm* (EPD No. 1.3.17 Mineral building products / Bricks, blocks and elements / Air-dried brick (adobe)). https://www.oekobaudat.de/OEKOBAU.DAT/datasetdetail/process.xhtml?uuid=59622fc0-d719-43bf-a16b-ae924ae0d276&version=20.19.120

Olufsen, S. N., Andersen, M. E., & Fagerholt, E. (2020). μ DIC: An open-source toolkit for digital image correlation. *SoftwareX*, *11*, 100391. https://doi.org/10.1016/j.softx.2019.100391

OpenNest—Parametric House. (2020, May 13). https://parametrichouse.com/opennest/

Oreb, J., Curić, H., Tomić, I., & Beyer, K. (2024). Masonry walls from reclaimed concrete demolition waste. *MATEC Web of Conferences*, *403*, 06004. https://doi.org/10.1051/matecconf/202440306004

Pan, M., & Pan, W. (2016). Advancing Formwork Systems for the Production of Precast Concrete Building Elements: From Manual to Robotic. *Modular and Offsite Construction (MOC) Summit Proceedings*. https://doi.org/10.29173/mocs1

Paschoalin Filho, J. A., Camelo, D. G., de Carvalho, D., Guerner Dias, A. J., & Marcondes Versolatto, B. A. (2020). Use of construction and demolition solid wastes for basket gabion filling. *Waste Management & Research*, *38*(12), 1321–1330. https://doi.org/10.1177/0734242X20922591

Reichenbach, S., & Kromoser, B. (2021). State of practice of automation in precast concrete production. *Journal of Building Engineering*, *43*, 102527. https://doi.org/10.1016/j.jobe.2021.102527

RIVA Stahl GmbH. (2021). *EPD Rebar* (EPD No. EPD-KIWA-EE-000133-EN).

Schaldenbrand, P. (2021, October 17). *Digital Image Correlation: Camera Considerations*. Siemens. https://community.sw.siemens.com/s/article/Digital-Image-Correlation-Camera-Considerations

Schreier, H., Orteu, J.-J., & Sutton, M. A. (2009). *Image Correlation for Shape, Motion and Deformation Measurements: Basic Concepts,Theory and Applications*. Springer US. https://doi.org/10.1007/978-0-387-78747-3

Scrivener, K. L., & Snellings, R. (2022). The Rise of Portland Cements. *Elements*, *18*(5), 308–313. https://doi.org/10.2138/gselements.18.5.308

Sembiring, A. C., Tampubolon, J., Sitanggang, D., Turnip, M., & Subash. (2019). Improvement of Inventory System Using First In First Out (FIFO) Method. *Journal of Physics: Conference Series*, *1361*(1), 012070. https://doi.org/10.1088/1742-6596/1361/1/012070

Statista. (2024a). *Global cement CO_2 emissions 1960-2023*. Statista. https://www.statista.com/statistics/1299532/carbon-dioxide-emissions-worldwide-cement-manufacturing

Statista. (2024b). *Global CO2 emissions by year 1940-2024*. Statista. https://www.statista.com/statistics/276629/global-co2-emissions/

Steel Projects. (n.d.). *Plate nesting software, sheet metal nesting software*. Steel Projects. Retrieved 21 January 2025, from https://www.steelprojects.com/en/solutions/features/plate-nesting/

Tam, V. W. Y., Soomro, M., & Evangelista, A. C. J. (2018). A review of recycled aggregate in concrete applications (2000–2017). *Construction and Building Materials*, *172*, 272–292. https://doi.org/10.1016/j.conbuildmat.2018.03.240

Tate, S. (n.d.). *Urbanite—Reusing Broken Concrete for Patios & Walls—Concrete Network*. ConcreteNetwork.Com. Retrieved 28 December 2024, from https://www.concretenetwork.com/concrete/demolition/urbanite-recycled-concrete.html

Thomas Gruppe. (n.d.-a). *Massivwände*. thomas gruppe. Retrieved 13 May 2025, from https://www.thomas-gruppe.de/betonbauteile/waende/massivwaende/

Thomas Gruppe. (n.d.-b). *Thomas Gruppe Standorte*. Retrieved 6 August 2025, from https://www.thomas-gruppe.de/unternehmen/thomas-gruppe/#standorte

thomas gruppe - Geschäftsfeld Betonbauteile. (2020). *EPD C30/37 Precast Wall Elements* (EPD No. EPD-THO-20200144-IBD1-EN). Institut Bauen und Umwelt e.V. (IBU).

Torrent, R. J. (2013). *Service Life Prediction: Theorecrete, Labcrete and Realcrete Approaches*.

TWS. (2025, February 11). Renting vs. Buying Temporary Walls for Construction Projects. *Temporary Wall Systems*. https://tempwallsystems.com/blog/the-e/

UEPG. (2021). *UEPG - Annual Report 2020—2021*. https://www.aggregates-europe.eu/wp-content/uploads/2023/03/Final_-_UEPG-AR2020_2021-V05_spreads72dpiLowQReduced.pdf

UNEA. (2022). *Sand and Sustainability: 10 strategic recommendations to avert a crisis*.

Uotila, U., Saari, A., & Joensuu, T. (2024). Demands for DfD data characteristics: A step towards enabling reuse of prefabricated concrete components. *Environmental Research: Infrastructure and Sustainability*, *4*(1), 015014. https://doi.org/10.1088/2634-4505/ad3579

USGS. (n.d.). *Cement Statistics and Information | U.S. Geological Survey*. Retrieved 19 January 2025, from https://www.usgs.gov/centers/national-minerals-information-center/cement-statistics-and-information

v studio. (2017, December 5). *The Sealing*. Designboom | Architecture & Design Magazine. https://www.designboom.com/readers/v-studio-sealing-debris-memorials-12-05-2017/

van Mier, J. G. M. van. (1997). *Fracture processes of concrete: Assesment of material parameters for fracture models*. CRC Press.

Vermeulen, J. (2016). *EU Construction & Demolition Waste Management Protocol*.

Wang, Q., Pantoja-Rosero, B. G., Santos, K. R. M. D., & Beyer, K. (2024). An image convolution-based method for the irregular stone packing problem in masonry wall construction. *European Journal of Operational Research*, *316*(2), 733–753. https://doi.org/10.1016/j.ejor.2024.01.037

Weber Vloeibare zandcement®. (2025). Saint-Gobain Weber Beamix. https://www.nl.weber/weber-vloeibare-zandcement

Yazdi, M. A., Dejager, E., Debraekeleer, M., Gruyaert, E., Van Tittelboom, K., & De Belie, N. (2020). Bond strength between concrete and repair mortar and its relation with concrete removal techniques and substrate composition. *Construction and Building Materials*, *230*, 116900. https://doi.org/10.1016/j.conbuildmat.2019.116900

Yiğit Hunce, S., Soyer, E., & Akgiray, Ö. (2016). Characterization of Granular Materials with Internal Pores for Hydraulic Calculations Involving Fixed and Fluidized Beds. *Industrial & Engineering Chemistry Research*, *55*(31), 8636–8651. https://doi.org/10.1021/acs.iecr.6b00953

Zabek, M., Konstantinou, T., & Klein, T. (2023). *D2.3. Sustainable requirements*. https://doi.org/10.5281/ZENODO.8239083

Zandonella Callegher, C., Grazieschi, G., Wilczynski, E., Oberegger, U. F., & Pezzutto, S. (2023). Assessment of Building Materials in the European Residential Building Stock: An Analysis at EU27 Level. *Sustainability*, *15*(11), 8840. https://doi.org/10.3390/su15118840

Appendix

Python Codes

Processing Scans

```
import cv2
import numpy as np
import csv

# Define the amount of rubble scanned
image_nbr = 113

# Define backdrop size in mm (adjust to distortion)
frame_size_v = 198
frame_size_h = 198

for i in range(1,image_nbr+1):


    # Paths
    directory =
"/Users/mvk/Documents/Python_Local/Cyclopean_Spolia/Scanning/
250410_Experiments/W01_largerubble30/Wall01"
    raw_scans = f"{directory}/Raw_Scans/rubble_{i:02}.jpg"
    contour_on_scan_path =
f"{directory}/Processed_Scans/contour_on_scan/contour_on_scan
_{i}.png"
    rubble_shape_path =
f"{directory}/Processed_Scans/rubble_shape/rubble_{i:02}.png"
    detailed_csv_files_path =
f"{directory}/Processed_Scans/detailed_csv_files/rubble_{i}.c
sv"
    csv_files_path =
f"{directory}/Processed_Scans/csv_files/rubble_{i}.csv"


    print("I tried to open: ",raw_scans)
    # Load the rubble image
    image = cv2.imread(raw_scans)

    # Check if the image was successfully loaded
    if image is None:
        print(f"Error: rubble image {i} not loaded.\n")
    else:
        print(f"Rubble image {i} loaded successfully!\n")

    # Resize the image based on the size of the backdrop and
multiply by 10 to generate a better resolution
    image_resize = cv2.resize(image, (frame_size_v*10,
frame_size_h*10))

    # Prepare the image to get the most accurate contour
    gray_image = cv2.cvtColor(image_resize,
cv2.COLOR_BGR2GRAY)
    blurred_image = cv2.GaussianBlur(gray_image, (5, 5), 30)
    contrast_image = cv2.convertScaleAbs(blurred_image,1,1)
    ret, binary_image = cv2.threshold(contrast_image, 0, 255,
cv2.THRESH_BINARY + cv2.THRESH_OTSU)

    # Find the contour
    contours, hierarchy = cv2.findContours(binary_image,
cv2.RETR_EXTERNAL, cv2.CHAIN_APPROX_SIMPLE)
    largest_contour = max(contours, key=cv2.contourArea)
    epsilon = 0.01 * cv2.arcLength(largest_contour, True)
    print(epsilon)
```

```
    approx_contour = cv2.approxPolyDP(largest_contour,
epsilon, True)
    hull_contour = cv2.convexHull(approx_contour)


    # Draw the contour on the original rubble image and save
it
    cv2.drawContours(image_resize, [hull_contour], -1, (0, 0,
255), 5)

    success = cv2.imwrite(contour_on_scan_path, image_resize)

    if success:
        print(f"Contour on rubble image {i} saved
successfully\n")
    else:
        print(f"Error saving contour on rubble image {i}\n")


    # Create an image which shows the shape of the rubble and
save it
    white_colour = (255, 255, 255)
    white_image = np.full_like(image_resize, white_colour)
    cv2.drawContours(white_image, [hull_contour], -1, (0, 0,
0), cv2.FILLED)
    success = cv2.imwrite(rubble_shape_path, white_image)

    if success:
        print(f"Rubble shape {i} saved successfully as
{rubble_shape_path}\n")
    else:
        print(f"Error saving rubble shape {i}\n")

    # Create a hulled csv file for further processing in
Grasshopper
    contour_points = hull_contour.reshape(-1, 2)  # Shape:
(N, 2)
```



```
    with open(csv_files_path, 'w', newline='') as csvfile:
        csv_writer = csv.writer(csvfile)
        for point in contour_points:
            x, y = point
            csv_writer.writerow([x, y])

        print("successfully saved rubble number ", i, " as a
csv file")


    # Create a detailed csv file for further processing in
Grasshopper
    contour_points = largest_contour.reshape(-1, 2)  # Shape:
(N, 2)

    with open(detailed_csv_files_path, 'w', newline='') as
csvfile:
        csv_writer = csv.writer(csvfile)
        for point in contour_points:
            x, y = point
            csv_writer.writerow([x, y])

        print("successfully saved rubble number ", i, " as a
csv file")


#cv2.imwrite(f"/Users/mvk/Documents/Python_Local/Cyclopean_Sp
olia/Scanning/250304_Rubble/Processed_Scans/test_folder/rubbl
e_{i:02}.png", binary_image)
```

Prepare contours as single svg for Deep Nest including numbering

```
import os
import csv

# ------------------------------------------------
# User-defined parameters
# ------------------------------------------------
image_nbr = 20  # How many CSV files do you have?
csv_dir =
"/Users/mvk/Documents/Python_Local/Cyclopean_Spolia/Scanning/
250313_Nesting/Processed_Scans/csv_02"
output_svg_path =
"/Users/mvk/Documents/Python_Local/Cyclopean_Spolia/Scanning/
250313_Nesting/Processed_Scans/250313_nesting_w2.svg"

# Rectangle SVG settings
rectangle_width = 2500
rectangle_height = 4000
rectangle_svg_path =
"/Users/mvk/Documents/Python_Local/Cyclopean_Spolia/Scanning/
250313_Nesting/Processed_Scans/rectangle_shape_portrait.svg"

# Grid layout
num_columns = 5      # How many shapes per row
spacing = 50.0       # Horizontal/vertical gap between shapes

# Optional scale factor if you want to resize all contours
scale_factor = 1.0

# Digit labeling settings
digit_scale = 0.2    # Scale factor for all digits
digit_color = "black"
digit_stroke_width = 0.5
# ------------------------------------------------
```



```
############################################################
################
# 1) Define a simple 7-segment representation for digits
############################################################
################
# Each segment is defined by start->end points in a
coordinate system ~8 wide, 10 tall.
# We gather them in a dictionary for easy use.
SEGMENTS = {
    'a': [(2,0),(6,0)],    # top horizontal
    'b': [(6,0),(6,5)],    # upper-right vertical
    'c': [(6,5),(6,10)],   # lower-right vertical
    'd': [(2,10),(6,10)],  # bottom horizontal
    'e': [(2,5),(2,10)],   # lower-left vertical
    'f': [(2,0),(2,5)],    # upper-left vertical
    'g': [(2,5),(6,5)],    # middle horizontal
}

# For each digit, define which segments appear
DIGIT_MAP = {
    '0': ['a','b','c','d','e','f'],        # omit 'g'
    '1': ['b','c'],
    '2': ['a','b','d','e','g'],
    '3': ['a','b','c','d','g'],
    '4': ['b','c','f','g'],
    '5': ['a','c','d','f','g'],
    '6': ['a','c','d','e','f','g'],
    '7': ['a','b','c'],
    '8': ['a','b','c','d','e','f','g'],
    '9': ['a','b','c','d','f','g'],
}

def make_digit_polylines(digit_char):
    """
    Returns a list of polylines (each polyline = list of
(x,y) points)
    for the specified single digit (0-9) in 7-segment style.
```

```
    """
    if digit_char not in DIGIT_MAP:
        return []  # unknown char, return empty

    segments_on = DIGIT_MAP[digit_char]
    polylines = []
    for seg in segments_on:
        polylines.append(SEGMENTS[seg])
    return polylines

def make_number_polylines(num_str):
    """
    For a multi-digit string (e.g. "12"), build a combined
list of polylines.
    We place each digit next to the previous one, with a
small offset in X.
    """
    x_offset = 0
    digit_width = 8  # approximate width for each digit in
the local coords
    result = []

    for ch in num_str:
        digit_lines = make_digit_polylines(ch)
        # Shift each segment by x_offset
        for line in digit_lines:
            shifted_line = [(pt[0] + x_offset, pt[1]) for pt
in line]
            result.append(shifted_line)
        # Move over to the right for the next digit
        x_offset += (digit_width + 2)  # 2 px gap between
digits
    return result

##################################################################
#################
```



```
# 2) Read the polygons from CSV and store (points,
rubble_index)
##################################################################
#################
all_polygons = []  # list of (points, rubble_num)

for i in range(1, image_nbr + 1):
    csv_file = os.path.join(csv_dir, f"rubble_{i}.csv")
    if not os.path.isfile(csv_file):
        print(f"Skipping missing file: {csv_file}")
        continue

    # Read points from CSV
    points = []
    with open(csv_file, 'r', newline='') as cf:
        reader = csv.reader(cf)
        for row in reader:
            if len(row) == 2:
                x, y = map(float, row)
                x *= scale_factor
                y *= scale_factor
                points.append((x, y))
    if points:
        all_polygons.append((points, i))

if not all_polygons:
    raise ValueError("No valid polygons found. Check your CSV
files.")

##################################################################
#################
# 3) Compute bounding boxes & arrange polygons in a grid
##################################################################
#################
def bounding_box(polygon):
    xs = [p[0] for p in polygon]
    ys = [p[1] for p in polygon]
```

```
    return (min(xs), max(xs), min(ys), max(ys))

polygons_bbox = [bounding_box(poly) for (poly, _) in
all_polygons]

arranged_polygons = []  # list of ((shifted_points),
rubble_num, (minx,maxx,miny,maxy))
x_cursor = 0.0
y_cursor = 0.0
row_height = 0.0
col_count = 0

layout_min_x = float('inf')
layout_min_y = float('inf')
layout_max_x = float('-inf')
layout_max_y = float('-inf')

for idx, (poly, rubble_num) in enumerate(all_polygons):
    minx, maxx, miny, maxy = polygons_bbox[idx]
    width = maxx - minx
    height = maxy - miny

    shifted_poly = []
    for (px, py) in poly:
        sx = x_cursor + (px - minx)
        sy = y_cursor + (py - miny)
        shifted_poly.append((sx, sy))

        layout_min_x = min(layout_min_x, sx)
        layout_min_y = min(layout_min_y, sy)
        layout_max_x = max(layout_max_x, sx)
        layout_max_y = max(layout_max_y, sy)

    # Store the shape plus its bounding box in the final
position
    arranged_polygons.append((shifted_poly, rubble_num,
                              x_cursor, y_cursor,
                              width, height))

    # Update row height for grid
    row_height = max(row_height, height)
    x_cursor += width + spacing
    col_count += 1
    # If we've filled one row, go to next
    if col_count >= num_columns:
        col_count = 0
        x_cursor = 0
        y_cursor += row_height + spacing
        row_height = 0

# Overall layout bounding box
svg_min_x = min(0, layout_min_x)
svg_min_y = min(0, layout_min_y)
svg_width = layout_max_x - svg_min_x + spacing
svg_height = layout_max_y - svg_min_y + spacing

svg_width = max(svg_width, 1)
svg_height = max(svg_height, 1)

##############################################################
################
# 4) Build the SVG for the arranged shapes + digit polylines
##############################################################
################
svg_header = f"""<svg
  xmlns="http://www.w3.org/2000/svg"
  width="{svg_width}"
  height="{svg_height}"
  version="1.1"
>
"""

svg_footer = "</svg>\n"
svg_shapes = []
```

```
for (shifted_points, rubble_num, cell_x, cell_y, cell_w,
cell_h) in arranged_polygons:
    # 4.1) Write the stone polygon
    stone_points_str = " ".join(f"{x},{y}" for x, y in
shifted_points)
    shape_id = f"rubble_{rubble_num}"
    stone_polygon = f"""  <polygon
    id="{shape_id}"
    points="{stone_points_str}"
    fill="none"
    stroke="black"
    stroke-width="1"
  />"""
    svg_shapes.append(stone_polygon)

    # 4.2) Create the digit polylines for the rubble number
    num_str = str(rubble_num)
    digit_lines = make_number_polylines(num_str)

    # The digit lines are in a local coordinate system (width
~ up to 8 * digits).
    # We want to center them inside the bounding box of this
stone (cell_w x cell_h).
    #  - So find their bounding box
    if digit_lines:
        digit_xs = [pt[0] for line in digit_lines for pt in
line]
        digit_ys = [pt[1] for line in digit_lines for pt in
line]
        dig_minx, dig_maxx = min(digit_xs), max(digit_xs)
        dig_miny, dig_maxy = min(digit_ys), max(digit_ys)
        seg_w = (dig_maxx - dig_minx)
        seg_h = (dig_maxy - dig_miny)

        # We'll scale them down a bit (digit_scale) plus fit
them into the bounding box
```



```
        # so they don't exceed cell_w or cell_h.
        # We'll do a minimal scale so the digits fit in about
half the shape size,
        # or you can adjust logic as needed.
        box_target_w = cell_w * 0.5  # only use half cell
width for digits
        box_target_h = cell_h * 0.5

        # scale needed to fit
        scale_w = box_target_w / max(seg_w, 1e-6)
        scale_h = box_target_h / max(seg_h, 1e-6)
        scale_fit = min(scale_w, scale_h) * digit_scale

        # Compute offset to center inside (cell_x, cell_y,
cell_w, cell_h)
        center_x = cell_x + (cell_w / 2.0)
        center_y = cell_y + (cell_h / 2.0)

        # Now transform each polyline
        digit_polyline_svgs = []
        for line in digit_lines:
            transformed = []
            for (dx, dy) in line:
                # Move line origin so top-left corner is
(0,0)
                # (i.e. subtract dig_minx, dig_miny)
                local_x = dx - dig_minx
                local_y = dy - dig_miny

                # scale
                local_x *= scale_fit
                local_y *= scale_fit

                # center in bounding box
                final_x = center_x - (seg_w * scale_fit)/2.0
+ local_x
```

```
                final_y = center_y - (seg_h * scale_fit)/2.0
+ local_y

                transformed.append((final_x, final_y))

            # Convert to an SVG <polyline>
            line_str = " ".join(f"{px},{py}" for px, py in
transformed)
            polyline_svg = f"""  <polyline
      fill="none"
      stroke="{digit_color}"
      stroke-width="{digit_stroke_width}"
      points="{line_str}"
    />"""
            digit_polyline_svgs.append(polyline_svg)

        # Add each digit polyline to the shapes
        svg_shapes.extend(digit_polyline_svgs)

################################################################
#################
# 5) Combine and write the single SVG file
################################################################
#################
svg_full = svg_header + "\n".join(svg_shapes) + "\n" +
svg_footer

os.makedirs(os.path.dirname(output_svg_path), exist_ok=True)
with open(output_svg_path, "w") as f:
    f.write(svg_full)

print(f"Created single SVG with {len(arranged_polygons)}
shapes in a grid + digit polylines.")
print(f" -> {output_svg_path}")

################################################################
#################
```



```
# 6) Create a separate SVG file for the rectangle
################################################################
#################
rect_svg = f"""<svg
  xmlns="http://www.w3.org/2000/svg"
  width="{rectangle_width}"
  height="{rectangle_height}"
  version="1.1"
>
  <rect
    x="0"
    y="0"
    width="{rectangle_width}"
    height="{rectangle_height}"
    fill="none"
    stroke="black"
    stroke-width="1"
  />
</svg>
"""

os.makedirs(os.path.dirname(rectangle_svg_path),
exist_ok=True)
with open(rectangle_svg_path, "w") as f:
    f.write(rect_svg)

print(f"Created separate rectangle SVG:\n ->
{rectangle_svg_path}")
```

muDIC adaptation to CS, DIC.py, main execution script

```
# This allows for running the example when the repo has been
cloned
import sys
from os.path import abspath
sys.path.extend([abspath(".")])
from os.path import dirname, abspath
repo_root = dirname(dirname(abspath(__file__)))
sys.path.insert(0, repo_root)

#MAURITZ: I changed the below to muDIC only from
muDIC.Examples (which didnt work)
import muDIC as dic
import logging

# Set the amount of info printed to terminal during analysis
logging.basicConfig(format='%(name)s:%(levelname)s:%(message)
s', level=logging.INFO)

# Path to folder containing images
path = r'/Users/mvk/Library/Mobile
Documents/com~apple~CloudDocs/Documents/Studium etc./TU
Delft/Graduation/Cyclopean
Spolia/Experiments/Documentation/0417/DIC_Videos/raw/cut/W1_f
rames' # Use this formatting on Linux and Mac OS
#path = r'c:\path\to\example_data\\'  # Use this formatting
on Windows

# Generate image instance containing all images found in the
folder
images = dic.IO.image_stack_from_folder(path,
file_type='.png')
images.set_filter(dic.filtering.lowpass_gaussian, sigma=1.)
```



```
# Generate mesh default:
mesher = dic.Mesher(deg_e=3, deg_n=3,type="q4")
# Generate mesh Mauritz:
#mesher = dic.Mesher(deg_e=3, deg_n=3,type="spline")

# If you want to see use a GUI, set GUI=True below
#Mauritz: I changed this from mesh =
mesher.mesh(images,Xc1=316,Xc2=523,Yc1=209,Yc2=1055,n_ely=36,
n_elx=9, GUI=False)
mesh =
mesher.mesh(images,Xc1=500,Xc2=3300,Yc1=100,Yc2=1800,n_ely=16
,n_elx=15, GUI=True)

# Instantiate settings object and set some settings manually
#Standard Settings:
"""settings = dic.DICInput(mesh, images)
settings.max_nr_im = 500
settings.ref_update = [23]
settings.maxit = 20
settings.tol = 1.e-6
settings.interpolation_order = 4"""

#Mauritz Settings:
settings = dic.DICInput(mesh, images)
settings.max_nr_im = 15
settings.ref_update = [10,20,30]
settings.maxit = 30
settings.tol = 1.e-2
settings.interpolation_order = 4

# If you want to access the residual fields after the
analysis, this should be set to True
settings.store_internals = True

# This setting defines the behaviour when convergence is not
obtained
settings.noconvergence = "ignore"
```

```
# Instantiate job object
job = dic.DICAnalysis(settings)

# Running DIC analysis
dic_results = job.run()

# Calculate field values
fields = dic.post.viz.Fields(dic_results,upscale=10)

# Show a field
viz = dic.Visualizer(fields,images=images)

# Uncomment the line below to see the results. Options:
truestrain, displacement, deformationgradient, engstrain,
coordinates, greenstrain, residual
common_vmin = -29.5
common_vmax = 29.5
#viz.show(field="truestrain", component = (1,1), frame=-1,
cmap = "RdBu",vmin=common_vmin, vmax=common_vmax)
viz.show(field="truestrain", component = (1,1), frame=-1,
cmap = "RdBu")


#viz.show(field="displacement", component = (1,1), frame=-1,
cmap = "RdBu")
```

```
import os
import logging

import matplotlib.pyplot as plt
import matplotlib as mpl
import numpy as np
from scipy.ndimage import map_coordinates
from muDIC.elements.b_splines import BSplineSurface
from muDIC.elements.q4 import Q4
import datetime

#MAURITZ
output_folder = "..."
#MAURITZ END

class Fields(object):
    # TODO: Remove Q4 argument. This should be detected
automaticaly
    def __init__(self, dic_results, seed=21, upscale=1,
interpolation_order=1):
        """
        Fields calculates field variables from the DIC-
results.
        The implementation is lazy, hence getter methods have
to be used.

        NOTE
        ----
        The fields are formatted as follows:

        * Vectors:
[elm_id,component_i,element_e_coord,element_n_coord,frame_id]
        * matrices:
[elm_id,component_i,component_j,element_e_coord,element_n_coo
rd,frame_id]


        Parameters
        ----------
        dic_results :
            The results from the DIC analysis
        seed : Integer
            The number of grid points which will be evaluated
in each direction
        upscale : Float
            Return values on a grid upscale times fines than
the original mesh

        Returns
        -------
        A Fields object
        """

        self.logger = logging.getLogger()

        # The type is implicitly checked by using the
interface
        self.__res__ = dic_results
        self.__settings__ = dic_results.settings
        self.interpolation_order = interpolation_order

        if isinstance(self.__settings__.mesh.element_def,
Q4):
            q4 = True
            seed = 1
            self.logger.info("Post processing results from Q4
elements. The seed variable is ignored and the values "
                             "are extracted at the element
centers. Use the upscale value to get interpolated fields.")
```

```
        else:
            q4 = False
            self.logger.info("Post processing results from B-
spline elements. The upscale variable is ignored. Use "
                             "the seed varialbe to set the
number of gridpoints to be evaluated along each element "
                             "axis.")

        self.__ee__, self.__nn__ =
self.__generate_grid__(seed)

        self.__F__, self.__coords__ =
self._deformation_gradient_(self.__res__.xnodesT,
self.__res__.ynodesT,

self.__settings__.mesh,

self.__settings__.mesh.element_def, self.__nn__,

self.__ee__)

        # To make the result formatting consistent across
element formulations, we arrange the elements onto a grid
        # with the same dimensions as the mesh. If up-scaling
is used, we determine the values between element centers
        # by using 3rd order spline interpolation.

        if q4:
            # Flatten things form multiple elements to a grid
of elements
            grid_shape = (self.__settings__.mesh.n_ely,
self.__settings__.mesh.n_elx)
            n_frames = self.__F__.shape[-1]
            self.__F2__ = np.zeros(
                (1, 2, 2, self.__settings__.mesh.n_elx,
self.__settings__.mesh.n_ely, self.__F__.shape[-1]))
            for i in range(2):
                for j in range(2):
                    for t in range(n_frames):
                        self.__F2__[0, i, j, :, :, t] =
self.__F__[:, i, j, 0, 0, t].reshape(grid_shape).transpose()

            self.__coords2__ = np.zeros(
                (1, 2, self.__settings__.mesh.n_elx,
self.__settings__.mesh.n_ely, self.__F__.shape[-1]))
            for i in range(2):
                for t in range(n_frames):
                    self.__coords2__[0, i, :, :, t] =
self.__coords__[:, i, 0, 0,
t].reshape(grid_shape).transpose()

            # Overwrite the old results
            # TODO: Remove overwriting results as this is a
painfully non-functional thing to do...
            self.__coords__ = self.__coords2__
            self.__F__ = self.__F2__

            self.__coords__ = self.__coords2__
            self.__F__ = self.__F2__

            if upscale != 1.:
                elms_y_fine, elms_x_fine =
np.meshgrid(np.arange(0, self.__settings__.mesh.n_elx - 1, 1.
/ upscale),

np.arange(0, self.__settings__.mesh.n_ely - 1, 1. / upscale))

                self.__F3__ = np.zeros(
                    (1, 2, 2, elms_x_fine.shape[1],
elms_x_fine.shape[0], self.__F__.shape[-1]))

                self.__coords3__ = np.zeros(
                    (1, 2, elms_x_fine.shape[1],
elms_x_fine.shape[0], self.__F__.shape[-1]))
```

```
                for i in range(2):
                    for t in range(n_frames):
                        self.__coords3__[0, i, :, :, t] =
map_coordinates(self.__coords__[0, i, :, :, t],

[elms_y_fine.flatten(),

elms_x_fine.flatten()],

order=self.interpolation_order).reshape(
                                elms_x_fine.shape).transpose()

                for i in range(2):
                    for j in range(2):
                        for t in range(n_frames):
                            self.__F3__[0, i, j, :, :, t] =
map_coordinates(self.__F__[0, i, j, :, :, t],

[elms_y_fine.flatten(),

elms_x_fine.flatten()],

order=self.interpolation_order).reshape(

elms_x_fine.shape).transpose()

                self.__coords__ = self.__coords3__
                self.__F__ = self.__F3__

    def __generate_grid__(self, seed):

        # TODO: Remove hack:
        if seed == 1:
            return np.meshgrid(np.array([0.5]),
                               np.array([0.5]))
```



```
        else:

            if np.ndim(seed) == 1:
                return np.meshgrid(np.linspace(0., 1.,
seed[0]),
                                   np.linspace(0., 1.,
seed[1]))

            else:
                return np.meshgrid(np.linspace(0., 1., seed),
                                   np.linspace(0., 1., seed))

    @staticmethod
    def _deformation_gradient_(xnodesT, ynodesT, msh, elm, e,
n):
        """
        Calculate the deformation gradient from the control
point positions
        and the element definitions.

        See the paper for the procedure.

        Parameters
        ----------
        xnodesT : ndarray
            Node position in the x direction
        ynodesT : ndarray
            Node position in the y direction
        msh : Mesh
            A Mesh object
        elm : Element
            A Element object containing the element
definitions
        e : ndarray
            The e coordinates of the element
        n : ndarray
            The n coordinates of the element
```

```
        """

        # Post Processing
        nEl = msh.n_elms
        ne = np.shape(e)[0]
        nn = np.shape(e)[1]

        # Evaluate shape function gradients on grid within
element
        Nn = elm.Nn(e.flatten(), n.flatten())
        dfde = elm.dxNn(e.flatten(), n.flatten())
        dfdn = elm.dyNn(e.flatten(), n.flatten())

        Fstack = []
        coord_stack = []

        for el in range(nEl):
            x_crd = np.einsum('ij,jn -> in', Nn,
xnodesT[msh.ele[:, el], :])
            y_crd = np.einsum('ij,jn -> in', Nn,
ynodesT[msh.ele[:, el], :])
            dxde = np.einsum('ij,jn -> in', dfde,
xnodesT[msh.ele[:, el], :])
            dxdn = np.einsum('ij,jn -> in', dfdn,
xnodesT[msh.ele[:, el], :])
            dyde = np.einsum('ij,jn -> in', dfde,
ynodesT[msh.ele[:, el], :])
            dydn = np.einsum('ij,jn -> in', dfdn,
ynodesT[msh.ele[:, el], :])

            c_confs = np.array([[dxde, dxdn], [dyde, dydn]])
            r_conf_inv = np.linalg.inv(np.rollaxis(c_confs[:,
:, :, 0], 2, 0))

            Fs = np.einsum('ijpn,pjk->ikpn', c_confs,
r_conf_inv)
```



```
            Fs = Fs.reshape((2, 2, ne, nn, -1))

            x_crd = x_crd.reshape((ne, nn, -1))
            y_crd = y_crd.reshape((ne, nn, -1))

            Fstack.append(Fs)

            coord_stack.append(np.array([x_crd, y_crd]))

        # Returns F(nElms, i, j, ide, idn , frame),
coords(nElms, i, ide, idn , frame)

        return np.array(Fstack), np.array(coord_stack)

    @staticmethod
    def _green_deformation_(F):
        """
        Calculate Green deformation tensor from deformation
as G = F^T * F
        :param F:
        :return:
        """
        E11 = F[:, 0, 0, :, :, :] ** 2. + F[:, 0, 1, :, :, :]
** 2.

        E12 = F[:, 0, 0, :, :, :] * F[:, 1, 0, :, :, :] +
F[:, 0, 1, :, :, :] * F[:, 1, 1, :, :, :]

        E22 = F[:, 1, 0, :, :, :] ** 2. + F[:, 1, 1, :, :, :]
** 2.

        E = np.array([[E11, E12], [E12, E22]])

        E[E == np.nan] = 0.

        return np.moveaxis(E, 2, 0)
```

```
    @staticmethod
    def _green_strain_(F):
        """
        Calculate Green strain tensor from F as G = 0.5*(F^T
* F -I)
        :param F: Deformation gradient tensor F_ij on the
form [nEl,i,j,...]
        :return: Green Lagrange strain tensor E_ij on the
form [nEl,i,j,...]
        """
        E11 = 0.5 * (F[:, 0, 0, :, :, :] ** 2. + F[:, 0, 1,
:, :, :] ** 2. - 1.)

        E12 = 0.5 * (F[:, 0, 0, :, :, :] * F[:, 1, 0, :, :,
:] + F[:, 0, 1, :, :, :] * F[:, 1, 1, :, :, :])

        E22 = 0.5 * (F[:, 1, 0, :, :, :] ** 2. + F[:, 1, 1,
:, :, :] ** 2. - 1.)

        E = np.array([[E11, E12], [E12, E22]])

        E[E == np.nan] = 0.

        return np.moveaxis(E, 2, 0)

    @staticmethod
    def _principal_strain_(G):
        E11 = G[:, 0, 0]
        E12 = G[:, 0, 1]
        E21 = G[:, 1, 0]
        E22 = G[:, 1, 1]

        E_temp = np.moveaxis(G, 1, -1)
        E = np.moveaxis(E_temp, 1, -1)

        eigvals, eigvecs = np.linalg.eig(E)
```



```
        # print(np.shape(eigvals))
        # print(np.shape(eigvecs))

        ld1 = np.sqrt(eigvals[:, :, :, :, 0])
        ld2 = np.sqrt(eigvals[:, :, :, :, 1])

        ev1 = eigvecs[:, :, :, :, 0, 0]
        ev2 = eigvecs[:, :, :, :, 0, 1]

        # print(np.shape(eigvals))
        # print(np.shape(eigvecs))
        # print(np.shape(ld1))
        # print(np.shape(ev1))

        ld = np.moveaxis(np.array([ld1, ld2]), 0, 1)
        ev = np.moveaxis(np.array([ev1, ev2]), 0, 1)
        print(np.shape(ld1))
        print(np.shape(ev1))

        return ld, ev

    @staticmethod
    def _engineering_strain_(E):
        """
        Calculate engineering strain from Green Lagrange
strain tensor E_ij as:
        eps_ii = sqrt(1+E_ii)-1 and
        gamma_ij = 2E_ij/sqrt((1+E_ii)*(1+E_jj))
        :param E: Green Lagrange strain tensor E_ij on the
form [nEl,i,j,...]
        :return: Engineering strain tensor eps_ij on the form
[nEl,i,j,...]
        """
        eps_xx = np.sqrt(1. + 2. * E[:, 0, 0, :]) - 1.
        eps_yy = np.sqrt(1. + 2. * E[:, 1, 1, :]) - 1.
```

```
        eps_xy = 0.5 * np.arcsin(2. * E[:, 0, 1, :] /
np.sqrt((1. + 2. * E[:, 0, 0, :]) * (1. + 2. * E[:, 1, 1,
:])))

        eps = np.array([[eps_xx, eps_xy], [eps_xy, eps_yy]])

        return np.moveaxis(eps, 2, 0)

    @staticmethod
    def _true_strain_(eps):
        """
        Calculate true strain tensor teps_ij from engineering
strain tensor eps_ij as:
        teps_ij = log(eps_ij+1)
        :param eps: Engineering strain tensor eps_ij on the
form [nEl,i,j,...]
        :return: True strain tensor teps_ij on the form
[nEl,i,j,...]
        """
        return np.log(eps + 1.)

    def true_strain(self):
        E = self._green_strain_(self.__F__)
        engineering_strains = self._engineering_strain_(E)
        return self._true_strain_(engineering_strains)

    def eng_strain(self):
        E = self._green_strain_(self.__F__)
        return self._engineering_strain_(E)

    def F(self):
        return self.__F__

    def green_strain(self):
        return self._green_strain_(self.__F__)

    def coords(self):
```



```
        return self.__coords__

    def disp(self):
        return self.__coords__[:, :, :, :, :] -
self.__coords__[:, :, :, :, 0, np.newaxis]

    def residual(self, frame_id):
        if self.__settings__.store_internals == False:
            raise ValueError("The analysis has to be run with
store_internals=True")
        if isinstance(self.__settings__.mesh.element_def,
Q4):
            raise NotImplementedError("Q4 residual fields are
not yet implemented")
        ref_id = ind_closest_below(frame_id, [ref.image_id
for ref in self.__res__.reference])
        ref = self.__res__.reference[ref_id]

        cross_correlation_product =
cross_correlation_products(self.__res__.Ic_stack[frame_id],
ref.I0_stack)
        self.logger.info("Cross correlation product is %f" %
cross_correlation_product)

        return np.abs(self.__res__.Ic_stack[frame_id] -
ref.I0_stack)

    def elm_coords(self, frame_id):
        ref_id = ind_closest_below(frame_id, [ref.image_id
for ref in self.__res__.reference])
        ref = self.__res__.reference[ref_id]
        return ref.e, ref.n


class Visualizer(object):
    def __init__(self, fields, images=False):
        """
```

```
        Visualizer for field variables.

        Parameters
        ----------
        fields : Fields object
            The Fields object contains all the variables that
can be plotted.
        images : ImageStack object
            The stack of images corresponding to Fields

        Returns
        -------
        A Visualizer Object
        """
        if isinstance(fields, Fields):
            self.fields = fields
        else:
            raise ValueError("Only instances of Fields are
accepted")

        self.images = images
        self.logger = logging.getLogger()

    def show(self, field="displacement", component=(0, 0),
frame=0, quiverdisp=False, **kwargs):
        """
        Show the field variable

        Parameters
        ----------
        field : string
            The name of the field to be shown. Valid inputs
are:
                "true strain"
                "eng strain"
                "disp"
                "green strain"
                "residual"

        component : tuple with length 2
            The components of the fields. Ex. (0,1).
            In the case of vector fields, only the first
index is used.
        frame : Integer
            The frame number of the field

        """

        keyword = field.replace(" ", "").lower()

        if keyword == "truestrain":
            fvar = self.fields.true_strain()[0, component[0],
component[1], :, :, frame]
            xs, ys = self.fields.coords()[0, 0, :, :, frame],
self.fields.coords()[0, 1, :, :, frame]

        elif keyword in ("F", "degrad",
"deformationgradient"):
            fvar = self.fields.F()[0, component[0],
component[1], :, :, frame]
            xs, ys = self.fields.coords()[0, 0, :, :, frame],
self.fields.coords()[0, 1, :, :, frame]

        elif keyword == "engstrain":
            fvar = self.fields.eng_strain()[0, component[0],
component[1], :, :, frame]
            xs, ys = self.fields.coords()[0, 0, :, :, frame],
self.fields.coords()[0, 1, :, :, frame]

        elif keyword in ("displacement", "disp", "u"):
            fvar = self.fields.disp()[0, component[0], :, :,
frame]
            xs, ys = self.fields.coords()[0, 0, :, :, frame],
self.fields.coords()[0, 1, :, :, frame]
```

```
        elif keyword in ("coordinates", "coords", "coord"):
            fvar = self.fields.coords()[0, component[0], :,
:, frame]
            xs, ys = self.fields.coords()[0, 0, :, :, frame],
self.fields.coords()[0, 1, :, :, frame]


        elif keyword == "greenstrain":
            fvar = self.fields.green_strain()[0,
component[0], component[1], :, :, frame]
            xs, ys = self.fields.coords()[0, 0, :, :, frame],
self.fields.coords()[0, 1, :, :, frame]

        elif keyword == "residual":
            fvar = self.fields.residual(frame)
            xs, ys = self.fields.elm_coords(frame)

        else:
            self.logger.info("No valid field name was
specified")
            return

        if np.ndim(fvar) == 2:
            if self.images:
                n, m = self.images[frame].shape
                plt.imshow(self.images[frame],
cmap=plt.cm.gray, origin="lower", extent=(0, m, 0, n))

            if quiverdisp:
                plt.quiver(self.fields.coords()[0, 0, :, :,
frame], self.fields.coords()[0, 1, :, :, frame],
                           self.fields.disp()[0, 0, :, :,
frame], self.fields.disp()[0, 1, :, :, frame],**kwargs)
            else:
                #MAURITZ: predefines the same legend values
for each image
```



```
                cf = plt.contourf(xs, ys, fvar, **kwargs)
                plt.colorbar(cf)
                plt.show()


    def save(self, field="displacement", component=(0, 0),
frame=0, quiverdisp=False, **kwargs):
        """
        Show the field variable

        Parameters
        ----------
        field : string
            The name of the field to be shown. Valid inputs
are:
                "true strain"
                "eng strain"
                "disp"
                "green strain"
                "residual"

        component : tuple with length 2
            The components of the fields. Ex. (0,1).
            In the case of vector fields, only the first
index is used.
        frame : Integer
            The frame number of the field

        """

        keyword = field.replace(" ", "").lower()

        if keyword == "truestrain":
            fvar = self.fields.true_strain()[0, component[0],
component[1], :, :, frame]
            xs, ys = self.fields.coords()[0, 0, :, :, frame],
self.fields.coords()[0, 1, :, :, frame]
```

```
        elif keyword in ("F", "degrad",
"deformationgradient"):
            fvar = self.fields.F()[0, component[0],
component[1], :, :, frame]
            xs, ys = self.fields.coords()[0, 0, :, :, frame],
self.fields.coords()[0, 1, :, :, frame]

        elif keyword == "engstrain":
            fvar = self.fields.eng_strain()[0, component[0],
component[1], :, :, frame]
            xs, ys = self.fields.coords()[0, 0, :, :, frame],
self.fields.coords()[0, 1, :, :, frame]

        elif keyword in ("displacement", "disp", "u"):
            fvar = self.fields.disp()[0, component[0], :, :,
frame]
            xs, ys = self.fields.coords()[0, 0, :, :, frame],
self.fields.coords()[0, 1, :, :, frame]

        elif keyword in ("coordinates", "coords", "coord"):
            fvar = self.fields.coords()[0, component[0], :,
:, frame]
            xs, ys = self.fields.coords()[0, 0, :, :, frame],
self.fields.coords()[0, 1, :, :, frame]


        elif keyword == "greenstrain":
            fvar = self.fields.green_strain()[0,
component[0], component[1], :, :, frame]
            xs, ys = self.fields.coords()[0, 0, :, :, frame],
self.fields.coords()[0, 1, :, :, frame]

        elif keyword == "residual":
            fvar = self.fields.residual(frame)
            xs, ys = self.fields.elm_coords(frame)
```



```
        else:
            self.logger.info("No valid field name was
specified")
            return

        if np.ndim(fvar) == 2:
            if self.images:
                n, m = self.images[frame].shape
                plt.imshow(self.images[frame],
cmap=plt.cm.gray, origin="lower", extent=(0, m, 0, n))

            if quiverdisp:
                plt.quiver(self.fields.coords()[0, 0, :, :,
frame], self.fields.coords()[0, 1, :, :, frame],
                           self.fields.disp()[0, 0, :, :,
frame], self.fields.disp()[0, 1, :, :, frame],**kwargs)
            else:
                #MAURITZ: predefines the same legend values
for each image
                # allow the caller to fix the color limits
once for all runs
                vmin = kwargs.pop('vmin', None)
                vmax = kwargs.pop('vmax', None)
                # if neither vmin nor vmax were passed, we
default to auto-scaling:
                norm = mpl.colors.Normalize(vmin=vmin,
vmax=vmax)
                cf = plt.contourf(xs, ys, fvar, vmin=vmin,
vmax=vmax, **kwargs)
            plt.colorbar(cf)
        #MAURITZ: save the file (I turned plt.show off)
        timestamp = datetime.datetime.now().strftime('%Y-%m-
%d %H:%M:%S')
        filename = os.path.join(output_folder,
f"displacement_frame_{timestamp}.png")
        plt.savefig(filename, dpi=300)
```

```
        print("successfully saved file under: ",filename, "in
",output_folder)
        plt.close()
        #MAURITZ END



def ind_closest_below(value, list):
    ind = 0
    for i, num in enumerate(list):
        if num < value:
            ind = i

    return ind


def cross_correlation_products(field_a, field_b):
    return np.sum(field_a * field_b) / (
            (np.sum(np.square(field_a)) ** 0.5) * (
            np.sum(np.square(field_b)) ** 0.5))
```

System Design Case Study Calculations

Building			
Stories	3		
Span	10	m	
m2 / wall	30	m2	
Stress	1.4	Mpa	
Safety Factors			
Q	1.35		
G	1.5		

Floors			
Floor Load	2	kN / m2	EN 1991-1-1 (Table 6.1 for residential)
Walls			
Material	Concrete		
Density	2400	kg/m3	
Load	23544	N/m3	
Thickness	0.22	m	
Length	6	m	
Height	3	m	
Total N	130528	N	
Windows	2		
Window Length	1.6	m	
Load Bearing Length	2.8	m	
Area	0.616	m2	
Area	616000	mm2	
m3 / wall	1.848	m3	
N/ wall	43509	N	
Snow			
Snow	0.7	kN / m2	
Snow total	21	kN	
Finishes			
Finishes	1	kN/m2	
Finishes total	30	kN	
Live Loads			
Live Loads	2	kN/m2	
Live Loads Total	60	kN	

Loads			
Dead Loads (Q)			
Walls	130.5	kN	176.2127136
Floors	180.0	kN	243
Finishes	90	kN	121.5
Live Loads (G)			
Live Loads	180.0	kN	270
Snow	21.0	kN	31.5
Total			
Loads	601.5	kN	842.2 kN
Stress	1.0	Mpa	1.4 Mpa

Rubble Distortion

	Stone 11.1	Stone 11.2	Stone 11.3	Stone 2.1	Stone 2.2	Stone 1.1	Stone 1.2
real length	33	84	77	78	45	62	47
image length	35	90	82	81	48	66	50
ratio	0.94	0.93	0.94	0.96	0.94	0.94	0.94

average ratio	0.942	
paper width	2100	pixels
final size	1979	pixels

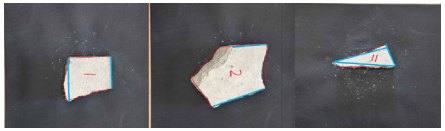

Preliminary Tests All Stacked Walls

20250225-044548

id	d_x	d_y	angle
51	3423.16129	444.653763	-98.746162
26	245.056663	110.957405	-205.82099
108	1080	400	86.9872131
111	2970	660	90
27	1930	250	64.5366516
118	1408.16707	851.63017	-90
14	101.59121	864.183214	-90
37	772.401902	856.48038	-1.332222
40	1370	1050	87.3974457
39	2170	1000	87.1375961
70	665.101992	1768.97164	0
5	3005.4236	1020.76143	-186.63251
74	390	2550	90
34	1685.13514	1368.46448	-264.28941
48	2391.93926	1512.30687	-213.69006
126	3411.21447	1549.40568	-171.38435
94	1292.44382	2384.14045	-102.09476
97	2050.75211	2420.0921	-8.1301041
112	3015.45123	2235.55465	-10.304848
73	3660	2440	90

20250225-012803

id	d_x	d_y	angle
13	3437.96564	204.112594	-171.8699
125	180.525082	225.705579	-85.683972
89	2279.84556	486.150579	-268.5679
120	189.883224	1178.0262	-7.9696121
51	1503.16129	444.653763	-98.746162
26	1040.95741	344.943337	-25.820992
73	760	1280	90
118	1264.89862	1276.73155	0
82	359.574657	1744.51117	-264.55967
119	2595.5771	1107.22992	-93.2397
11	3682.60661	926.661345	-87.70939
40	2885.44728	1358.123	-182.60255
15	2523.70059	1166.71214	-165.37913
116	1843.48479	1590.13756	-91.735703
61	1470	1810	4.39870548
79	3769.04089	2120.00294	-180
95	2395.04646	2248.51336	-9.462326
31	2960	2060	73.5596161
58	345.690119	2155.15186	-84.427803
88	1254.72031	2328.0676	-87.739498

20250225-050506

id	d_x	d_y	angle
75	3584.26268	547.924749	-106.99082
8	246.768216	369.75857	-189.6052
22	1253.04898	223.129373	-266.72951
108	3702.72116	1267.73293	-183.01279
122	2758.19923	439.526297	-94.085617
118	3050	880	90
17	1941.72792	345.084806	-180
124	3260	1460	86.1859207
25	579.677557	1009.48438	-257.00538
36	1390.76377	1019.72291	-85.030259
33	2940	1580	42.7093887
9	1830	1010	90
63	494.298792	2169.37476	-180
1	1400	1930	45
3	2380	2120	4.01417542
94	2379.15169	1283.29213	-192.09476
88	3271.9324	2354.72031	-267.7395

20250225-092926

id	d_x	d_y	angle
38	3380	380	88.4088593
24	642.749726	29.1602634	-86.552613
123	6.44391408	1157.61337	-180
41	2431.75892	362.836057	-101.76829
14	3423.704	997.887212	-180
68	3389.01961	1727.52469	-269.3704
50	2750	1030	5.57219744
15	1630	160	14.6208744
70	961.028365	1085.10199	-180
2	400.92769	1573.92593	-38.659809
32	1870.84611	701.868257	-61.189205
54	1149.47634	1779.24774	-185.90615
18	2317.37643	1011.6033	-180
80	1865.69684	1892.73958	-186.58195
74	2491.01148	2092.98587	0
94	452.44382	2484.14045	-102.09476
79	1460	2410	90
26	2920.95741	2084.94334	-25.820992

20250225

id	d_x	d_y	angle
70	601.028365	625.101992	-180
22	3333.04898	223.129373	-266.72951
54	1619.24774	530.523658	-5.9061508
123	2510	640	0
2	2176.07407	330.92769	-218.65981
63	380	1560	90
23	1016.49971	860.998842	-266.63354
74	1541.01148	1392.98587	0
86	1750	1240	3.23970008
79	3659.04384	1320.96205	-90
37	2353.51962	1452.4019	-181.33222
31	2888.97571	1508.67769	-16.440384
71	398.878623	1913.69384	-88.619646
100	3545.74437	1981.939	-180
26	1445.05666	1560.95741	-205.82099
124	3002.83576	2324.80405	-3.8140793
66	2290.18453	2419.93612	0
49	1470	2150	90

Preliminary Tests Selected Walls

20250225-022132

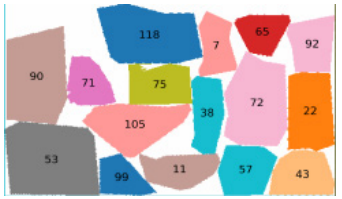

Status: Tested

Sequence	id	d_x	d_y	angle
1	1	455.677174	497.214293	-135
2	92	145.447275	1544.43214	-176.98721
3	5	3430	260	83.367485
5	44	1192.65405	288.364881	-38.659809
6	14	2687.88721	316.296002	0
8	61	3407.5195	1092.393	-85.601295
12	64	2041.01665	604.081215	-193.2764
13	20	3020	1090	9.81930065
14	88	2220	1130	2.26050186
15	79	3769.04089	2260.00294	-180
16	83	1450	1190	82.170929
17	36	970.277087	1330.76377	-265.03026
19	9	1731.48707	1432.80711	-180
20	26	3010.95741	1994.94334	-25.820992
25	66	2510.2484	2260.12065	-90
26	82	1459.57466	2114.51117	-264.55967
	49	775.667532	2045.35065	-180

20250225 - 1524004

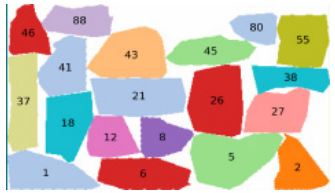

Status: Broken

Sequence	id	d_x	d_y	angle
1	125	180.525082	225.705579	-85.683972
2	53	3478.00823	437.704243	-16.699242
5	58	2560	550	40.8150826
6	86	1354.87497	185.317933	-266.7603
8	97	1820.75211	1000.0921	-8.1301041
12	73	1241.96229	974.127095	-90
18	106	686.871392	1114.01524	0
21	71	1436.30616	1208.87862	-268.61965
26	78	2559.95406	1475.01413	-180
27	103	3240	1310	69.4439545
37	81	146.906343	1430.54042	-181.39718
38	100	3477.68337	1736.19463	-90
41	54	678.724083	1899.7714	-95.906151
43	89	1346.15058	1900.15444	-88.567904
45	119	2525.5771	2087.22992	-93.2397
46	37	93.5196195	2142.4019	-181.33222
55	127	3380.28773	2024.98171	-267.51045
80	49	2870	2160	90
88	108	840	2450	86.9872131

20250225 - 150028

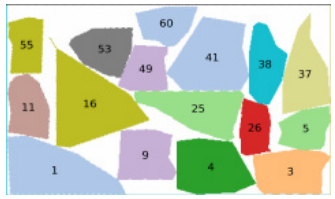

Status: Broken

	id	d_x	d_y	angle
1	76	348.22899	376.060646	-81.940896
3	129	3263.00491	344.090424	-266.53177
4	87	2256.95033	331.757555	-90
5	17	3546.81272	863.35689	-90
9	4	1627.61304	412.1109	-86.905942
11	120	179.883224	1418.0262	-7.9696121
16	28	859.528017	1071.28807	-31.138973
25	24	2430.83974	902.749726	-266.55261
26	116	3016.67361	1116.81117	-181.7357
37	19	3696.55165	1368.44315	-180
38	96	2940	1650	0
41	65	2317.36769	1982.13901	-220.81509
49	115	1495.72689	1593.42875	-180
53	55	973.026778	1879.52394	-262.87498
55	2	106.074074	1910.92769	-218.65981
60	15	1950	2100	14.6208744

Wall 01

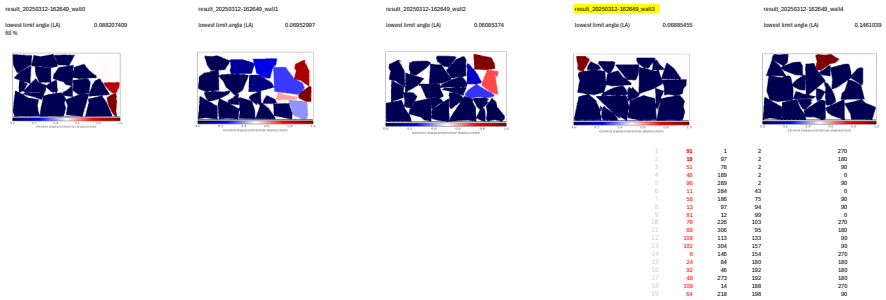

Wall 02

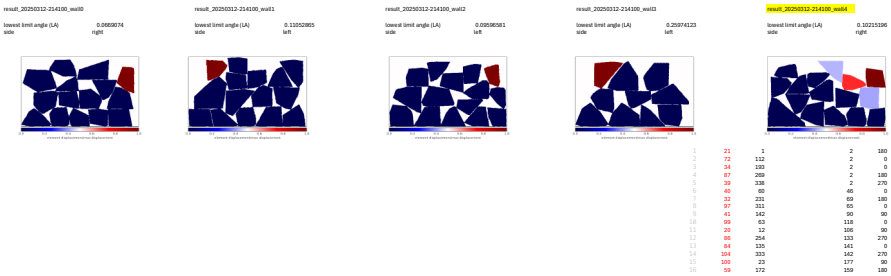

Wall 03

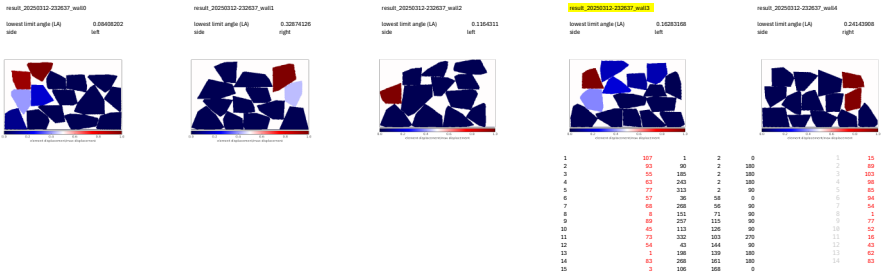

Wall_Number	Wall Name	smallest Rubble Size	largest Rubble Size	lowest Infill %	highest Infill %	cm2 wall	cm2 rubble	average cm2 rubble	rubble pieces needed	Rubble for scan	Pixel Size	Canvas Size	Infill %	Stones placed	Computing Time	Tries
1	Large_Stones01	75	150	25%	35%	1000	750	58.9	13	14	41706	147440	28%	12	05:18:00	4
2	Large_Stones02	75	150	25%	35%	1000	750	58.9	13	14	44890	147440	30%	10	06:48:00	7
3	Large_Stones03	75	150	25%	35%	1000	750	58.9	13	14	42781	147440	29%	10	07:55:00	9
4	Large_Stones04	75	150	25%	35%	1000	750	58.9	13	14	46521	147440	32%	10	14:15:00	8
5	Large_Stones05	75	150	25%	35%	1000	750	58.9	13	14	44820	147440	30%	13	07:04:00	8
6	Small_Stones01	25	75	25%	35%	1000	750	26.2	29	40	47968	147440	33%	35	03:13:00	5
7	Small_Stones02	25	75	25%	35%	1000	750	26.2	29	40	46239	145015	32%	29	02:51:00	6
8	Small_Stones03	25	75	25%	35%	1000	750	26.2	29	40	47529	145015	33%	30	17:08:00	8
9	Small_Stones04	25	75	25%	35%	1000	750	26.2	29	40	47543	145015	33%	30	09:24:00	7
10	Small_Stones05	25	75	25%	35%	1000	750	26.2	29	40	48840	145015	34%	35	08:43:00	5
11	Human	75	150	45%	55%	1000	550	58.9	10	14	55553	289850	19%			
12	Human	75	150	45%	55%	1000	550	58.9	10	14	62426	289850	22%			
13	Human	75	150	45%	55%	1000	550	58.9	10	14	52691	289850	18%			
14	Human	75	150	45%	55%	1000	550	58.9	10	14	63825	289850	22%			
15	Human	75	150	45%	55%	1000	550	58.9	10	14	63747	289850	22%			
16	Stone_Infill01	25	150	10%	20%	1000	900	45.8	20	14	57918	289850	20%			
17	Stone_Infill02	25	150	10%	20%	1000	900	45.8	20	14	57000	289850	20%			
18	Stone_Infill03	25	150	10%	20%	1000	900	45.8	20	14	56936	289850	20%			
19	Stone_Infill04	25	150	10%	20%	1000	900	45.8	20	14	53431	289850	18%			
20	Stone_Infill05	25	150	10%	20%	1000	900	45.8	20	14	60321	289850	21%			
21	Concrete01	0	0	100%	100%	1000						147440	100%			
22	Concrete02	0	0	100%	100%	1000						147440	100%			
23	Concrete03	0	0	100%	100%	1000						147440	100%			
24	Concrete04	0	0	100%	100%	1000						147440	100%			
25	Concrete05	0	0	100%	100%	1000						147440	100%			

LCA Case Study Wall Thickness Calculation

Wall Type	Brick	Precast Wall	C30 Concrete	R-C30 Concrete	Rammed Earth	CS Wall 30%	CS Wall 20%
net Load (kN)	100 kN	100 kN	100 kN	100 kN	100 kN	100 kN	100 kN
nfcd (compressive strength)	8.00 MPa	20.00 MPa	20.00 MPa	20.00 MPa	1.33 MPa	3.33 MPa	3.33 MPa
b (overall width of wall)	4000 mm	4000 mm	4000 mm	4000 mm	4000 mm	4000 mm	4000 mm
e (exxentricity of Ned)	50 mm	50 mm	50 mm	50 mm	50 mm	50 mm	50 mm
slenderness ratio		25	25	25		25	
thickness based on compression		101 mm	101 mm	101 mm		108 mm	108 mm
thickness based on slenderness		120 mm	120 mm	120 mm		220 mm	220 mm
thickness based on norm	240 mm	100 mm	140 mm	140 mm	300 mm		
final thickness	240 mm	120 mm	140 mm	140 mm	300 mm	220 mm	220 mm
m3 for 1 m2 wall	0.24 m3	0.12 m3	0.14 m3	0.14 m3	0.30 m3	0.22 m3	0.22 m3
GWP	27 kg	48 kg	32 kg	32 kg	3 kg	23 kg	20 kg
	117%	206%	140%	136%	12%	100%	88%
PENRT	283 MJ	380 MJ	138 MJ	135 MJ	37 MJ	150 MJ	134 MJ
	189%	254%	92%	90%	25%	100%	89%

LCA EPD Data

Product			Brick	Precast Wall	Rammed Earth	C30 Concrete	R-C30 Concrete	CS Wall 20%	CS Wall 30%	Rebar	Rebar per Wall
					1.3.17 Mineral building products / Bricks, blocks and elements / Air-dried brick (adobe)						
EPD			EPD-BDZ-20210062-ICG1-DE	EPD-THO-20200144-IBD1-EN		EPD-IZB-201431-IBG2-DE	EPD-Kiwa-EE-171735-EN	EPD-IZB-2023041 8-IBA1-DE	EPD-IZB-2023041 8-IBA1-DE	EPD-KIWA-EE-000133-EN	EPD-KIWA-EE-000133-EN
Date			04.08.21	44067	2018	41481	45418	45219	45219	44306	44306
Density		kg/m3	2000	2577	2000	1	1	1	1	1	1
Weight Unit		kg	0	1000	2000	2400	2148.88	2400	2400	7850	7850
Volume Unit		m3	0	2.58	1	2400	2148.88	2400	2400	1	1
Unit in EPD			m2	t	m3	m3	m3	m3	m3	kg	kg
Factor to m3			1.00	2.58	1	1	1	0.2	0.3	7850	78.5
Compressive Strength			12.00 MPa	30.00 MPa	2.00 MPa	30.00 MPa	30.00 MPa	5.00 MPa	5.00 MPa		
Safety Factor			1.5	1.5	1.5	1.5	1.5	1.5	1.5		
Design Strength			8.00 MPa	20.00 MPa	1.33 MPa	20.00 MPa	20.00 MPa	3.33 MPa	3.33 MPa		
Indicator	Direction	Unit	Production	Production	Production	Production	Production	Production	Production	Production	Production
Energy / m3			A1-A3	A1-A3	A1-A3	A1-A3	A1-A3	A1-A3	A1-A3	A1-A3	A1-A3
Use of renewable primary energy (PERE)	Input	MJ	0	0	0	82.7	0	0	0	0	0
Primary energy resources used as raw materials (PERM)	Input	MJ	0	0	0	0	0	0	0	0	0
Total use of renewable primary energy resources (PERT)	Input	MJ	0	0	0	82.7	0	0	0	0	0
Use of non-renewable primary energy (PENRE)	Input	MJ	0	0	0	984	0	0	0	0	0
Non-renewable primary energy resources used as raw materials (PENRM)	Input	MJ	0	0	0	0	0	0	0	0	0
Total use of non-renewable primary energy resources (PENRT)	Input	MJ	1180	3169.71	123.9	984	962	146.2	219.3	8399.5	0
Input of secondary material (SM)	Input	kg	0	0	0	116.2	0	0	0	0	0
Use of renewable secondary fuels (RSF)	Input	MJ	0	0	0	182	0	0	0	0	0
Use of non renewable secondary fuels (NRSF)	Input	MJ	0	0	0	354.8	0	0	0	0	0
Use of net fresh water (FW)	Input	m3	0	0	0	0.23	0	0	0	0	0
Hazardous waste disposed (HWD)	Output	kg	0	0	0	0	0	0	0	0	0
Non-hazardous waste disposed (NHWD)	Output	kg	0	0	0	0	0	0	0	0	0
Radioactive waste disposed (RWD)	Output	kg	0	0	0	0	0	0	0	0	0
Components for re-use (CRU)	Output	kg	0	0	0	0	0	0	0	0	0
Materials for Recycling (MFR)	Output	kg	0	0	0	0	0	0	0	0	0
Material for Energy Recovery (MER)	Output	kg	0	0	0	0	0	0	0	0	0
Exported electrical energy (EEE)	Output	MJ	0	0	0	0	0	0	0	0	0
Exported thermal energy (EET)	Output	MJ	0	0	0	0	0	0	0	0	0
Environmental Impact Indicators / m3			**A1-A3**	**A1-A3**	**A1-A3**	**A1-A3**	**A1-A3**	**A1-A3**	**A1-A3**	**A1-A3**	0
Global warming potential (GWP)		kg CO2 eq.	113	461.283	9.349	231.9	225.776	25.8	38.7	704.93	7.0493
Ozone Depletion Potential (ODP)		kg R11 eq.	0	1.3117E-06	0	7.35E-07	0	0	0	0	0
Photochemical Ozone Creation Potential (POCP)		kg Ethene e	0	0.577248	0	0.323	0	0	0	0	0
Acidification potential (AP)		kg SO2 eq.	0	0.1293654	0	0.0513	0	0	0	0	0
Eutrophication potential (EP)		kg Phospha	0	0.0664866	0	0.0393	0	0	0	0	0
Abiotic depletion potential for non fossil resources (ADPE)		kg Sb eq.	0	0.00035563	0	0.000418	0	0	0	0	0
Abiotic depletion potential for fossil resources (ADPF)		MJ	0	2860.47	0	845.2	0	0	0	0	0
Energy as of EPD			A1-A3	A1-A3	A1-A3						0
Use of renewable primary energy (PERE)	Input	MJ	0	0	0	82.7	0	0	0	0	0
Primary energy resources used as raw materials (PERM)	Input	MJ	0	0	0	0	0	0	0	0	0
Total use of renewable primary energy resources (PERT)	Input	MJ	0	0	0	82.7	0	0	0	0	0
Use of non-renewable primary energy (PENRE)	Input	MJ	0	0	0	984	0	0	0	0	0
Non-renewable primary energy resources used as raw materials (PENRM)	Input	MJ	0	0	0	0	0	0	0	0	0
Total use of non-renewable primary energy resources (PENRT)	Input	MJ	1180	1230	123.9	984	962	731	731	1.07	0
Input of secondary material (SM)	Input	kg	0	0	0	116.2	0	0	0	0	0
Use of renewable secondary fuels (RSF)	Input	MJ	0	0	0	182	0	0	0	0	0
Use of non renewable secondary fuels (NRSF)	Input	MJ	0	0	0	354.8	0	0	0	0	0
Use of net fresh water (FW)	Input	m3	0	0	0	0.23	0	0	0	0	0
Hazardous waste disposed (HWD)	Output	kg	0	0	0	0	0	0	0	0	0
Non-hazardous waste disposed (NHWD)	Output	kg	0	0	0	0	0	0	0	0	0
Radioactive waste disposed (RWD)	Output	kg	0	0	0	0	0	0	0	0	0
Components for re-use (CRU)	Output	kg	0	0	0	0	0	0	0	0	0
Materials for Recycling (MFR)	Output	kg	0	0	0	0	0	0	0	0	0
Material for Energy Recovery (MER)	Output	kg	0	0	0	0	0	0	0	0	0
Exported electrical energy (EEE)	Output	MJ	0	0	0	0	0	0	0	0	0
Exported thermal energy (EET)	Output	MJ	0	0	0	0	0	0	0	0	0
Environmental Impact Indicators as of EPD	**Direction**	**Unit**	**A1-A3**	A1-A3	A1-A3	A1-A3		129	129	0 A1-A3	
Global warming potential (GWP)		kg CO2 eq.	113	179	9.349	231.9	225.776			0.0898	0.0898
Ozone Depletion Potential (ODP)		kg R11 eq.	0	5.09E-07	0	7.35E-07		0	0	0	0
Photochemical Ozone Creation Potential (POCP)		kg Ethene e	0	0.224	0	0.323		0	0	0	0
Acidification potential (AP)		kg SO2 eq.	0	0.0502	0	0.0513		0	0	0	0
Eutrophication potential (EP)		kg Phospha	0	0.0258	0	0.0393		0	0	0	0
Abiotic depletion potential for non fossil resources (ADPE)		kg Sb eq.	0	0.000138	0	0.000418		0	0	0	0
Abiotic depletion potential for fossil resources (ADPF)		MJ	0	1110	0	845.2		0	0	0	0